

Universidade do Minho
Escola de Engenharia

Nuno Adriano Leite Mendes

**Seismic Assessment of
Ancient Masonry Buildings:
Shaking Table Tests and Numerical Analysis**

Tese de Doutoramento
Estruturas / Engenharia Civil

Trabalho efectuado sob a orientação do
Professor Doutor Paulo José Brandão Barbosa Lourenço

Co-Orientador:
Doutor Alfredo Peres de Noronha Campos Costa

DECLARAÇÃO

Nuno Adriano Leite Mendes

Correio electrónico: nunomendes@civil.uminho.pt

Tel. 253517210

Número do Bilhete de Identidade: 12305989

Título da tese:

**Seismic Assessment of Ancient Masonry Buildings:
Shaking Table Tests and Numerical Analysis**

Ano de conclusão: 2012

Orientador:

Professor Doutor Paulo José Brandão Barbosa Lourenço

Co-Orientador:

Doutor Alfredo Peres de Noronha Campos Costa

Designação do Doutoramento:

Engenharia Civil

Escola de Engenharia

Departamento de Engenharia Civil

É AUTORIZADA A REPRODUÇÃO INTEGRAL DESTA TESE APENAS PARA EFEITOS DE INVESTIGAÇÃO,
MEDIANTE DECLARAÇÃO ESCRITA DO INTERESSADO, QUE A TAL SE COMPROMETE.

Guimarães, ___/___/_____

Assinatura: _____

Acknowledgments

The present work was carried out at the Department of Civil Engineering of the University of Minho and at the National Laboratory for Civil Engineering (Lisbon). This thesis would not be completed without the help of all that were involved in my work and I would like to express my gratitude to:

- Professor Paulo Lourenço, my supervisor, for his full support, encouragement, interesting discussions and careful reading;
- Doctor Alfredo Campos Costa, my co-supervisor, for the permanent and interesting discussions and tremendous help in the experimental tests;
- Doctor Ema Coelho for accepting me in the Earthquake Engineering and Structural Dynamics Division (NESDE) of the National Laboratory for Civil Engineering (Lisbon);
- Professors Daniel Oliveira, Graça Vasconcelos and Luís Ramos of the University of Minho for their support and interest in my work;
- Doctors Alexandra Carvalho, Paulo Candeias, Luís Mendes and Maria João Falcão of the NESDE for the support in the shaking table tests;
- My colleagues Leonardo Avila and Ana Araújo for the tremendous support in the final works of the thesis;
- Tommaso Scappaticci and Guang Yang for the collaboration in the numerical analyses;

- Technicians of the NESDE, Artur Santos, Gonçalo Vitor and Susana Almeida, and Engineer Pedro Alves for their help and support in the laboratory works;
- My colleague João Leite for the careful reading of the thesis;
- My colleagues José Pedro Cunha e Rui Silva for the interesting discussions and friendship during this work;
- The Portuguese Science Foundation (FCT) for the grant awarded during 2006 to 2010 (Contract SFRH/BD/32190/2006);
- BEL company for the materials and application of the strengthening elements used in the strengthened mock-up;
- And finally, but not the least, my family and my friends for the patient, encouragement and support during all work.

Abstract

Ancient masonry buildings were built for many centuries taking into account only vertical static loads, without reference to any particular seismic code. The different types of masonry present common features that are directly related to the high seismic vulnerability of this type of buildings, such as the high specific mass, the low tensile strength, low to moderate shear strength and low ductility (brittle behaviour). Besides the material properties, the seismic behaviour of ancient masonry buildings depends on other factors, such as geometry of the structure, connection between orthogonal walls, connections between structural walls and floors, connections between walls and roof, foundation strength, stiffness of the floors and strength of the non-structural elements.

The Portuguese housing stock consists of several building typologies in which some of them present construction features associated with poor seismic performance. Thus, it is necessary to intervene in these types of buildings with the purpose of reducing their seismic vulnerability. The “gaioleiro” buildings correspond to a Portuguese building typology built between the 19th century and the beginning of the 20th century, and are believed to present the highest seismic vulnerability of the housing stock of Portugal. These buildings are, generally, four to six stories high, with stone masonry walls, timber floors and roof, and still remain in use nowadays.

Motivated by the above reasons, this thesis aims at evaluating the seismic vulnerability of the “gaioleiro” buildings and proposing a strengthening technique to reduce it. The study involved shaking table tests and several types of numerical analysis.

The tests were carried out on the shaking table of the National Laboratory for Civil Engineering (Lisbon). The experimental program involved the definition of a prototype representative of the average features of the “gaioleiro” buildings, which was later used for the construction of the mock-ups. Due the size and payload capacity of the shaking table, two mock-ups were built using a reduce scale: non-strengthened and strengthened mock-ups. The seismic load is composed by two orthogonal and uncorrelated accelerograms which induce, simultaneously, in-plane and out-of-plane behaviour of the mock-ups. In the strengthened mock-up steel elements were used to improve the connection between walls and floors, and ties in the upper storeys.

Through the experimental program the dynamic properties of the mock-ups, the vulnerability curves, the crack patterns and the collapse mechanisms were obtained, and the efficiency of the strengthening technique adopted to reduce the seismic vulnerability of the “gaioleiro” buildings was evaluated.

The experimental results were used for validating the numerical model of the non-strengthened mock-up, which was later used in non-linear dynamic with time integration and pushover analyses. Furthermore, a sensitivity analysis varying the proprieties of the numerical model was carried out.

The seismic vulnerability curves obtained from the dynamic identification tests show that the strengthened mock-up presents a reduction of the damage indicator of about 46% with respect to the non-strengthened mock-up. The results of the seismic tests show that the damage of the non-strengthened mock-up concentrates at the facades and the strengthening technique adopted improved significantly the seismic behaviour of the mock-up, leading to the conclusion that the strengthening technique was efficient in the reduction of its seismic vulnerability.

Finally, the sensitivity analysis shows that the Young’s modulus of the masonry walls, the Young’s modulus of the timber floors and the compressive non-linear properties are the parameters that most influence the seismic behaviour of the numerical model. The stiffness of the floors influences significantly the capacity strength and the collapse mechanism of the structure. Thus, the strengthening of the floors is also an effective solution for reducing of the seismic vulnerability of the “gaioleiro” buildings, namely by improving the out-of-plane response of the walls.

Resumo

Os edifícios antigos de alvenaria foram construídos durante muitos séculos tendo em consideração apenas ações estáticas e verticais, sem referência a qualquer regulamento sísmico. Os diferentes tipos de alvenaria apresentam características comuns que estão relacionadas diretamente com a grande vulnerabilidade sísmica deste tipo de edifícios, tais como a elevada massa específica, a baixa resistência à tração, a baixa a moderada resistência ao corte e a baixa ductilidade (comportamento frágil). Além das propriedades dos materiais, o comportamento sísmico dos edifícios antigos de alvenaria depende de outros fatores, tais como: geometria da estrutura, ligação entre paredes ortogonais, ligação entre paredes e pavimentos, ligação entre paredes e cobertura, resistência da fundação, rigidez dos pavimentos e resistência dos elementos não estruturais.

O parque habitacional de Portugal é constituído por várias tipologias de edifícios, entre as quais algumas apresentam características de construção associadas a um mau desempenho sísmico. Assim, torna-se necessário intervir nestas tipologias de edifícios, tendo por objetivo reduzir a sua vulnerabilidade sísmica. Os edifícios gaioleiros correspondem à tipologia de edifícios construídos no final do século XIX e inícios do século XX, e acredita-se que apresentem a maior vulnerabilidade sísmica do edificado de Portugal. Estes edifícios têm, geralmente, quatro a seis pisos, paredes de alvenaria de pedra, pavimentos e cobertura em estrutura de madeira e encontram-se ainda em utilização nos dias de hoje.

Tendo em consideração o anteriormente referido, a presente tese tem como principais objetivos a avaliação e redução da vulnerabilidade sísmica dos edifícios gaioleiros. O estudo envolveu ensaios em plataforma sísmica e diferentes tipos de análises numéricas.

Os ensaios foram realizados na plataforma sísmica do Laboratório Nacional de Engenharia Civil (Lisboa). O programa experimental envolveu a definição de um protótipo representativo das características correntes dos edifícios gaioleiros, que posteriormente foi utilizado para a construção dos modelos experimentais. Devido às dimensões e limite de capacidade de carga da plataforma sísmica, foram ensaiados dois modelos experimentais à escala reduzida: modelo não reforçado e reforçado. A ação sísmica aplicada é composta por dois acelerogramas ortogonais e não correlacionáveis que induzem, simultaneamente, comportamento no plano e para fora do plano dos

modelos experimentais. No modelo reforçado utilizaram-se elementos metálicos para melhorar a ligação entre as paredes e os pavimentos, e tirantes nos pisos superiores.

O programa experimental permitiu obter as propriedades dinâmicas dos modelos, as curvas de vulnerabilidade, os padrões de fendilhação e os mecanismos de colapso, bem como concluir sobre a eficiência da técnica de reforço adotada na redução da vulnerabilidade dos edifícios gaioleiros.

Os resultados experimentais foram utilizados na calibração de modelos numéricos. Estes foram, posteriormente, utilizados em análise não lineares dinâmicas e estáticas. Além disso, foi realizada uma análise de sensibilidade variando as propriedades do modelo numérico.

Como principais conclusões sobre os ensaios em plataforma sísmica, as curvas de vulnerabilidade sísmica obtidas através dos ensaios de identificação dinâmica demonstraram que o modelo reforçado apresenta uma redução do indicador de dano de cerca de 46% relativamente ao modelo não reforçado. Os resultados dos ensaios sísmicos demonstraram que o dano do modelo não reforçado concentra-se nas fachadas e que a técnica de reforço adotada melhorou significativamente o comportamento sísmico do modelo, concluindo-se que a técnica de reforço foi eficiente na redução da sua vulnerabilidade sísmica.

Por último, os resultados da análise de sensibilidade demonstraram que o módulo de elasticidade das paredes, o módulo de elasticidade dos pavimentos e as propriedades não-lineares em compressão são os parâmetros com maior influência no comportamento sísmico do modelo numérico. A rigidez dos pavimentos tem influência significativa na capacidade resistente e no mecanismo de colapso da estrutura. Assim, o reforço dos pavimentos é também uma solução efetiva para a redução da vulnerabilidade sísmica dos edifícios gaioleiros, melhorando sobretudo a resposta para fora do plano das paredes.

Contents

Chapter 1

Introduction.....	1
1.1 Motivation for assessing of the seismic vulnerability of masonry structures.....	1
1.2 Background of methods to assess the seismic vulnerability.....	2
1.3 Seismic behaviour of ancient masonry structures	4
1.4 Focus of the thesis	13
1.5 “Gaioleiro” buildings.....	15
1.6 Outline of the thesis	22

Chapter 2

Shaking table tests setup	25
2.1 Introduction.....	25
2.2 Prototype definition	27
2.3 Mock-ups definition.....	28
2.4 Mock-ups construction	36
2.5 Test setup	39
2.6 Instrumentation	41
2.7 Input signals.....	46
2.8 Characterization of the materials	51
2.9 Final remarks	54

Chapter 3

Shaking table tests results.....	55
3.1 Introduction.....	55
3.2 Methodologies used in the analyses of the results.....	56
3.2.1 Dynamic identification tests	56
3.2.2 Seismic tests	61

3.3 Crack patterns	64
3.4 Dynamic identification tests	70
3.4.1 Non-strengthened mock-up	70
3.4.2 Strengthened mock-up	77
3.4.3 Comparison of the results of the dynamic identification test	81
3.5 Results of the seismic tests	84
3.5.1 Non-strengthened mock-up	84
3.5.2 Strengthened mock-up	89
3.5.3 Comparison of the results of the seismic test	94
3.6 Conclusions.....	98

Chapter 4

Preparation and validation of the numerical model	101
4.1 Introduction.....	101
4.2 Preparation of the numerical model.....	102
4.3 Calibration of the dynamics properties.....	104
4.3.1 Modal updating methods	104
4.3.2 Results of the modal updating	106
4.4 Non-linear dynamic analysis with time integration.....	115
4.4.1 Analysis tools	115
4.4.2 Non-linear dynamic analysis for Earthquake 25%.....	121
4.4.3 Non-linear dynamic analysis with Earthquake 100%	126
4.5 Scale effect discussion.....	128
4.6 Conclusions.....	131

Chapter 5

Sensitivity analysis.....	133
5.1 Introduction.....	133
5.2 Results for the reference numerical model	134
5.3 Non-linear dynamic parametric analysis	140
5.3.1 Stiffness of the masonry walls.....	140
5.3.2 Stiffness of the timber floors	142
5.3.3 Compressive non-linear properties of the masonry.....	144
5.3.4 Tensile non-linear properties of the masonry	147
5.3.5 Damping	149

5.3.6	Vertical component of the earthquake	149
5.4	Pushover parametric analysis	151
5.4.1	Stiffness of the masonry walls	152
5.4.2	Stiffness of the timber floors	152
5.4.3	Compressive non-linear properties of the masonry	154
5.4.4	Tensile non-linear properties of the masonry	155
5.4.5	Pushover analysis proportional to the first mode	157
5.5	Conclusions.....	158
 Chapter 6		
Conclusions and future work		
163		
6.1	Conclusions.....	163
6.1.1	Experimental research	164
6.1.2	Numerical study.....	165
6.2	Future work.....	167
 References		
169		
 Annex A		
Input signals		
179		
 Annex B		
Modal updating		
201		
 Annex C		
Non-linear dynamic parametric analysis		
209		
 Annex D		
Pushover parametric analysis		
219		

Index of figures

Figure 1.1 – Methodologies of seismic vulnerability assessment (adapted from Sousa 2006)	4
Figure 1.2 – Examples of masonry: (a) rubble walls (b) ashlar walls (International Correspondence Schools 2008); (c) single, double and three leaf walls (Mascarenhas 2003)	5
Figure 1.3 – Typical deformation and damage of unreinforced masonry buildings (adapted from Tomažević 1999)	7
Figure 1.4 – In-plane structural models of masonry walls: (a) cantilever walls connected by flexible floors; (b) coupled walls with pier hinging; (c) coupled walls with spandrel hinging (adapted from Paulay and Priestley 1992)	8
Figure 1.5 – In-plane collapse mechanisms of the piers (adapted from Yi 2004)	9
Figure 1.6 – In-plane behaviour of the spandrels (Magenes et al. 2000)	9
Figure 1.7 – In-plane behaviour of masonry walls (FEMA 306 1998).....	10
Figure 1.8 – Out-of-plane behaviour of the walls of masonry buildings with rigid floors (adapted from Tomažević 1999)	10
Figure 1.9 – Example of shear failure of: (a) piers (Penna 2008); (b) spandrels (Dazio and Beyer 2010)	11
Figure 1.10 – Example of out-of-plane collapse mechanisms: (a) wall of the top floor (Lagomarsino 2012); (b) parapet and wall collapse and successful strengthening with ties (arrow) (Ingham et al. 2011)	11
Figure 1.11 –Schematic contributions of connections and diaphragm stiffness to the overall floor stiffness (Brignola et al. 2008)	13
Figure 1.12 – Evolution of the current construction processes of the Lisbon building stock (Silva 2001)	14
Figure 1.13 – Examples of “gaioleiro” buildings, Lisbon, Portugal	16
Figure 1.14 – Facade of a “gaioleiro” buildings (Appleton 2005).....	16
Figure 1.15 – Urban layout and apartment plan of “gaioleiro” buildings: (a) block of buildings; (b) geometry of the typical apartment	17
Figure 1.16 – Thickness of the load-bearing walls of the “gaioleiro” buildings: (a) typical reduction of thickness in elevation (Appleton 2003); (b) example of a building in Lisbon with constant thickness. (Dimensions in meters)	18
Figure 1.17 – Walls of the “gaioleiro” buildings: (a) load-bearing wall with rubble masonry; (b) load-bearing wall with solids bricks (adapted from Andrade 2011).....	19

Figure 1.18 – Connection of the floors to the masonry load-bearing walls: (a) insertion of the timber joist a pocket of the wall; (b) improving of the connection through steel anchors; (c) connection with rim joist (adapted from Appleton 2003)	20
Figure 1.19 – Cross section of the “gaioleiro” building’s roof (adapted from Appleton 2005)	20
Figure 1.20 – Elements of the “gaioleiro” buildings: (a) sunrooms; (b) external stairs (Andrade 2011); (c) lift.....	21
Figure 2.1 – Geometry of the non-strengthened mock-up: (a) facades; (b) gable walls; (c) plan; (d) connection floor-gable wall; (e) connection floor-facade. (Dimensions in meters)	32
Figure 2.2 – Strengthened mock-up: (a) facades; (b) plan; (c) section AA’; (d) section BB’; (e) section CC’. (Dimensions in meters)	34
Figure 2.3 – Steel cables of the strengthened mock-up: (a) plan of the two top floors; (b) connection of the cables to the corners; (c) connection of the cables to the middle of the facades; (d) turnbuckle.....	35
Figure 2.4 – Construction of the non-strengthened mock-up.....	36
Figure 2.5 – Details of the: (a) corners and overlapping corner stones; (b) spandrels...	37
Figure 2.6 – Details of the floors construction: (a) bent nails connecting the rim joists to the masonry walls; (b) timber prop and lime mortar used to fix the rim joists	37
Figure 2.7 – General view of the: (a) non-strengthened mock-up; (b) strengthened mock-up.....	38
Figure 2.8 – Shaking table: (a) 3D general view; (b) plan	43
Figure 2.9 – Images of Accelerometers: (a) piezoelectric accelerometer (PCB 2010); (b) capacitive accelerometer (ENDEVCO 2010).....	44
Figure 2.10 – Accelerometers setup: (a) North facade; (b) East gable wall; (c) South facade; (d) West gable wall	45
Figure 2.11 – Pseudo acceleration response spectrums at 1:3 reduced scale: (a) North-South direction; (b) East-West direction	46
Figure 2.12 – Time histories of the input signals at 1:3 reduced scale	47
Figure 2.13 – Comparison between the target and measured input signals using the peak values of the time histories	49
Figure 2.14 – Comparison between the target and measured of the input signals using the integral parameters: (a) Root Mean Squares; (b) Arias Intensity; (c) Input Energy	50
Figure 2.15 – Input signals of the dynamic identification tests: (a) North-South (longitudinal) direction; (b) East-West (transversal) direction.....	51
Figure 2.16 – Strain-stress diagrams of the uniaxial compressive tests.....	52
Figure 2.17 – Strain-stress diagrams of the diagonal compressive tests.....	53

Figure 3.1 – Theoretical evolution of the damage indicator as function of the amplitude of the seismic action	59
Figure 3.2 – Scheme of out-of-plane displacements relative to the corners ($u_{corners}$)	62
Figure 3.3 – Crack patterns of the non-strengthened mock-up: Earthquake 25% - 100%	65
Figure 3.4 – Examples of the damage for the non-strengthened mock-up (Earthquake 100%): (a) spandrel; (b) pier.....	66
Figure 3.5 – Crack patterns of the strengthened mock-up: Earthquake 25% - 100%....	67
Figure 3.6 – Crack patterns of the strengthened mock-up: Earthquake 125% and 150%	69
Figure 3.7 – Mode shapes of the DI 0 (dynamic identification test before the first seismic test) of the non-strengthened mock-up.....	71
Figure 3.8 – Variation of the FRF's along the dynamic identification tests of the non-strengthened mock-up at position: (a) E4.5; (b) N2.3	72
Figure 3.9 – Evolution of the frequencies of the non-strengthened mock-up and their variation with respect to the DI 0	73
Figure 3.10 – Seismic vulnerability curves of the non-strengthened mock-up in both directions, using as input the nominal peak ground acceleration (PGA_{no})	75
Figure 3.11 – Seismic vulnerability curves of the non-strengthened mock-up in both directions, using as input the equivalent peak ground acceleration (PGA_{eq})	76
Figure 3.12 – Seismic vulnerability curves of the non-strengthened mock-up in both directions using as input the nominal input energy	76
Figure 3.13 – Mode shapes of the DI 0 (dynamic identification test before the first seismic test) of the strengthened mock-up.....	78
Figure 3.14 – Evolution of the frequencies of the strengthened mock-up and their variation with respect to the DI 0	79
Figure 3.15 – Seismic vulnerability curves of the strengthened mock-up in both directions, using as input the nominal peak ground acceleration (PGA_{no})	80
Figure 3.16 – Seismic vulnerability curves of the strengthened mock-up in both directions using as input the nominal input energy	81
Figure 3.17 – Comparison between the seismic vulnerability curves of the non-strengthened (NSM) and strengthened (SM) mock-ups relating the input energy with the damage indicator d using: (a) the first transversal mode; (b) the first longitudinal mode	82
Figure 3.18 – Comparison between the seismic vulnerability curves of the non-strengthened and strengthened mock-ups and the mock-ups tested by Candeias (2008).....	83

Figure 3.19 – Average out-of-plane acceleration amplification at floor levels for the facades of the non-strengthened mock-up	84
Figure 3.20 – Average out-of-plane acceleration amplification at floor levels for the gable walls of the non-strengthened mock-up	85
Figure 3.21 – Average out-of-plane displacement at floor levels for the facades of the non-strengthened mock-up	86
Figure 3.22 – Average out-of-plane displacement at floor levels for the gable walls of the non-strengthened mock-up	86
Figure 3.23 – Average out-of-plane relative displacement with respect to the corners at floor levels for the facades of the non-strengthened mock-up	87
Figure 3.24 – Average out-of-plane relative displacement with respect to the corners at floor levels for the gable walls of the non-strengthened mock-up	88
Figure 3.25 – Average in-plane drift for the facades of the non-strengthened mock-up	89
Figure 3.26 – Average out-of-plane acceleration amplification at floor levels for the facades of the strengthened mock-up	90
Figure 3.27 – Average out-of-plane acceleration amplification at floor levels for the gable walls of the strengthened mock-up	90
Figure 3.28 – Average out-of-plane displacement at floor levels for the facades of the strengthened mock-up.....	91
Figure 3.29 – Average out-of-plane displacement at floor levels for the gable walls of the strengthened mock-up.....	91
Figure 3.30 – Average out-of-plane relative displacement with respect to the corners at floor levels for the facades of the strengthened mock-up.....	92
Figure 3.31 – Average out-of-plane relative displacement with respect to the corners at the floor levels for the gable walls of the strengthened mock-up.....	93
Figure 3.32 – Average in-plane drift for the facades of the strengthened mock-up.....	94
Figure 3.33 – Comparison of the average out-of-plane acceleration amplification at the: (a) 3 rd floor of the facades; (b) 4 th floor of the gable walls.....	95
Figure 3.34 – Comparison of the average out-of-plane displacement at the: (a) 3 rd floor of the facades; (b) 4 th floor of the gable walls	96
Figure 3.35 – Comparison of the average out-of-plane relative displacement with respect to the corners at the: (a) 3 rd floor of the facades; (b) 4 th floor of the gable walls	97
Figure 3.36 – Comparison of the average in-plane drift at the 3 rd floor of the facades. 97	
Figure 4.1 – Numerical model: (a) general view; (b) detail of the floors	103
Figure 4.2 – Variables used in the modal updating: (a) Model 1; (b) Model 2; (c) Model 3; (d) Model 4.....	107
Figure 4.3 – Results of the modal updating for the: (a) Model 1; (b) Model 2; (c) Model 3; (d) Model 4.....	109

Figure 4.4 – Results of the optimization of the Model 3: (a) residuals of the objective function; (b) frequency comparison and errors; (c) <i>MAC</i> matrix; (d) <i>NMD</i> values.....	111
Figure 4.5 – <i>COMAC</i> values in the: (a) transversal direction; (b) longitudinal direction	113
Figure 4.6 – Numerical mode shapes (Model 3): (a) general view; (b) comparison between the numerical (marker line) and experimental (grey line) DOF's in the transversal and longitudinal direction	114
Figure 4.7 – Adopted hysteretic behaviour	117
Figure 4.8 – Viscous damping of the numerical model	121
Figure 4.9 – Comparison of the average maximum out-of-plane acceleration amplification at floors levels: (a) facades; (b) gable walls.....	122
Figure 4.10 – Comparison of the average maximum out-of-plane displacement at floors levels: (a) facades; (b) gable walls.....	123
Figure 4.11 – Comparison of the average maximum out-of-plane relative displacement with respect to the corners at floors levels: (a) facades; (b) gable walls	123
Figure 4.12 – Comparison of the average of the maximum in-plane drifts of the facades	124
Figure 4.13 – Comparison of the Root Mean Square of displacement at the central vertical alignment of the: (a) South facade; (b) East gable wall.....	125
Figure 4.14 – Comparison of the damage for the Earthquake 25%: (a) experimental crack pattern; (b) maximum tensile principal strains at the external surface.....	126
Figure 4.15 – Comparison of the damage for the Earthquake 100%: (a) experimental crack pattern; (b) maximum tensile principal strains at the external surface.....	127
Figure 4.16 – Maximum acceleration amplifications of the Earthquake 25% for the reduced and full models at the middle of the: (a) North facade; (b) East gable wall.....	129
Figure 4.17 – Maximum displacements of the Earthquake 25% for the reduced and full models at the middle of the: (a) North facade; (b) East gable wall	129
Figure 4.18 – Maximum displacements of the Earthquake 100% for the reduced and full models at the middle of the: (a) North facade; (b) East gable wall	130
Figure 4.19 – Maximum displacements of the Earthquake 25% with linear behaviour for the reduced and full models at the middle of the: (a) North facade; (b) East gable wall.....	131
Figure 5.1 – Envelope of the response obtained from the non-linear dynamic analysis with time integration and capacity curve obtained from the pushover analysis of the reference model in the: (a) transversal direction; (b) longitudinal direction	136

Figure 5.2 – Maximum tensile principal strains at the external surface of the non-linear dynamic analyses of the reference model: (a) Earthquake 100%; (b) Earthquake 300% 137

Figure 5.3 – Maximum tensile principal strains at the external surface of the pushover analysis of the reference model in the: (a) transversal direction; (b) longitudinal direction..... 138

Figure 5.4 – Maximum out-of-plane displacement of the reference model at the middle of the: (a) North facade; (b) East gable wall 139

Figure 5.5 – Maximum in-plane drift of the reference model of the: (a) North facade; (b) East gable wall..... 139

Figure 5.6 – Envelope of the response varying the Young’s modulus of the masonry walls in the: (a) transversal direction; (b) longitudinal direction 141

Figure 5.7 – Maximum out-of-plane displacement, obtained from the dynamic analysis, varying the Young’s modulus of the masonry walls at the middle of the: (a) North facade; (b) East gable wall 142

Figure 5.8 – Envelope of the response varying the Young’s modulus of the floors in the: (a) transversal direction; (b) longitudinal direction..... 143

Figure 5.9 – Maximum tensile principal strains at the external surface, obtained from the dynamic analysis, varying the Young’s modulus of the floors: (a) $0.1x E_{floors,ref}$; (b) $10x E_{floors,ref}$ 144

Figure 5.10 – Maximum out-of-plane displacement, obtained from the dynamic analysis, varying the Young’s modulus of the floors at the middle of the: (a) North facade; (b) East gable wall..... 144

Figure 5.11 – Envelope of the response varying the compressive strength in the: (a) transversal direction; (b) longitudinal direction 145

Figure 5.12 – Maximum out-of-plane displacement, obtained from the dynamic analysis, varying the compressive strength at the middle of the: (a) North facade; (b) East gable wall..... 145

Figure 5.13 – Maximum tensile principal strains at the external surface, obtained from the dynamic analysis, varying the compressive strength: (a) $0.5x f_{c,ref}$; (b) $2.0x f_{c,ref}$ 146

Figure 5.14 – Envelope of the response varying the compressive fracture energy in the: (a) transversal direction; (b) longitudinal direction 147

Figure 5.15 – Envelope of the response varying the tensile strength in the: (a) transversal direction; (b) longitudinal direction 148

Figure 5.16 – Envelope of the response varying the tensile fracture energy in the: (a) transversal direction; (b) longitudinal direction 148

Figure 5.17 – Envelope of the response varying the damping ratio in the: (a) transversal direction; (b) longitudinal direction..... 149

Figure 5.18 – Envelope of the response including the vertical component of the earthquake in the: (a) transversal direction; (b) longitudinal direction . 150

Figure 5.19 – Capacity curves varying the Young’s modulus of the masonry walls in the: (a) transversal direction; (b) longitudinal direction	152
Figure 5.20 – Capacity curves varying the Young’s modulus of the timber floors in the: (a) transversal direction; (b) longitudinal direction	153
Figure 5.21 – Maximum tensile principal strains at the external surface, obtained from the pushover analysis in the longitudinal direction, varying the Young’s modulus of the floors: (a) $0.1 \times E_{floors,ref}$; (b) $10 \times E_{floors,ref}$	153
Figure 5.22 – Capacity curves varying the compressive strength in the: (a) transversal direction; (b) longitudinal direction	154
Figure 5.23 – Capacity curves varying the compressive fracture energy in the: (a) transversal direction; (b) longitudinal direction	155
Figure 5.24 – Capacity curves varying the tensile strength in the: (a) transversal direction; (b) longitudinal direction	155
Figure 5.25 – Maximum tensile principal strains at the external surface, obtained from the pushover analysis in the longitudinal direction, varying the tensile strength: (a) $0.5 \times f_{t,ref}$; (b) $2.0 \times f_{t,ref}$	156
Figure 5.26 – Capacity curves varying the tensile fracture energy in the: (a) transversal direction; (b) longitudinal direction	156
Figure 5.27 – Capacity curves of the pushover analysis proportional to the first mode in the: (a) transversal direction; (b) longitudinal direction	157
Figure 5.28 – Maximum tensile principal strains at the external surface, obtained from the pushover analysis proportional to the mode shape of the first mode in the: (a) transversal direction; (b) longitudinal direction	158

Index of tables

Table 1.1 – Typical mechanical properties of the masonry (Tomažević 1999)	6
Table 1.2 – Building typologies and corresponding construction periods (Oliveira and Cabrita 1985).....	14
Table 2.1 – Scale factors of the Cauchy and Froude similitude laws (Carvalho 1998) .	29
Table 2.2 – Shaking table tests carried out on the non-strengthened mock-up	40
Table 2.3 – Shaking table tests carried out on the strengthened mock-up	40
Table 2.4 – Characteristics of the LNEC 3D shaking table (LNEC 2010)	42
Table 2.5 – Characteristics of the actuators of the shaking table (LNEC 2010).....	42
Table 2.6 – Strength stress of the lime mortar and limestone specimens.....	52
Table 2.7 – Results of the axial compression tests	53
Table 2.8 – Results of the diagonal compression tests	54
Table 3.1 – Damping ratios of the non-strengthened mock-up	74
Table 3.2 – Damping ratios of the strengthened mock-up	79
Table 4.1 – Material properties of the first numerical model (not calibrated)	103
Table 4.2 – Material properties of the Model 3 after modal updating.....	110
Table 4.3 – Material properties of the masonry walls	121
Table 4.4 – Frequencies of the reduced and full numerical models	128
Table 5.1 – Linear material properties of the reference model	134
Table 5.2 – Non-linear material properties of the masonry walls of the reference model	134
Table 5.3 – Frequencies of the updated and reference full numerical models	135
Table 5.4 – Parameters considered in the non-linear dynamic sensitivity analysis	140
Table 5.5 – Parameters considered in pushover sensitivity analysis.....	151

Chapter 1

Introduction

1.1 Motivation for assessing of the seismic vulnerability of masonry structures

Natural disasters are an effect of natural hazards (tornados, volcanic eruptions, landslides, tsunamis or earthquakes) that caused millions of deaths (1975-2007) and severe socio-economic impacts, affecting the development of many countries. From this perspective, earthquakes are one of the most devastating natural hazards on Earth. According to Hough and Bilham (2006), earthquakes caused 6 million fatalities in 500 years (1500-2000). In the last decade, several earthquakes that caused 1,000 or more deaths occurred, namely (USGS 2012): the earthquake in Japan (2011) of magnitude 9 with 20,896 deaths; magnitude 7 earthquake in Haiti Region (2010) alone triggered disastrous destruction and 316,000 deaths; the earthquake in Southern Sumatra (Indonesia 2009) of magnitude 7.5 caused 1,117 deaths; in 2008 the earthquake in Eastern Sichuan (China) of magnitude 7.9 caused 87,587 deaths; the 2006 earthquake in Indonesia (magnitude 6.3) caused 5,749 deaths; in 2005 the earthquake in Pakistan of magnitude 7.6 and the earthquake in Northern Sumatra (Indonesia) of magnitude 8.6 caused 86,000 and 1,313 deaths, respectively; the 9.1 magnitude earthquake in Sumatra (2004) caused 227,898 deaths; in 2003 the earthquake of magnitude 6.6 in Iran and the earthquake of magnitude 6.8 in Algeria caused 31,000 and 2,266 deaths, respectively; the earthquake in the Hindu Kush Region (Afghanistan) of magnitude 6.1 caused 1,000 deaths. In Portugal, it is estimated that the 1755 earthquake and the subsequent tsunami

(about 30 minutes after the earthquake) that occurred in Lisbon destroyed about eighty-five per cent of the buildings and about 30,000 to 40,000 people were killed (the population of Lisbon at that time was about 200,000 people, meaning that 15% to 20% of the people were killed). However, earthquakes hardly kill people, being the collapse of the buildings the main reason of the deaths. This means that efforts should be conducted to reduce the seismic vulnerability of buildings.

The cities are areas with a concentration of elements of risk (people, buildings, bridge, infrastructures, etc.). Teheran (8.5 million), Jakarta (8.5 million) and Mexico City (18.1 million) are examples of large cities that suffered from earthquakes in the past.

Ancient masonry buildings are one of the most vulnerable elements of risk. These were built for many centuries according to the experience of the builder, taking into account simple rules of construction and without reference to any particular seismic code. Furthermore, in seismic areas, unreinforced masonry structures represent an important part of the building stock. Thus, in the recent decades the study of the vulnerability of ancient buildings is receiving much attention due to the increasing interest in the conservation of the built heritage and the awareness that life and property must be preserved. The seismic assessment of ancient masonry buildings is particularly difficult and depends on several factors. Besides the quality of masonry materials and the distribution of structural walls in plan, also the connection between the walls and floors influences significantly the seismic resistance (Tomažević et al. 1996).

1.2 Background of methods to assess the seismic vulnerability

Seismic vulnerability assessment can be applied to housing, cultural heritage buildings (monuments), essential facilities (hospitals, fireman's headquarters, police stations), infrastructure (roads, water, power grids) and any other type of buildings (e.g. schools or concert halls). Taking into account this diversity and the objectives pursued (seismic assessment of an individual building, or of a given building typology or even at regional level), different methods to assess the seismic vulnerability can be used.

Different classifications of methods to assess the seismic vulnerability have been proposed in the recent years. Corsanego and Gavarini (1993) divided the approaches developed in Italy in three main methods: (a) typological; (b) mechanistic; and (c) hybrid. The first method is based on the definition of building typologies, taking into account the construction technology (materials, geometry, type of horizontal diaphragms, connections between the elements, etc.), and the vulnerability is assessed through damage caused in real earthquakes and is expressed in probabilistic terms for each typology. Mechanistic methods assess the seismic vulnerability through theoretical mechanical models of the buildings. At a territorial (regional) level, simplified analytical models of the structure schemes can be used. In the hybrid methods,

quantitative (e.g. numerical analyses) and qualitative (e.g. experts' opinions) information on the building are combined to assess the seismic vulnerability.

Besides these three main groups, Corsanego and Gavarini (1993) proposed other types of classification of assessment methods for seismic vulnerability taking into account the kind of measure used to define the seismic vulnerability (quantitative and qualitative methods), the sort of results that emerge (direct, indirect and conventional methods) and prevalent source of knowledge (statistical, analytical and subjective methods).

Palacios (2004) presented a research about the methods of seismic vulnerability assessment, in which two main methods were highlighted: probabilistic methods (observed vulnerability) and deterministic methods (predicted vulnerability). The probabilistic methods are mainly used to study a group of buildings and are based on statistical data of past earthquake damage. However, depending on the source of statistical data, four sub-groups can be defined:

- Empirical methods, which are based on observed earthquake damage data.
- Judgment methods, which are based on experts' opinions.
- Analytical methods, which are based on analytically simulated damage data.
- Hybrid methods, which are based on combinations of different sources.

On the other hand, deterministic methods are mainly used to assess the seismic vulnerability of single structural units and they refer to the performance point of existing structures, before and after strengthening, and to the design of new structures.

Considering how and on the basis of what knowledge the methods have been derived, Giovinazzi (2005) classified the seismic vulnerability methods in three main groups: (a) observed vulnerability methods (empirical or statistical), which are based on the statistical observation of damage data of past events as a function of the felt intensity; (b) analytical methods, based on the mechanical calculation of the building behaviour and (c) method based on the expert judgment. Giovinazzi (2005) refers also the possibility of hybrid methods, taking into account the recent experiences.

More recently, Sousa (2006) presented the methodologies for seismic vulnerability assessment in a chart (Figure 1.1), being the methods divided in two main groups: (a) mechanistic and (b) statistical/empirical. The first group (mechanistic methods) includes the analytical methods to assess the seismic vulnerability at individual level, using procedures similar to those used in structural analysis, and at regional level, through simplified mechanistic models, as the capacity spectrum method (ATC-40 1996). The second group (statistical/empirical methods) refers to methods based on the damage statistical data observed in real earthquakes and/or expert opinion. These methods are usually used to assess the seismic vulnerability of large samples of buildings. Sousa (2006) divided this group in three classes: (a) methods based on the data collection of damage caused by earthquakes, in which the vulnerability is assessed by building typologies (Braga et al. 1982), (b) indirect and rating methods, in which the capacity of the buildings to resist seismic action is evaluated first, and its correlation

with damage is done afterwards (Barbat and Pujades 2004), (c) hybrid methods, in which the characteristics of the two different methods are combined (Giovinazzi and Lagomarsino 2003).

This short review on methods to assess the seismic vulnerability leads to the conclusion that its classification criteria is not consensual. Although the authors refer, in general, the same procedures for seismic assessment, they use different criteria for the organization of the methods.

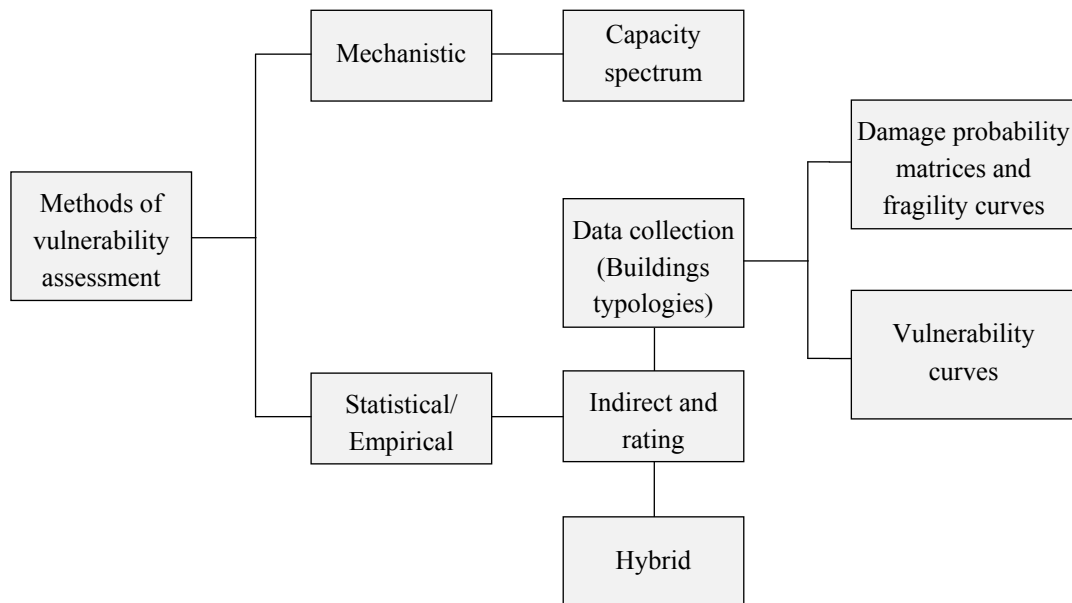


Figure 1.1 – Methodologies of seismic vulnerability assessment (adapted from Sousa 2006).

1.3 Seismic behaviour of ancient masonry structures

The seismic behaviour of ancient masonry buildings is particularly difficult to characterize and depends on several factors, namely the material properties, the geometry of the structure, the foundations, the connections between walls and floors, the connections between walls and roof, the stiffness of the horizontal diaphragms and the building condition. Furthermore, the strength of “non-structural” elements (partition walls) and their connection to the load-bearing walls also contribute for the performance of ancient masonry buildings.

Masonry is a composite material that consists of units and mortar, which has been used for construction of housing and some of the most important monuments around the world. Units are such as bricks, blocks, ashlar, irregular stones and others. Mortar can be clay, bitumen, chalk, lime/cement based mortar, glue or other. The huge number of possible combinations generated by the geometry, nature and arrangement of units as

well as the characteristics of the joints raises doubts about the accuracy of the term *masonry*. Figure 1.2 presents examples of masonry walls with different bond and number of leaves.

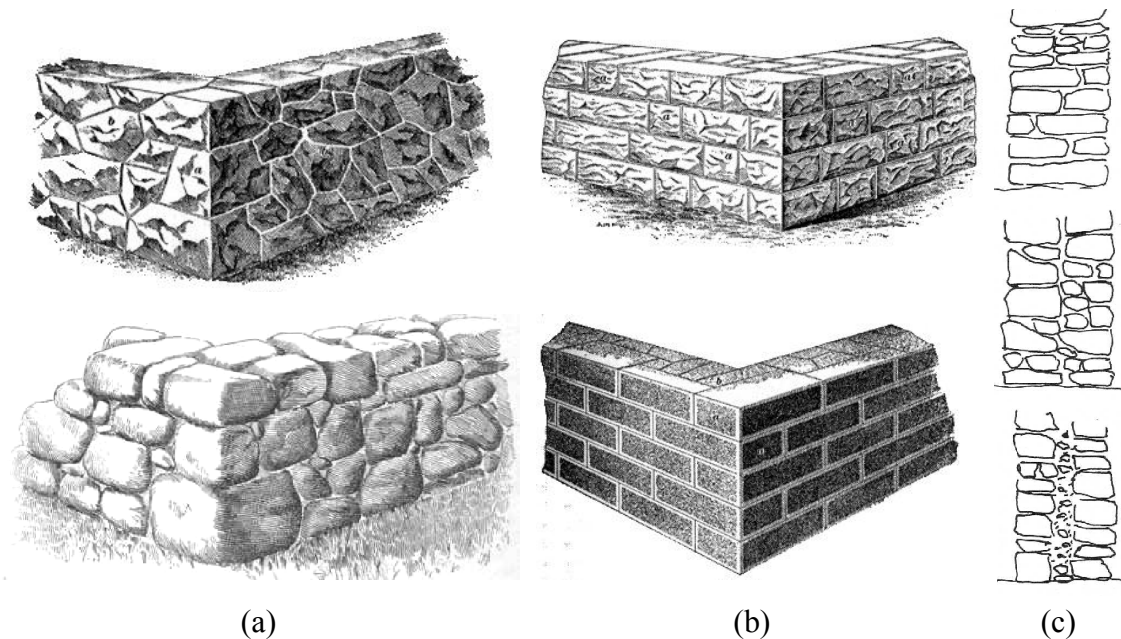


Figure 1.2 – Examples of masonry: (a) rubble walls (b) ashlar walls (International Correspondence Schools 2008); (c) single, double and three leaf walls (Mascarenhas 2003).

The strength of masonry depends on the unit and mortar properties as well as on the construction technique. The compressive strength of the units may range from 5 MPa (limestone units of low quality) to over 130 MPa (limestone units of good quality). The strength of the mortar also presents high deviations and depends on the proportion of its components (cement, lime, sand and water) used in the mix (Paulay and Priestley 1992). The compressive strength of the mortar of ancient masonry buildings ranges from 1.5 MPa to 3.5 MPa (Toumbakari 2002, Valluzi et al. 2004). Furthermore, the strength and failure modes of the masonry are also dependent on the loading direction and combination of the loads (Lourenço 1996). Nevertheless, the mechanical behaviour of different types of masonry has some common features: high specific mass, low tensile strength, low to moderate shear strength and low ductility (quasi-brittle behaviour). The specific mass of stone masonry ranges between 1700 kg/m^3 to 2200 kg/m^3 (Pinho 2000). Table 1.1 presents typical values of the mechanical properties of the stone and brick masonry.

The features of masonry allow it to be a material mainly for structural elements under compressive stresses caused by vertical static loads (e.g. walls, arches, vaults and columns subject to the self-weight). Masonry properties have direct influence on the seismic performance of unreinforced masonry buildings, therefore, this material has been considered unsuitable for the construction of buildings in seismic zones. The

inertial forces induce tensile and shear stresses which may lead to the failure of masonry elements and, consequently, to local or global collapse of the building. In Lourenço (1996), Paulay and Priestley (1992) and Tomažević (1999) more information is given about the mechanical behavior of the masonry.

Table 1.1 – Typical mechanical properties of the masonry (Tomažević 1999).

	Stone masonry	Brick masonry
Compressive strength [MPa]	0.3-0.9	1.5-10.0
Tensile strength [MPa]	0.08-0.21	0.10-0.70
Young's modulus [MPa]	200-1000	1500-3800
Shear modulus [MPa]	70-90	60-165

(characteristic values)

The in-plane and in-elevation regularity as well as simplicity (geometry, mass and stiffness distribution) are aspects that improve the seismic performance of masonry structures, preventing local damage and decreasing the torsional effects. These criteria as well as a set of material properties requirements, design and detailing rules are present in modern codes (EN 1998-1 2004, FEMA 440 2005, OPCM 3274 2003), which aim at a good seismic performance of masonry buildings in terms of strength capacity and adequate collapse mechanisms. However, ancient masonry buildings were not built according to any particular code and a great number of unreinforced masonry buildings subjected to earthquakes presented serious damage or even total collapse. Masonry buildings are composed by load-bearing walls, in which in-plane the dimensions are significantly larger than the thickness. Thus, the seismic performance of masonry buildings depends on the application direction of the horizontal load. Figure 1.3 presents the typical deformation and damage at the load-bearing walls of a simple unreinforced masonry building subjected to a seismic action in one direction. In the plane of the walls diagonal and horizontal cracks are observed, due to shear and bending, respectively. The walls orthogonal to the direction of the seismic action present vertical cracks at the middle and the corners due the out-of-plane bending. Existing masonry buildings present several types of geometry and material properties, which may lead to different damage and collapse mechanisms. However, the types of damage generally occurring in unreinforced masonry buildings due to the seismic action are (Tomažević 1999):

- Cracks between walls and floors;
- Cracks at the corners and at wall intersections;
- Out-of-plane collapse of the perimetral walls;
- Cracks in spandrels beams and/or parapets;
- Diagonal cracks in structural walls;
- Partial disintegration or collapse of structural walls;
- Partial or complete collapse of the buildings.

For more information about the damage occurring in unreinforced masonry buildings see e.g. D'Ayala and Speranza (2002) and Carocci (2001).

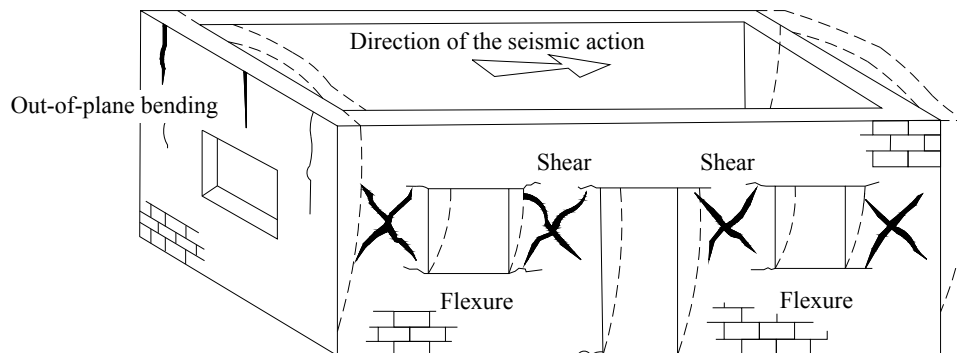


Figure 1.3 – Typical deformation and damage of unreinforced masonry buildings (adapted from Tomažević 1999).

As previously referred, the seismic performance of unreinforced masonry buildings depends on several aspects. As the experimental and numerical models developed in this thesis aim at evaluating the seismic performance of masonry buildings with load-bearing walls and timber floors, only the seismic behaviour of the masonry walls and of the floors are discussed next.

The in-plane behaviour of masonry walls depends on the geometry of piers, spandrels and openings, and three configurations of walls can be distinguished. Cantilever walls (Figure 1.4a) connected by floors, which even if rigid in their plane are flexible in the orthogonal direction and do not transfer the moments resulting from the bending of the walls. This configuration is assumed as the best masonry structural model for a ductile response, as the walls act as props and the maximum moments and energy dissipation occurs at the base of the walls. The coupled walls with pier hinging (Figure 1.4b) present piers weaker than the spandrels and, consequently, the damage tend to initiate at the piers. The piers, in general, at the lowest storey will either fail due to the diagonal compression (shear failure) or by the crushing of masonry, requiring high ductility at this floor level. However, the shear failure of the piers is not favourable to the ductility and energy dissipation of the structure. The coupled walls with spandrel hinging (Figure 1.4c) occur when spandrels are weaker than the piers. Here, spandrels behave as coupling beams, connecting the walls and transferring bending moments. Damage occurs at both elements and energy dissipation is distributed over the entire structure. The behaviour of coupled walls with spandrel hinging is the most desirable wall configuration (Paulay and Priestley 1992, Tomažević 1999).

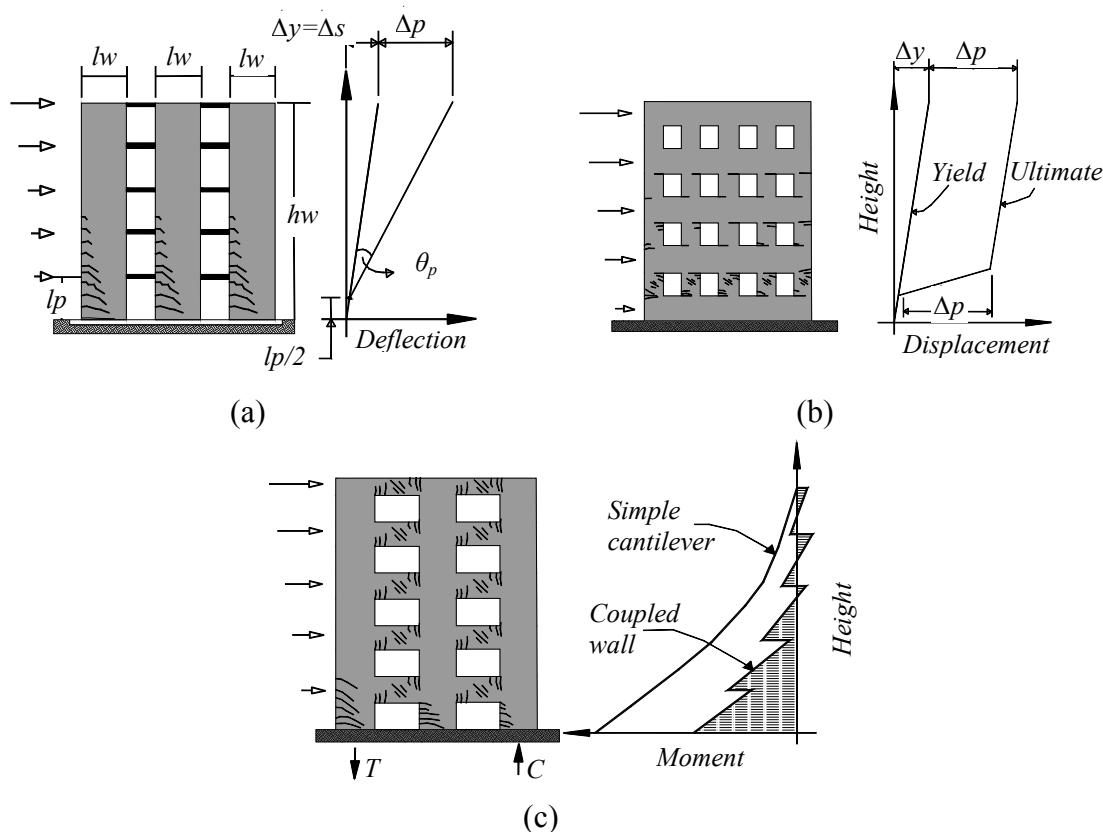


Figure 1.4 – In-plane structural models of masonry walls: (a) cantilever walls connected by flexible floors; (b) coupled walls with pier hinging; (c) coupled walls with spandrel hinging (adapted from Paulay and Priestley 1992).

In what concerns the seismic behaviour of piers, the typical in-plane collapse mechanisms (Figure 1.5) are (Magenes and Calvi 1997, Yi 2004):

- Rocking: the high bending causes horizontal cracks at the top and at the bottom of the pier. The failure of the pier occurs by overturning of the wall;
- Sliding: when the horizontal forces at the piers are larger than the shear strength of the bed joints (low vertical load and low friction coefficient), where horizontal cracks develop and the pier presents sliding movement along the bed joints;
- Diagonal tension: the principal tensile stress caused by the seismic action exceeds the tensile strength of masonry and the pier presents diagonal cracks. The cracks can propagate along the mortar bed joints and head joints or go through the units, depending on the strength of the mortar, mortar-unit interface and unit;
- Toe crushing: the toes of the piers are usually zones of high compressive stresses and when the principal compressive stress caused by the seismic action exceeds the compressive strength of the masonry a compressive failure (crushing) can occur.

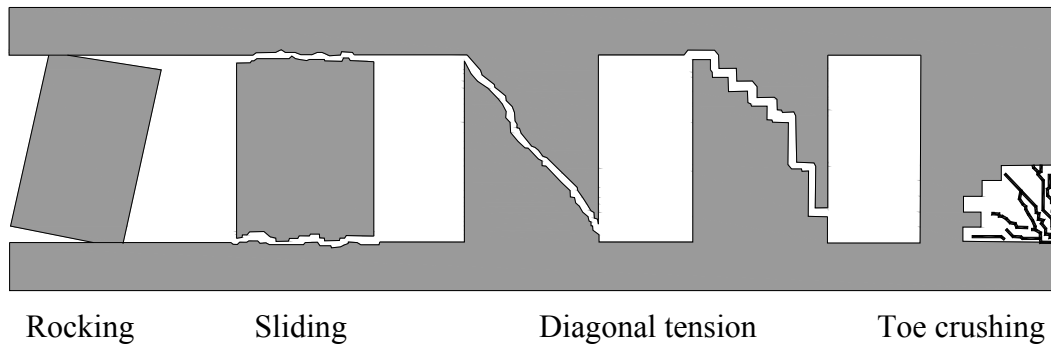


Figure 1.5 – In-plane collapse mechanisms of the piers (adapted from Yi 2004).

The behaviour of spandrels is similar to the behaviour of piers. However, two aspects have to be taken into account: (a) the axis of the spandrel is horizontal and not vertical as in the piers; (b) the normal stress existing in the spandrels, caused by vertical loads, is significantly lower than the one in the piers. The first aspect is important for regular masonry, due to orthotropic behaviour, while irregular masonry presents, in general, isotropic behaviour, independent from the load direction. The second aspect has consequences in both types of masonry, as the normal stress influences the seismic behaviour of spandrels. Figure 1.6a presents the in-plane behaviour of the spandrels subjected to a seismic action, in which shear stresses initially occur and can lead to them to collapse (Figure 1.6b). In masonry buildings with reinforced elements that prevent such collapse mechanisms (Figure 1.6c), diagonal compression occurs and this increases the bending strength of the spandrel. In these conditions, the spandrels present two possible collapse mechanisms (Magenes et al. 2000):

- Collapse due to high compression of diagonal strut (similar to the collapse for combined axial and bending forces of a pier);
- Collapse due to diagonal tension (shear failure).

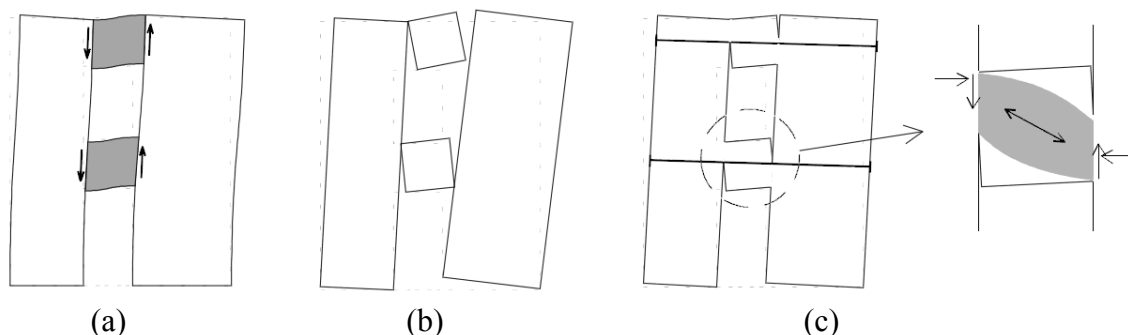


Figure 1.6 – In-plane behaviour of the spandrels (Magenes et al. 2000).

FEMA 306 (1998) also presents the typical damage and collapse mechanisms of the in-plane behavior of unreinforced masonry walls subjected to a seismic action (Figure 1.7). The walls without openings (URM1) can present rocking, toe crushing, sliding and diagonal tension. Furthermore, these walls can also present sliding at the

wall/foundation interface and foundation rocking. The collapse mechanisms of the walls with openings, i.e. at the spandrels (URM3) or at the piers (URM2 and URM4), is defined by their geometry. Finally, the unusual collapse of the “joints”, caused by diagonal tension, is also possible (URM5).

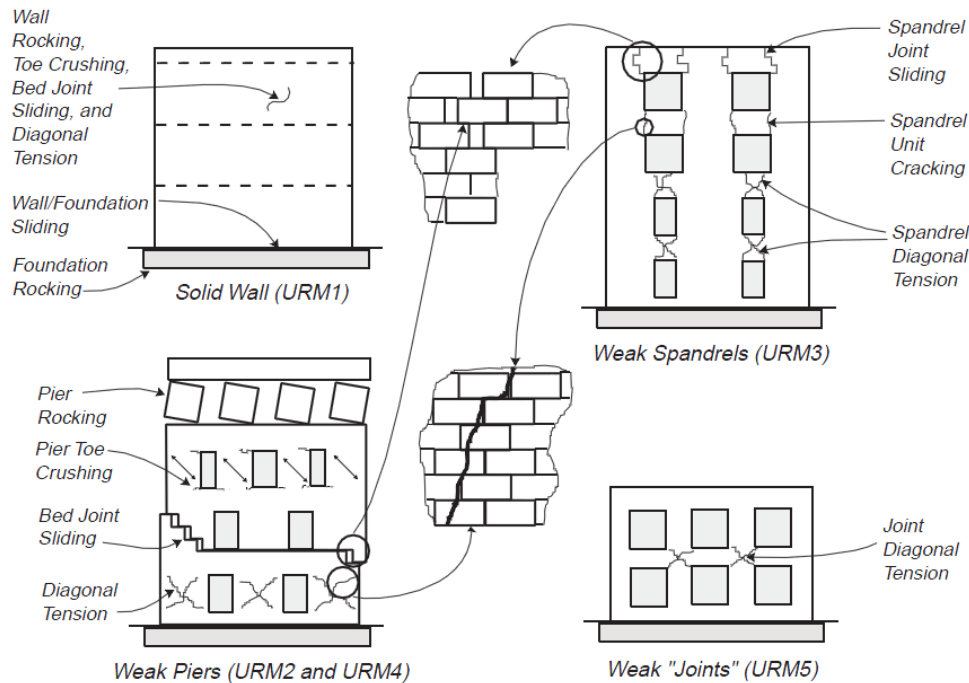


Figure 1.7 – In-plane behaviour of masonry walls (FEMA 306 1998).

The out-of-plane behavior of unreinforced walls is complex and depends on the connection between walls and floors, the connection between walls and roof, and the in-plane stiffness of the floors. When the floors are rigid and have sufficient strength, masonry walls have local effects as shown in Figure 1.8. On the other hand, when the floors are flexible or the connection between the walls and the floors is weak, the walls present a global behavior (independent of the floor levels) with collapses involving one or more floors and, consequently, present lower stiffness and strength (Candeias 2008).

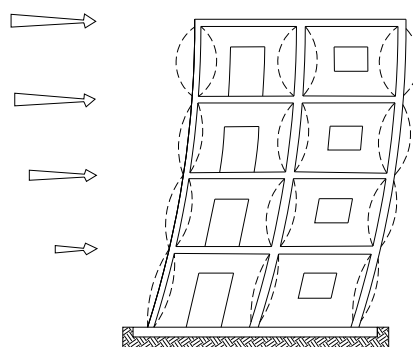


Figure 1.8 – Out-of-plane behaviour of the walls of masonry buildings with rigid floors (adapted from Tomažević 1999).

Figure 1.9 presents examples of the in-plane damage, namely the shear failure of piers and spandrels, in which diagonal cracks are observed. Figure 1.10 presents examples of out-of-plane collapse of masonry walls, with the collapse of masonry walls versus successful strengthening with ties (Figure 1.10b).



Figure 1.9 – Example of shear failure of: (a) piers (Penna 2008); (b) spandrels (Dazio and Beyer 2010).

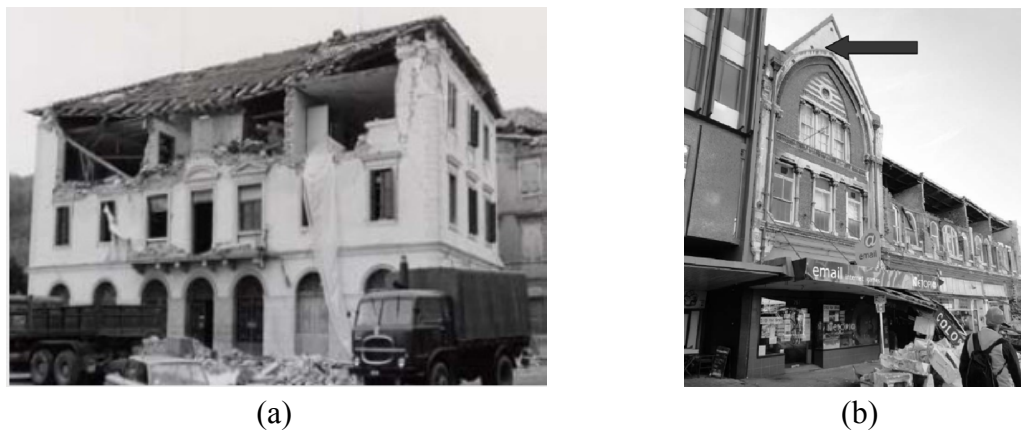


Figure 1.10 – Example of out-of-plane collapse mechanisms: (a) wall of the top floor (Lagomarsino 2012); (b) parapet and wall collapse and successful strengthening with ties (arrow) (Ingham et al. 2011).

Diaphragms distribute the inertial forces to the building's vertical resisting elements. The distribution capacity of lateral loads through the diaphragms is dependent on the in-plane stiffness of the diaphragms and on the connection between walls and diaphragms. In contrast to a rigid diaphragm, in which the in-plane stiffness is so large that the distribution among the vertical elements is affected only by the location and lateral stiffness of these structural elements, a flexible diaphragm (timber floors) usually exhibits significant bending and shear deformations under horizontal loads, influencing the distribution of the load among the elements of the structure.

Research conducted on flexible diaphragms, e.g. Brignola et al. (2008), Bruneau (1994) [1], Bruneau (1994) [2], Paquette and Bruneau (2006), Tomažević et al. (1996) and Yi (2004), showed that flexible diaphragms lead to the following behaviour:

- The overall stiffness of the floors (Figure 1.11), which controls the out-of-plane behaviour of the masonry walls, is a combination of the in-plane stiffness of the diaphragm ($k_{eq,d}$) and the stiffness of the connections between floors and walls (k_c). Thus, the total deformation of the floors is given by the sum of the deformations of the diaphragm and connections. When the connections are rigid ($k_c = \infty$) the overall deformation is only a function of the internal stiffness of the diaphragm. On the other hand, when the diaphragms are rigid ($k_{eq,d} = \infty$), the stiffness of the connections is taken into account. The equivalent stiffness of the floors ($k_{eq,d+c}$), which should be used in the assessment, design and strengthening analyses, is given by the combination of both contributions ($1/k_{eq,d+c} = 1/k_{eq,d} + 1/k_c$) (Brignola et al. 2008);
- The flexible diaphragms have large deformation capacity, high strength and low mass. The earthquakes show that the failure of flexible diaphragms itself is rare. In general, the failure mechanisms of flexible diaphragms are related to the lack of connections or weak connections between the masonry walls and diaphragms. Furthermore, the masonry walls vibrate in the out-of-plane direction under seismic load and tend to separate from the diaphragms, meaning that the diaphragm may slip off its supports and collapse if the diaphragm is not suitably connected to the walls (Bruneau 1994 [2]);
- Strong diaphragms present amplifications of up 3 or 4 times the input acceleration, velocities and displacements in the elastic range (Bruneau 1994 [1] citing Ewing et al. 1981 and SEAOC 1986). On the other hand, flexible diaphragms have a highly non-linear hysteretic behaviour for large peak ground accelerations, which is favourable to reduce the diaphragm's accelerations and velocities at mid-span (Bruneau 1994 [1]);
- Strengthening of the horizontal diaphragms is a natural solution for a better performance, even if an increase of the in-plane stiffness *per se* is not enough to improve the global response of the building. The seismic performance of the unreinforced masonry buildings also depends of the stiffness and strength of the connections between floors and walls Yi (2004).

The importance of the flexibility of the floor diaphragms and of the connections between these and the masonry walls plays an important role in the global and local response of masonry buildings under seismic load.

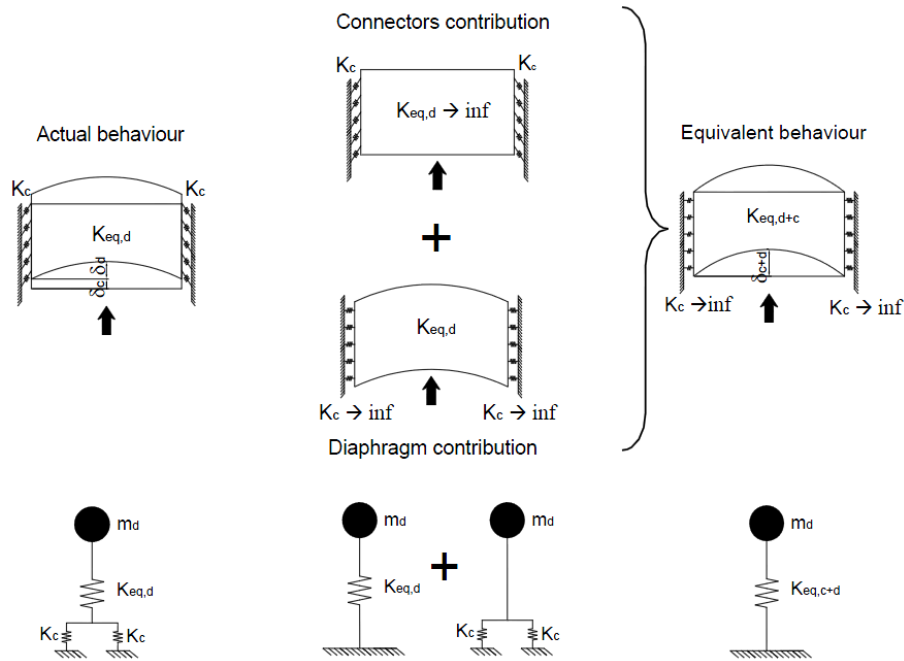


Figure 1.11 –Schematic contributions of connections and diaphragm stiffness to the overall floor stiffness (Brignola et al. 2008).

1.4 Focus of the thesis

The Portuguese housing stock consists of several building typologies (Table 1.2 and Figure 1.12), in which some of them present construction features associated with poor seismic performance, mainly the masonry buildings. Thus, it is necessary to intervene in these types of buildings with the purpose of reducing their seismic vulnerability. This thesis aims at evaluating the seismic vulnerability of a masonry building typology – the “gaioleiro” buildings (see Section 1.5) and proposing a strengthening technique to reduce it. The study involved an experimental program and several types of numerical analysis.

In the experimental program, an unusual method to assess the seismic vulnerability of “gaioleiro” buildings and to obtain the seismic vulnerability curves, as it involves shaking table tests, was used. This method is representative of the main features of the building typology, which can be assumed as typological, and the seismic vulnerability is assessed through an experimental test. The proposed procedure involves four main phases:

- 1- Definition of the prototype representative of the building typology;
- 2- Preparation of the mock-up, usually, in reduced scale;
- 3- Application of the seismic action through shaking table tests. The action is applied with gradually increase of seismic intensity. This involves carrying out several successive seismic tests with different amplitudes;

4- Characterization of the dynamic properties (natural frequencies) of the mock-up during the seismic testing.

The general objective of these experimental vulnerability curves is to relate a parameter of the response of the structure (e.g. damage indicator) with the seismic amplitude applied at the base. The main advantages of this experimental method is to evaluate the seismic performance of structures relating quantitative parameters (maximum displacement, acceleration, drifts, damage indicator, etc) with the collapse mechanism and crack patterns observed (qualitative parameters) and the possibility to compare directly the efficiency of strengthening techniques (strengthened and non-strengthened mock-ups). This gives strong reliability to the interpretation and conclusions about the seismic behaviour of the structures. However, the method presents also disadvantages. The experimental tests are expensive and the method does not take into account the deviations in the characteristics of the building typology. Thus, this experimental method should be complemented with a numerical study. Later in this work, a detailed description of the experimental method used to assess the seismic vulnerability is presented.

Table 1.2 – Building typologies and corresponding construction periods (Oliveira and Cabrita 1985).

Building typology	Construction period
Stone masonry buildings	Up to 1755
“Pombalino” and similar buildings	From 1755 to 1870
“Gaioleiro” buildings	From 1870 to 1930
Masonry buildings with reinforced concrete slabs	From 1930 to 1940
Mixed buildings of reinforced concrete and brick masonry	From 1940 to 1960
Reinforced concrete buildings	After 1960

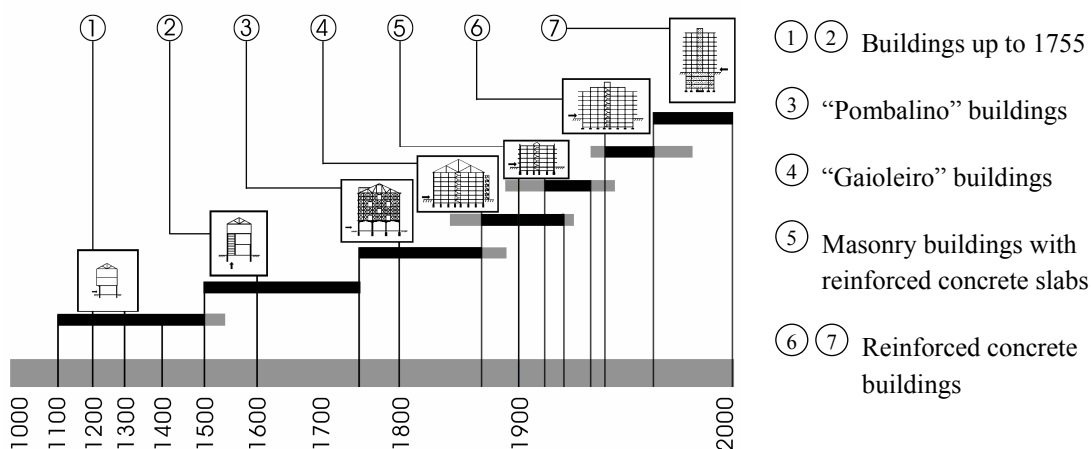


Figure 1.12 – Evolution of the current construction processes of the Lisbon building stock (Silva 2011).

With respect to the numerical study, the calibration of the numerical model is the first task and is based on the results of the shaking table tests. Once the experimental tests on buildings are made with a reduced scale mock-up, the study of the size effect becomes relevant. Non-linear dynamic analysis with time integration and several types of pushover analyses are done, aiming at evaluating different techniques of structural analysis. Finally, a sensitivity study taking into account the deviation in the characteristics of the “gaioleiro” buildings is also carried out.

1.5 “Gaioleiro” buildings

The “gaioleiro” buildings (Figure 1.13) constitute a Portuguese building typology that was built between the end of 19th century and beginning of the 20th century. These buildings characterize a transition period from the anti-seismic practices used in the “pombalino” buildings originated after the earthquake of 1755, see e.g. Ramos and Lourenço (2004), and the modern reinforced concrete frame buildings. The “gaioleiro” buildings are, usually, four to six stories high, with masonry walls and timber floors and roof. The external walls are, usually, in rubble masonry with lime mortar (Pinho 2000).

“Gaioleiro” can be related to a derogatory definition regarding the quality of the construction from the buildings of this typology in comparison to the “gaiola” (cage) of the “Pombalino” buildings, used in the reconstruction of Lisbon after earthquake of 1775. This definition can also be associated to the mass exodus for the cities, which occurred at that time, and to the need of lodging all these people in housing buildings. This need has, as consequence, led to a lack of quality control in the construction techniques (low cost buildings) and to the idea that people were put in “gaiolas” (cages). Finally, Appleton (2005) mentions that the definition of “gaioleiro” was initially assigned to workers who built this type of buildings and then came to designate what they built. This means that the definition of the term “gaioleiro” building is not clear and its origin is not known.

The above description of “gaioleiro” buildings is general (as building typology), but not enough to know, in detail, the characteristics of its elements that are associated to the seismic performance. Furthermore, a concept of building typology is used to group buildings with common characteristics and to distinguish them from the others. However, this concept is not objective and depends on the criteria used to define the typologies. Thus, to assess the seismic performance of the “gaioleiro” buildings it is necessary to know in detail their common characteristics, as well the dispersion that exists in this typology.



Figure 1.13 – Examples of “gaioleiro” buildings, Lisbon, Portugal.

First of all, the facades of the “gaioleiros” buildings present common elements, which can help us to identify this type of buildings. In the facades, as shown in Figure 1.14, the following elements can be observed (Appleton 2005):

- Entrance door (A): it can be in timber or steel, and painted with enamel.
- Windows (B): they are in softwood and painted with enamel.
- Balcony guard (C): they are in steel and, also, painted with enamel. Besides its functional characteristic, they are a decorative element of the facades.
- Lintel (D): generally, the “Lioz” stone (a type of limestone of Portugal) is used.
- Tiles (E): this type of buildings can also present a strip of tiles.



Figure 1.14 – Facade of a “gaioleiro” buildings (Appleton 2005).

“Gaioleiro” buildings are usually semi-detached and belong to a block of buildings (Figure 1.15a). Pounding can be taken in account when the adjacent buildings present different heights or the separation distance is not large enough to accommodate the displacements (Gulkan et al. 2002 and Viviane 2007). It is noted the “block” effect is usually beneficial and provides higher strength to the building, as shown in (Ramos and Lourenço 2004). In plan, the apartments of this type of buildings are distinguished by its narrow shape (Figure 1.15b), leading to the construction of large shafts for light and ventilation of the interior divisions. The stairs are located, approximately, at the central position of the plan, resulting in some structural symmetry. According to the study carried out by Appleton (2005) on a block in Lisbon with 20 “gaioleiro” buildings, the implantation area ranges from 127.8 m² and 529.0 m², with widths ranging between 6.5 m and 15.2 m, and depths between 16.5 m and 28.0 m.

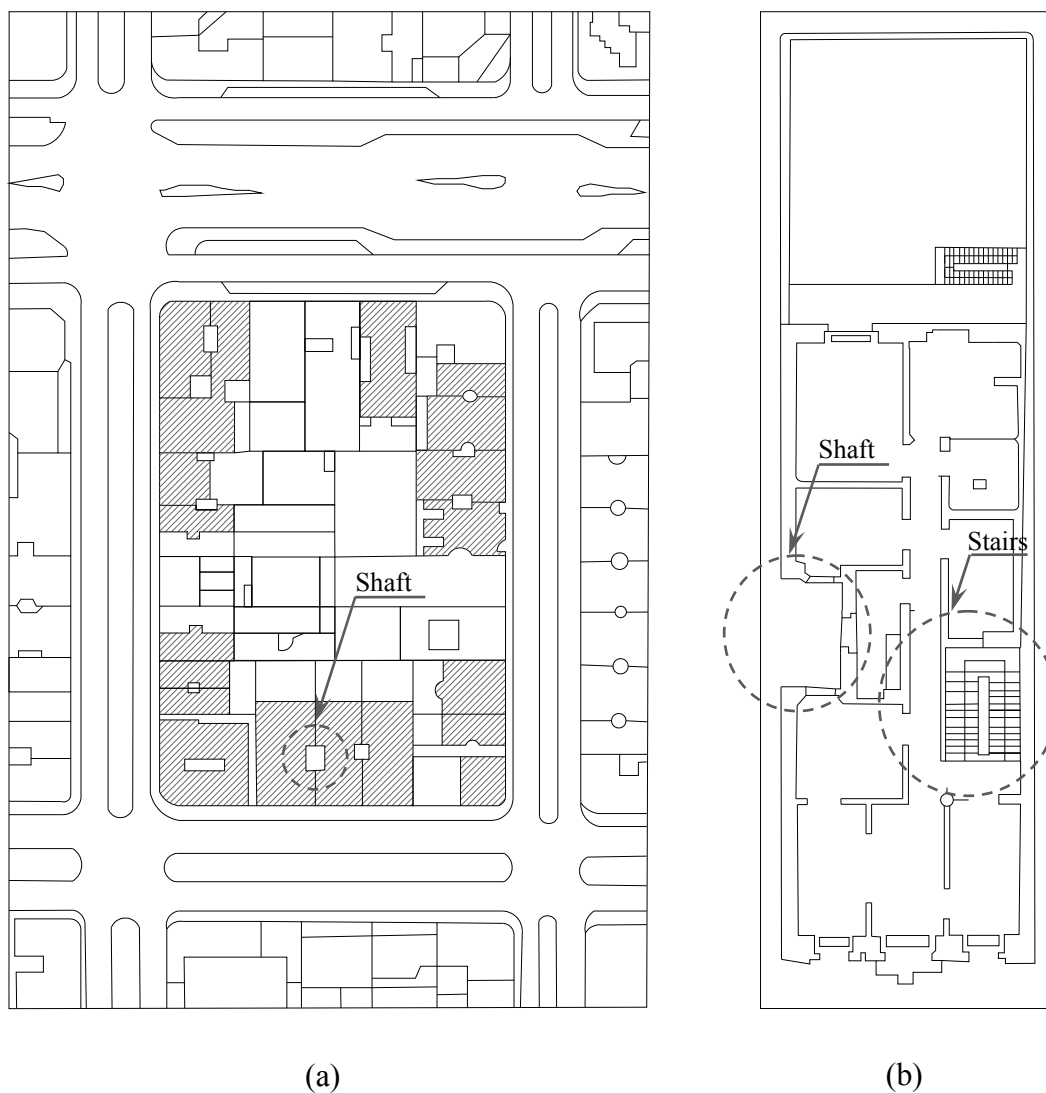


Figure 1.15 – Urban layout and apartment plan of “gaioleiro” buildings: (a) block of buildings; (b) geometry of the typical apartment.

The “gaioleiro” buildings are characterized by lack of structural continuity, in which connections between the orthogonal load-bearing walls, the load-bearing walls and the partition walls, and the load-bearing walls and the floors are not, in general, adequate (Cabrita et al. 1993 and Pinho 2000). The load-bearing walls present, in general, a reduction of thickness in elevation of the building. Figure 1.16a shows the typical cross section of the load-bearing walls. However, for a “gaioleiro” building undergoing rehabilitation works in Lisbon, constant thickness in elevation was observed (Figure 1.16b). The partition walls are, usually, in lath timberwork and lime mortar. According Pinho (2000) the walls of the “gaioleiro” buildings can be divided in three types:

- Masonry load-bearing walls: built with rubble masonry and lime mortar (Figure 1.17a). The stone ranging from strong to relatively weak limestone. These walls have a thickness ranging from 0.90 m at the ground-floor and 0.50 m at the top floor, and they are located, for example, in the front and back facades of the buildings.
- Load-bearing walls with solid bricks (Figure 1.17b): the thickness ranges between 0.15 m and 0.30m. They can be located in the gable walls and, sometimes, internally in the buildings.
- Partition walls in lath timber and lime mortar: the thickness is, on average, equal to 0.15 m. In these walls, the load-bearing capacity is low as they are light partition walls.

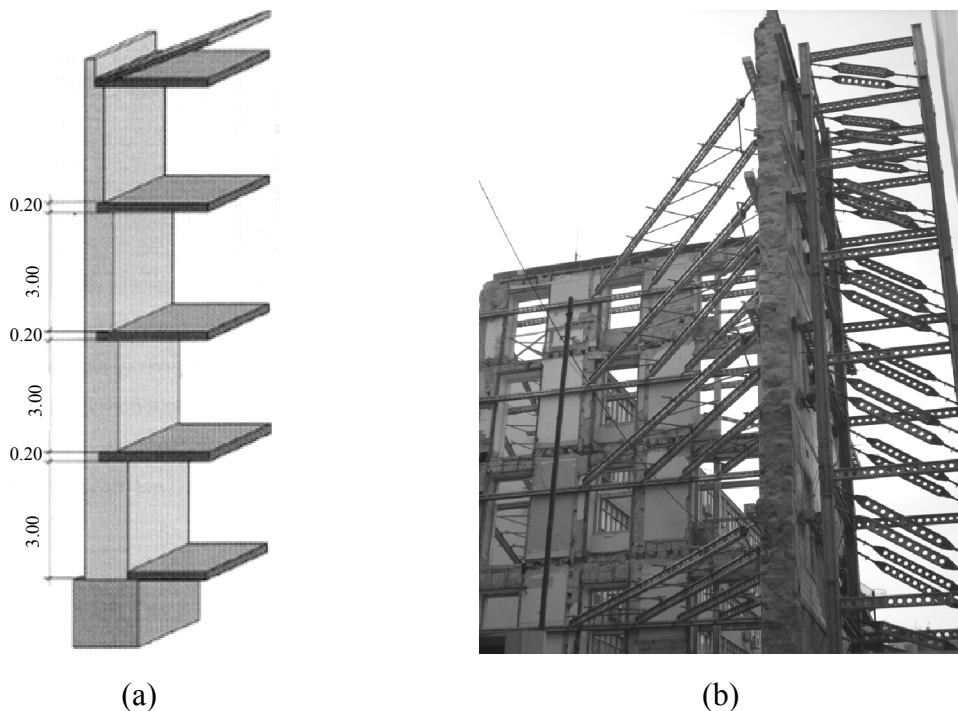


Figure 1.16 – Thickness of the load-bearing walls of the “gaioleiro” buildings:
(a) typical reduction of thickness in elevation (adapted from Appleton 2003);
(b) example of a building in Lisbon with constant thickness. (Dimensions in meters).

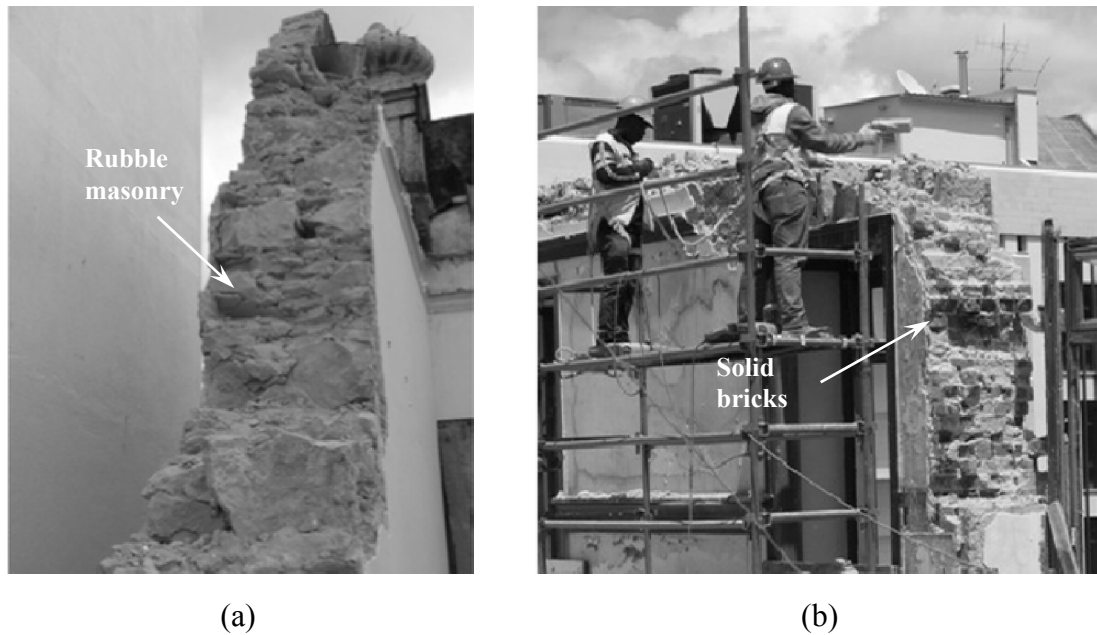


Figure 1.17 – Walls of the “gaioleiro” buildings: (a) load-bearing wall with rubble masonry; (b) load-bearing wall with solids bricks (adapted from Andrade 2011).

Regarding the mechanical properties of the load-bearing masonry walls, the information available in the literature is scarce. Silva and Soares (1997) carried out tests on load-bearing walls of “gaioleiro” buildings, in which values from 0.8 MPa to 1.5 MPa for compressive strength and values from 700 MPa to 1000 MPa for Young’s modulus (about 1000 times the compressive strength) were obtained.

In Lisbon, most of the “gaioleiro” buildings are set on soft soils, with low to medium strength and compactness. Only few buildings are set on rock (Silva and Soares 1997). The foundations of this type of buildings are composed by ditches filled with hard stone masonry and lime mortar. The geometry of the foundations is varies and depends, essentially, on the building height, on the type of wall and on the type and depth on the foundation soil. However, there are “gaioleiro” buildings with different heights and similar foundation widths, which is, approximately, equal to the double of the walls thickness (Appleton 2005).

The floors are, essentially, of two types: (a) with timber frame and; (b) with steel frame. The floors with steel frame belong to a later period from the floors with timber frame and are less common, appearing in balconies, kitchens and bathrooms. The floors with timber frame are more common and are composed by several elements: (a) timber joists oriented in the direction of the shortest span; (b) floorboards; (c) ring joists. The most simple connection between floors and masonry walls correspond to the insertion of the timber joist into a pocket of the wall with only a few centimetres of support (Figure 1.18a). The width and height of the timber joist ranges, on average, from 0.07 m to 0.08 m and from 0.16 m to 0.22 m, respectively. The spacing among timber joist ranges from 0.20 m to 0.40 m. Covering floorboards with about 0.02 m of thickness is placed over

the joists. The connection between floors and masonry walls could be improved through the incorporation of steel anchors, nailed to the timber joists and embedded into the walls (Figure 1.18b). In buildings with rim joists (Figure 1.18c), the connection was done through this element, which was anchored to the masonry wall (Andrade 2011, Appleton 2003 and Candeias 2008).

The “gaioleiro” buildings’ roofs are, usually, in timber frames with one or two slopes in simple buildings, or with several slopes in more complex buildings. Some of these buildings also present a mansard roof, which is more sloped and complex than frames with two slopes. The mansard roof allows the increment of usable building area (Andrade 2011). The roof is covered by ceramic tiles (Figure 1.19).

During the 19th century, sunrooms (Figure 1.20a) began to appear in the back facade of the “gaioleiro” buildings, where a very small compartment to place a toilet was also installed. These sunrooms were also used as junk rooms (Pinho 2000). Later, external steel stairs were also added (Figure 1.20b), aggregated to the sunrooms, by imposition of the fireman. The lift (Figure 1.20c), which was a luxury equipment in the 20th century, is not very common in the “gaioleiro” buildings and appears only in buildings of noble families.

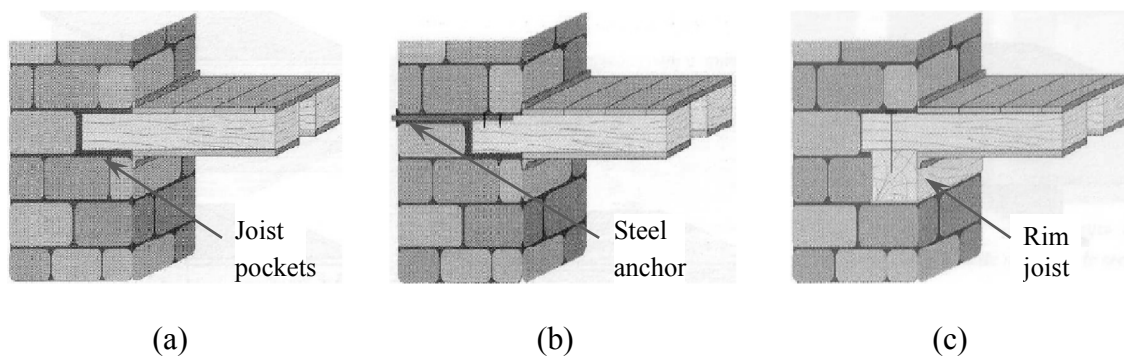


Figure 1.18 – Connection of floors to masonry load-bearing walls: (a) insertion of timber joist at the pocket of the wall; (b) improving of the connection through steel anchors; (c) connection with rim joist (adapted from Appleton 2003).

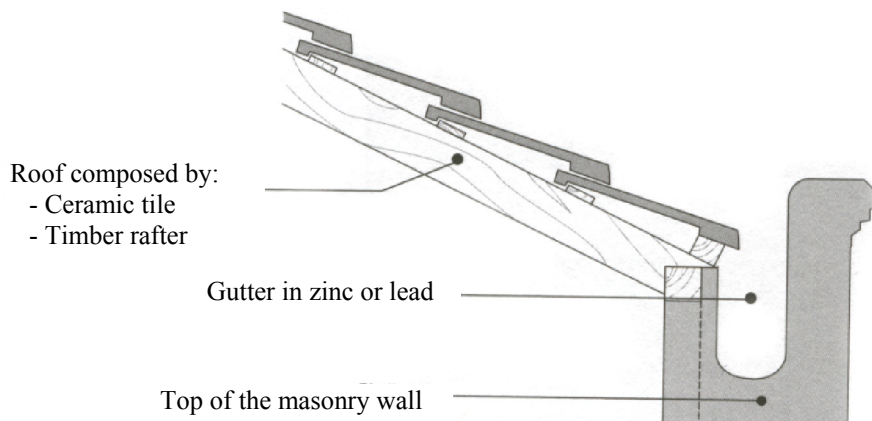


Figure 1.19 – Cross section of the “gaioleiro” building’s roof (adapted from Appleton 2005).

As mentioned before, the “gaioleiro” building typology ends with the emergence of reinforced concrete, which was initially used in the floors, originating masonry buildings with reinforced concrete slabs, but eventually replaced masonry as the structural material. This type of buildings is still in use nowadays and in significant number. According to the Census (1991) (cited by Silva 2001), the total number of buildings in Lisbon up to the earthquake 1775, the “pombalino” and the “gaioleiro” buildings is about 28,000 buildings (almost 50% of the Lisbon housing stock).

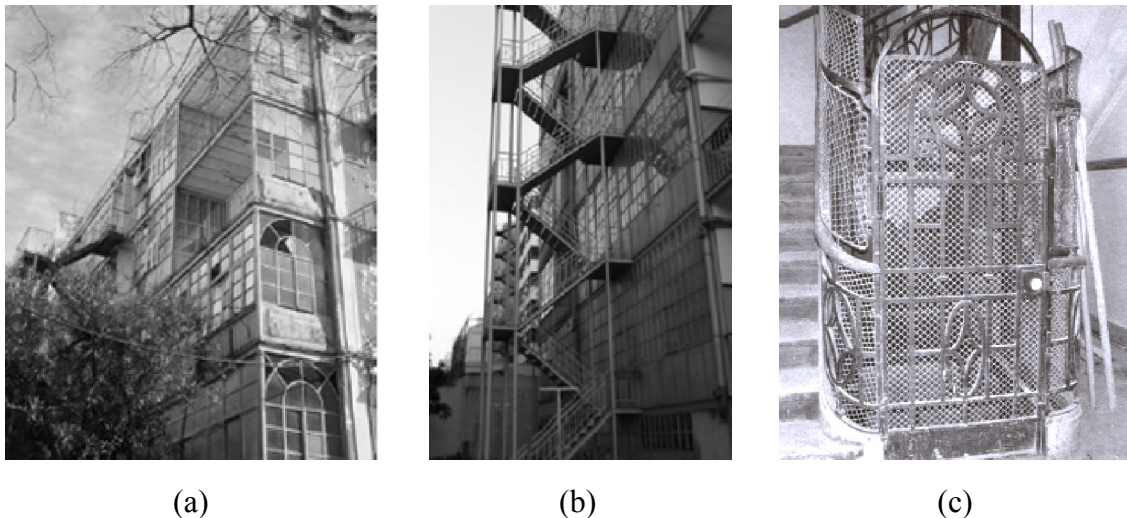


Figure 1.20 – Elements of the “gaioleiro” buildings: (a) sunrooms; (b) external stairs (Andrade 2011); (c) lift.

Some research on the assessment and improvement of the “gaioleiro” buildings has already been carried out. Candeias (2008) carried out experimental shaking table tests on the performance of “gaioleiro” buildings using two non-strengthened (Model 0 and 00) and three strengthened (Models 1 to 3) mock-ups. Model 1 aims at improving the connections between walls and floors by using steel connectors and composite strips. In Model 2 the mock-up was strengthened using ties at the two top floors. Model 3 was strengthened with ties and composite strips in the piers. The results of the tests showed that the models present different cracks patterns and global seismic behaviour in the transversal and longitudinal directions. Furthermore, the seismic performance of the strengthened mock-ups presented slight improvements with respect to the behaviour of the non-strengthened mock-ups, with a reduction of the out-of-plane displacements of the walls and an increase of the seismic coefficient and energy dissipation. Mendes and Lourenço (2009) present a numerical study on the seismic behaviour of these “gaioleiro” tests. This study included non-linear dynamic analysis with time integration and several types of pushover analysis. The results of the non-linear dynamic analysis showed that the damage concentrates at the facades (walls with openings) and at the base of the structure. The pushover analyses are not able to

simulate the out-of-plane response, simulating correctly only the in-plane damage. Branco and Guerreiro (2011) carried out a numerical study on seismic behaviour of a “gaioleiro” building, with two main objectives: (a) evaluation of different techniques of strengthening of the building floors, namely using concrete slabs, composite steel-concrete slabs, metal grids or steel ties; (b) seismic protection of the buildings using different solutions, namely insertion of concrete walls, the use of a base isolation technique and application of viscous dampers. In what concerns the first objective, the composite slab and the steel ties were the best solution to reduce the floor displacements and to improve the distribution of horizontal forces to the load-bearing walls. In terms of seismic protection of the building and considering the measured displacements, the strengthening technique with concrete walls presented the best response. However, the results of the solution with viscous dampers were very close to the ones obtained with concrete walls and are the best at the foundation level.

1.6 Outline of the thesis

In order to address the issue of seismic vulnerability of the “gaioleiro” buildings, this thesis is organized in six Chapters as follows:

- **Chapter 1** provides an introduction to the work, with the motivation for assessing the seismic vulnerability of masonry buildings, the background of the methods to assess the seismic vulnerability, an overview on seismic behaviour of ancient masonry buildings, the focus of the thesis, a description of “gaioleiro” buildings, as well as, the outline of the thesis.
- **Chapter 2** presents the preparation of the tests carried out for assessment of the seismic vulnerability of the “gaioleiro” buildings”, namely shaking table tests and dynamic identification tests of two mock-ups (non-strengthened and strengthened mock-ups), including the prototype definition, mock-up at reduced scale definition and construction, the test planning and the characterization of the materials.
- **Chapter 3** presents the results of the seismic tests and dynamic identification tests. The dynamic identification was used to evaluate the decrease of the frequencies of the modes of the mock-ups after each seismic test, which is associated to the decrease of the stiffness, and defined a damage indicator. The damage indicator was related to the seismic action applied at the base of the mock-ups - vulnerability curves; which were used to compare the efficient of the strengthening technique. The results of the seismic shaking

table tests allow to define several parameters of acceleration and displacement of the response of the mock-ups. These quantitative parameters and the crack patterns were used to evaluate the seismic behaviour of the mock-ups.

- **Chapter 4** presents the preparation and validation of the numerical model of the non-strengthened mock-up. The finite element model was prepared at reduced scale and based on a masonry macro-modelling strategy. A modal updating based on the frequencies and mode shapes estimated in the dynamic identification tests was carried out. The dynamic response of the numerical model under seismic action was validated through the comparison between the results obtained from the non-linear dynamic with time integration and the ones obtained from the shaking table tests of the non-strengthened mock-up. Finally, the full model of the non-strengthened mock-up was also prepared and a scale effect discussion is also presented.

- **Chapter 5** presents the sensitivity analysis taking into account the deviations on features of the “gaioleiro” buildings. The main objective of the sensitivity analysis is to compare the response of the structure as a function of the variations of its properties with respect to the response of a reference model. The sensitivity analysis was carried out for two types of structural analysis, namely for the non-linear dynamic analysis with time integration and for the pushover analysis proportional to the mass of the structure. The Young’s modulus of the masonry walls, Young’s modulus of the timber floors, the compressive and tensile non-linear properties (strength and fracture energy) were the properties considered in both type of analysis. Additionally, in the dynamic analysis, the influences of the viscous damping and of the vertical component of the earthquake were evaluated. Finally, a pushover analysis proportional to the modal displacement of the first mode in each direction was also carried out.

- **Chapter 6** presents the main conclusions from each chapter and a proposal for future works.

Shaking table tests setup

2.1 Introduction

The experimental methods used in seismic engineering remain irreplaceable. Besides the fact that they lead directly to conclusions on the performance of the seismic behaviour of structures, these methods are essential for the calibration of numerical models. Numerical modelling has been increasingly used to assess the performance of civil engineering structures in the last decades (Carvalho 1998). However, numerical models, which usually include several parameters, have to reproduce the real behaviour of structures. After calibration, numerical models can be used as a computational laboratory to study the sensitivity of the response to the input (material and geometric properties, types of connections, boundary conditions, etc.), which is impractical through an experimental programme. This means that the optimal approach for novel developments in seismic engineering combines experimental and numerical tools.

There are several types of experimental tests that can be realized in laboratory to evaluate the performance of structures, namely: (a) static monotonic tests; (b) quasi-static cyclic tests; (c) pseudo-dynamic tests; (d) shaking table tests.

Static monotonic tests are the simplest ones. Basically, they consist of an application of an increasing load in a given direction to the structure and of the measurement of the obtained response, in general, in terms of displacements and strains. Testing can be carried out with displacement control, aiming at obtaining the response of the structure

in the post-peak range. Although it is possible to carry out this type of testing on full structures, static monotonic tests have been mainly used to study structural elements (beams, columns, etc.). However, this type of testing is more representative of structures under static loads and less adequate to evaluate the seismic behaviour, since it is not able to adequately describe the dynamic and inelastic response of structures. For examples of static monotonic tests on ancient masonry elements see e.g. Binda et al. (2006) and Vasconcelos (2005).

Static cyclic tests do not require very complex equipment and can be carried out on full structures, general at reduced scale, or on structural elements of those structures. In these tests the load is applied slowly (quasi-static) by imposing forces or displacements. The cyclic tests are usually performed with increasing amplitude in both ways (positive and negative), aiming at reproducing the dynamic behaviour occurring, for example, in earthquakes. Ideally, any displacement imposed at the structure should be representative of the dynamic response but the interaction between the input excitation and the response (non-linear) of the structure cannot be considered. For examples of the static cyclic tests on masonry elements see e.g. Griffith et al. (2007) and Oliveira (2003).

Pseudo-dynamic tests consist of a combination of static tests by imposing displacements and an analytical method to define those displacements during the test. The analytic method is based on the description of the dynamic response of the structure idealized through a model with a finite number of degrees of freedom, in which the inertia forces, viscous damping forces and the seismic excitation are computed analytically, whereas the restoring forces are measured on the experimental model from each integration time. This type of tests is more complex than the previous ones and is more suitable for structures with concentrated masses, since each actuator applied to the structure is associated to a single degree of freedom. For examples of static pseudo-dynamic tests on large structures see e.g. Paquette and Bruneau (2006) and Pinto et al. (2002).

Shaking table tests are able to simulate most accurately the excitation of structures under seismic loading. Basically, the shaking table is a rigid platform, where mock-ups are fixed, moved by hydraulic actuators. The most complex shaking tables have six degree of freedom (three translational and three rotational), which require a complex control system. Even if the shaking tables can be rather large, usually the mock-ups are prepared at reduced scale given the size of full civil engineering structures. This type of tests can be assumed as the most adequate to study the seismic behaviour of structures in laboratory. However, the costs to build this type of facility and the cost of making the mock-ups are themselves high. Furthermore, the preparation of mock-ups at reduced scale, using laws of similitude, is difficult and only partly represents reality. For examples of shaking table tests on large structures see e.g. Lindt et al. (2011) and Moaveni et al. (2010).

This Chapter focus on shaking tables tests carried out at the National Laboratory for Civil Engineering in Lisbon (Portugal). Two mock-ups – non-strengthened and strengthened, were prepared at reduced scale and tested in the shaking table, by

imposing excitation in two orthogonal directions. The main objectives of the present work were to assess directly the seismic performance of the “gaioleiro” buildings and to evaluate the performance of a strengthening technique. Next, a detailed description about the shaking table setup is presented.

2.2 Prototype definition

The experimental programme aims at assessing the seismic performance of a building typology – “gaioleiro” buildings. Thus, the first step is the definition of a prototype representative of the “gaioleiro” buildings. The prototype is defined according the main characteristics of the buildings that make up the typology. It is noted that in Section 1.5 a description of the “gaioleiro” buildings was done.

Candeias (2008) carried out a study on the seismic performance of the “gaioleiro” buildings and defined prototypes representative of this typology, based on the survey of Appleton (2005), including twenty “gaioleiro” buildings in Lisbon. Three types of prototypes were defined: (a) an isolated building with rectangular plan, with two facades with 28.6% of opening area, two gable walls without openings and a roof with two slopes; (b) a semi-detached building with rectangular plan, with two facades with 28.6% of opening area, two gable walls with shaft and one opening in each floor, and a roof with two slopes; (c) a corner building with irregular plan, with two facades with 30.8% of opening area, two gable walls with shaft and one opening in each floor, and a roof with four slopes. All prototypes have four floors with 3.60 m of interstory height, thickness of the walls (limestone) constant and equal to 0.45 m, flexible timber floors and dimensions in plan equal to 9.45x12.45 m².

The different prototypes defined by Candeias (2008) allow to consider different aspects of the behaviour of the “gaioleiro” buildings. First, the significant difference of geometry between gable walls without openings and facades with high percentage of opening. Thus, the isolated and semi-detached prototypes, in which the facades and gable walls are orthogonal, present two horizontal directions with a significant different stiffness and strength. A second aspect is the absence of the partition walls. Although all elements of a building can contribute for its seismic behaviour, in this type of buildings the connections between partition walls and masonry load-bearing walls are often weak and the contribution of the partition walls was considered negligible. Another relevant aspect is presence of shafts in two prototypes. The geometry of the shaft walls (“U” shape) reduces the in-plane and increases the out-of-plane strength of the gable walls. Finally, the prototype that represents the corner building has the two facades orthogonal between themselves, as well as the gable walls, resulting in a non-symmetric building and including large torsional effect.

The experimental research previously carried out by Candeias (2008) is a significant contribution for evaluating the seismic performance of the “gaioleiro” buildings, even if masonry was replaced by a substitute material in these tests. Given the fact that the costs and the time duration involved in the shaking table tests are very high, only the mock-up of the prototype of the isolated building was built and tested here, with the consideration of real masonry walls. After the definition of the prototype, the next step corresponds to the construction of the mock-up.

2.3 Mock-ups definition

In shaking table tests, mock-ups are prepared to reproduce the geometrical, physical and dynamical characteristics of the prototypes. However, mock-ups are usually simplified due to difficulties related to its execution in laboratory. Moreover, given the size of the prototype and the size and load capacity of the facilities, reduced scale mock-ups are usually considered. It is difficult to fulfil the similitude laws using very small scales, e. g. with respect to the preparation of masonry units and reinforcement elements. Here, due to the size and payload capacity of the LNEC shaking table the mock-up had to be geometrical reduced, using a law of similitude.

Physically, the similitude corresponds to the equivalence between objects or phenomena that actually are different (Sonin 2001). For a reduced scale mock-up to be able to reproduce the dynamic behaviour of its prototype, it must satisfy the similitude of (Carvalho 1998): (a) geometry; (b) relationship between stresses and strains of the materials; (c) mass and gravity forces; (a) initial and boundary conditions.

Geometry similitude is usually obtained from the direct application of the scale factors. This can be difficult to achieve accurately for all the details of the prototype for large scale factors. Stress-strain relationships are much more difficult to reproduce in the mock-ups, even when the same material is used in the prototype and mock-up. Very reduced scales require the use of specific materials (different from the original ones), and phenomena such as the bond between a reinforcement bar and concrete can be complex to scale. The similitude of mass and gravity forces is obtained using the Cauchy and Froude similitude laws (Carvalho 1998). The Cauchy number, see Equation (2.1), corresponds to the ratio between inertial forces and restoring forces:

$$Cauchy\ number = \frac{\rho L^3 v^2}{E L^2} = \frac{\rho v^2}{E} \quad (2.1)$$

and the Froude number, see Equation (2.2), relates the inertial forces and gravity forces:

$$\text{Froude number} = \frac{\rho L^3 v^2}{\rho L^3 g} = \frac{v^2}{L g} \quad (2.2)$$

in which ρ is the specific mass, L is the length, v is the velocity, E is the Young's modulus and g is the gravity acceleration.

Table 2.1 presents the scale factors of several parameters for both similitude laws, assuming that the material of the prototype and mock-up are the same ($E_p/E_m=1$). Taking into account only the Cauchy similitude law, the accelerations in the mock-up (a_m) are equal to λ times (scale factor) the accelerations in the prototype (a_p). However, in the experimental test it is not possible to scale the gravity acceleration. This means that the relationship between inertial forces and gravity forces is not respected (Froude number).

Table 2.1 – Scale factors of the Cauchy and Froude similitude laws (Carvalho 1998).
(Example with scale factor λ equal to 3)

Parameter	Symbol	Cauchy	Cauchy and Froude
Length	L	$L_p/L_m=\lambda=3$	$L_p/L_m=\lambda=3$
Young's Modulus	E	$E_p/E_m=1$	$E_p/E_m=\lambda=1$
Specific mass	ρ	$\rho_p/\rho_m=\lambda=1$	$\rho_p/\rho_m=\lambda^{-1}=1/3$
Area	A	$A_p/A_m=\lambda^2=9$	$A_p/A_m=\lambda^2=9$
Volume	V	$V_p/V_m=\lambda^3=27$	$V_p/V_m=\lambda^3=27$
Mass	m	$m_p/m_m=\lambda^3=27$	$m_p/m_m=\lambda^2=9$
Displacement	d	$d_p/d_m=\lambda=3$	$d_p/d_m=\lambda=3$
Velocity	v	$v_p/v_m=1$	$v_p/v_m=\lambda^{1/2}=3^{1/2}$
Acceleration	a	$a_p/a_m=\lambda^{-1}=1/3$	$a_p/a_m=1$
Weight	W	$W_p/W_m=\lambda^3=27$	$W_p/W_m=\lambda^2=9$
Force	F	$F_p/F_m=\lambda^2=9$	$F_p/F_m=\lambda^2=9$
Moment	M	$M_p/M_m=\lambda^3=27$	$M_p/M_m=\lambda^3=27$
Stress	σ	$\sigma_p/\sigma_m=1$	$\sigma_p/\sigma_m=1$
Strain	ε	$\varepsilon_p/\varepsilon_m=1$	$\varepsilon_p/\varepsilon_m=1$
Time	t	$t_p/t_m=\lambda=3$	$t_p/t_m=\lambda^{1/2}=3^{1/2}$
Frequency	f	$f_p/f_m=\lambda^{-1}=1/3$	$f_p/f_m=\lambda^{-1/2}=3^{-1/2}$

(p and m designate prototype and mock-up, respectively)

For a realistic simulation of dynamic behaviour, Cauchy and Froude similitude laws must be accomplished simultaneously. In this case, the specific mass in the mock-up (ρ_m) is equal to λ times the specific mass in the prototype (ρ_p). The preparation of materials, in laboratory, with the same stress-strain relationship and different specific mass is difficult. Thus, it is usual to prepare the mock-up with the same material of the prototype and to add masses on the mock-up. As an example, concentrated masses at floors levels can be added in reinforced concrete frame structures and distributed masses (steel plates) can be added in the walls of masonry structures.

Although the problem associated to the specific mass in the Cauchy and Froude similitude laws can be solved by adding masses to the mock-up, another important aspect should be taking into account. If only the Cauchy similitude is used, the mass of the the prototype (m_p) is equal to λ^3 times the mass of mock-up (m_m). However, if both similitude laws are used, the mass of the the prototype (m_p) is equal to λ^2 times the mass of mock-up (m_m). This means that the total mass of the mock-ups prepared using both similitude laws are λ times heavier than the mock-ups built taking only into account the Cauchy law of similitude. In the first case, the natural frequencies of the mock-ups are lower than the ones obtained using only the Cauchy law of similitude. This aspect is an advantage of preparing mock-ups taking into account the Cauchy and Froude similitude laws, because the shaking tables are more accurate in the low range of frequencies. It is noted that shaking tables have payload capacities and the total mass of the mock-ups can define the type of law of similitude to be adopted.

Finally, the boundary conditions are, usually, not difficult to replicate, as the soil-structure interaction is not simulated. In general, the connection between the platform and mock-up is done through reinforced concrete beams or foundation slabs. However, shaking table tests are usually done applying several seismic actions in the same mock-up without repairing it, resulting in successive tests on mock-ups all with a different initial condition. This procedure is usually adopted, due to the costs involved in the constructions of the mock-ups.

In the literature about experimental tests, different criteria to prepare reduced mock-ups can be found. For instance, Tomažević (2000) presents a method to build mock-ups at reduced scale based on the similitude of dynamic behaviour and failure mechanism, which requires similar distribution of mass and stiffness and similar working stress level (stress/compressive strength ratio) in the load-bearing walls of the prototype and mock-up, respectively. According to this method, and for full models, the materials adopted for the mock-up are different from the original ones defined in the prototype (a different Young's modulus is required).

As previously mentioned, the LNEC shaking table has, in plan, 4.6 x 5.6 m² (see Section 2.6) and the mock-up had to be geometrical reduced. Taking into account the size and payload capacity of the shaking table, the Cauchy law of similitude with a scale factor equal to 1:3 was adopted (Table 2.1). The same material (limestone and lime mortar) was used in the prototype and mock-up.

The mock-up has four floors, two facades with openings, two gable walls without openings, timber floors and the top ceiling. Due to the difficulties in reproducing the gable roof at reduced scale, this was not considered in the mock-up. Thus, the horizontal forces transferred from the roof to the walls under an earthquake, which can aggravate the out-of-plane mechanism of walls, were not taken into account. However, it is also noted that vertical component of the self-weight of the roof increases the compressive stress in the masonry walls and the presence of the tie-beams can heavily reduce the horizontal thrust, meaning that the simplification is not expected to provide a major change in the response. The external walls have a single leaf of irregular stone masonry and the partition walls were not considered.

The geometry of the non-strengthened mock-up (Figure 2.1a and 2.1b) results directly from the application of the scale factor to the prototype, resulting in an experimental model 3.15 m wide and 4.15 m deep, with 0.17 m of wall thickness. The interstory height is equal to 1.20 m. In the construction of the timber floors (Figure 2.1c), medium-density fiberboard (MDF) panels, with thickness equal to 0.012 m, connected to a set of timber joists oriented in the direction of the shortest span, were used. The panels were cut in rectangles ($0.57 \times 1.05 \text{ m}^2$) and nailed to the joists, keeping a joint of about 1 mm for separating the panels. The purpose was to simulate flexible floors with weak diaphragmatic action. In order to avoid elements with small cross section, as a result of application of the scale factor, each timber joist corresponds to a set of three real joists, resulting in a cross section with $0.100 \times 0.075 \text{ m}^2$ (width and height) spaced each 0.35 m. The floor has rim joists, connected using bent nails to the gable walls ($0.035 \times 0.150 \text{ m}^2$), as well as in the facades ($0.035 \times 0.075 \text{ m}^2$). The timber joists were inserted 0.05 m into the gable walls (Figure 2.1d). The connection between floors and facades is weaker as the MDF panels are connected to the rim joists, which are only connected to the masonry wall by bent nails (Figure 2.1e).

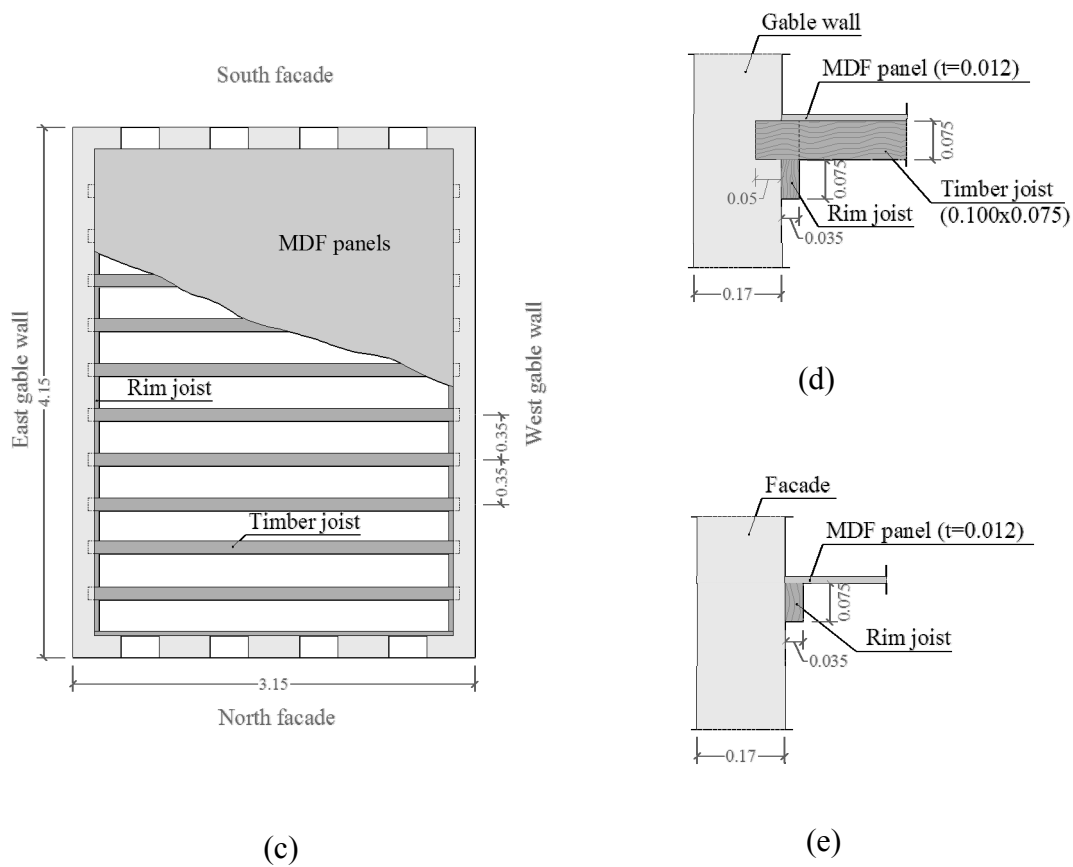
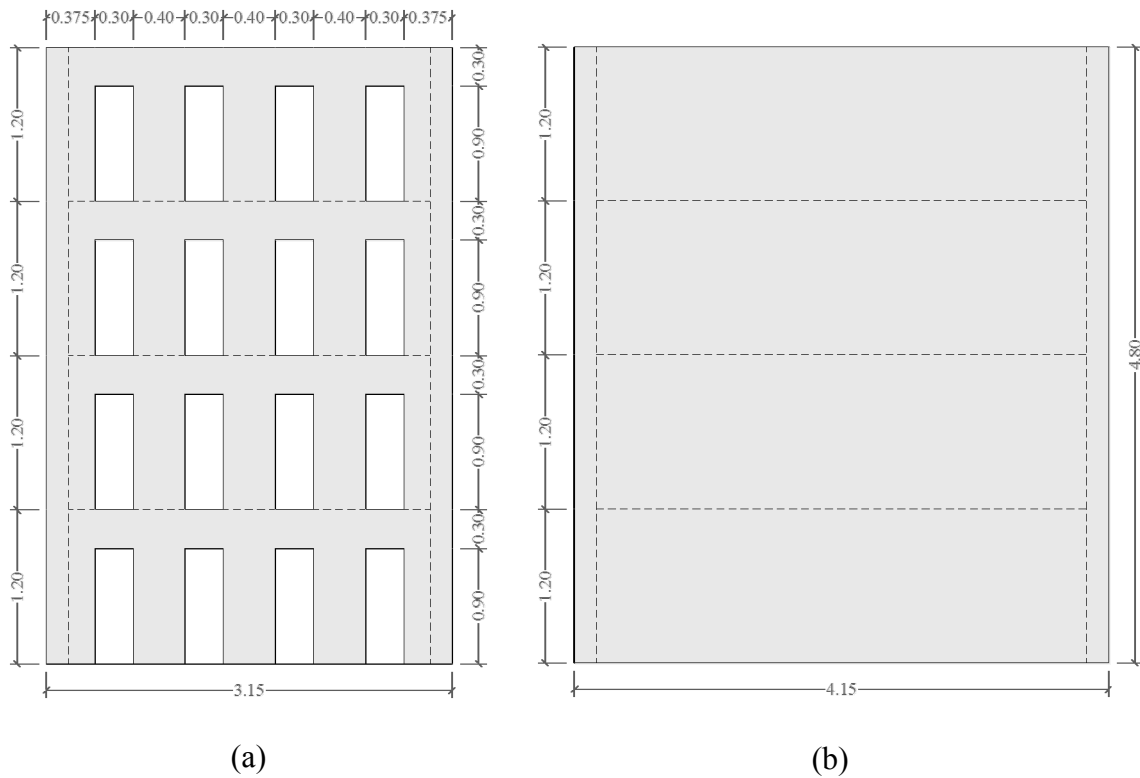


Figure 2.1 – Geometry of the non-strengthened mock-up: (a) facades; (b) gable walls; (c) plan; (d) connection floor-gable wall; (e) connection floor-facade. (Dimensions in meters).

The strengthened mock-up (Figure 2.2a) presents the same geometry of the non-strengthened one. The main goals of the strengthening techniques were to improve the connection between the floors and the masonry walls, mainly to the gable walls, and to prevent the out-of-plane collapse of the facades. The “gaioleiro” buildings present usually weak connection between floors and masonry walls and high percentage of openings in the facades. Furthermore, total or partial collapse of the facades is observed in similar buildings struck by earthquakes in the past. The design of the strengthening elements was based on the out-of-plane response of the facades. A beam was assumed for design at floor level with length of the facades (3.15 m) and cross section equal to the one for the spandrel ($0.30 \times 0.17 \text{ m}^2$). A linear static analysis with the inertial forces was made and the inertial forces were calculated considering the maximum out-of-plane acceleration of the facades obtained from the non-strengthened mock-up tests.

The improvement of the connections between floors and masonry walls was done using steel angles (S235) at all floor levels placed internally in the mock-up (Figure 2.2b). In the gable walls, the steel angles are connected to the masonry by chemical anchors (M8) spaced each 0.25 m, through the rim joists (Figure 2.2c). The steel angles are also connected to the timber joists and MDF panels by bolts (Figure 2.2d). Additionally, timber elements to constrain the rotation of the timber joists were used (Figure 2.2b). This strengthening technique allows an efficient connection between floors and gable walls. In the facades, the connection between floors and masonry walls was improved using steel angles inside and steel plates outside of the mock-up. These steel elements were connected among themselves by bolts spaced each 0.25 m (Figure 2.2e). Furthermore, the connection between MDF panels and rim joists was also improved by additional nails (Figure 2.2e). It is expected that some beam effect (steel angle + masonry + steel plate) prevents the out-of-plane displacements of the facades and improves the in-plane behaviour, because the spandrels are now connected by steel elements. It is noted that no steel plates were added at the external surface of the gable walls. Although the mock-up is representative of an isolated “gaioleiro” building, the adopted strengthening techniques aim to be general and should be applicable to the adjacent buildings.

In the two top floors steel cables were also installed (Figure 2.3a). Each floor has two pairs of stainless steel cables (AISI 316), with diameter equal to 3 mm, connecting the middle of the facades to the corners of the opposite facades, transferring the inertial forces in the out-of-plane direction of the facades to the plane of the gable walls. The cables are connected to the masonry walls with an external steel plate (Figure 2.3b), preventing the punching in the masonry, and to the steel angles (Figure 2.3c) in the corners and in the middle of facades, respectively. Each steel cable is made by two half-cables joined by turnbuckles, aiming at providing a slight prestress (Figure 2.2d).

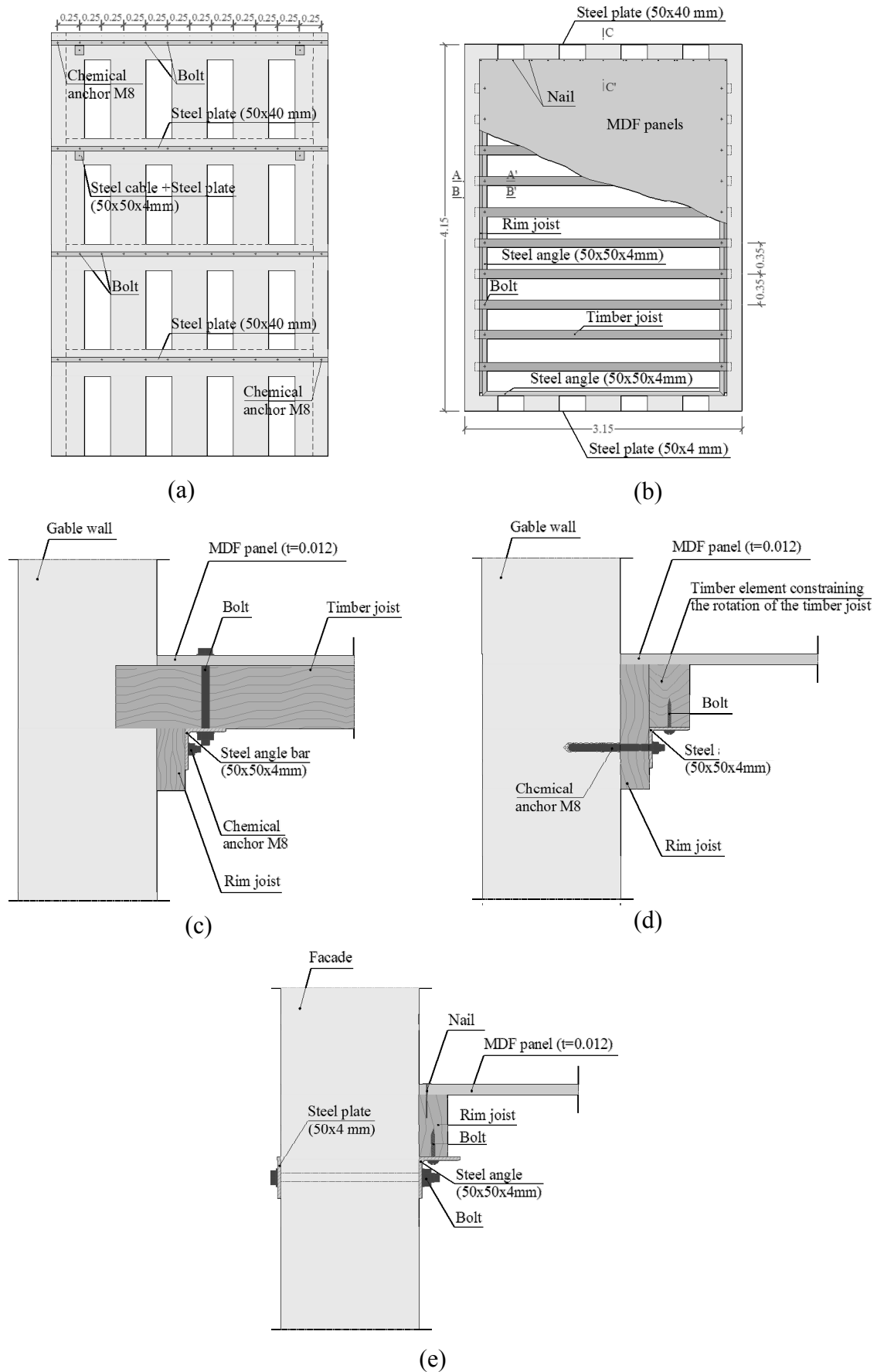


Figure 2.2 – Strengthened mock-up: (a) facades; (b) plan; (c) section AA'; (d) section BB'; (e) section CC'. (Dimensions in meters).

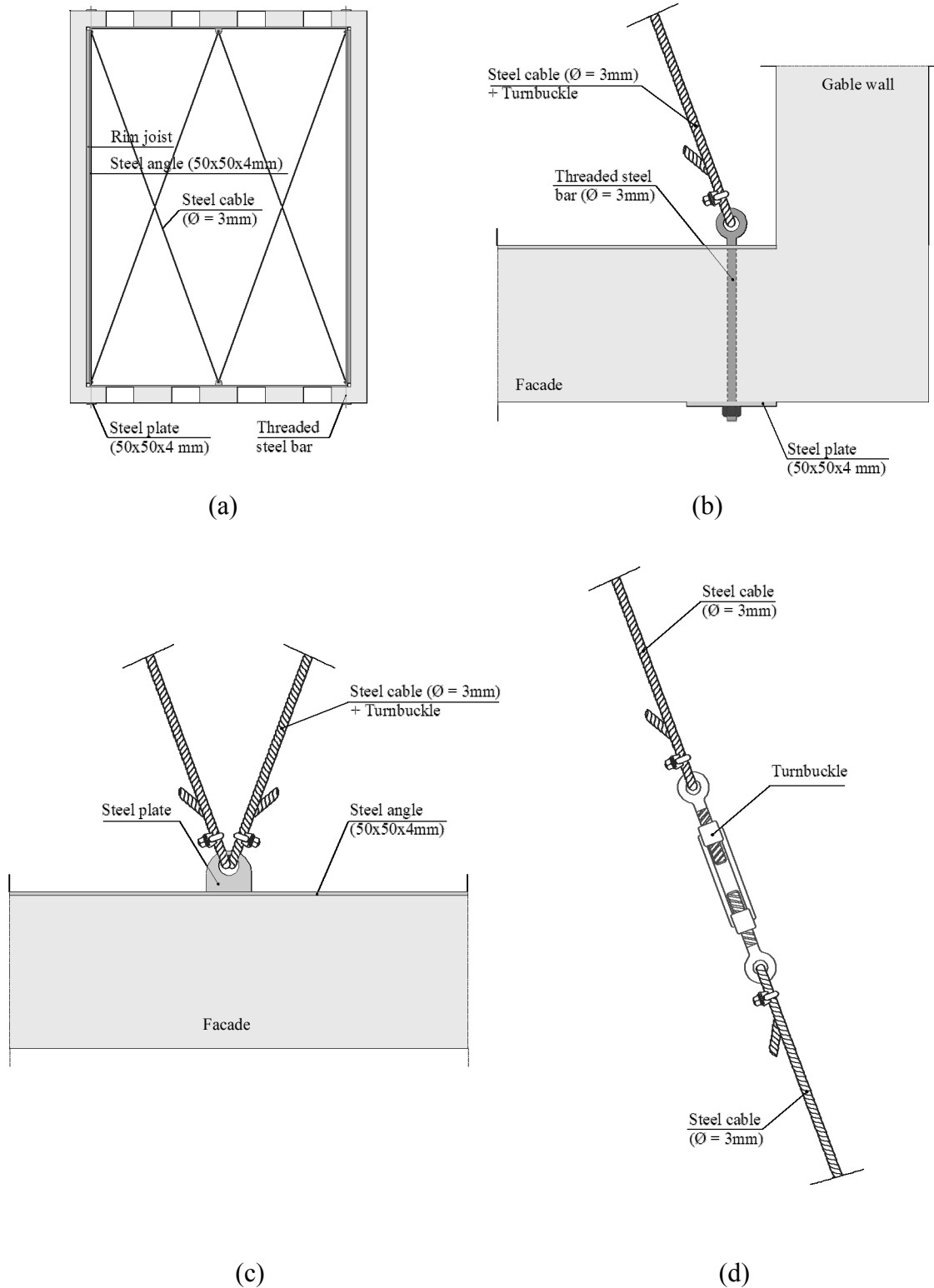


Figure 2.3 – Steel cables of the strengthened mock-up: (a) plan of the two top floors; (b) connection of the cables to the corners; (c) connection of the cables to the middle of the facades; (d) turnbuckle.

2.4 Mock-ups construction

The construction of the mock-ups was made outside of the shaking table on a reinforced concrete slab specifically designed for this purpose. The slab has plan dimensions of 4.40x4.90 m², four steel elements to lift the mock-ups during the transportation in the laboratory, and holes conveniently drilled to fix the mock-ups to the shaking table. The self-weight of the slab is about 108 kN and has to be added to the mass of the mock-ups to define the total mass on the shaking table. The non-strengthened mock-up was built floor by floor, in a way that the load-bearing walls of a given floor were initially built, followed by the construction of the respective timber floor. The timber floors were built one week after the construction of the load-bearing walls to allow the hardening of the lime mortar.

The load-bearing stone walls were built with specialised workmanship and using formworks in the outside of the mock-up, assuring the verticality of the masonry walls (Figure 2.4). Although in reality the formworks are not used in the construction of these buildings, traditional masonry was usually adequately built and the idea of the present was not to add any geometrical imperfections. The openings were made using timber frame (Figure 2.4). Two aspects of construction require attention. First, a traditional masonry pattern was adopted, with corners featuring an interlocked connection of the masonry units between facades and gable walls (Figure 2.5a). Second, the construction of the spandrels at reduced scale is rather complex. In general, the first masonry course over the openings of the lintels of the “gaioleiro” buildings is composed by several stone units with small arching action. Thus, in the first course of the spandrels, three small units were used (Figure 2.5b).



Figure 2.4 – Construction of the non-strengthened mock-up.

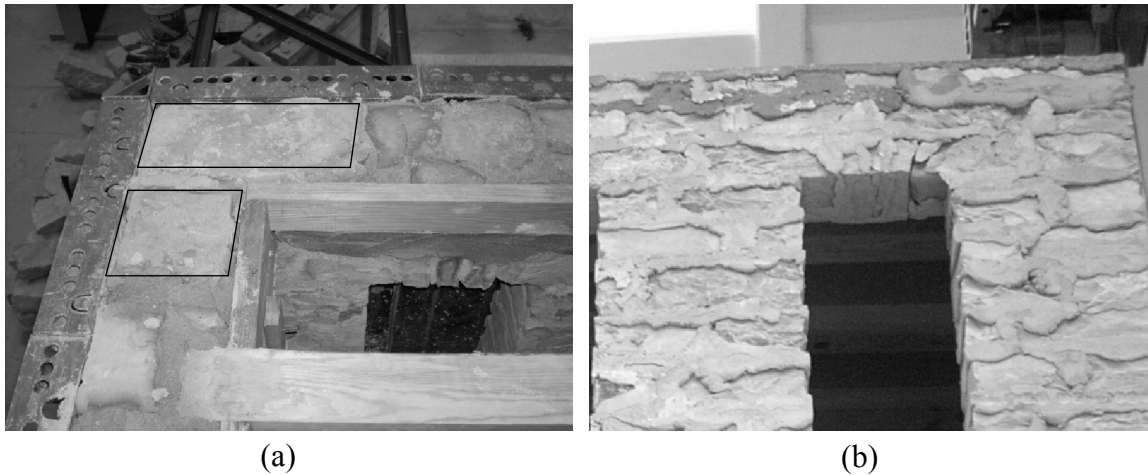


Figure 2.5 – Details of the: (a) corners and overlapping corner stones; (b) spandrels.

The construction of the timber floors involved several steps carried out in the following order: (a) placement of the rim joists in the gable walls and facades; (b) placement of the rim joists in direction of the shortest span; (c) nailing of the MDF panels to timber joists and to the rim joists. The connection between rim joists and masonry walls was made by curved nails, as originally done in this type of buildings (Figure 2.6a). Additionally, a wedged support in lime mortar under of the rim joist was also done. Initially and during the hardening of the lime mortar, timber props were used to position these elements (Figure 2.6b).

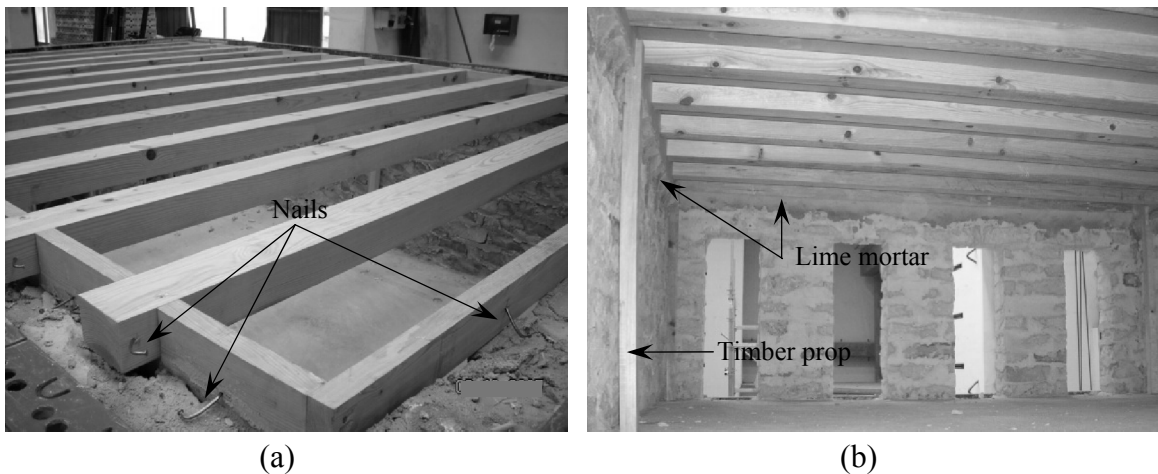


Figure 2.6 – Details of the floors construction: (a) bent nails connecting the rim joists to the masonry walls; (b) timber prop and lime mortar used to fix the rim joists.

The seismic test on the non-strengthened mock-up aims at obtaining moderate damage and not full collapse. After the seismic tests, the piers and the spandrels of the facades were repaired, aiming at re-establishing the initial conditions of the mock-up. Afterwards, the mock-up was strengthened and tested again. The strengthening of the mock-up was carried out by BEL Company and did not present any difficulties. First, the strengthening of the connection between floors and masonry walls was carried out,

with the installation of the steel angles and their welding in the corners. Finally, the steel cables were installed in the two top floors.

Although the prestress in the cables was not measured, each cable had a turnbuckle which allowed to obtain similar prestress in all the cables. The natural frequencies of the steel cables are directly related to the prestress installed. Forced dynamic identification tests, using a hammer to apply the excitation on the cables, were carried out and the turnbuckles were adjusted aiming at obtaining similar natural frequencies in all steel cables (about 12.5 Hz).

The mock-ups did not include the mass of the partition walls or even live load. Although experimentally the mass could be included by adding inert masses fixed to the timber floors (e.g. sand bags or steel elements), the inertial forces of all masonry buildings are mainly related with the mass of the thick masonry walls. The self-weight of the mock-ups is about 220 kN and the self-weight of the foundation slab is equal to 108 kN. Thus, the total mass (mock-up + slab) on the shaking table is about 328 kN and its maximum load capacity is equal to 392 kN. The weight of the mock-up was the main reason for selecting of only the Cauchy similitude law for construction on a 1:3 reduced scale. If Cauchy and Froude similitude laws would be respected, additional masses had to be added to the mock-ups and the total self-weight would be about 768 kN, exceeding the load capacity of the shaking table. The mock-ups were tested with an age equal or older than 28 days to allow mortar curing. Figure 2.7 shows the final aspect of the non-strengthened and strengthened mock-ups.

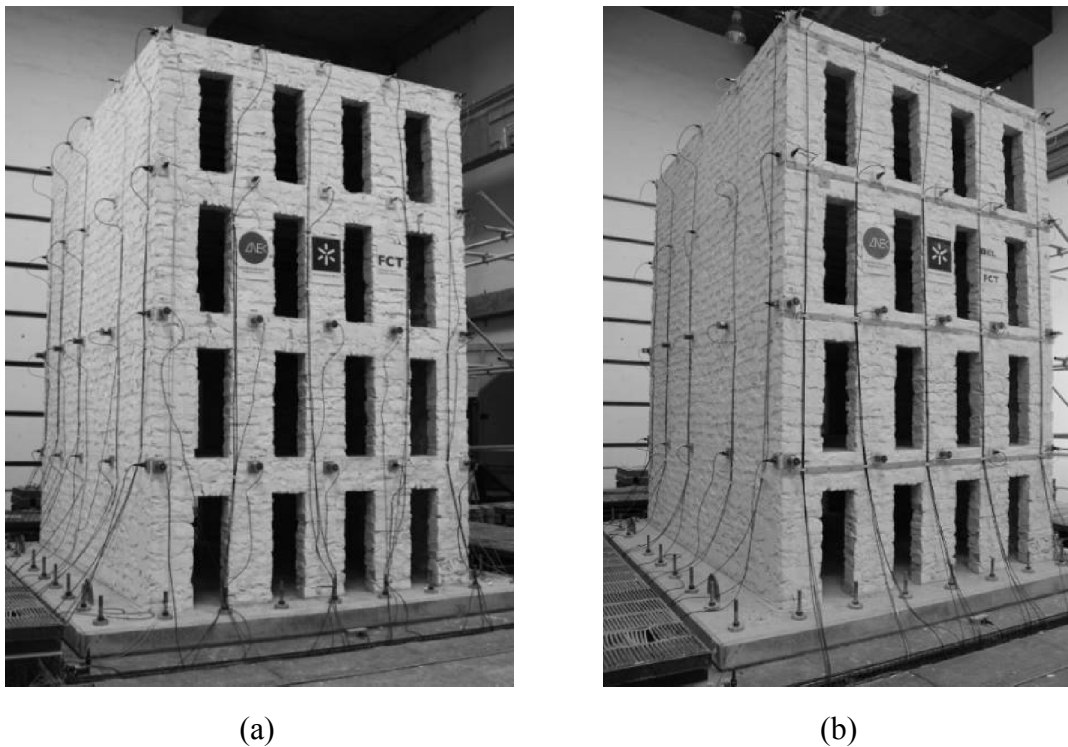


Figure 2.7 – General view of the: (a) non-strengthened mock-up; (b) strengthened mock-up.

2.5 Test setup

The main objectives of the shaking table tests carried out are to assess the seismic performance of the “gaioleiro” buildings and to validate the efficiency of a strengthening technique. These objectives were carried out through two experimental procedures: (a) the evaluation of the response of the mock-ups based on the results obtained in the seismic tests (e.g. crack patterns and displacements at floor levels) with increasing seismic amplitude applied at base; (b) the definition of the seismic vulnerability curves based on the decreasing of the natural frequencies of the mock-ups with the application of seismic tests with increasing amplitude.

The seismic tests were performed at the LNEC 3D shaking table by imposing accelerograms compatible with the design response spectrum defined by the Eurocode 8 (EN 1998-1 2004). The accelerograms were imposed with increasing amplitude in two uncorrelated orthogonal directions that should present approximately the same *PGA* (Peak Ground Acceleration). Thus, several seismic tests were carried out on the same mock-up, measuring its response by accelerometers, placed on floor levels, and recording the damage that occurred. It is noted that the mock-ups were not repaired before applying the next seismic action. This means that the mock-ups accumulated damage with the shaking table tests and, consequently, the initial conditions are not the same for the different tests. The mock-ups only present ideal initial condition (no damage) in the first seismic test. In the subsequent analysis of the results, this issue will be discussed with some detail (see Section 3.2.1).

The methodology for defining the seismic vulnerability curves through experimental tests is, usually, based on the identification of the dynamic properties of the mock-ups (natural frequencies, mode shapes and damping ratios) along a series of seismic tests with increasing input excitations (Degée et al. 2007, Bairrão and Falcão 2009). The dynamic properties give inherent information of the mock-up and its evolution is related to the stiffness and, consequently, to the damage caused by a given seismic input. Thus, dynamic identification tests at the shaking table (forced vibration tests) were also carried out, aiming at characterizing the dynamic properties initially and after each seismic test. The tests for the characterization of the dynamic properties were done applying a series of accelerations at the base of the mock-ups, in two orthogonal directions and specifically prepared for this type of tests, being the response measured by accelerometers placed at floor levels. Besides these tests, dynamic identification tests using output only techniques were also carried out with the mock-up outside the shaking table and on the shaking table. For more information about these tests see Mendes et al. (2010) [1].

The shaking table tests of the non-strengthened mock-up involved four seismic tests with amplitudes equal to 25%, 50%, 75% and 100% of the code amplitude and five dynamic identification tests (Table 2.2). Additionally, in the strengthened mock-up two extra seismic tests were done, with amplitudes of the seismic action equal to 125% and

150% of the code amplitude. Due to serious damage of the mock-up in the last stage, it was not possible to carry out the dynamic identification after the final seismic test (Table 2.3).

Table 2.2 – Shaking table tests carried out on the non-strengthened mock-up.

Number	Identification	Description
1	DI 0	Dynamic identification test before the first seismic test
2	Earthquake 25%	Seismic test with amplitude equal to 0.25 code
3	DI 1	Dynamic identification after seismic test Earthquake 25%
4	Earthquake 50%	Seismic test with amplitude equal to 0.50 code
5	DI 2	Dynamic identification after seismic test Earthquake 50%
6	Earthquake 75%	Seismic test with amplitude equal to 0.75 code
7	DI 3	Dynamic identification after seismic test Earthquake 75%
8	Earthquake 100%	Seismic test with amplitude equal to 1.00 code
9	DI 4	Final dynamic identification test

Table 2.3 – Shaking table tests carried out on the strengthened mock-up.

Number	Identification	Description
1	DI 0	Dynamic identification before the first seismic test
2	Earthquake 25%	Seismic test with amplitude equal to 0.25 code
3	DI 1	Dynamic identification after seismic test Earthquake 25%
4	Earthquake 50%	Seismic test with amplitude equal to 0.50 code
5	DI 2	Dynamic identification after seismic test Earthquake 50%
6	Earthquake 75%	Seismic test with amplitude equal to 0.75 code
7	DI 3	Dynamic identification after seismic test Earthquake 75%
8	Earthquake 100%	Seismic test with amplitude equal to 1.00 code
9	DI 4	Dynamic identification after seismic test Earthquake 100%
10	Earthquake 125%	Seismic test with amplitude equal to 1.25 code
11	DI 5	Dynamic identification after seismic test Earthquake 125%
12	Earthquake 150%	Seismic test with amplitude equal to 1.50 code

2.6 Instrumentation

The experimental program aims at simulating the behaviour of the “gaioleiro” buildings under seismic action in laboratory, with the intention to relate the seismic action applied at the base of the mock-ups with the response of their masonry walls. This work was carried out in the Earthquake Engineering and Structural Dynamics Division (NESDE) of LNEC. Besides the construction of the mock-ups, the preparation of the tests involved the following tasks: (a) selection and preparation of the facility to simulate the seismic scenario; (b) selection and setup of the devices to measure the response of the mock-ups; (c) preparation of the acquisition systems to record the input and output signals.

The tests were carried out in the LNEC 3D shaking table. This facility allows developing seismic tests in which the global movements are the combination of three translational degrees of freedom according with the orthogonal axes (two horizontal) i.e. transversal and longitudinal, and one vertical. The shaking table consists of three main components: (a) the platform in which models are placed, (b) the guiding system, which ensures that the table moves only in the desired degrees of freedom, and (c) the hydraulic actuators that include the control system and impose the movements to the table (Coelho and Carvalhal 2005). The platform is a welded steel slab with a shape similar to a triangular prism, in which the top ($4.60 \times 5.60 \text{ m}^2$) corresponds to the side where the models are fixed. The whole structure is very rigid globally and locally, with moderate self-weight.

The guiding system ensures that the platform only moves in the desired translational degrees of freedom, avoiding rotational movements around the orthogonal axes (Table 2.4). For that purpose the system has external torsional bars connected to the table and controlling the movements of the shaking table (LNEC 2010). The actuator system is composed by hydraulic actuators and an associated control system. Each of the actuators is composed by a hydraulic cylinder with double effect (tension-compression), possessing one or more servo-valves and a set of hydraulic components, control and safety commands (Coelho and Carvalhal 2005). The seismic platform possesses four hydraulic actuators (Table 2.5), namely: (a) a vertical one, with nominal capacity of 300 kN; (b) one according with the horizontal direction, with a nominal capacity of 1000 kN; and (c) two actuators according to the transversal direction, in a push-pull arrangement, with nominal capacity of $2 \times 300 \text{ kN}$ (LNEC 2010). All the actuators possess a stroke of about 145 mm, excluding the safety margin. The total mass of the shaking table is 40 ton. The control of the shaking table is done by means of a mixed system (analog/digital) associated to a central computer (Instron 8580 Control Tower) with capacity up to eight channels ADC – 16 bits. Figures 2.8a and 2.8b present a 3D general view of the shaking table and the identification of the directions considered in this work, respectively.

Table 2.4 – Characteristics of the LNEC 3D shaking table (LNEC 2010).

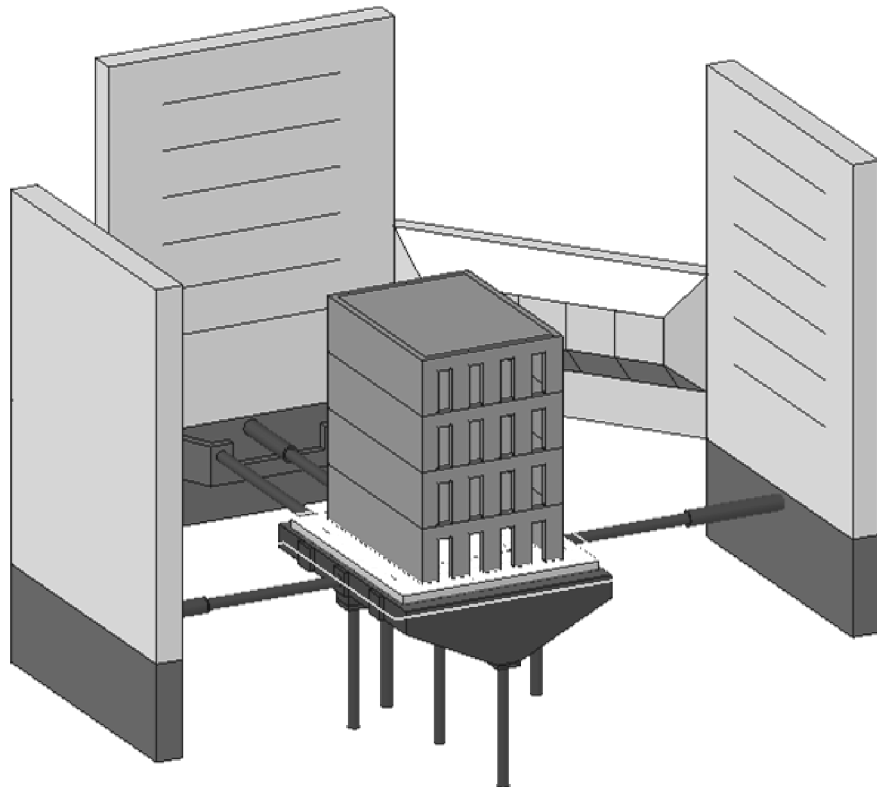
Frequency range		Hz	0.1 – 40	
Stroke (effective/maximum)	Horizontal	mm _{pp}	290/400	
	Vertical	mm _{pp}	290/400	
Maximum velocity (nominal/limit)	Horizontal	Transversal	cm/s	70.1/121.5
		Longitudinal	cm/s	41.9/72.6
	Vertical	cm/s	42.4/73.5	
Maximum acceleration for bare table	Horizontal	Transversal	m/s ²	18.75
		Longitudinal	m/s ²	9.38
	Vertical	m/s ²	31.25	
Yaw/Pitch/Roll	Rotation degree	°	N/A	
	Velocity	rad/s	N/A	
Maximum overturning moment		kN.m	N/A	
Maximum mock-up dead weight		kN	392	
Maximum compensated dead weight		kN	392	

Table 2.5 – Characteristics of the actuators of the shaking table (LNEC 2010).

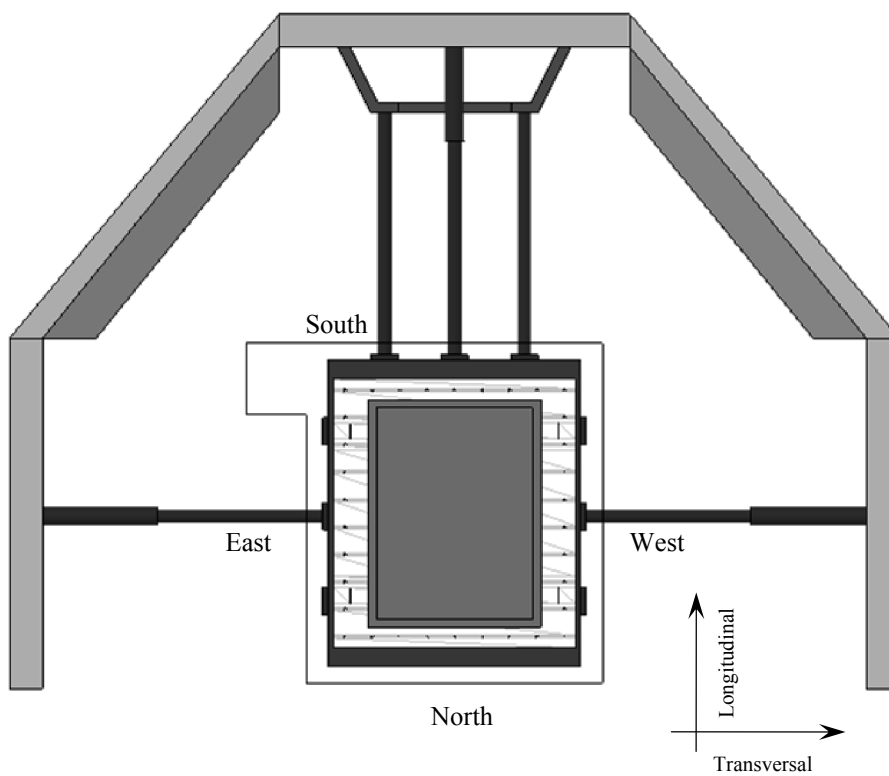
Direction	Manufacturer	Maximum total force [kN]	Number of units/axis
Longitudinal	INSTRON	1250	1
Transversal	INSTRON	750	2
Vertical	INSTRON	375	1

The type and setup of devices used in the tests for measuring the response of the mock-ups was defined according to the expected behaviour of this type of buildings under seismic action. Given the high concentration of mass at the masonry walls and the flexible floors, high inertial forces in the out-of-plane direction of the walls are expected. Furthermore, the high percentage of openings at the facades can lead to a concentration of damage here, mainly in the spandrels. Finally, the asymmetric damage that can occur in the spandrels near the corners can cause different behaviour of the corners.

In shaking table tests, displacement transducers (LVDT) and accelerometers are usually used to measure the response of the mock-ups. Here, the large dimensions of the mock-ups and the measurements devices available in the LNEC led to the selection of accelerometers to capture the out-of-plane response of the masonry walls. The signals of the seismic action applied at the base of the mock-ups were measured by accelerometers and LVDT's pre-installed on the platform and on the actuators. It is noted that the time history of displacements can be obtained from the double integration of the acceleration signals.



(a)



(b)

Figure 2.8 – Shaking table: (a) 3D general view; (b) plan.

Two types of accelerometers were used in the shaking table tests: (a) piezoelectric accelerometers; (b) capacitive accelerometers. A piezoelectric accelerometer (Figure 2.9a) is a one spring-mass-damper system, which produces an electric output proportional to the acceleration. This type of accelerometers is not capable of measuring the DC component (response at 0 Hz) and does not need external power source. A capacitive accelerometer (Figure 2.9b) has the advantage of measuring the uniform acceleration signals but requires the supply of energy to measure.

The capacitive accelerometers, with a sensitivity of 200 mV/g (± 10) and a measurement range of ± 0.5 g pk are fixed to the platform of the shaking table and were used to measure the two components of the seismic action applied at the base of the mock-ups. The piezoelectric accelerometers were used to measure the response of the structure at floor levels in the seismic and dynamic identification tests. Three types of piezoelectric accelerometers with different sensitivity and measurement range were used:

- AA: sensitivity equal to 10000 mV/g and measurement range equal to ± 0.5 g pk;
- AB: sensitivity equal to 1000 mV/g and measurement range equal to ± 5.0 g pk;
- AC: sensitivity equal to 100 mV/g and measurement range equal to ± 50.0 g pk.

In the dynamic identification tests the most sensitive accelerometers (AA and AB) were used, because the amplitude of the signals applied at the base of the mock-ups is low. On the other hand, the maximum accelerations obtained in the seismic tests are higher than 0.5 g and, consequently, types AB and AC were adopted in this case. In both type of tests, a setup composed by 5 accelerometers in each masonry wall per floor level was adopted, resulting in 20 accelerometers for each wall. In total, 80 out-of-plane accelerations of the mock-ups were measured (Figure 2.10), giving detailed information of the out-of-plane response of the masonry walls.



(a)



(b)

Figure 2.9 – Images of Accelerometers: (a) piezoelectric accelerometer (PCB 2010); (b) capacitive accelerometer (ENDEVCO 2010).

The acquisition of the 84 channels (80 output acceleration channels, 2 input acceleration channels fixed to the platform of the shaking table, and 2 input displacement channels fixed to the actuators) were carried using two SCXI chassis of the National Instruments connected by a trigger. Modules NI SCXI-1530 and NI SCXI-1140 were used for signal conditioning of accelerations and displacements. The damage occurring in the mock-ups was registered for each seismic test by photos, video or drawings of the cracks after each seismic test.

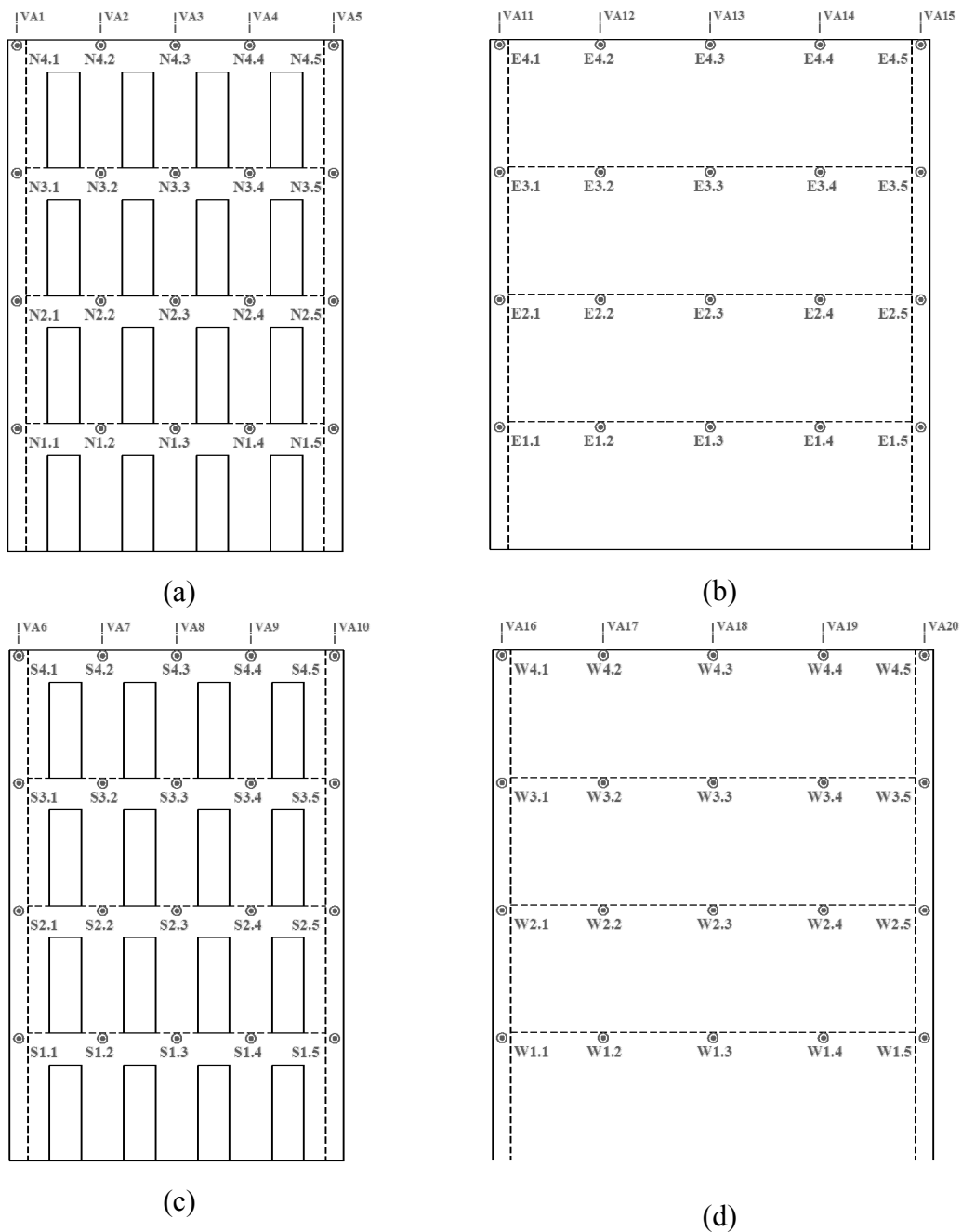


Figure 2.10 – Accelerometers setup: (a) North facade; (b) East gable wall; (c) South facade; (d) West gable wall.

(VA corresponds to the vertical alignments considered)

2.7 Input signals

There are few earthquake records and they correspond to a unique seismic event, with a set of random parameters (frequency content, duration, etc.) that will never occur again and that may not be satisfactory for design purposes. Thus, in shaking table tests and numerical dynamic analyses with time integration many authors use artificial accelerograms, in which the amplitude of their response spectrum is defined by the codes. A software such as SIMQKE_GR (Gelfi 2006) or LNEC-SPA (Mendes 2008) can be used to generate artificial accelerograms.

Here, two artificial accelerograms were generated based on stochastic methods and techniques of finite fault modelling, with parameters adequate for Portugal (Carvalho 2007) with a duration equal to 30 s (intense phase). The response spectrum of the accelerograms is compatible with the type 1 design response spectrum defined by Eurocode 8 (EN 1998-1 2004) and Portuguese National Annex for Lisbon ($ag_r = 1.5 \text{ m/s}^2$), with a damping ratio equal to 5% and a type *A* soil (rock, $S = 1$). The range of frequencies of the accelerograms is 0.7-40 Hz (1.428-0.025 s), which was defined taking into account the features of the shaking table (Table 2.4).

Due to the Cauchy law of similitude (Table 2.1) the acceleration and the time were increased and decreased three times, respectively. Figure 2.11 presents the pseudo acceleration response spectrum, at reduced scale of 1:3, for the accelerograms adjusted to the spectrum of the Eurocode 8 (EN 1998-1 2004) for both directions. Figure 2.12 shows the time history of acceleration, velocities and displacements. The maximum acceleration, velocity and displacement are equal to 4.66 m/s^2 , 20.53 cm/s and 1.43 cm , respectively, which are lower than the limits of the shaking table (Table 2.4).

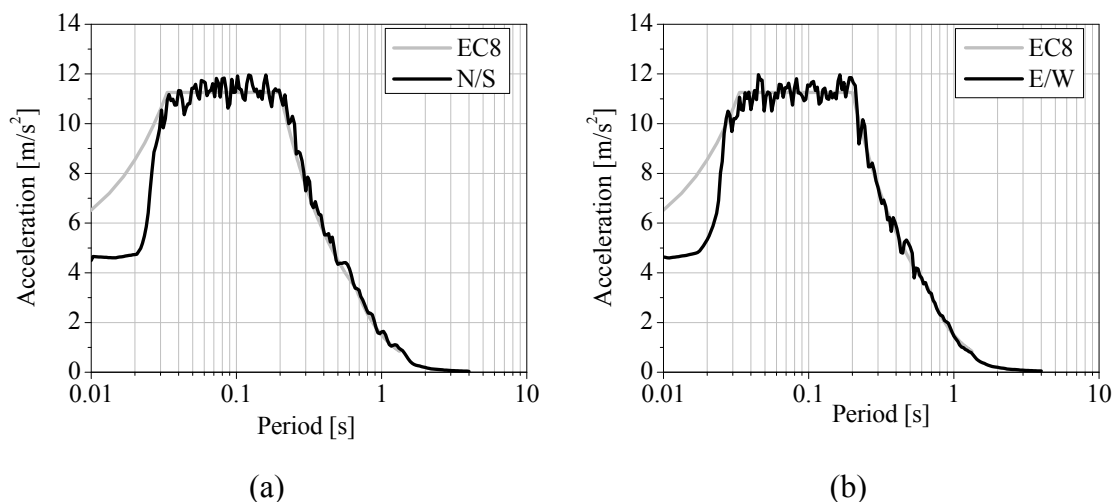


Figure 2.11 – Pseudo acceleration response spectra at 1:3 reduced scale: (a) North-South direction; (b) East-West direction.

(Fourier filter: 0.7-40 Hz; 1.428-0.025 s)

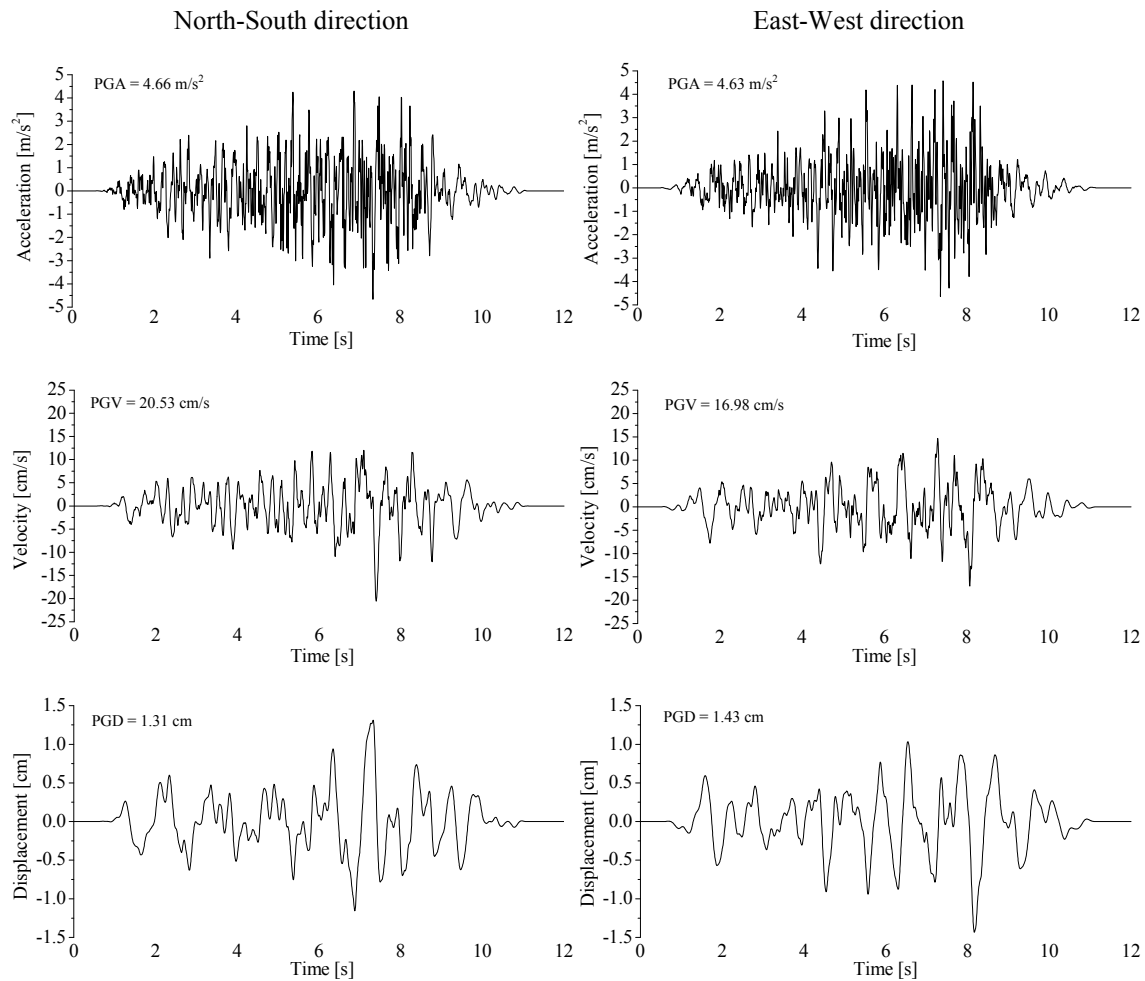


Figure 2.12 – Time histories of the input signals at 1:3 reduced scale.
(Fourier filter: 0.7-40 Hz)

The signals presented in the Figure 2.12 correspond to the target signals of the Earthquake 100%, which the shaking table should provide. The shaking table was calibrated using an inert mass equal to the total mass of the mock-up plus the foundation slab. It is noted that the mock-ups are not inert masses and, during the seismic tests, the input signals measured at the base of the mock-ups will present some deviations with respect to the target. A comparison between the expected input (target) and the real input (measured) by the shaking table in the seismic tests is therefore needed. This comparison was done here using several parameters usually adopted in seismic engineering to characterize the signals of earthquakes. All the signals were filtered by using a bandwidth Fourier filter with a frequency range between 0.7 and 25 Hz. The following peak values of the time histories were used (Cozenza and Manfredi 2000, Kramer 1996):

$$\text{Peak Ground Acceleration : } PGA = \max \left| \ddot{u}_g(t) \right| \quad (2.3)$$

$$\text{Peak Ground Velocity : } PGV = \max \left| \dot{u}_g(t) \right| \quad (2.4)$$

$$\text{Peak Ground Displacement : } PGD = \max \left| u_g(t) \right| \quad (2.5)$$

in which $\ddot{u}_g(t)$, $\dot{u}_g(t)$ and $u_g(t)$ are the time histories of accelerations, velocities and displacements, respectively, at the base of the mock-up.

The peak value is the maximum value of the amplitude occurring in a time history and is, usually, used by codes to design structures, particularly the *PGA*. This parameter is not representative of the entire history of amplitudes of the signal. For instance, the damages caused in the same structure by two earthquakes with the same *PGA* but with different duration and frequency content will not be equal, because, among others aspects, the energy applied to the structure is not the same. Thus, the measured and target input signals were also compared using integral parameters, which take into account the history of amplitudes occurring in a time history, namely (Cozenza and Manfredi 2000, Kramer 1996):

$$\text{Root Mean Square : } RMS_x = \sqrt{\frac{1}{t_d} \int_0^{t_d} x^2(t) dt} \quad (2.6)$$

$$\text{Arias Intensity : } IA = \frac{\pi}{2g} \int_0^{t_d} \ddot{u}_g(t) dt \quad (2.7)$$

$$\text{Input Energy : } E = m \int_0^{t_d} \left| \ddot{u}_g(t) \dot{u}_g(t) \right| dt \quad (2.8)$$

$$\text{Cumulative Absolute Velocity : } CAV = \int_0^{t_d} \left| \ddot{u}_g(t) \right| dt \quad (2.9)$$

$$\text{Specific Energy Density : } SED = \int_0^{t_d} \left| \dot{u}_g(t) \right|^2 dt \quad (2.10)$$

in which x is the time history of accelerations, velocities or displacements, g is the gravity acceleration, m is the mass of the mock-up and t_d is the duration of the time history.

In the seismic tests of the non-strengthened mock-up, the peak values of the measured input signals show a deviation, on average, of about 14% and 6%, with respect to the target, in the North-South (longitudinal) and East-West (transversal) directions, respectively (Figure 2.13). Considering the Root Mean Squares (Figure 2.14a), in which the peak value has a lower contribution, the deviations decrease and are, on average, equal to 7% and 6% in the longitudinal and transversal directions, respectively. In the seismic tests of the strengthened mock-up, the signals in the longitudinal direction of the Earthquakes 100% and 150% present *PGA*'s significantly higher than the targets ones (Figure 2.13). However, the deviations in the Root Mean Squares (Figure 2.14a) are, on average, equal to 12% and 10% in the longitudinal and transversal directions, respectively. The higher deviations occur in the accelerations, as can be observed by *PGA* and *IA* parameters (Figure 2.14b), mainly in the last two earthquakes (125% and 150%) of the strengthened mock-up. Taking into account the Input Energy (Figure 2.14c), the average of the input signal deviations are about 6% and 18% for the non-strengthened and strengthened mock-ups, respectively. In conclusion, the deviations are within reasonable limits, with higher deviations for the seismic tests of the strengthened mock-up, mainly in the longitudinal direction and in the seismic tests with amplitude equal to 125% and 150%. It is noted that the maximum target amplitude was 150% (as this value was only estimated in the beginning) and the shaking table was calibrated for the Earthquake 100% with an inert mass. For more information about the comparison between the target and measured input signals see Annex A.

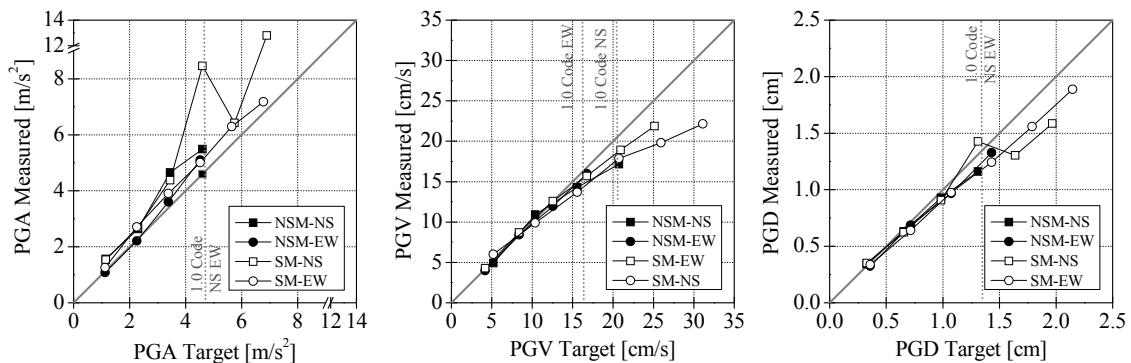


Figure 2.13 – Comparison between the target and measured input signals using the peak values of the time histories.

(Fourier filter: 0.7-25 Hz; NSM: Non-Strengthened Mock-up; SM: Strengthened Mock-up; NS: North-South (longitudinal); EW: East-West (transversal))

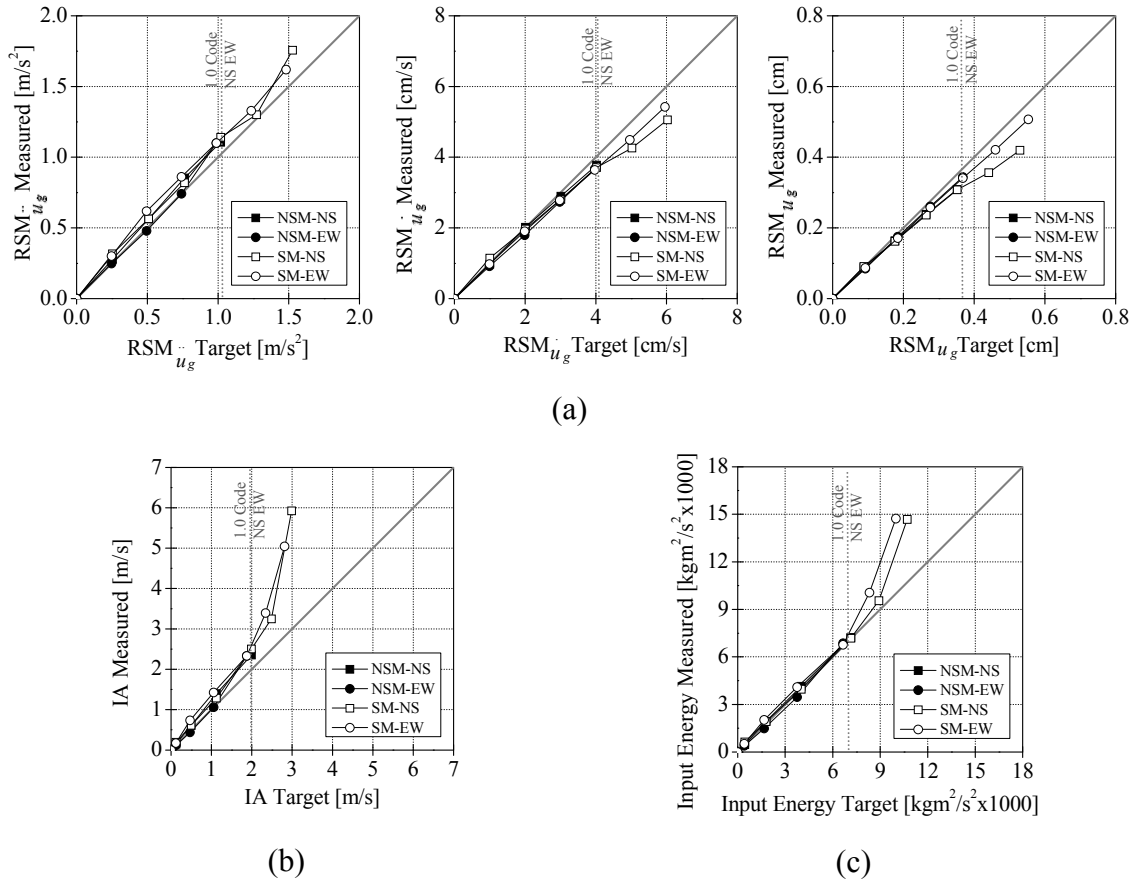
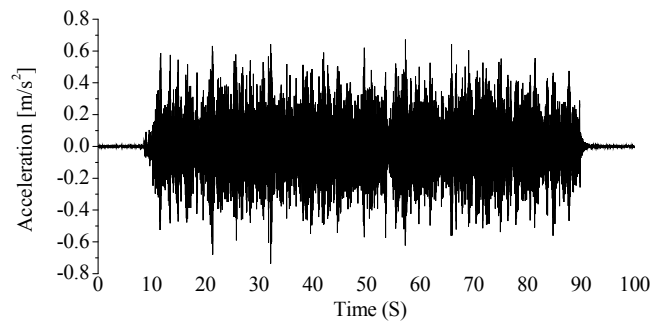
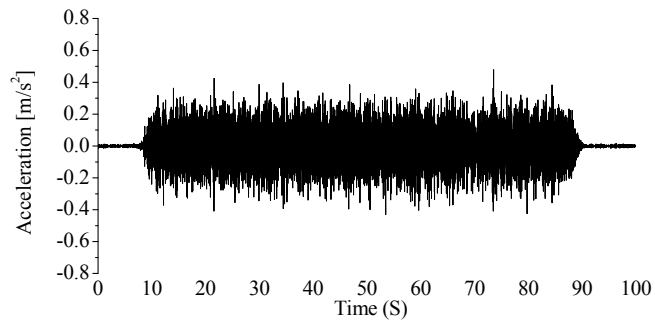


Figure 2.14 – Comparison between the target and measured of the input signals using the integral parameters: (a) Root Mean Squares; (b) Arias Intensity; (c) Input Energy. (Fourier filter: 0.7-25 Hz; NSM: Non-Strengthened Mock-up; NSM: Strengthened Mock-up; NS: North-South (longitudinal); EW: East-West (transversal))

The input signals used in the dynamic identification tests (Figure 2.15) correspond to a “white noise”, with large frequency range and low amplitude, aiming at avoiding further damage in the mock-ups. These signals are artificial and were applied directly at the base of the mock-ups without scale factors, because they are only intended to identify the dynamic properties and do not have influence on the seismic tests. The duration of the signals are about 80 s (intense phase) and the maximum amplitudes are about 0.8 m/s^2 and 0.4 m/s^2 in the longitudinal and transversal directions, respectively. The amplitude of the signal applied in the longitudinal direction is, approximately, the double of the amplitude of the signal in the transversal direction, because the mock-ups are much stiffer in the longitudinal direction.



(a)



(b)

Figure 2.15 – Input signals of the dynamic identification tests: (a) North-South (longitudinal) direction; (b) East-West (transversal) direction.

2.8 Characterization of the materials

The load-bearing walls of the mock-ups were built with limestone units from the South of Portugal and lime mortar. The technique of construction and the material properties were defined taking into account the information available in the literature (e.g. Pinho 2000) and the experience of the masons involved in the construction, which are experts in “gaioleiro” buildings. During the construction of the non-strengthened mock-up, 66 specimens of lime mortar ($0.040 \times 0.040 \times 0.160 \text{ m}^3$) and 31 specimens of limestone units ($0.050 \times 0.050 \times 0.125 \text{ m}^3$) were also prepared, aiming at characterizing the mechanical properties. The lime mortar is composed by lime, cement and sand in the proportions of 2:1:6 by volume.

Tests of flexural and compressive strength of the lime mortar, according to the standard NP EN 196-1 (2006), and tests of compressive strength of the limestone, according to the standard ASTM D2938-95 (ASTM Standard D2938-95 2002), were carried out at LNEC. The age of the mortar specimens is over 28 days. Table 2.6 presents the average value and the coefficient of variation (CV) of the results obtained for the specimens. The flexural and compressive strength of the lime mortar is on average equal to 0.65 MPa and 2.47 MPa, respectively. The compressive strength of the limestone is on average equal to 131 MPa. As a reference, Toumbakari (2002) carried out tests on lime

mortar specimens, with proportions 2:1:11 (lime, cement, sand) by volume, and limestone obtained from demolished buildings in Belgium. The mortar was prepared to reproduce a relatively “weak” historic mortar. The flexural and compressive strength obtained in the mortar tests were 1.20 MPa and 3.40 MPa, respectively. In the limestone tests, the compressive strength obtained was equal to 55 MPa. Valluzzi et al. (2004) carried out also tests in limestone of the North-Eastern of Italy and mortar composed by lime, natural hydraulic lime and sand (3:1:12), with a ratio lime/sand equal to 1:3 and a ratio water/lime equal to 0.5 by volume. The compressive strength of the limestone was approximately 160 MPa and compressive strength of the mortar, after 28 days, was 1.57 MPa.

Table 2.6 – Strength stress of the lime mortar and limestone specimens.

	Lime mortar		Limestone
	Flexural	Compressive	Compressive
Average of the strength [MPa]	0.65	2.47	131
CV [%]	16	16	25

In order to determine the Young’s modulus, the Poisson ratio, the compressive and the tensile strengths of masonry, ten wallets were prepared for axial and diagonal compression tests (Mendes et al. 2010 [2]). The specimens are squared with 1.0 m by 1.0 m and the thickness is equal to 0.17 m (thickness of the walls of the mock-up at 1:3 reduced scale). In these tests, a static hydraulic system was used, in which the applied load, with displacement control, was measured directly. Two vertical and two horizontal LVDT’s were used in each surface. Figures 2.16 and 2.17 present the strain-stress diagrams, considering the average of the LVDT’s, for the uniaxial and diagonal compression tests, respectively.

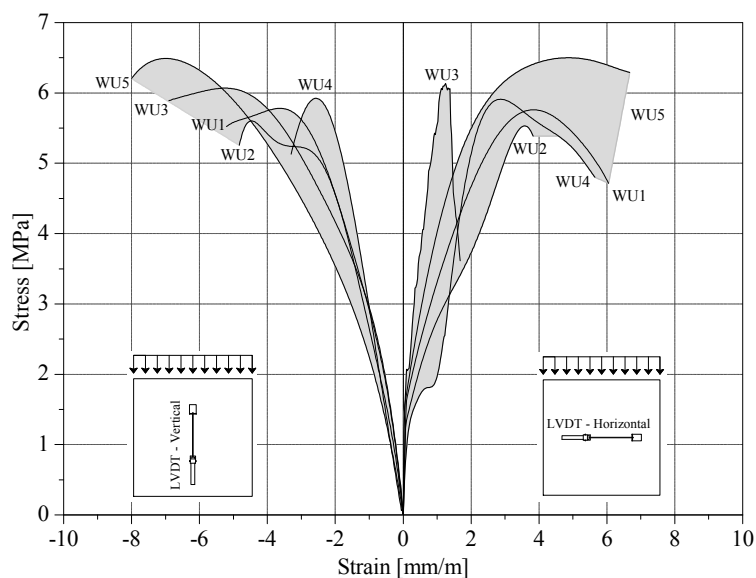


Figure 2.16 – Strain-stress diagrams of the uniaxial compressive tests.

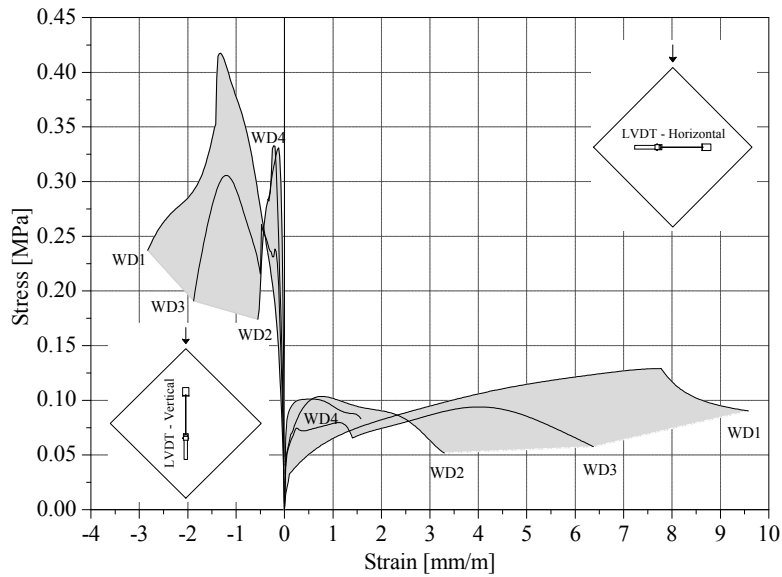


Figure 2.17 – Strain-stress diagrams of the diagonal compressive tests.

Table 2.7 presents the results obtained in the axial compression tests. The compressive strength is on average equal to 6.00 MPa and was determined assuming a uniform stress in the cross-section of the wallets. This value is rather high with respect to the one obtained by Silva and Soares (1997) (0.8 MPa to 1.5 MPa), which is explained by the usage of single leaf walls, higher strength mortar and larger size stone units. The Young's modulus and Poisson ratio were calculated from the variation of the strains (average of the vertical and horizontal LVDT's) between 0.05 and 0.20 of the compressive strength. The average of the Young's modulus is equal to 3.37 GPa. The last three specimens presented unexpected values of Poisson ratio. Thus, due to lack of data, this parameter was not statically analyzed. The Young's modulus presents a significant coefficient of variation (20%) and the value of the last specimen WU5 (2.51 GPa) appears to deviate markedly from other specimens of the sample. The Grubbs and Dixon criteria for testing outliers (ASTM Standard E178-02 2002) were used, indicating that the Young's modulus of the specimen WU5 should not be considered as an outlier.

Table 2.7 – Results of the axial compression tests.

Specimen	Specific mass [kg/m ³]	Compressive strength [MPa]	Young's modulus [GPa]	Poisson ratio
WU1	2182	5.807	4.07	0.23
WU2	2135	5.554	3.32	0.20
WU3	2171	6.173	3.97	0.09
WU4	2141	5.925	3.00	0.44
WU5	2182	6.561	2.51	0.05
Average	2162	6.004	3.37	-
CV [%]	1	6	20	-

In the standard interpretation of the diagonal compression test, the diagonal tensile strength is obtained by assuming that the specimen collapses when the principal stress, σ_I , at its centre achieves its maximum value. According to Frocht theory (Frocht 1931), as reported by Calderini et al. (2009) [1], the principal stresses at the centre of the specimen are equal to: σ_I (tensile strength) = $0.5 P/A$ and $\sigma_{II} = -1.62 P/A$, in which P is the load and A is the transversal area of the specimen. Table 2.8 presents the principal stresses obtained in the diagonal compression tests. The average of the tensile strength is equal to 0.10 MPa, which is rather low. It is noted that according to Grubbs and Dixon criteria the principal stresses of the specimen WD1 are outliers and were not considered in the average of the results.

Table 2.8 – Results of the diagonal compression tests.

Specimen	Specific mass [kg/m ³]	Tensile strength (σ_I) [MPa]	Principal stress (σ_{II}) [MPa]
WD1	2118	0.130 [†]	-0.422 [†]
WD2	2129	0.104	-0.338
WD3	2153	0.096	-0.310
WD4	2159	0.103	-0.332
WD5	2141	0.098	-0.318
Average*	2140	0.100	-0.325
CV [%]	1	4	4

([†] outlier according to Grubbs and Dixon criteria; * discarding outliers)

2.9 Final remarks

In this Chapter a description of the setup for the shaking table tests was done, including the selection of the prototype, the definition of the mock-ups at 1:3 reduced scale, the instrumentation of the mock-ups, the generation and comparison of the input signals with respect to the target ones and the characterization of the mechanical properties of the masonry walls. Two mock-ups were considered – non-strengthened and strengthened – with the latter resulting from strengthening the damage non-strengthened mock-up after testing. The non-strengthened mock-up has four floors, two facades with openings, two gable walls without openings and timber floors. After the first series of seismic tests the non-strengthened mock-up was repaired, strengthened and tested again. In the strengthened mock-up steel angles and plates at the floor levels were used. In the two top floors, steel cables were also installed for tying opposite facade walls.

The seismic tests were performed at the LNEC 3D shaking table by imposing accelerograms, with increasing amplitude, in two horizontal orthogonal directions inducing in-plane and out-of-plane response of the mock-ups. Before the initial and subsequent seismic tests, dynamic identification tests were also done, aiming at evaluating the decrease of the natural frequencies with the seismic tests. In the next Chapter, the results of the seismic and dynamic identification tests are presented.

Shaking table tests results

3.1 Introduction

In this Chapter, the results of the tests carried out at LNEC 3D shaking table are presented. It is noted that two types of tests were done: (a) seismic tests, in which the seismic action was applied with increasing amplitude in two uncorrelated orthogonal directions; (b) dynamic identification tests, aiming at evaluating the decrease of the dynamic properties of the mock-ups. An important aspect to take into account is the initial condition of the mock-ups. Several seismic tests were done on the same mock-up without repairing and re-establishing the initial conditions. This means that the mock-ups accumulated damage along the seismic tests. Although the different initial conditions of the mock-ups can influence the results, the costs involved in the shaking table tests of mock-ups are high and this procedure is commonly used. This procedure of testing reduces significantly the costs of the tests and is acceptable, particularly when the objective is to compare different techniques of construction or strengthening solutions.

The methodologies for analysing the results are first presented here, followed by the crack patterns, and the different results obtained in the dynamic identification tests and seismic tests. A comparison of the performance of the mock-ups (non-strengthened and strengthened) is also presented. Finally, the conclusions of the experimental program are provided.

3.2 Methodologies used in the analyses of the results

A total of 80 accelerometers (20 for each wall) were used to measure the response of the mock-ups, both in the seismic and in the dynamic identification tests (Figure 2.10). The time histories of acceleration were obtained directly, from the accelerometers, which provide the full range of accelerations experienced by each wall. The time histories of velocity and displacement can be indirectly obtained from the integration of the time histories of acceleration. These are the three main parameters of the mock-ups response that are obtained from the accelerometers. However, different processing of the signals can be adopted to evaluate the behaviour of the mock-ups. The seismic performance of the mock-ups can be experimentally studied using simple parameters, such as the peak values of acceleration, velocities or displacements, or using more complex techniques, such as the evolution of the dynamic properties as a function of the applied seismic action. Next, the adopted methodologies for processing the signals and for evaluating the seismic performance of the mock-ups in the seismic and identification tests are presented.

3.2.1 Dynamic identification tests

The dynamic identification tests aim at estimating the dynamic properties, namely the frequencies, mode shapes and damping ratios of the mock-ups. Dynamic identification tests before the first seismic test (DI 0) and after each seismic test were carried out, aiming at evaluating the variation of the dynamic properties of the mock-ups along the testing as a function of the seismic action amplitude applied. The change of the dynamic properties, such as the decrease of the frequencies, is related to the change of the stiffness of the structure and, consequently, to the damage concept usually used to define the degradation of the mechanical and strength properties of materials or structural elements. Thus, the main objective of these tests is to define a damage indicator based on the decrease of frequencies and to compare the seismic performance of the mock-ups.

The experimental modal identification techniques can be divided in three main groups (Ramos 2007): (a) input/output vibration tests, where the excitation applied on the structure and the vibration response are measured; (b) output only vibration tests, where only the vibration response is measured during the service conditions of the structure; (c) free vibration tests, where the structure is forced to an initial deformation and is then quickly released. Here, the identification of the modal properties of the mock-ups was carried through input/output vibration tests, in which the excitation was applied by the shaking table in two orthogonal directions. The input signals applied at the base of the mock-ups in the dynamic identification tests correspond to a “white noise” and are uncorrelated (Figure 2.15).

Several methods can be used to identify the dynamic properties through input/output vibration tests, such as the Peak Picking, Circle Fit, Rational Fraction Polynomial or Complex Exponential. These methods are classified according the type of domain (frequency or time domain), the type of formulation (indirect or direct), the type of estimates (global or local), the number of the degrees of freedom (SDF - Single Degree of Freedom or MDF - Multiple Degree of Freedom), the number of the input/output signals (SISO - Single Input and Single Output; SIMO - Single Input and Multiple Output or MIMO- Multiple Input and Multiple Output). For details about the methods, see Caetano (2000).

Taking into account that in the dynamic identification tests two inputs and eighty outputs were measured (MIMO), the Rational Fraction Polynomial (RFP), also called Orthogonal Polynomial (OP), method was used. This method is developed in the frequency domain and the theoretical expression used for the Frequency Response Functions (FRF's) is based on the rational fraction polynomial of the response and excitation. In this formulation a viscous damping model is adopted and the unknown polynomial coefficients are obtained from a curve-fitting process. After obtaining the polynomial coefficients, the next stage of the modal analysis involves the calculation of the modal parameters. The modal parameters are obtained by solving the polynomial expressions (numerator and denominator) of the theoretical equation of the FRF's. The natural frequencies ω_i and the damping ratios ζ_i , for each mode i , are obtained from the denominator and the complex modal constants A_i are obtained from the numerator of the FRF's. The shape of the modes ϕ_i (eigenvectors) is derived from the modal constants A_i . In this thesis, the modal parameters were only identified for defining a quantitative measure of the damage of the mock-ups. Details on the calculation of the FRF's and the experimental modal parameters are given in Bendat and Piersol (2000), Ewins (2000), Maia and Silva (1997) and Rodrigues (2004).

In the dynamic identification tests, the input and output acceleration signals were measured at the shaking table and at the mock-ups, respectively, with sampling frequency equal to 250 Hz. The signals were firstly processed aiming at obtaining the dynamic properties of the mock-ups, namely by removing the DC components (0 Hz) and by filtering using a lowpass Fourier filter with a cutting frequency equal to 40 Hz. Thus, the frequency of Nyquist is equal to 125 Hz, which is higher than the frequency of cutting from the applied filter. In the estimation of the FRF's, 2^{10} (1024) samples per frame filled with a minimum number of zeros (padding) and Hanning windows with overlap equal to $2/3$ were used, aiming at decreasing the deviation of the FRF's and at allowing the application of the Fast Fourier Transform algorithm. This set of operations to process the signals was carried out in the software LNEC-SPA (Mendes 2008).

Once obtained the dynamic properties of the mock-ups, the variation of the frequency of the modes can be used to quantify the evolution of the damage. Taking into account the fundamental relation between natural frequency, mass and stiffness of a single degree of freedom system (Chopra 2001):

$$\omega_{i,n}^2 = \frac{K_{i,n}}{M_{i,n}} \quad (3.1)$$

$$(2\pi f_{i,n})^2 = \frac{K_{i,n}}{M_{i,n}} \quad (3.2)$$

where ω is the natural frequency, K is the generalized stiffness, M is the generalized mass and f is the frequency of mode n in the dynamic identification test i . Assuming isotropic damage (Lemaitre and Desmorat 2005) between the first dynamic identification (DI 0) and the dynamic identification n , as in Candeias (2008),

$$K_{i,n} = (1 - d_{2,i,n}) K_{i,0} \quad (3.3)$$

and the d_2 damage indicator of the mode i in the dynamic identification n is equal to:

$$d_{2,i,n} = 1 - \frac{M_{i,n} f_{i,n}^2}{M_{i,0} f_{i,0}^2} \quad (3.4)$$

Assuming that the modes shapes do not change significantly throughout the testing, the damage indicator d_2 can be approximated by:

$$d_{2,i,n} = 1 - \left(\frac{f_{i,n}}{f_{i,0}} \right)^2 \quad (3.5)$$

where the damage indicator d_2 is proportional to the quadratic ratio between the frequency of the n and the first (DI 0) dynamic identification tests, i.e. the damage is a linear function of the variation of the stiffness. The damage indicator ranges from zero (initial condition and theoretical absence damage) to one (collapse of the structure or full damage). This formulation can be linked to simple models where damage occurs by breakage of parallel fibres such as pure tension. The first transversal mode of the mock-ups, which provides the highest contribution to the dynamic behaviour, is mainly related to the bending stiffness. The bending stiffness change has a cubic relationship with the damage, understood here as a reduction of the cross section by losing the extreme fibres. Taking into account the variation of the bending stiffness, the damage indicator $d_{2/3}$ varies according to the following equation:

$$d_{2/3,i,n} = 1 - \left(\frac{f_{i,n}}{f_{i,0}} \right)^{\frac{2}{3}} \quad (3.6)$$

As the dynamic behaviour of the mock-ups depends on several modes, which are associated to different types of stiffness, an intermediate relationship between variation of stiffness and damage is adopted next. Therefore, for simplicity, the damage indicator d is assumed to be linearly proportional to the ratio between the frequency n and the first frequency (DI 0) in the dynamic identification tests:

$$d_{i,n} = 1 - \frac{f_{i,n}}{f_{i,0}} \quad (3.7)$$

Figure 3.1 presents the three damage indicators (d_2 , $d_{2/3}$ and d) as a function of the seismic amplitude, assumed to be proportional to the frequency change. The damage indicator progress is significantly different in the three models. For instance, if the seismic amplitude is equal to half the one that causes the collapse of the structure (damage indicator equal to 1), the level of damage is equal to 0.75, 0.50 and 0.37 according the d_2 , d and $d_{2/3}$ formulations, respectively. The scales of damage will be also discussed in the analysis of the results of the dynamic identification tests of the non-strengthened mock-up.

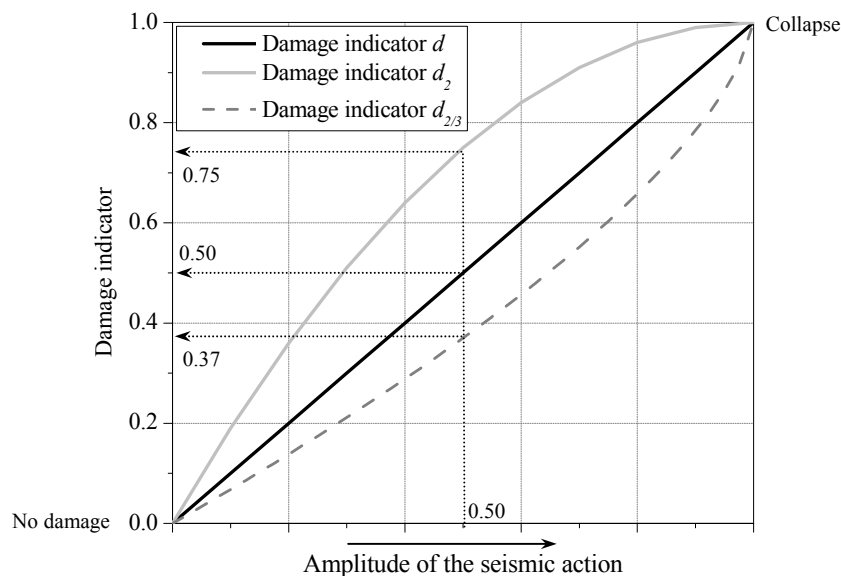


Figure 3.1 – Theoretical evolution of the damage indicator as function of the amplitude of the seismic action.

As previously referred, the formulation used to evaluate the damage is only valid if the mode shapes do not change significantly along the testing. Therefore, the Model Assurance Criterion (MAC) was used to compare the change in the modes shapes Ewins (2000):

$$MAC_{u,d} = \frac{\left| \sum_{j=1}^m \phi_j^u \phi_j^d \right|^2}{\sum_{j=1}^m (\phi_j^u)^2 \sum_{j=1}^m (\phi_j^d)^2} \quad (3.8)$$

where ϕ^u and ϕ^d are the eigenvectors for two different dynamic identification tests and m is the number of degrees of freedom. The MAC value ranges from zero to one, corresponding to the absence of correlation or perfect match between the two eigenvectors. The eigenvectors were normalized in a way that the maximum value of the modal displacement is equal to one.

Finally, the experimental vulnerability curves were obtained, relating the damage indicator d for the estimated modes with the seismic amplitude applied at the base. The amplitude of the seismic action was characterized by the nominal peak ground acceleration PGA_{no} (Equation (2.3)) and Input Energy E (Equation(2.8)). The mock-up does not have the same initial conditions, i.e. before application of the seismic input the mock-up presents cumulative damage. Therefore, the damage observed in the nominal seismic test k is not only caused by the seismic action applied in this particular test, but it is also related with the excitation of the previous seismic tests. Then, the characterization of the input series through the peak values must be adjusted taking into account the test sequence. Equation (3.9) presents a proposal, adapted from Coelho et al. (1999), to determine the equivalent PGA (PGA_{eq}) through the use of the energy concept:

$$PGA_{eq,k} = \left(\frac{E_{ac,k}}{E_{no,k}} \right)^{0.5} PGA_{no,k} \quad (3.9)$$

in which E_{ac} is the accumulated energy until the actual test k , and E_{no} and PGA_{no} are the nominal energy and peak ground acceleration in the test k , respectively. This proposal does not take into account the response of the mock-up (damage) observed in the test k . Furthermore, this proposal is only valid for a test planning in which the seismic action is increased by scaling the accelerograms, and in which the damage and the PGA_{no} increase with testing. It is noted that Equation (3.9) corresponds to the theoretical relationship between PGA and Input Energy (target signals). In the subsequent analysis, the PGA was updated taking into account the real relationship between PGA and Input Energy applied at the base of mock-ups through the regression of potential curves.

3.2.2 Seismic tests

The equation of motion of a Single Degree Freedom (SDF) system subject to a ground acceleration $\ddot{u}_g(t)$ (Chopra 2001):

$$m\ddot{u}(t) + c\dot{u}(t) + ku(t) = -m\ddot{u}_g(t) \quad (3.10)$$

shows that the linear dynamic behaviour depends on the mass m , damping c and stiffness k of the system. Furthermore, the response of the SDF system is given in terms of relative acceleration $\ddot{u}(t)$, relative velocity $\dot{u}(t)$ and relative displacement $u(t)$ at each instant of time t . In the seismic tests of the mock-ups, the total accelerations were obtained directly from the accelerometers, while the total velocities and displacements were obtained from the integration, in the frequency domain, of the acceleration. Finally, the relative velocities and displacements of the mock-ups were obtained subtracting the respective velocities and displacements at the base of the mock-ups. It is noted that 80 accelerometers (5 at each floor level of each wall) were used to measure the response of the mock-ups (Figure 2.10) and that four and six seismic tests were carried out on the non-strengthened and strengthened mock-ups, respectively (in the Earthquake 150% of the strengthened mock-up, the response was not measured). Thus, a total of 960 and 1200 signals of the response of the mock-ups (acceleration, velocities and displacements) were processed. In all signals the DC components (0 Hz) was removed and a bandpass Fourier filter (0.7-25 Hz) was applied. The highest frequency of cutting was defined aiming at including the modes with highest contribution for the dynamic behaviour of the mock-ups and at reducing the noise associated to the high frequencies.

As the number of measured signals is rather high and it is difficult to use all signals to compare the performance of the mock-ups along the testing program, the response of the mock-ups was analysed by merging the signals of acceleration and displacements (or relative displacements) at the floor levels. Thus, the performance of the mock-ups was evaluated by using only four parameters of response at the floor levels for each masonry wall.

The first parameter of the response of the mock-ups concerns the average of the maximum amplification of acceleration ($Amplification_{acc,ave}$) at the floor level f :

$$Amplification_{acc,ave,k,f} = \frac{\sum_{j=1}^5 \max \left| \frac{\ddot{u}(t)_{k,f,j}}{PGA_k} \right|}{5} \quad (3.11)$$

where the PGA is the peak ground acceleration in the respective direction and j is the accelerometer number at the floor levels in the seismic test k . As this parameter includes also the vertical alignments of accelerometers at the corner, it can be assumed as a global parameter of the response in the two main directions of the mock-ups.

The average of maximum displacements (u_{ave}) at the floor levels f for the seismic tests k is given by:

$$u_{ave,k,f} = \frac{\sum_{j=1}^5 \max |u(t)_{k,f,j}|}{5} \quad (3.12)$$

The parameter u_{ave} is also a global parameter of the response in terms of displacement in the longitudinal and transversal directions of the mock-ups.

It is expected that the masonry walls, mainly in the non-strengthened mock-up, present a significant out-of-plane deformation with respect to the corners ($u_{corners}$) and this local effect should be evaluated. Figure 3.2 presents a scheme of the out-of-plane deformation with respect to the corners, where it is observed that $u_{corners}$ correspond to displacement normal to the plane defined by the corner displacements, in the longitudinal or transversal direction, assuming an infinitely stiff floor. Furthermore, $u_{corners}$ are measured only for the three central accelerometers at each floor level.

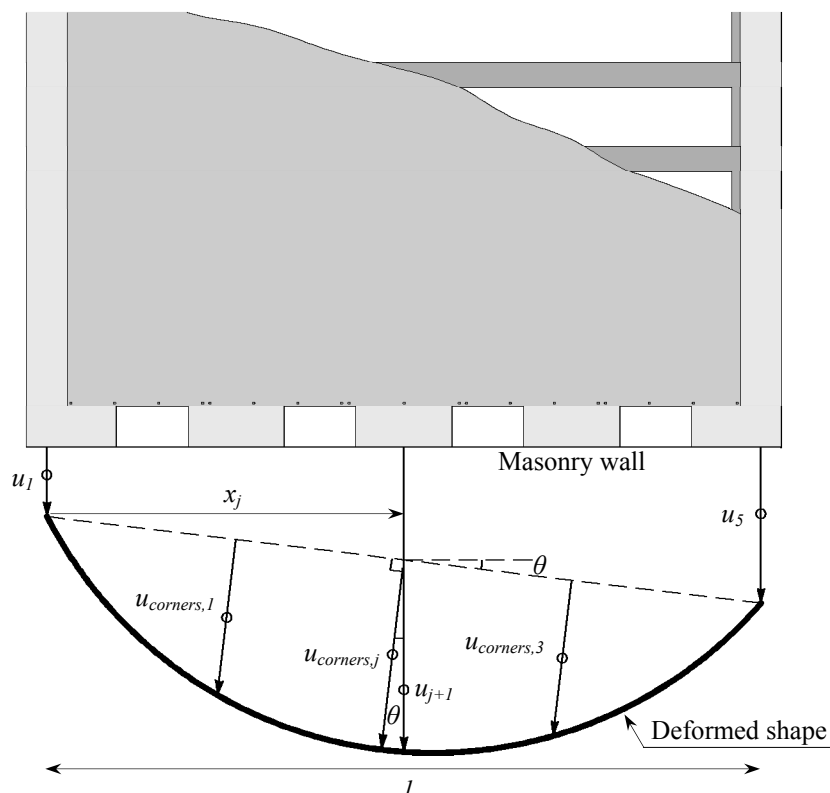


Figure 3.2 – Scheme of out-of-plane displacements relative to the corners ($u_{corners}$).

For each instant of time t , the out-of-plane displacements with respect to the corners are calculated by:

$$u(t)_{corners,k,f,j} = \left(u(t)_{k,f,j+1} - u(t)_{1,k,f} - \frac{u(t)_{5,k,f} - u(t)_{1,k,f}}{l} x_{k,f,j} \right) \cos \theta_{k,f}(t) \quad (3.13)$$

where $u(t)_{k,f,j+1}$ is the displacement in the longitudinal or transversal direction of the mock-up at the floor f in seismic test k and j is the vertical alignment of accelerometers ($j = 1$ to 3), $u(t)_1$ and $u(t)_5$ are the displacements in the longitudinal or transversal direction of the first and last corners, respectively, x is the distance from the first corner to the vertical alignment j and l is the distance between corners (Figure 3.2).

The local deformation of the masonry walls is given in terms of average of maximum out-of-plane displacements with respect to the corners at the floor level f and for each seismic test k ($u_{ave,corners}$):

$$u_{ave,corners,k,f} = \frac{\sum_{j=1}^3 \max |u(t)_{corners,k,f,j}|}{3} \quad (3.14)$$

Finally, the drift (or interstory drift) in the plane of the masonry, at the instant of time t , between the floors j and $j-1$, in percentage, is given by:

$$Drif(t)_{in-plane,f \rightarrow f-1,a,k} = \left(\frac{u(t)_{in-plane,f,a,k} - u(t)_{in-plane,f-1,a,k}}{h_f} \right) \times 100 \quad (3.15)$$

where $u(t)_{in-plane,f,a,k}$ is the in-plane displacement at the floor level f in the seismic test k for the a (left or right) vertical alignment of accelerometers oriented in the plane of the masonry wall in study, and h is the interstory height. Here, the in-plane drifts are given in terms of average of the maximum drifts obtained from the vertical alignments on the left and right of the masonry walls ($Drift_{in-plane,ave}$):

$$Drif(t)_{in-plane,ave,f \rightarrow f-1,k} = \frac{\max |Drif(t)_{in-plane,f \rightarrow f-1,left,k}| + \max |Drif(t)_{in-plane,f \rightarrow f-1,right,k}|}{2} \quad (3.16)$$

The four parameters of the response of the mock-ups at the floors levels ($Amplification_{acc,ave}$, u_{ave} , $u_{ave,corners}$ and $Drift_{in-plane,ave}$) will be related to the nominal peak ground acceleration (PGA_{no}) applied at the base.

3.3 Crack patterns

The evolution of the damage along the testing program is fundamental in the assessment of the seismic performance of the mock-ups and, although the seismic action was not increased until collapse of the mock-ups, the cracks allow to identify the collapse mechanism. Furthermore, the damage observed as crack patterns should be related to the quantitative results obtained from the dynamic identification and seismic tests, giving further reliability to the conclusions. Therefore, the cracks patterns are the first results of the shaking table tests to be discussed. It is noted that the seismic action was applied in two orthogonal directions, inducing simultaneously in-plane and out-of-plane response of the mock-ups, and making the analysis of results rather complex.

Before the first seismic test, the non-strengthened mock-up did not present any relevant damage that could influence its subsequent behaviour. In the first seismic tests, the non-strengthened mock-up does not present significant damage. Only a few cracks are observed (Figure 3.3). However, as shown in the results of the dynamic identification tests, after this seismic test the non-strengthened mock-up presents a significant reduction in the frequency of the first mode. This may be related to micro cracks that occurred in the mortar during the Earthquake 25%, which are not visible in the end of the seismic test due the self-weight action or floor action. During the dynamic identification (DI 1) the micro cracks can decrease the frequency of the first transversal mode. During the Earthquakes 50% and 75% the damage increases, as expected, concentrating in the spandrels. The corners of the openings are points of concentration of stress and, consequently, cracking near to these points occurs. In the Earthquake 75%, some separation between the floors at the third floor and the East gable wall is also observed. The gable walls do not present significant damage.

After Earthquake 100%, the mock-up presents a high concentration of damage at the facades (Figure 3.3). Almost all the spandrels present damage caused by diagonal tension, related to the in-plane behaviour of the facades (Figure 3.4a). Furthermore, almost all piers at the fourth floor present horizontal cracks, either at the ends or within the height of the element (Figure 3.4b). The first horizontal cracks are mainly related to the in-plane behaviour of the facades, with in-plane rocking of the piers. On the other hand, the horizontal cracks within the height of the element are mainly related to the out-of-plane bending of the piers. It is known that the vertical compressive stress is favourable to the behaviour of the masonry under horizontal loads, preventing in-plane and out-of-plane collapse mechanisms. Taking into account that the axial force at the top of the mock-up is low, the piers at the fourth floor are more vulnerable to the horizontal loads, as shown in the cracks patterns. Contrarily to what is observed in the facades, the gables walls do not present any significant damage. The timber floors and corners do not also present any damage and the MDF panels remain connected to the timber joists.

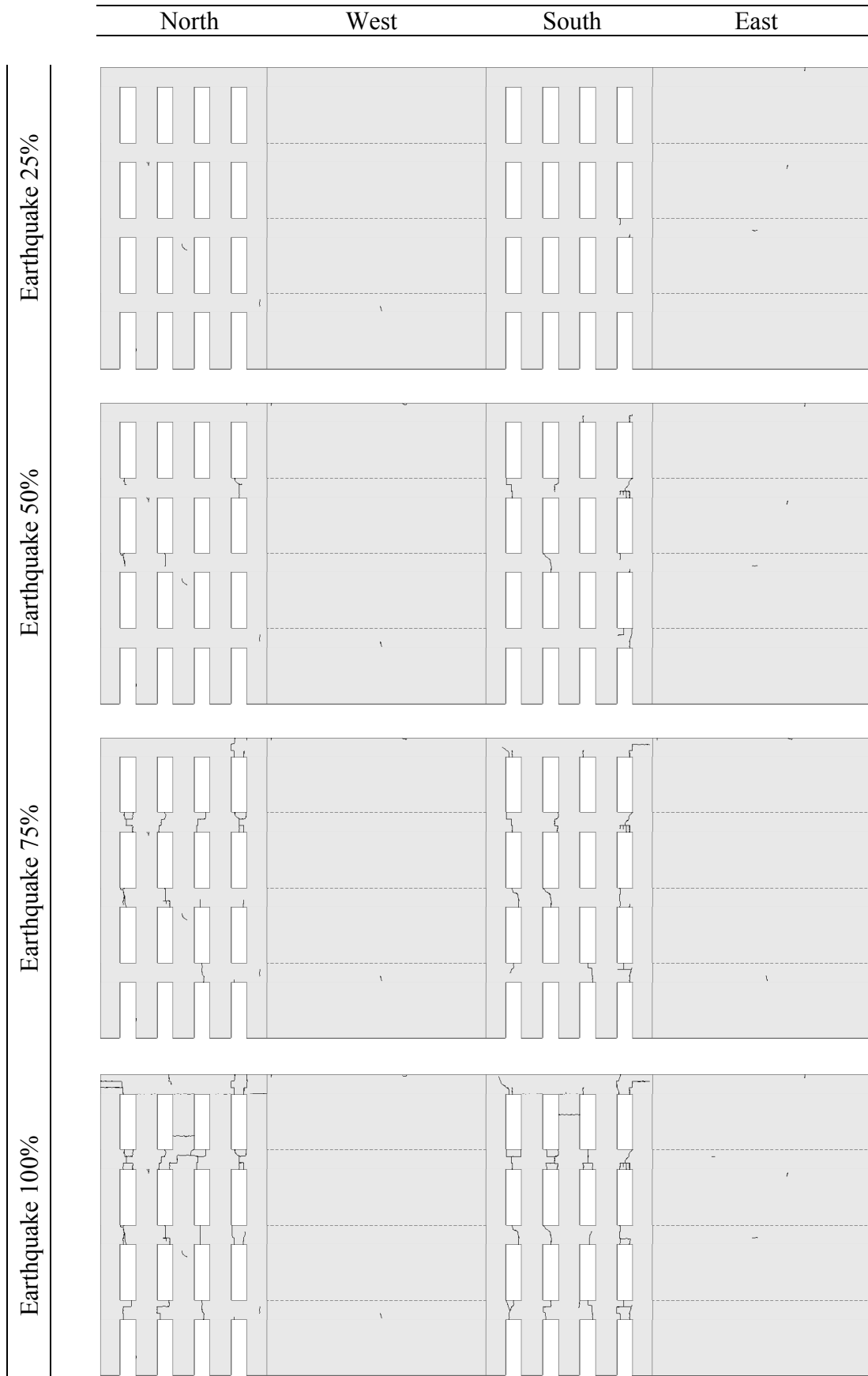


Figure 3.3 – Crack patterns of the non-strengthened mock-up: Earthquake 25% - 100%.

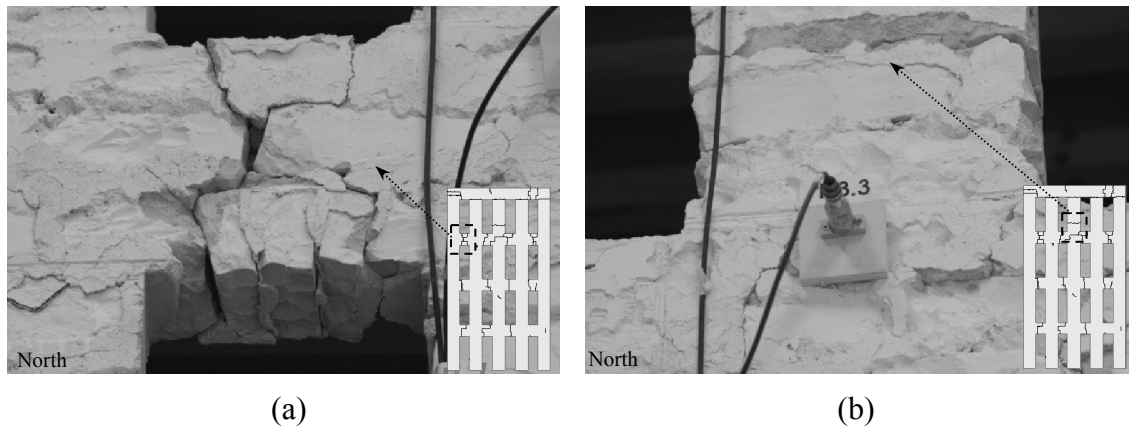


Figure 3.4 – Examples of the damage for the non-strengthened mock-up (Earthquake 100%): (a) spandrel; (b) pier.

The non-strengthened mock-up (Earthquake 100%) presents substantial damage, corresponding to a grade 3 for masonry buildings according to the European Macroseismic Scale 1998 (Grünthal 1998). It would be convenient to increase the seismic amplitude, aiming at obtaining severe damage in the mock-up and, consequently, at exploring the mechanisms that lead to collapse. However, the non-strengthened mock-up was subsequently used to test a strengthening technique and no further seismic test was carried out. According to the damage observed in the Earthquake 100% and considering the weak connection between floors and facades, it is expected that, by increasing the seismic amplitude, the damage concentrates at the spandrels and top piers. This would lead to partial or global collapse of facades, which is common in this type of buildings and typically observed in earthquakes.

As previously mentioned, after Earthquake 100% the non-strengthened mock-up was repaired, aiming at re-establishing its initial condition. However, the crack pattern of the strengthened mock-up presents a horizontal crack at the central pier of the North facade for the Earthquake 25% (Figure 3.5), leading to the conclusion that the non-strengthened mock-up was not adequately repaired in this area. Except for the horizontal crack with small width, after the Earthquake 25% the strengthened mock-up does not present any damage and, as shown later from the dynamic identification tests, the frequency of the first transversal mode exhibits a very low decrease.

After the Earthquakes 50% and 75%, the strengthened mock-up presents crack patterns significantly different from the ones obtained for the non-strengthened mock-up. Contrarily to the observed in the non-strengthened mock-up, in which several spandrels present damage (Figure 3.3), after Earthquake 75% the facades of the strengthened mock-up present low damage at the spandrels and only a few horizontal cracks at the two top floors (Figure 3.5). The two horizontal cracks observed in the piers at the middle of the South facade may be related with some initial damage, as a local mode at the third floor of the South facade will be presented later. Furthermore, after Earthquake 75% the East gable wall presents a horizontal crack at the top.

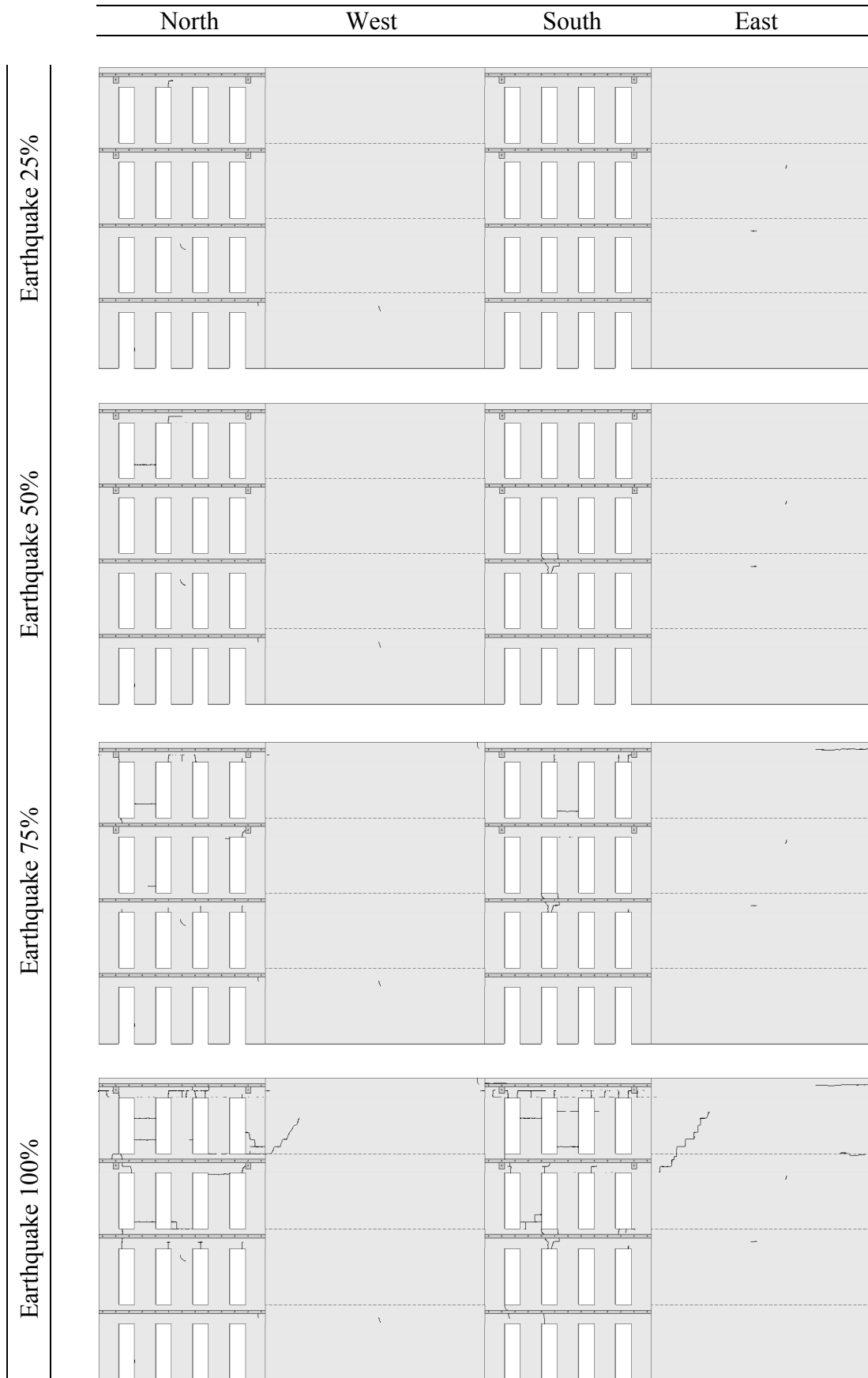


Figure 3.5 – Crack patterns of the strengthened mock-up: Earthquake 25% - 100%.

After Earthquake 100%, the damage in the strengthened mock-up concentrates at the top floors, mainly at the facades. In comparison to the non-strengthened mock-up, this mock-up presents less damage at the spandrels, leading to the conclusion that the steel plates and angles improved the performance of the lintels with respect to the diagonal tension collapse mechanism. The piers of the two top floors present several horizontal cracks. This type of damage is related to the in-plane rocking and out-of-plane bending of the piers. It is noted that the strengthening elements modify the boundary condition of the piers, decreasing the out-of-plane displacements at their ends. Thus, and due to the out-of-plane inertial forces, the relative displacements between a point at the interior and the ends of piers increase, causing the observed horizontal cracks. However, these horizontal cracks present very low thickness.

During the Earthquake 100%, the gable walls of the strengthened mock-up presented significantly different behaviour from the non-strengthened mock-up. According to the crack patterns, the gable walls of the strengthened mock-up present diagonal cracks, indicating that part of the out-of-plane inertial forces of the facades were transferred by the strengthening elements to the gable walls. Furthermore, the masonry near the anchors of the steel cables presents damage, leading also to the conclusion that the steel cables are able to transfer the inertial forces from the facades to the gables walls. The timber floors do not present damage. Thus, the strengthening elements improved the seismic performance of the mock-up, reducing the damage at the spandrels, transferring inertial forces from the facades to the gable walls and, consequently, taking advantage of the strength of each structural element of the mock-up. As the strengthened mock-up presents moderate damage at this stage, in which the spandrels remain connected by the steel elements and the global collapse of the facades is not expected, a new seismic test was done (Earthquake 125%).

The crack pattern of the Earthquake 125% (Figure 3.6) is mainly an evolution of the damage observed in the previous seismic test, with concentration of damage at two top floors and increase of the diagonal and horizontal cracks at the top of the gable walls. Although the damage increases, the strengthened mock-up does not present significant damage and a final seismic test was carried out (Earthquake 150%).

After the last seismic test, the damage of the strengthened mock-up concentrates at the two top floors, with cracks at the spandrels, at the piers and at the nodes spandrel/ pier (Figure 3.6). The damage at the two first floors is low in comparison to the one observed in the non-strengthened mock-up even for Earthquake 100% (Figure 3.3). The cracks at the spandrels are mainly related to the diagonal tension caused by the in-plane behaviour of the facades. However, the spandrels remain connected by the steel strengthening elements. In the seismic test, the in-plane rocking and out-of-plane bending of the piers at the fourth floor were clearly observed. It is noted that the collapse of the central pier at the floor of the North facade may be related to the initial damage of the strengthened mock-up, because the opposite pier at the South facade did not collapse and after Earthquake 25% a horizontal crack at the pier at the North facade

was observed. Furthermore, and in contrast to what was observed in the non-strengthened mock-up, the gable walls present diagonal cracks due to the in-plane behaviour, indicating that the strengthening elements were able to transfer the out-of-plane inertial forces from the facades to the plane of the gable walls and to prevent the global collapse of the facades. The gable walls present also horizontal cracks at the third floor, which are caused by the out-of-plane response of the walls at the top of the mock-up and are related to the high out-of-plane inertial forces and low in-plane vertical forces.

The main conclusion is that the crack patterns of the two mock-ups are much different. The non-strengthened mock-up (Earthquake 100%) presents only damage at the facades, mainly at the spandrels of all floors. On the other hand, the damage of the strengthened mock-up (Earthquake 100% and 150%) is distributed among the several masonry elements of the facades (spandrels, piers and nodes spandrel/pier) and gable walls. Furthermore, the first two floors do not present serious damage. The strengthening elements were able to transfer the out-of-plane inertial of the facades to the gable walls, leading to a crack pattern of the strengthened mock-up that is typical of structures with box behaviour, in which the out-of-plane horizontal forces are transferred to the orthogonal walls, taking advantage of the strength of each structural element and improving the global seismic performance.



Figure 3.6 – Crack patterns of the strengthened mock-up: Earthquake 125% and 150%.

3.4 Dynamic identification tests

3.4.1 Non-strengthened mock-up

In the non-strengthened mock-up five dynamic identification tests (DI 0 to DI 4) were done. DI 0 and DI 4 correspond to the first (without damage) and to the final (after Earthquake 100%) dynamic tests, respectively (Table 2.2). A high coherence (close to 1) between the input and output signals were obtained for each direction, mainly for the accelerometers AA (most sensitive accelerometers). This is a good indicator of the quality of the results and several peaks in the FRF's were clearly identified.

In the first dynamic tests (DI 0) of the non-strengthened mock-up eleven mode shapes, ranging from 4.93 Hz to 33.22 Hz, were estimated (Figure 3.7): (a) three transversal; (b) six longitudinal; (c) one distortional; (d) one combined. The first mode is a transversal mode, as expected, and its frequency is equal to 4.93 Hz. The frequency of the first longitudinal mode is equal to 12.08 Hz, which is significantly higher than the frequency of the first transversal mode, because the mock-up is much stiffer in the longitudinal direction. The transversal modes are associated to the global behaviour of the mock-up and were clearly identified in the FRF's. The longitudinal modes are mainly related to the local behaviour of the facades and can be distinguished by the type of in-elevation curvature (single, double and triple). The first longitudinal mode has a low contribution of the gable walls, however, the maximum amplitudes are clearly observed out-of-plane for the facades. In this mode the two facades are in phase and present a single curvature deformed shape. On the other hand, in the second longitudinal mode the facades present also single curvature but are in contra-phase. This behaviour is related to the in-plane flexibility of the floors and to the weak connections between floors and facades. Due to the imperfections of the mock-up, the frequency of the local mode with second curvature of the North (18.65 Hz; 18.90 Hz) and South (24.14 Hz) does not present the same value. It is noted that, due to the presence of two peaks very close in the FRF's, the mode with second curvature of the North facade was not clearly identified (3rd and 4th longitudinal modes). Furthermore, a combined mode was also estimated, in which the mode with second curvature of the North facade is combined with the out-of-plane behaviour of the gable walls (transversal direction). The estimated mode with the higher frequency (33.22 Hz) corresponds to the local mode with third curvature of the South facade. For the North facade, this type of mode was not identified. Finally, a distortional mode (8.45 Hz) was also estimated, in which the facades present in-plane translations in contra-phase. This mode further demonstrates the flexibility of the floors.

The modes shapes provide indications of the expected dynamic behaviour under seismic loading. Taking into account the interpretation of the modes shapes done, it is expected that the facades present high out-of-plane displacements, with respect to the corners, in the seismic testing, which is typical of this type of buildings.

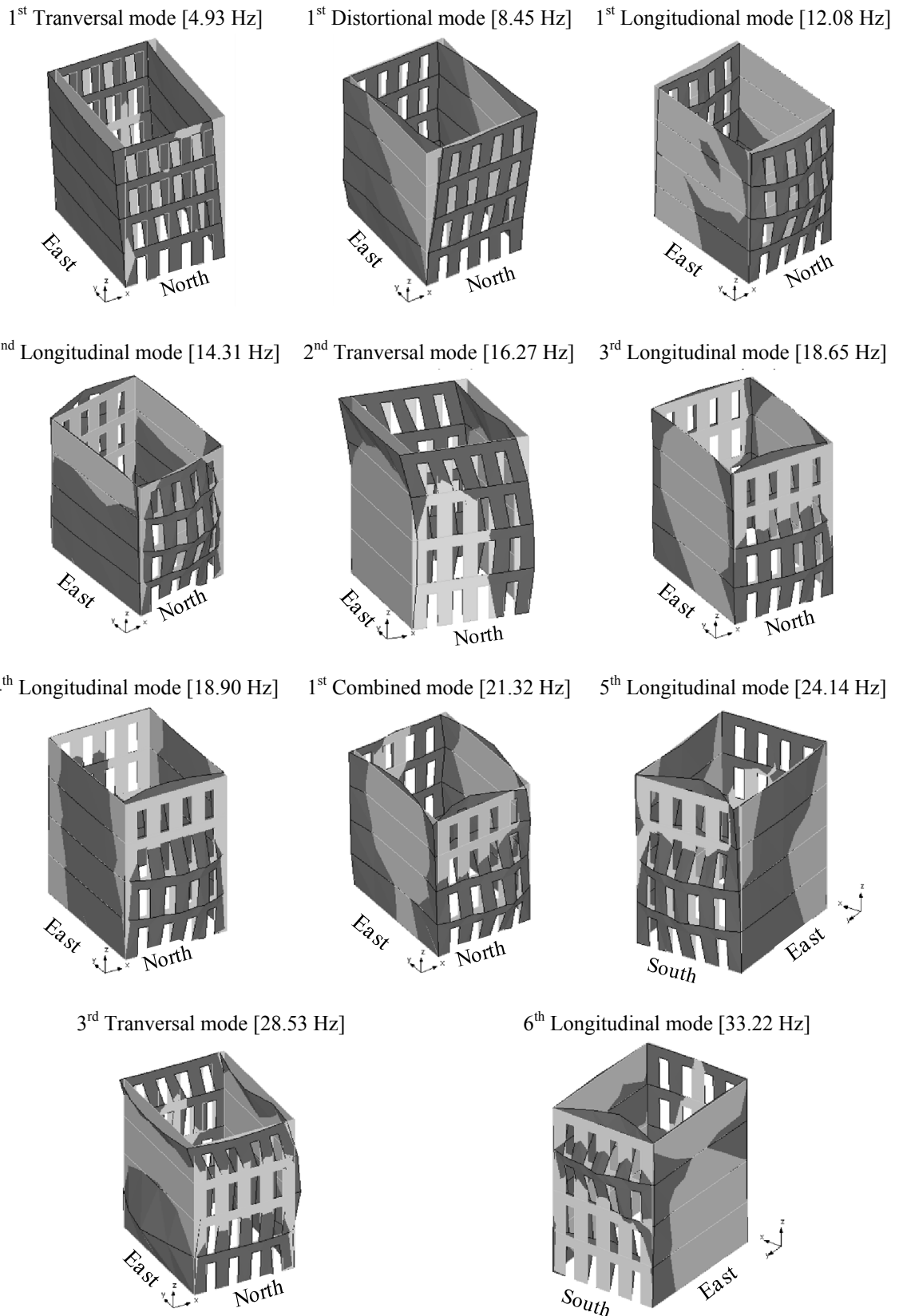
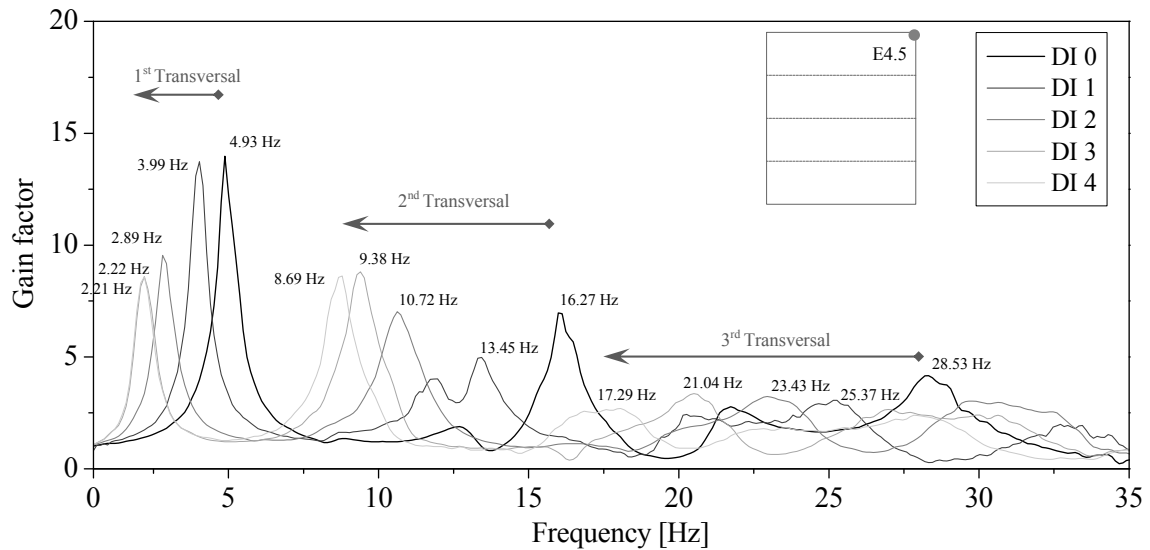
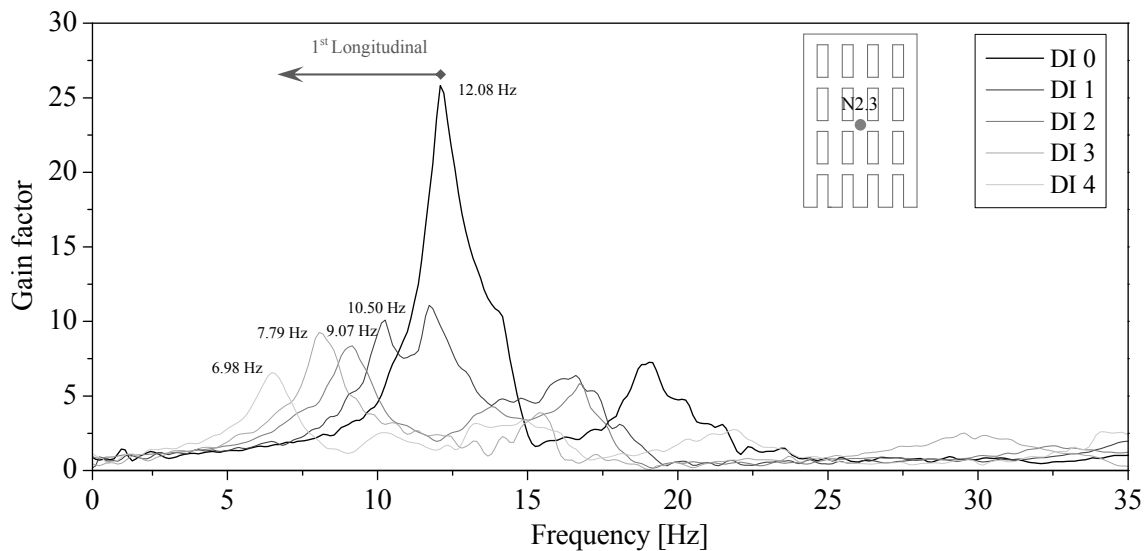


Figure 3.7 – Mode shapes of the DI 0 (dynamic identification test before the first seismic test) of the non-strengthened mock-up.



(a)



(b)

Figure 3.8 – Variation of the FRF's along the dynamic identification tests of the non-strengthened mock-up at position: (a) E4.5; (b) N2.3.

The procedure of dynamic identification of the dynamic properties was repeated through the testing and the variations in the FRF's were obtained. As an example, in Figure 3.8 the FRF's obtained along the testing program at the points E4.5 (transversal direction) and N2.3 (longitudinal direction) are plotted. The first and the second transversal modes are clearly identified and, as expected, a decrease of their frequencies is observed. The identification of the third transversal mode is more difficult, due to the high frequencies of this mode. Other interesting aspect of the FRF's is related to the range of variation of the frequencies. It is observed that the range of variation of the frequency increases from the first to the third transversal mode (Figure 3.8a). However,

this does not mean that the frequency variation of the third transversal mode is higher than the frequency variation of the first transversal mode. In the FRF's of the point N2.3, as expected, a decrease of the first longitudinal mode is observed (Figure 3.8b). In the FRF of the first dynamic identification (DI 0) at this point, the second longitudinal mode (14.31 Hz) is not clearly identified due to the high gain factor of the peak of the first longitudinal mode (12.08 Hz). Furthermore, the peak of the longitudinal mode with second curvature of the North facade is not well defined. Using all the accelerometers of this facade, it was found that the North facade present two similar modes (longitudinal mode with second curvature) with frequencies very close (18.65 Hz; 18.90 Hz) caused by the imperfections of the mock-up.

Figure 3.9 presents the evolution of the frequencies along the testing. It is noted that the combined and fourth longitudinal modes were only identified in the DI 0, and that the first distortional, the third longitudinal and the fifth longitudinal modes were not identified in all the dynamic identification tests. Furthermore, the frequency of the local longitudinal mode with second curvature of the North facade is assumed equal to 18.65 Hz, because the MAC between this mode shape and the similar one identified in the subsequent dynamic identification is the highest. The increase of damage modifies the frequencies of the modes, as expected, and several aspects render the identification of the dynamic properties along the testing complex, such as: (a) modes that increase significantly the gain factor in the FRF's and that overlap with the peaks of other modes; (b) presence of new local modes with frequencies close to the modes initially identified; (c) modes that change significantly its shape.

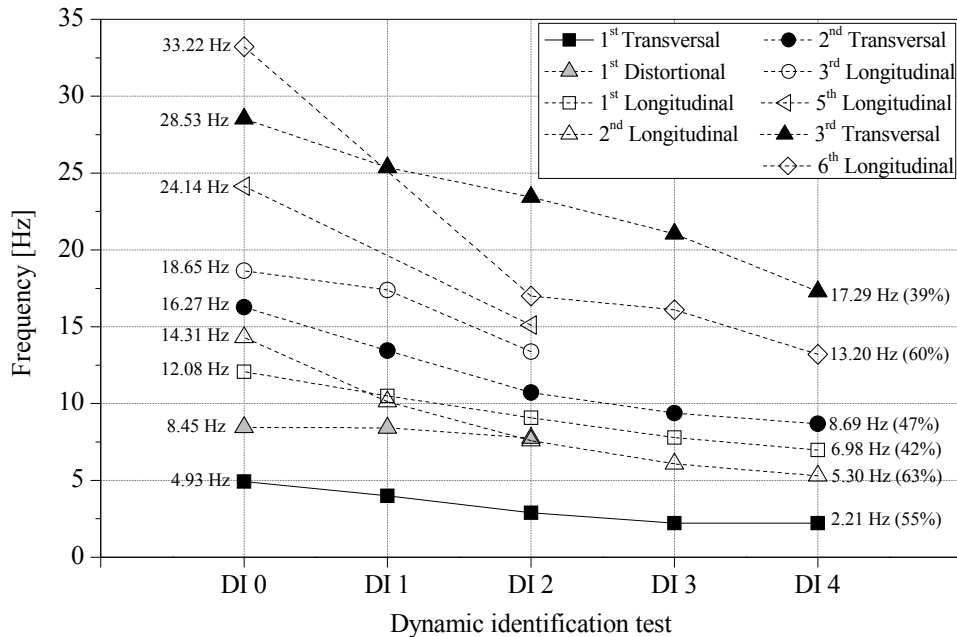


Figure 3.9 – Evolution of the frequencies of the non-strengthened mock-up and their variation with respect to the DI 0.

In the final dynamic identification tests, the frequency of the first mode remains almost equal to the previous test (2.22 Hz to 2.21 Hz). Probably, after the Earthquake 75%, the first transversal mode is mainly related with the stiffness of the gable walls connected by the floors. It is also possible that after the Earthquake 75% all the spandrels, in particular the ones near the corners, present damage which is not visible in the end of the seismic test, due to the self-weight action. The applied excitation on the mock-up for dynamic identification may reopen the cracks at the spandrels providing facades and gable walls not connected (DI 3 and DI4). It should be also taken into account that, in the first transversal mode, all the mass moves in the same direction and that the modal components increase in elevation with a distribution, approximately, linear and parallel to the orientation of the cracks at the spandrels.

Along the testing, the first transversal mode presented *MAC's* equal, on average, to 0.95 and a frequency variation of about 55%, with respect to DI 0. The others modes presented lower *MAC's* (lower than 0.80) along the testing. This means that, although the mode shape is similar, the mode is not exactly the same, due to the damage that was occurring. For this reason, in Figure 3.9 only the frequencies of the first transversal mode were connected by solid line.

Besides frequencies and mode shapes, the damping ratios were also estimated. Table 3.1 presents the damping ratio estimated along the testing. Only the first transversal, third transversal and first distortional modes presented an expected evolution of damping ratio, with a constant increase of the damping ratio along the testing. As an example, the damping ratio of the first transversal mode in the DI 0 is equal to 3.20% and it increases to 5.95% in the last dynamic identification test. Still, the damping ratio is a very sensitive parameter and difficult to estimate experimentally, particularly in masonry structures.

Table 3.1 – Damping ratios of the non-strengthened mock-up.

Mode	DI 0 [%]	DI 1 [%]	DI 2 [%]	DI 3 [%]	DI 4 [%]
1 st Transversal	3.20	4.49	5.10	5.84	5.95
1 st Distortional	4.54	5.90	9.94	-	-
1 st Longitudinal	3.70	3.19	7.20	1.37	12.63
2 nd Longitudinal	4.93	3.87	6.97	14.39	7.56
2 nd Transversal	3.39	4.13	5.09	3.93	4.19
3 rd Longitudinal	2.58	4.48	6.61	-	-
4 th Longitudinal	3.67	-	-	-	-
1 st Combined	4.74	-	-	-	-
5 th Longitudinal	2.77	-	6.51	-	-
3 rd Transversal	4.04	4.35	5.13	7.89	9.90
6 th Longitudinal	4.01	-	3.73	4.36	5.79

In the Figure 3.10, the seismic vulnerability curves of the non-strengthened mock-up are presented. These curves were defined relating the damage indicator d (Equation (3.7)), for each mode, with the input of the seismic tests in terms of nominal peak ground acceleration (PGA_{no}). Here, only the five modes (the three transversal and the first two longitudinal modes) in which the frequencies could be estimated in all dynamic tests were considered. Although the damage influences all the modes, the stiffness components of the structural elements (e.g. in-plane and out-of-plane bending) do not have the same contribution for all modes and, consequently, different variations in the frequencies of the modes are found, as observed in the Figure 3.10. The damage indicator increases along the testing for the considered modes and is in agreement with the evolution of the damage observed in cracks patterns. The maximum damage indicator for the first transversal mode is equal to 0.55 (Earthquake 100%) and remains almost equal to the previous test, as mentioned above. The highest damage indicator is equal to 0.63 and occurs for the second longitudinal mode. On average, the damage indicator is equal to 0.47 and 0.53 for the transversal and longitudinal modes, respectively. According to the linear and cubic evolution of the damage as a function of the stiffness, the maximum damage indicator d_2 and $d_{2/3}$ (Equations (3.5) and (3.6)) for the first transversal mode is equal to 0.80 and 0.41, respectively. The first value seems rather high in comparison to the qualitative damage observed in the Earthquake 100% (Figure 3.3) and is not recommended. On the contrary, the damage indicator $d_{2/3}$ (0.41) is relatively close to the adopted damage indicator d (0.55) and could also be adopted, leading to the conclusion that the adopted quadratic evolution of the damage as a function of the stiffness (linear evolution as a function of the frequency) is according to the damage observed, materialized in degradation of the shear and the bending stiffness.

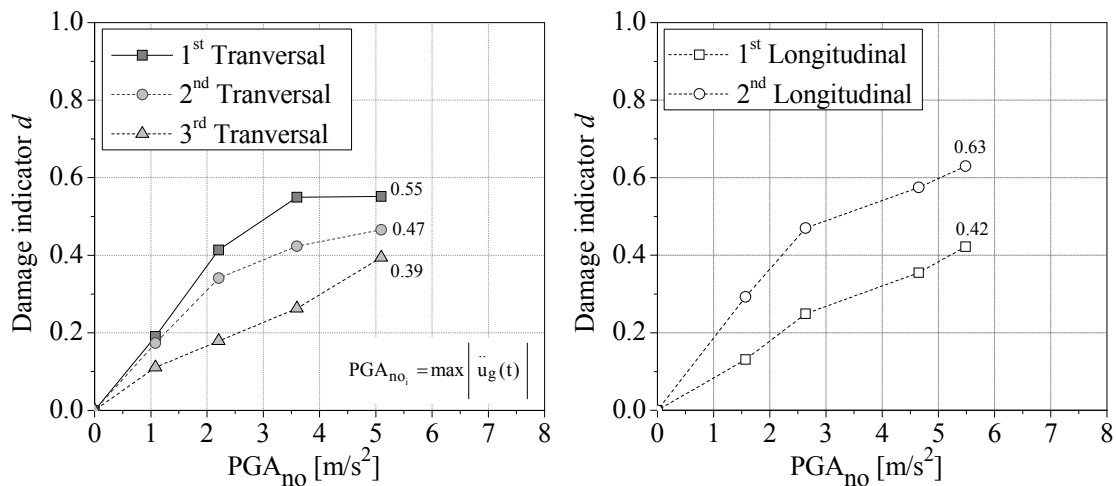


Figure 3.10 – Seismic vulnerability curves of the non-strengthened mock-up in both directions, using as input the nominal peak ground acceleration (PGA_{no}).

In order to take into account the different initial condition of the mock-up along the testing, the seismic vulnerability curves using the equivalent peak ground acceleration PGA_{eq} (Equation (3.9)) were also plotted (Figure 3.11). According to this proposal, the PGA to cause the same damage in the Earthquake 100% is equal to 6.89 m/s^2 and 7.59 m/s^2 , which corresponds to an increase of about 35% of the PGA_{no} . Finally, the seismic vulnerability curves using the input energy as the representative parameter of the seismic action, which is the integral parameter that best fitted the target signals, were also plotted (Figure 3.12). This integral parameter will be used next to compare the performance of the mock-ups.

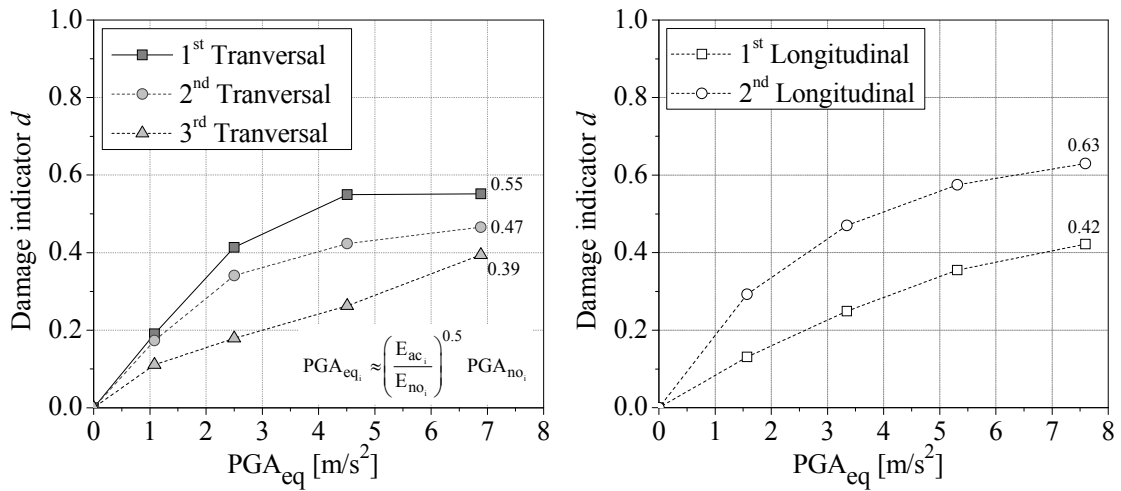


Figure 3.11 – Seismic vulnerability curves of the non-strengthened mock-up in both directions, using as input the equivalent peak ground acceleration (PGA_{eq}).

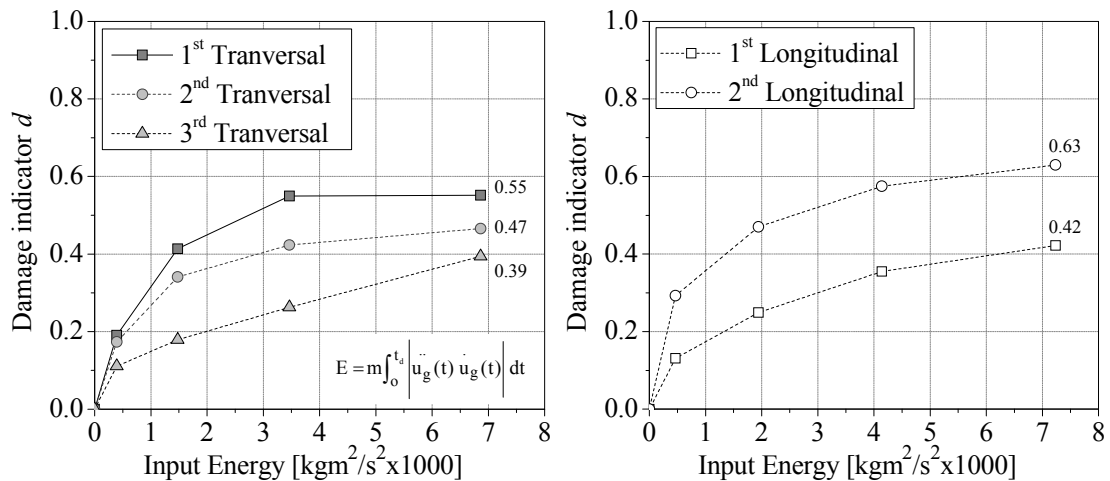


Figure 3.12 – Seismic vulnerability curves of the non-strengthened mock-up in both directions using as input the nominal input energy.

3.4.2 Strengthened mock-up

In the strengthened mock-up six dynamic identification tests (DI 0 to DI 5) were done. Due to serious damage of the mock-up, it was not possible to carry out the dynamic identification after the Earthquake 150%. In the first dynamic identification test, nine modes were estimated and related to the ones obtained for the non-strengthened mock-up (Figure 3.13). The frequency of the first mode (transversal) is equal to 4.51 Hz, which is a decrease of about 8.5% and presents the highest *MAC* (about 0.96) with respect to the first transversal mode estimated in the non-strengthened mock-up. The frequencies of the other transversal modes also decreased, namely from 16.27 Hz to 15.62 Hz and from 28.53 Hz to 25.83 Hz for the second and third transversal modes, respectively. It is noted that two very close peaks (25.03 Hz and 25.83 Hz) with similar mode shape (third transversal mode) were identified. The selection of the frequency of 25.83 Hz was based on the *MAC*. This decrease of frequency in the transversal modes can be related with some cracks that were not totally filled during the repair of the non-strengthened mock-up.

The most relevant differences between the modes of the non-strengthened and strengthened mock-ups occur in the longitudinal direction. In fact, the first longitudinal mode of the strengthened mock-up increased its frequency (13.37 Hz) and presents a shape significantly different than the first longitudinal mode estimated in the non-strengthened mock-up (12.08 Hz). The strengthening elements changed the mode shape of the longitudinal mode, decreasing significantly the out-of-plane modal components of the facades and increasing the contribution of the gables walls. Thus, the new longitudinal mode is clearly more global than the longitudinal mode estimated in the non-strengthened mock-up. The mode shape of this mode also presents a particularity at the middle of the third floor of the South facade. This particularity is clear in the FRF's, in which a local mode of the South facade (21.96 Hz) was identified (Figure 3.13). This mode is probably related with localized damage in the masonry walls of the South facade and/or with a weak connection between the South facade and the floors at the third floor. The third and sixth longitudinal modes were also estimated and present frequencies equal to 30.01 Hz and 31.80 Hz, respectively. The other longitudinal modes were not identified for the strengthened mock-up, including the second longitudinal mode. It is noted that the second longitudinal mode is a local mode of the facades in contra-phase (Figure 3.7) and should not occur due to the strengthening, since the improvement of the connection between walls and floors and the steel cables prevent the separation of the facades. In general, the *MAC*'s of the longitudinal modes between the DI 0 of the non-strengthened and strengthened mock-ups are low. For example, the *MAC* of the first longitudinal mode is equal to 0.45. Finally, the first distortional mode was also estimated and its frequency is equal to 9.19 Hz.

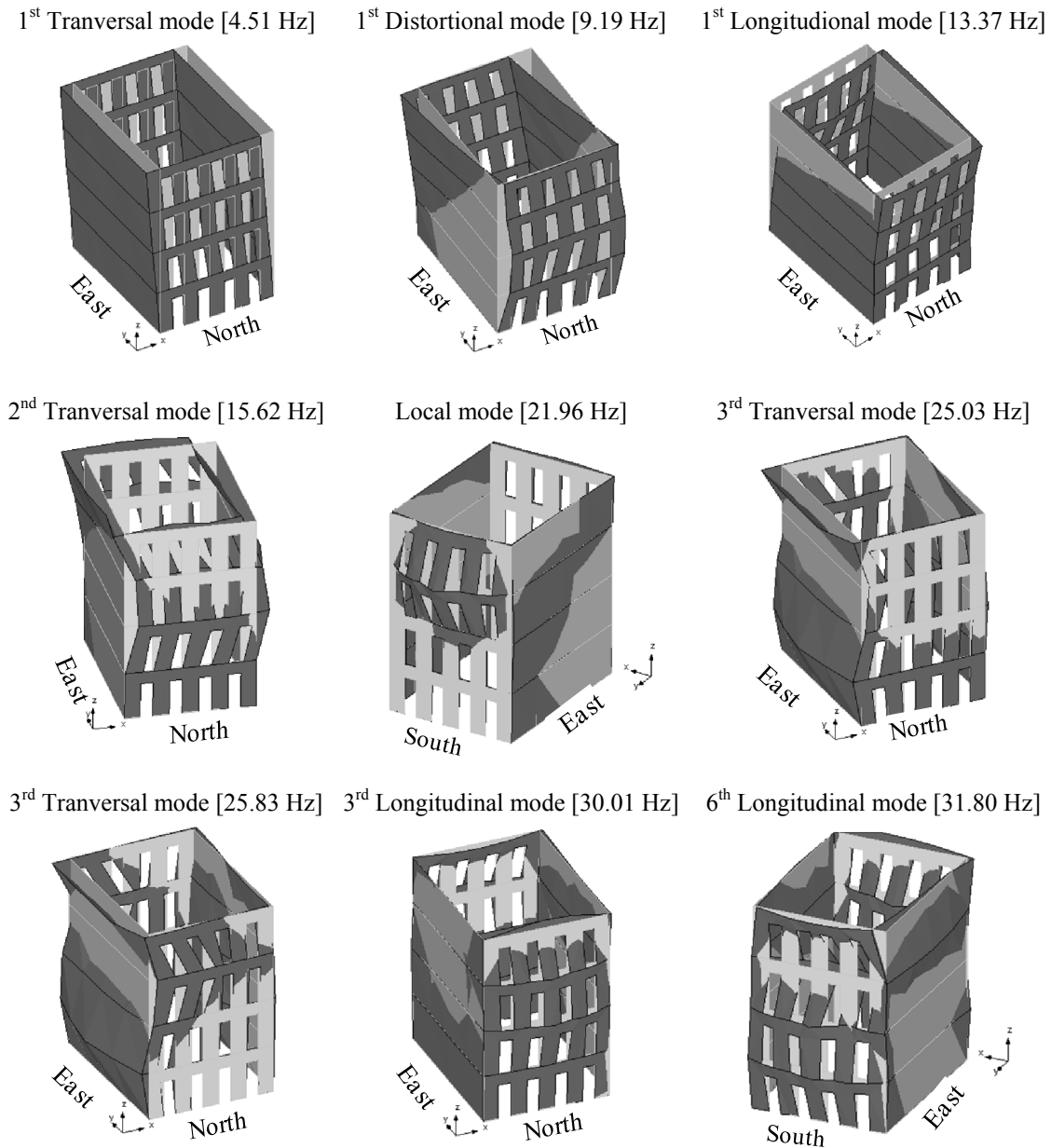


Figure 3.13 – Mode shapes of the DI 0 (dynamic identification test before the first seismic test) of the strengthened mock-up.

Taking into account the comparison between the mode shapes of the strengthened mock-up (Figure 3.13) and the non-strengthened mock-up (Figure 3.7), it is expected that the strengthening will improve the seismic performance of the mock-up, namely preventing the out-of-plane displacement of the facades and the separation between gable walls due to the cracks at the spandrels.

Along the testing, only the transversal modes and the sixth longitudinal modes were estimated in the dynamic identification (Figure 3.14). The *MAC* of the first transversal mode along the testing is on average equal to 0.98 and the frequency after Earthquake 125% is equal to 2.75 Hz (DI 5), which corresponds to a decrease of about 39% with respect to the DI 0. After Earthquake 125%, the frequency of the first longitudinal mode presented a decrease about 28% with respect to DI 0. The highest

variation of the frequency occurred for the second transversal mode (50%). As the first transversal mode presented high *MAC*'s along the testing, only the frequencies of this mode were connected by solid line in the Figure 3.14.

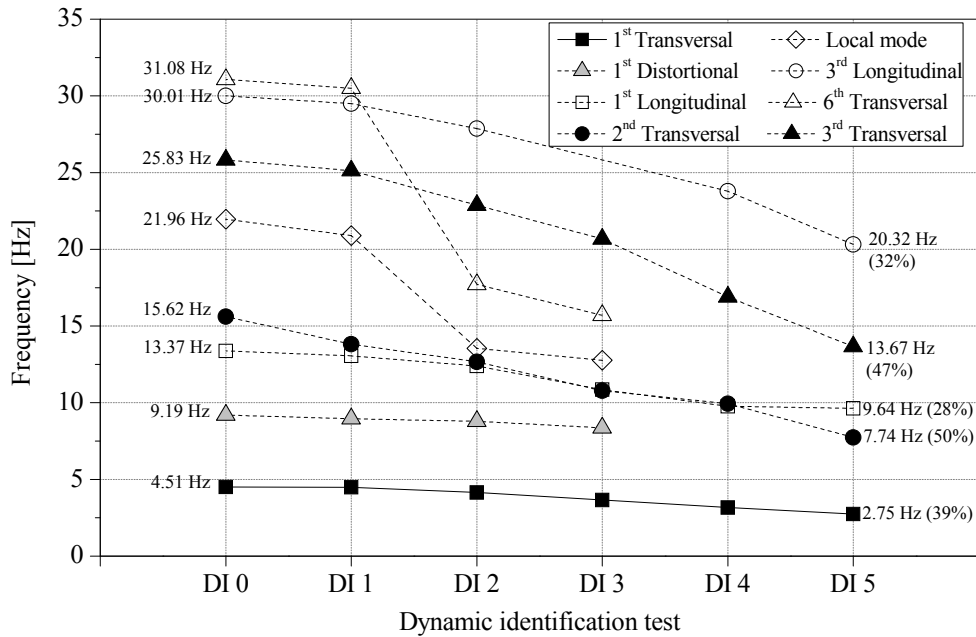


Figure 3.14 – Evolution of the frequencies of the strengthened mock-up and their variation with respect to the DI 0.

Table 3.2 presents the damping ratios estimated along the testing. The damping ratios of the first transversal mode increase from DI 0 (3.53%) to DI 4 (5.34%). In DI 5 the damping ratio presents an unexpected decrease (4.04%). In DI 0 the damping ratio of the first transversal mode of the strengthened mock-up (3.53%) is similar to the one estimated in non-strengthened mock-up (3.20%). The damping ratio of the first longitudinal mode (7.48%) is higher than the damping ratio of the first transversal mode (DI 0) and presents an unexpected variation along the testing. As previously referred, the damping ratio is difficult a parameter to estimate experimentally.

Table 3.2 – Damping ratios of the strengthened mock-up.

Mode	DI 0 [%]	DI 1 [%]	DI 2 [%]	DI 3 [%]	DI 4 [%]	DI 5 [%]
1 st Transversal	3.53	4.29	4.47	4.49	5.34	4.04
1 st Distortional	4.12	4.23	3.66	4.77	-	-
1 st Longitudinal	7.48	7.63	4.96	5.53	4.13	5.64
2 nd Transversal	1.49	2.11	2.31	3.00	6.00	5.73
Local mode	5.08	4.56	4.26	6.87	-	-
3 rd Transversal	2.84	-	-	-	-	-
3 rd Transversal	1.25	3.20	4.05	5.66	7.63	5.67
3 rd Longitudinal	3.03	2.57	3.81	-	2.52	5.76
6 th Longitudinal	0.65	4.24	5.90	7.03	-	-

The seismic vulnerability curves of the non-strengthened mock-up (Figures 3.15 and 3.16), relating the damage indicator d with the nominal peak ground acceleration (PGA_{no}) and with the nominal input energy, were also plotted. As the PGA_{no} in the longitudinal direction was not always increasing along the testing, the proposal to adapt the PGA as function of the initial condition of the strengthened mock-up is not valid and, consequently, the seismic vulnerability curves using the PGA_{eq} were not plotted. After Earthquake 125% (DI 5), the damage indicator is equal to 0.39, 0.47, 0.50 for the first, second and third transversal modes, respectively. After Earthquake 25% (Figure 3.15), the first transversal mode presents a very low damage indicator (0.01), indicating that the damage after this seismic test is insignificant, as can be observed in the crack pattern (Figure 3.5). Even if some damage at the facades was caused by the low amplitude seismic action, the strengthening elements enforce the connection of the spandrels and prevent the reopening of cracks during the dynamic identification test.

Due to the high and unexpected PGA_{no} in the longitudinal direction of the Earthquake 100% (Figure 3.15), the seismic vulnerability curve in this direction presents a peculiar behaviour, in which the damage indicator d for the Earthquake 125% increases with a decreasing of the PGA , in comparison to the Earthquake 100%. In fact, the damage present in the seismic test i is always equal or higher to the damage of the seismic test $i-1$, even if the PGA in the seismic test i is lower than the previous one. However, using as a parameter of the seismic action the input energy, which is an integral parameter less sensitive to the peak values, the seismic vulnerability curves present the expected behaviour, in which the damage indicator increases with the seismic action (Figure 3.16). The first longitudinal mode presents the lowest damage indicator (0.28), varying linearly until Earthquake 100% (0.27) and remaining almost constant after Earthquake 125% (0.28). The comparison between the mock-ups using the seismic vulnerability curves, defined using the frequencies of the modes, is presented in the next Section.

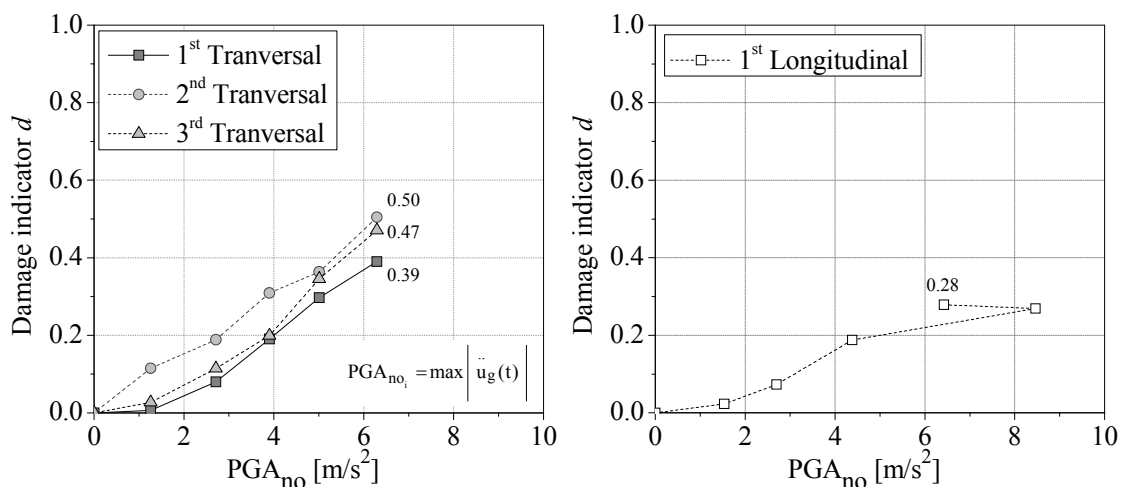


Figure 3.15 – Seismic vulnerability curves of the strengthened mock-up in both directions, using as input the nominal peak ground acceleration (PGA_{no}).

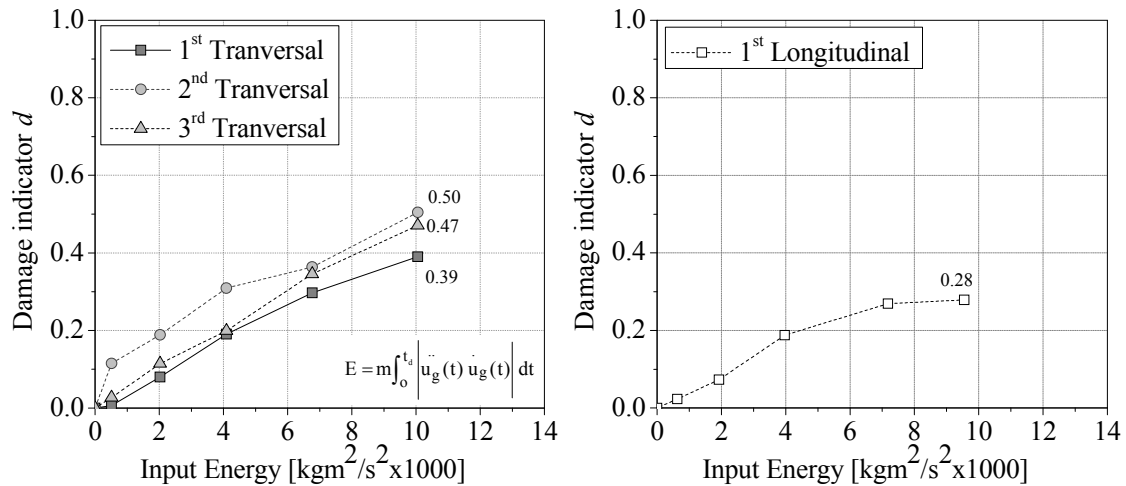


Figure 3.16 – Seismic vulnerability curves of the strengthened mock-up in both directions using as input the nominal input energy.

3.4.3 Comparison of the results of the dynamic identification test

In the first comparison of the seismic performance of the mock-ups, the seismic vulnerability curves for the first mode in each direction were used. Here, the seismic vulnerability curves that relate the damage indicator d with the input energy applied at the base of the mock-ups were adopted (Figure 3.17). In the seismic vulnerability curves of the first transversal mode, the highest variation of the damage indicator occurred in the Earthquake 25% (Figure 3.17a), as there is almost no damage for the strengthened mock-up at this stage. It is noted that the tensile strength of the masonry is very low (Table 2.8) and it is expected that, even under low seismic amplitude, the non-strengthened mock-up develops micro-cracks, mainly in the mortar, which are not visible but reopen in the dynamic identification tests and, consequently, decrease the frequencies. On the other hand, in the strengthened mock-up these micro-cracks have less influence in the dynamic identification testes, because the strengthening elements prevent their reopening. This means that the strengthening elements enforce the connection of the masonry structural elements, providing dynamic box behaviour for the structure and, consequently, improving its seismic performance. In the Earthquake 100% the strengthened mock-up presents a reduction of the damage indicator of about 46% with respect to the non-strengthened mock-up, leading to the conclusion that the strengthening was efficient in decreasing the seismic vulnerability of the mock-up. Even in the Earthquake 125%, the damage indicator of the strengthened mock-up (0.39) is lower than the damage indicator of the non-strengthened mock-up in the Earthquake 100% (0.55).

In the seismic vulnerability curves of the first longitudinal mode (Figure 3.17b), the variation of the damage indicator of the strengthened mock-up with respect to the non-

strengthened mock-up remains almost constant along the testing. In the Earthquake100%, the damage indicator of the strengthened mock-up presents a reduction of about 36% with respect to the non-strengthened mock-up. However, the comparison between these seismic vulnerability curves should be done with caution and not assuming that the first longitudinal modes are exactly the same for the non-strengthened and strengthened mock-ups, as the *MAC*'s in along the testing are low.

The conclusions obtained from the seismic vulnerability curves for the Earthquake 100% (transversal and longitudinal directions) are in agreement to the damage observed in the crack patterns, in which all the spandrels of the non-strengthened mock-up are damaged and in which the damage of the strengthened mock-up concentrates only in the two top floors. Damage at the spandrels of the first and second floors is low in this case.

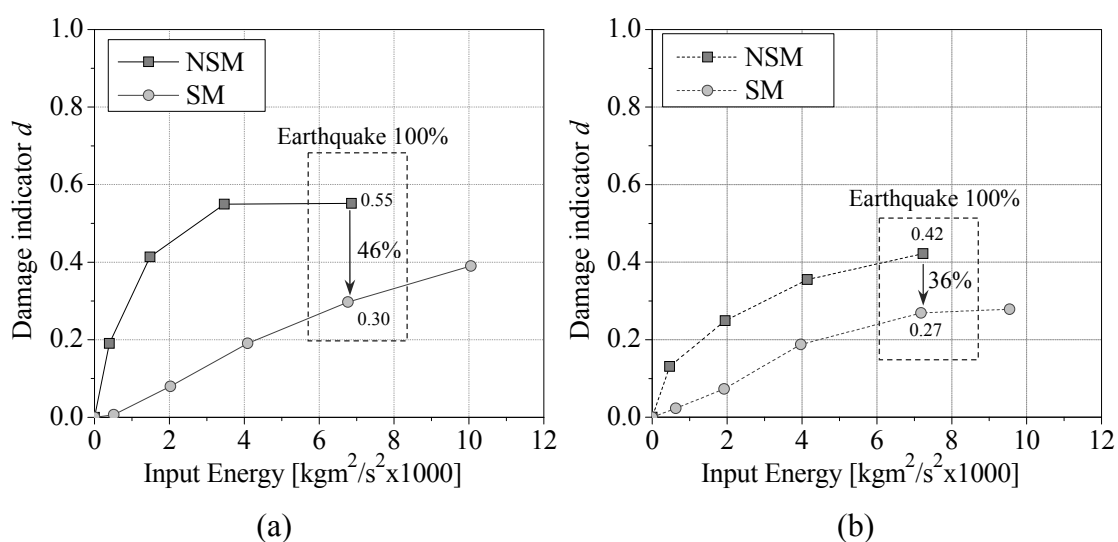


Figure 3.17 – Comparison between the seismic vulnerability curves of the non-strengthened (NSM) and strengthened (SM) mock-ups relating the input energy with the damage indicator *d* using: (a) the first transversal mode; (b) the first longitudinal mode.

Finally, a comparison between the mock-ups tested in this thesis and the mock-ups tested by Candeias (2008) is also made. In Figure 3.18 the seismic vulnerability curves for the different mock-ups are presented. In order to make the comparison with the mock-ups tested by Candeias (2008), the seismic vulnerability curves were defined relating PGA_{no} with the damage indicator *d* obtained from the frequencies of the first transversal mode, which is the one that presented the highest *MAC*'s along the testing. In the Earthquake 100%, the non-strengthened mock-ups (Model 0 and 00) tested by Candeias (2008) present damage indicators (0.54 and 0.60) lower than the one of the non-strengthened mock-up (NSM) tested in this work (0.80). It is noted that the frequencies of the non-strengthened mock-ups Model 0 and 00 are equal to 4.70 Hz and

4.10 Hz, respectively, which correspond to a variation of about 5% and 17% with respect to the NSM, respectively. Furthermore, in the Earthquake 100% and according to this method of seismic assessment, the strengthened mock-ups tested by Candeias (2008) do not present any efficiency in reducing the seismic vulnerability of the non-strengthened mock-ups. Only Model 1 presents a low decrease of the damage indicator (0.58) with respect to Model 00 (0.60). The highest reduction of the damage indicators are obtained for the low amplitudes of seismic action, namely to Earthquake 25%. It is noted that the mock-ups tested by Candeias (2008) did not present the same initial condition and that, according to the analysis of the seismic test results, the adopted strengthening techniques improved the seismic performance in comparison to the non-strengthened mock-ups. However, this method for assessing the seismic vulnerability provides a reduction of the damage indicator of about 46% for the strengthened mock-up in this work, with respect to the non-strengthened mock-up (Figure 3.18), leading to a similar conclusion that the strengthening elements adopted here improved the seismic performance of the mock-up.

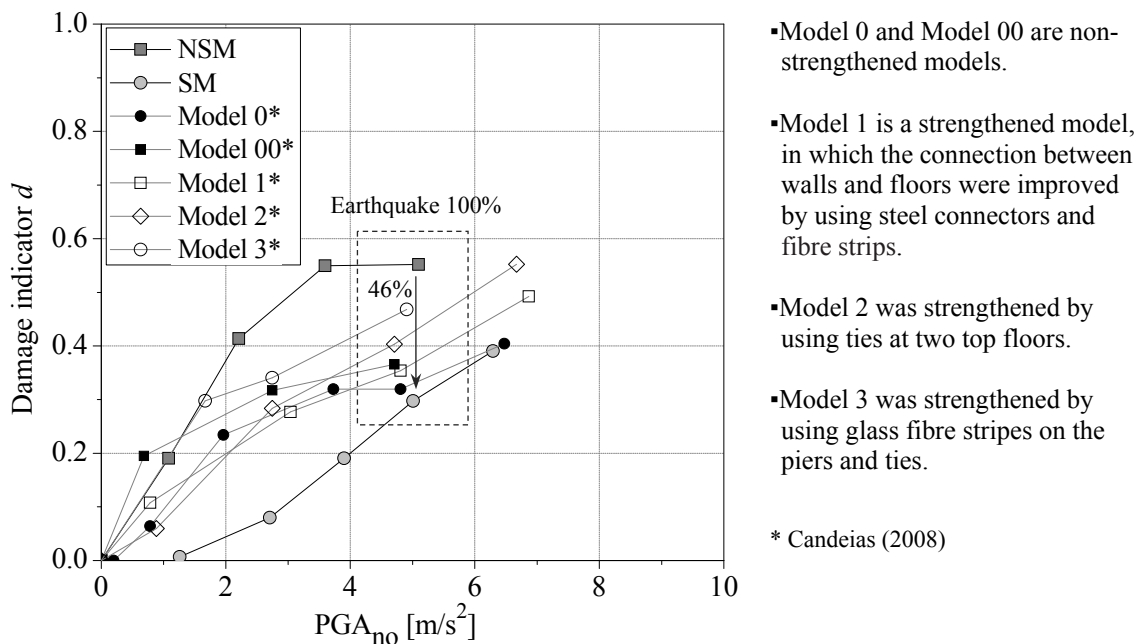


Figure 3.18 – Comparison between the seismic vulnerability curves of the non-strengthened and strengthened mock-ups and the mock-ups tested by Candeias (2008).

3.5 Results of the seismic tests

3.5.1 Non-strengthened mock-up

In the non-strengthened mock-up, four seismic tests with increasing amplitude were carried out (25%, 50%, 75% and 100% of the code seismic action). According to the methodology defined in Section 3.2.2, the seismic performance of the non-strengthened mock-up was analysed for each masonry wall, by using four parameters of control of the response, namely: (a) the average out-of-plane acceleration amplification at each floor level ($Amplification_{acc,ave}$); (b) the average out-of-plane displacement at each floor level (u_{ave}); (c) the average out-of-plane relative displacement with respect to the corners at each floor level ($u_{ave,corners}$); (d) the average of the in-plane drift at each floor level ($Drift_{in-plane,ave}$).

Starting by the analysis of the response in terms of acceleration, the maximum average amplification of acceleration ($Amplification_{acc,ave}$) for the Earthquake 25% (Figures 3.19 and 3.20) occurred at the top floor and is similar in both directions (2.6). In general, the amplification of acceleration in the facades increases from the Earthquake 25% to 50% and decreases progressively in the next two earthquakes. The highest increase of amplification occurs either at the third floor or at the top (Figure 3.19). The behaviour of the gable walls is similar to the facades, with a decrease of the acceleration from the first to the final seismic test in all floor levels. The maximum amplification occurred at the top floor (Figure 3.20).

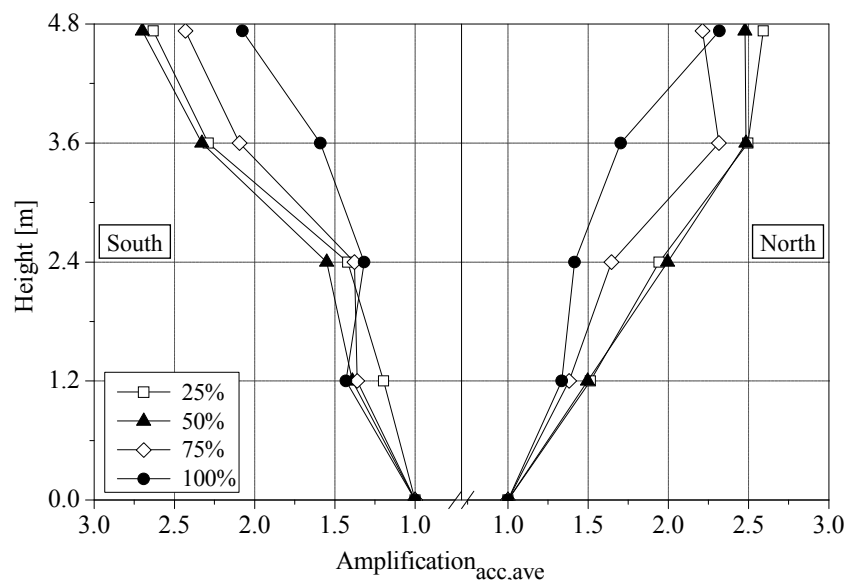


Figure 3.19 – Average out-of-plane acceleration amplification at floor levels for the facades of the non-strengthened mock-up.

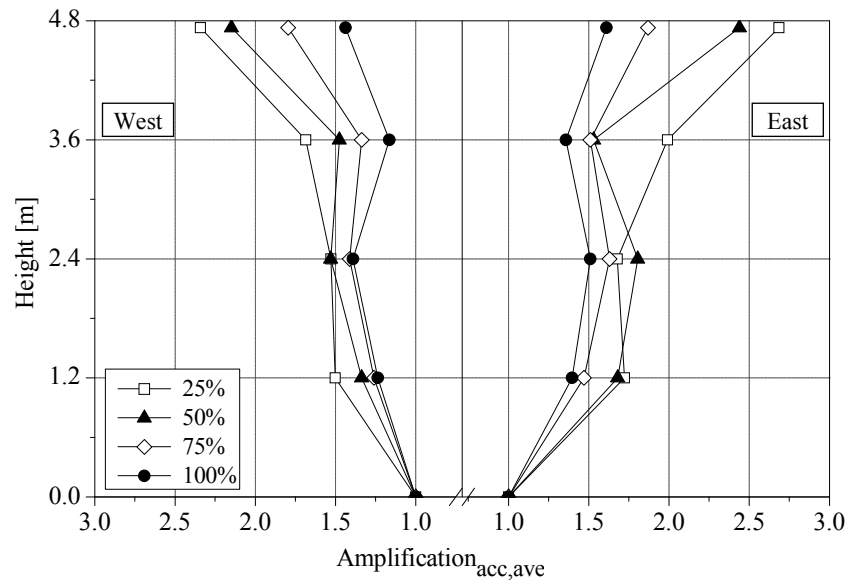


Figure 3.20 – Average out-of-plane acceleration amplification at floor levels for the gable walls of the non-strengthened mock-up.

The analysis of the evolution of the amplification of the acceleration is indicative of the stiffness of the mock-ups. It is expected that increasing the seismic amplitude, the damage increases and, consequently, the amplification of the acceleration decreases. Taking into account the amplification of the acceleration, all the floors of the non-strengthened mock-up presents damage, and particularly the top floors. This conclusion is according to the damage observed in the crack patterns, in which almost all lintels of the facades present damage (Figure 3.3). However, the analysis of the behaviour of the non-strengthened mock-up by using the amplification of the acceleration does not allow to distinguish the level of the damage in the different masonry walls (facades and gable walls).

In the Figures 3.21 and 3.22 the average of the maximum displacements at the floor levels (u_{ave}), including the five vertical alignments for each masonry wall, are presented. As expected, the displacements increase with the seismic amplitude. The displacements of the gable walls are much higher than the displacements of the facades, which agree with the significant difference of stiffness between the longitudinal and transversal direction. As an example, the ratio between the first longitudinal (12.08 Hz) and transversal (4.93 Hz) frequencies of the non-strengthened mock-up is equal to 2.5 and the ratio between the maximum displacement in the Earthquake 25% of the gable walls (top floor) and facades (third floor), is on average equal to 2.7. This ratio decreases slightly for the Earthquake 100% (2.5), indicating that for this seismic test the increase of maximum displacement at the facades is higher than the increase of the maximum displacement at the gable walls. This agrees with the concentration of damage at the facades and, consequently, with the expected increase of the out-of-plane displacements in these walls. Furthermore, the shape in elevation of the average of the maximum

displacements of the facades and gable walls are different. The maximum displacements of the facades increase from the base to the third floor and decrease at the top of the mock-up, particularly in the last seismic tests. The maximum average of the displacements at the masonry walls with openings occurs at the third floor of the North facade and is equal to 1.3 cm (Earthquake 100%). On the contrary, in the gable walls the increase in elevation of the average of the maximum displacements is approximately linear, with the maximum occurring at the top of the walls and being equal to 3.0 cm (Earthquake 100%).

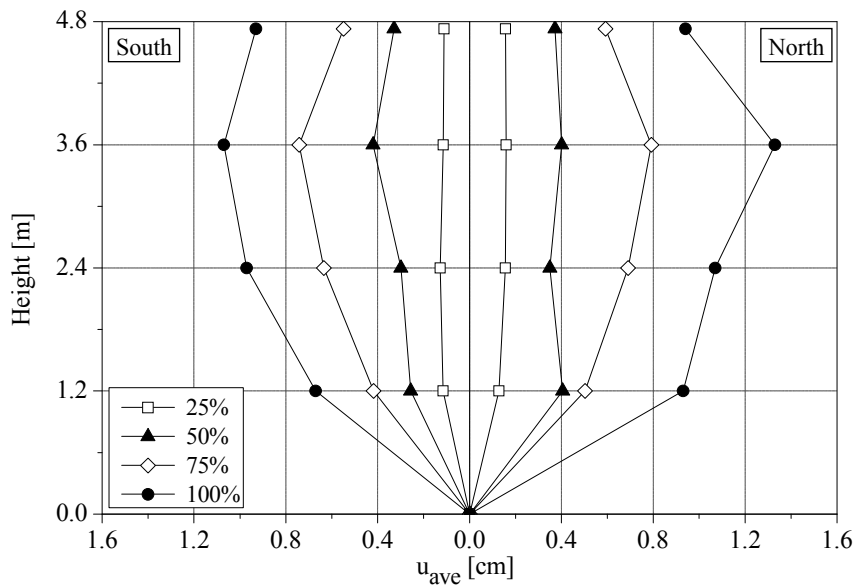


Figure 3.21 – Average out-of-plane displacement at floor levels for the facades of the non-strengthened mock-up.

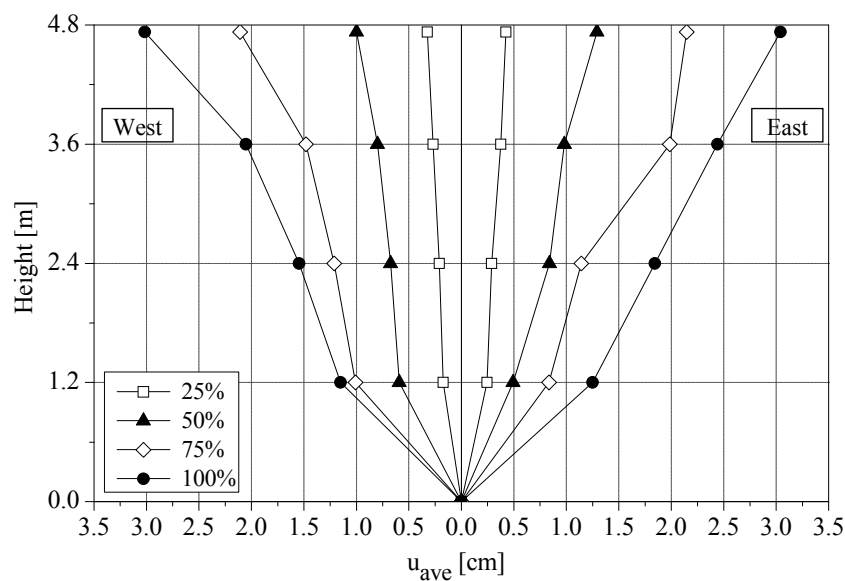


Figure 3.22 – Average out-of-plane displacement at floor levels for the gable walls of the non-strengthened mock-up.

The average of the maximum displacements (u_{ave}) is mainly a global parameter of the response of the mock-up at the floor levels, since it also includes the vertical alignments of accelerometers at the corners. Thus, the average of the maximum out-of-plane relative displacements with respect to the corners ($u_{ave, corners}$) was also plotted. It is noted that these displacements are orthogonal to a plane defined through the displacements of the corners for each time instant, i.e. they are not orthogonal to the plane of the masonry walls, and the average of the maximums only includes the three central vertical alignments of accelerometers. This relative displacement is a local parameter of the response of the walls and is associated to the out-of-plane bending.

The average of the maximum out-of-plane relative displacements increases progressively with the seismic amplitude applied at the base of the non-strengthened mock-up (Figures 3.23 and 3.24). In general, the facades (Figure 3.23) present a similar behaviour, in which the maximum occurs at the third floor for all seismic tests. The maximum value is equal to 1.2 cm and occurs at the third floor of the North facade (Earthquake 100%), which is according to the damage observed in the crack patterns at this floor level. In the Earthquake 25%, the gable walls (Figure 3.24) presents similar behaviour, with an increase of displacements from the base to the third floor and a decrease at the top of the walls. However, after this seismic test the top floor of the gable walls presents a peculiar and rather non-symmetric behaviour. This may be related to imperfections of the mock-up, mainly in the connections between floors and gable walls.

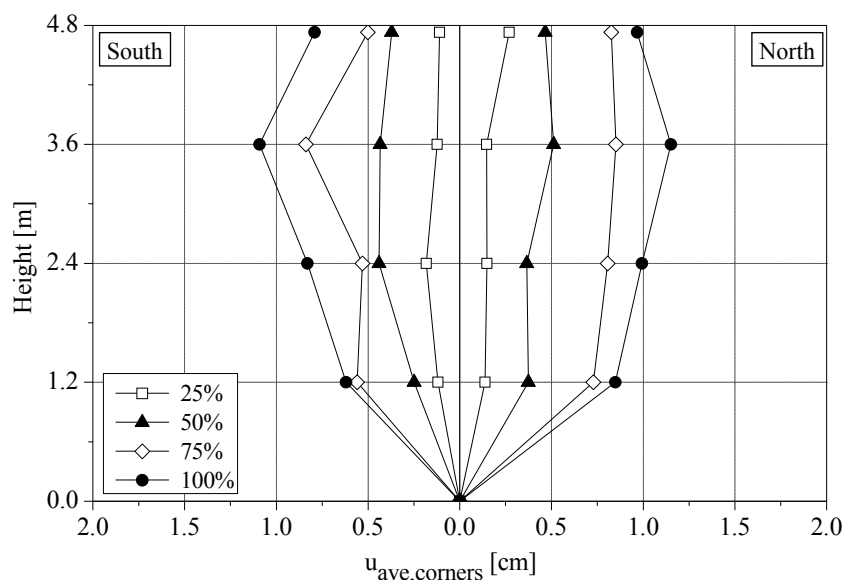


Figure 3.23 – Average out-of-plane relative displacement with respect to the corners at floor levels for the facades of the non-strengthened mock-up.

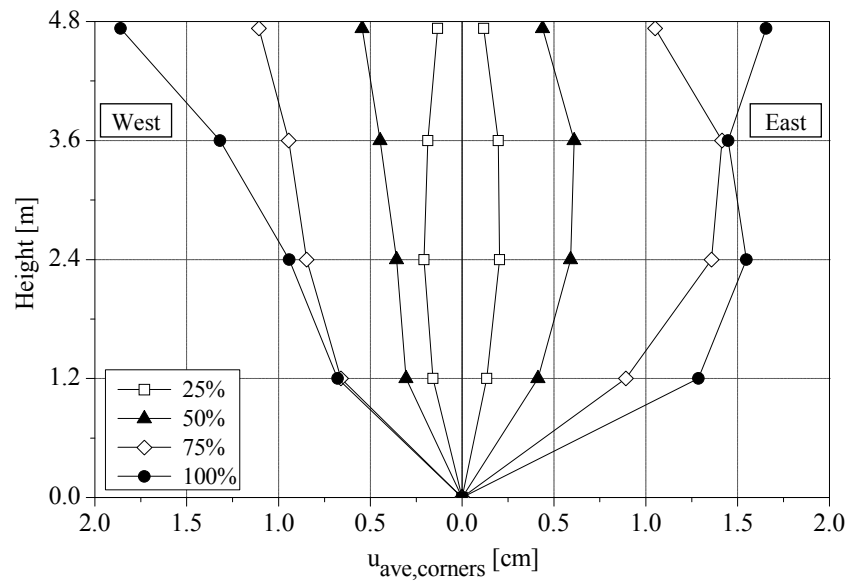


Figure 3.24 – Average out-of-plane relative displacement with respect to the corners at floor levels for the gable walls of the non-strengthened mock-up.

Finally, the averages of the maximum in-plane drifts of the facades ($Drift_{in-plane,ave}$) were also plotted (Figure 3.25). In general, the in-plane drifts increase from the base of the facades to the third floor and decrease at the top, with exception of the drifts for the Earthquake 75%, in which the drift at the third floor decreases in comparison to the drift of the second floor. The distribution in elevation of the drift is according to the damage observed in the crack patterns, in which the two top floors present the highest drifts and level of damage. The maximum in-plane drift is equal to 1.4% (Earthquake 100%) and occurred between the second and third floors of the South facade. The in-plane drifts of the gable walls are very low and are not presented here, because the in-plane stiffness of the walls is rather high and no damage was observed.

The analysis of the seismic performance of the non-strengthened mock-up by use of quantitative parameters, obtained from the seismic tests, is according to the expected behaviour of this type of buildings. The response of the non-strengthened mock-up shows that the facades present a significant response in the out-of-plane direction of the walls as a consequence of the flexible timber floors and of the weak connections between the floors and the masonry wall. The parameters of the response of the mock-up, mainly the average of maximum out-of-plane relative displacements with respect to the corners ($u_{ave, corners}$) and the average of the in-plane drifts of the facades ($Drift_{in-plane,ave}$), presents a non-linear increase along the testing, which is due to the concentration of damage at the facades.

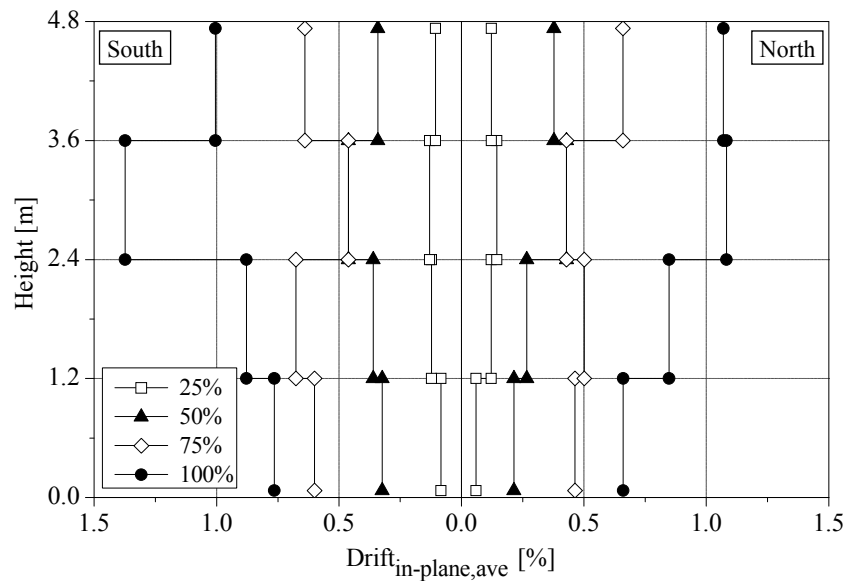


Figure 3.25 – Average in-plane drift for the facades of the non-strengthened mock-up.

3.5.2 Strengthened mock-up

The test planning used for the non-strengthened mock-up was repeated for assessing the seismic performance of the strengthened mock-up. Additionally, two seismic tests with amplitude equal to 1.25 and 1.50 of the code seismic action were also carried out. Due to safety reasons, in the Earthquake 150% the accelerometers were removed and, consequently, the response of the mock-up was not recorded.

The average of the maximum of the acceleration amplification ($Amplification_{acc,ave}$) of facades of the strengthened mock-up presents, in general, similar behaviour for the different amplitudes (Figure 3.26). The amplification increases until the Earthquake 50% and, after this seismic test, remains almost constant. However, the third floor of the South facade presents a distinct behaviour, in which the variation of the amplification is highest along the testing and presents also the highest absolute average of the maximum of the acceleration amplification (2.3 in the Earthquake 50%). The variations of the amplification at the two first floors of the gable walls are very low, in comparison to the two top floors, mainly until the Earthquake 100% (Figure 3.27). The maximum average of the amplification of the gable walls is about 2.5 and occurs at the top of the walls (Earthquake 25%). The highest variation of the amplification at the top floors of the gable agrees with the concentration of damage observed at these floors in the crack patterns.

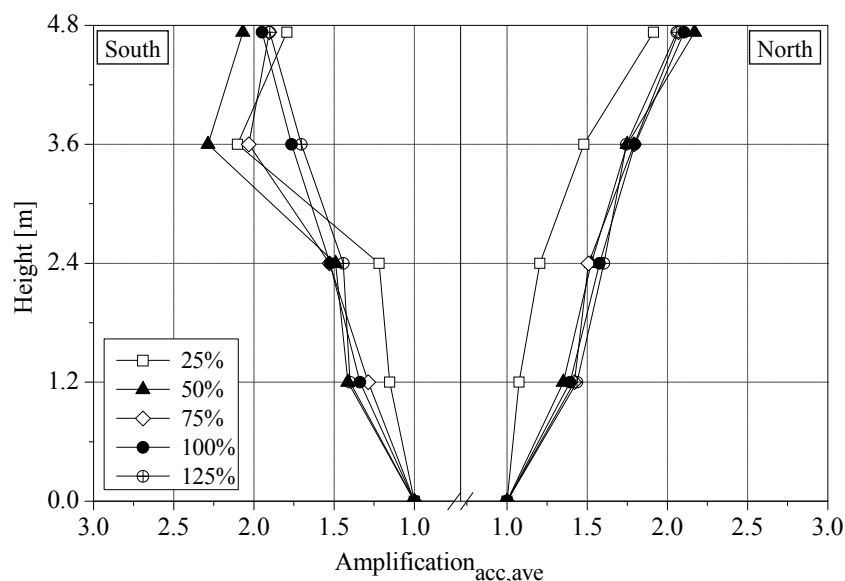


Figure 3.26 – Average out-of-plane acceleration amplification at floor levels for the facades of the strengthened mock-up.

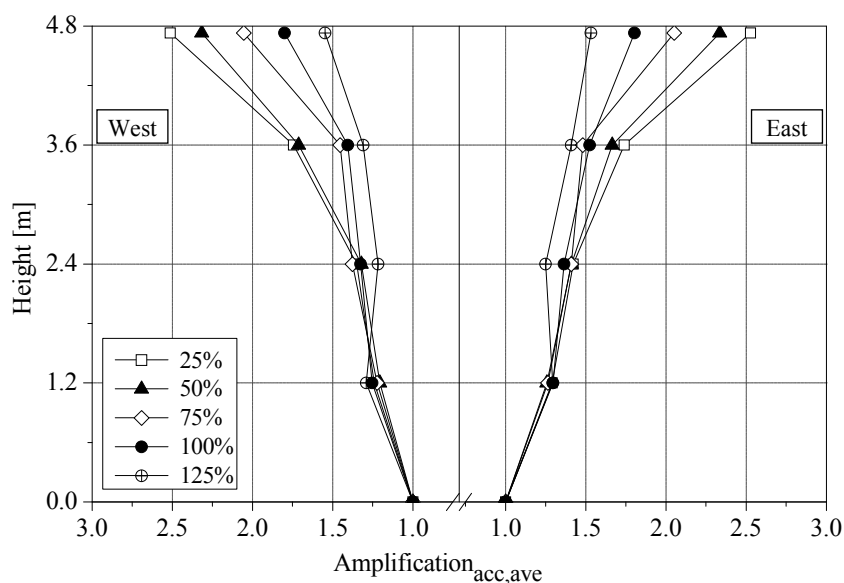


Figure 3.27 – Average out-of-plane acceleration amplification at floor levels for the gable walls of the strengthened mock-up.

The average of the maximum displacements at the floor levels (u_{ave}) of the facades is, in general, constant in elevation (Figure 3.28), and the maximum in the Earthquake 100% is equal to 1.0 cm. This value is lower than the maximum displacement of the non-strengthened mock-up (1.3 cm) and is related to the contribution of the strengthening elements for decreasing the amplitude of the out-of-plane response of the facades. Even in the Earthquake 125%, the maximum displacement of the strengthened mock-up is lower than the maximum displacement of the non-strengthened mock-up (1.1 cm). The

displacements u_{ave} of the gable walls present a low increase in elevation up to the second floor along the testing (Figure 3.29). The two top floors present the highest increase of displacements, with a maximum in the Earthquake 100% of about 2.8 cm at the top of the walls, which corresponds to a lower decrease with respect to the non-strengthened mock-up (3.0 cm). The variation of the displacements u_{ave} with increasing seismic amplitude agrees with the low damage at observed in the crack patterns.

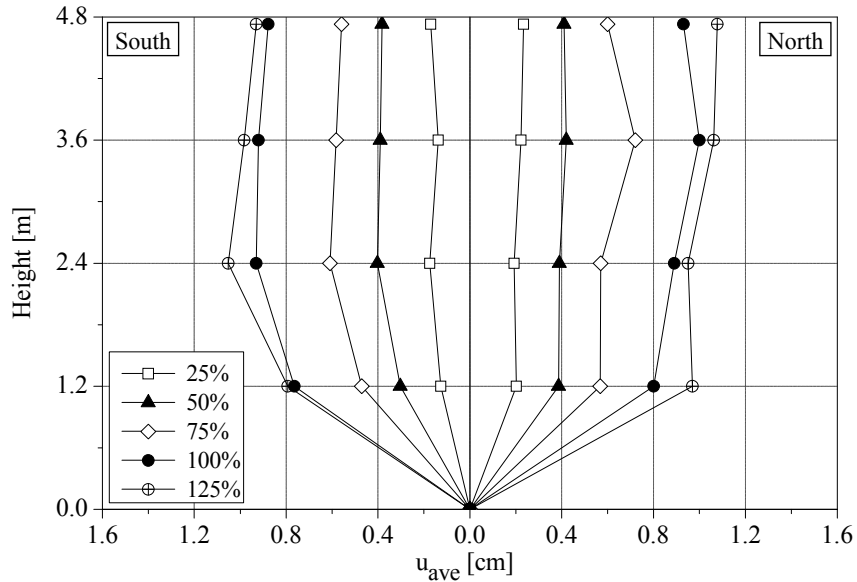


Figure 3.28 – Average out-of-plane displacement at floor levels for the facades of the strengthened mock-up.

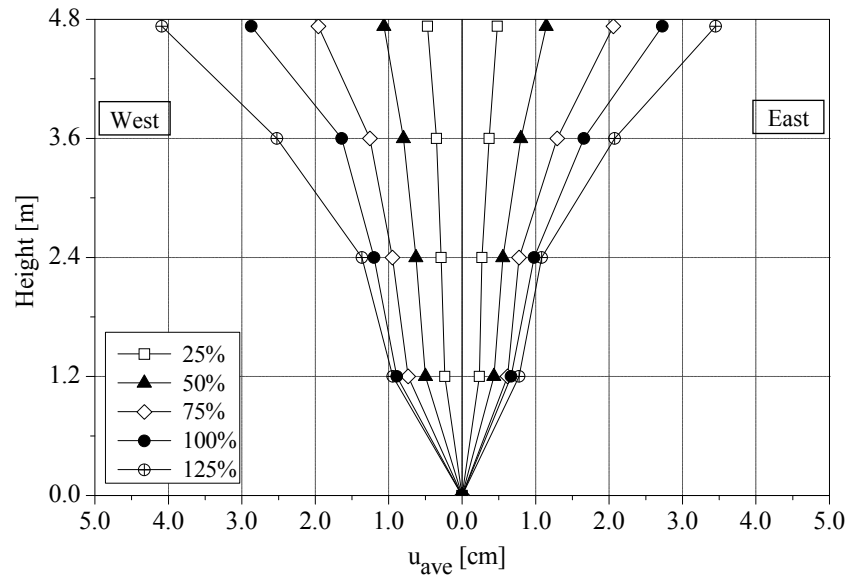


Figure 3.29 – Average out-of-plane displacement at floor levels for the gable walls of the strengthened mock-up.

The facades of the strengthened mock-up present the maximum of the average out-of-plane relative displacement with respect to the corners ($u_{ave, corners}$) at the second and at the top floors (Figure 3.30). It is noted that the maximum displacement $u_{ave, corners}$ of the non-strengthened mock-up in the Earthquake 100% occurs at the third floor (1.2 cm). The strengthening elements improved the out-of-plane response of the strengthened mock-up. For instance, in the Earthquake 100% a reduction of about 50% of the maximum out-of-plane response of the North facade was obtained for the second and top floors. In the third floor of the North facade, the reduction of the maximum displacement $u_{ave, corners}$ is about 80%, with respect to the non-strengthened mock-up. The South facade presents displacements $u_{ave, corners}$ higher than the ones of the North facades, which may be related to the imperfections in the strengthening of the mock-up and to some initial damage at the South facade. However, even this facade presents a reduction, with respect to the South facade of the non-strengthened mock-up, of the displacement $u_{ave, corners}$ of about 22% for the second and top floors and for 56% at the third floor. The maximum displacement $u_{ave, corners}$ is equal to 0.9 cm and occurs at the top of the South facade in the Earthquake 125%.

The displacements $u_{ave, corners}$ of the gable walls (Figure 3.31) present the maximum at the third floor and feature a significant reduction at the two first floors with respect to the non-strengthened mock-up. In the Earthquake 100%, the maximum displacement $u_{ave, corners}$ of the third floor of the strengthened mock is equal, on average, to 1.1 cm, which corresponds to a reduction of about 24% with respect to the non-strengthened mock-up. The top floor presents also a significant reduction, on average, of about 48% (Earthquake 100%). The maximum displacement $u_{ave, corners}$ is equal to 1.4 cm and occurs at the third floor of the West gable wall (Earthquake 125%). These results show that the steel angles improved also the out-of-plane behaviour of the gable walls.

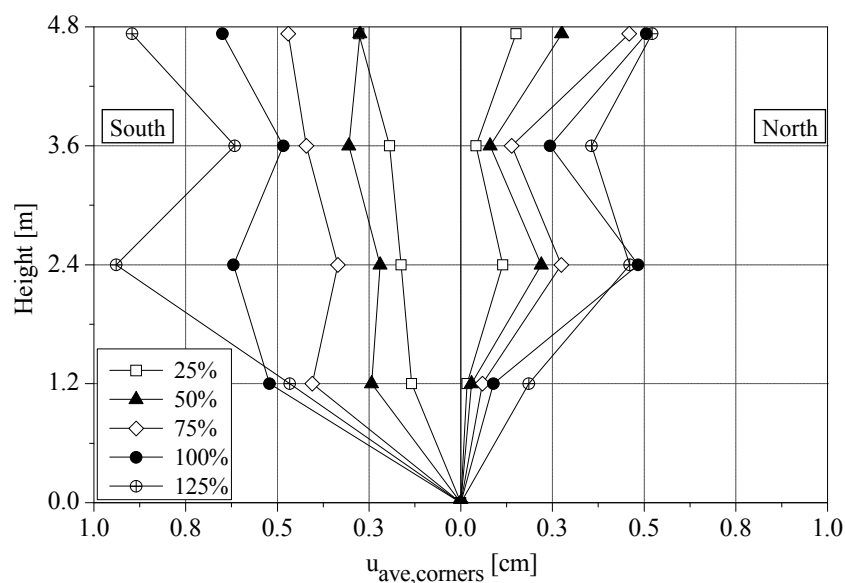


Figure 3.30 – Average out-of-plane relative displacement with respect to the corners at floor levels for the facades of the strengthened mock-up.

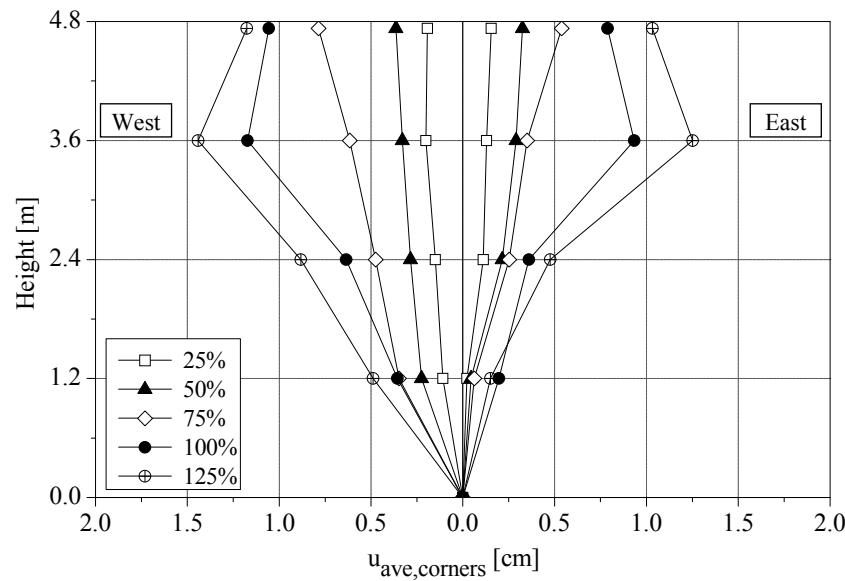


Figure 3.31 – Average out-of-plane relative displacement with respect to the corners at the floor levels for the gable walls of the strengthened mock-up.

Finally, the average maximum in-plane drift of the facades ($Drift_{in-plane,ave}$) was also plotted (Figure 3.32). The highest reduction of the in-plane drift, with respect to the non-strengthened mock-up, occurs at the first floor and is on average equal to 66% (Earthquake 100%). The second and third floors present also a significant reduction of the $Drift_{in-plane,ave}$, namely 34% and 31%, respectively. However, the top floor of the strengthened mock-up (1.5%) presents an increase of the in-plane drift of about 43%. This is related to the concentration of damage at the top floor and to the in-plane rocking of the piers and out-of-plane behaviour of the gables walls at this floor. The maximum in-plane drift is equal to 2.8% and occurs at the top of the South facade (Earthquake 125%). It is noted that the top floor of the strengthened mock-up presented behaviour clearly different from the other floors, mainly in the Earthquake 150% in which horizontal cracks at the third floor of the gable walls were observed.

The results previously presented allow already to conclude that the adopted strengthening technique improved the seismic performance of the mock-up, mainly preventing the out-of-plane collapse of the masonry walls. In the following Section a direct comparison of the seismic performance of the mock-ups is presented, in which several parameters for controlling the response are related to the seismic action applied at the base.

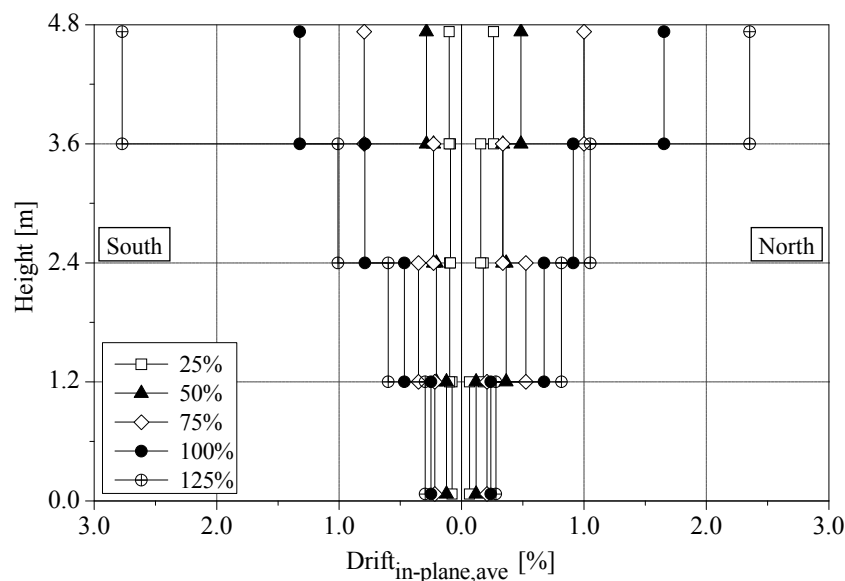


Figure 3.32 – Average in-plane drift for the facades of the strengthened mock-up.

3.5.3 Comparison of the results of the seismic test

This Section aims at comparing the main results of the seismic tests and at concluding on the improvement of the adopted strengthening techniques. Thus, seven parameters to control the response of the mock-up are related to the amplitude of the seismic action (PGA_{no}): (a) average maximum acceleration amplification at the third floor of the facades and at top of the gable walls ($Amplification_{acc,ave}$); (b) average maximum displacement at the third floor of the facades and at top of the gable walls (u_{ave}); (c) average maximum relative displacement with respect to the corners at the third floor of the facades and at the top of the gable walls ($u_{ave,cornerRadius}$); (d) average maximum in-plane drift at the third floor of the facades ($Drift_{in-plane,ave}$). The locations to control the response correspond to the floors in which the non-strengthened mock-up presents the maximum values. It is stressed again that the results here presented correspond to the average of the results of the facades and to the average of the results of the gable walls.

In the Figure 3.33 the average maximum acceleration amplification ($Amplification_{acc,ave}$) of the third floor and of the top of the gable walls are related to the PGA_{no} in the longitudinal and transversal direction, respectively. The third floor of the facades of the non-strengthened mock-up presents a progressive decrease after Earthquake 50% and is significant higher than the strengthened mock-up. Even if it presents significant low $Amplification_{acc,ave}$ in the first seismic tests, in the Earthquake 100% the strengthened mock-up presents an amplification 8% higher than the non-strengthened mock-up (Figure 3.33a). In Earthquake 100%, the top of the gable walls (Figure 3.33b) of the strengthened mock-up presents also amplification higher than the non-strengthened mock-up (18%). This means that the strengthened mock-up presents lower degradation

of the stiffness and, consequently, less damage than the non-strengthened mock-up, leading to the conclusion that the strengthening technique improved the seismic performance of the mock-up.

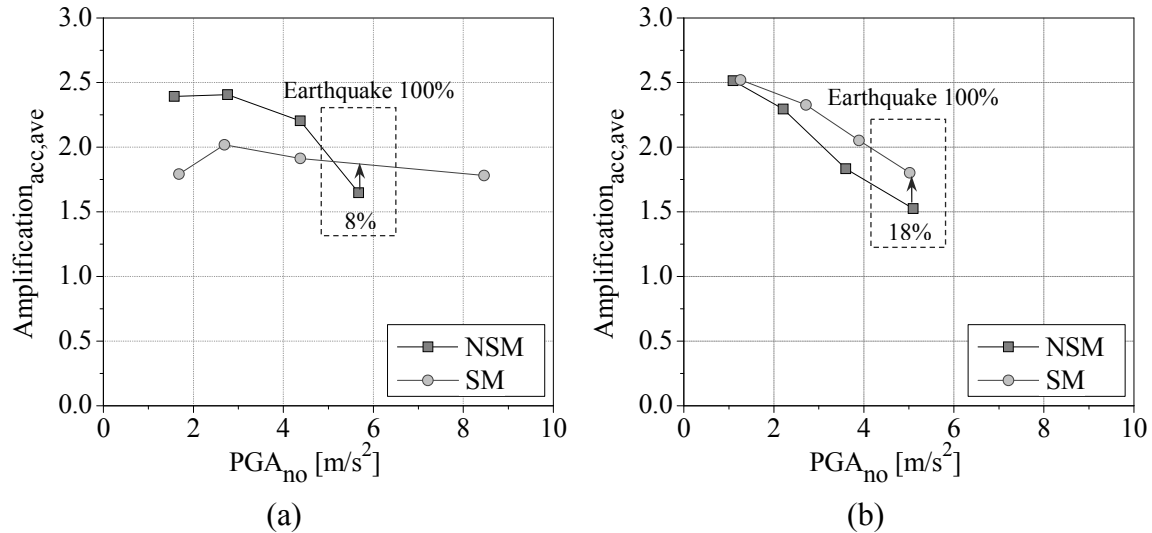


Figure 3.33 – Comparison of the average out-of-plane acceleration amplification at the: (a) 3rd floor of the facades; (b) 4th floor of the gable walls.

With respect to the average maximum displacement (u_{ave}), the third floor of the facades of the strengthened mock-up (Figure 3.34a) presents a reduction of about 20% with respect to the non-strengthened mock-up (Earthquake 100%). This means that the strengthening elements improved the out-of-plane response of the facades. However, in the Earthquake 100% the top of the gable walls of the strengthened mock-up only presents a reduction of about 8% (Figure 3.34b). It is noted that the displacements u_{ave} are mainly a global parameter of the response of the mock-ups in the longitudinal and transversal directions, which are obtained from the average of the maximum displacements of the five vertical accelerometers, including the two corners, occurring at different times of the seismic test. Taking into account that the transversal direction of the mock-ups is the most flexible (highest displacements), the non-strengthened and the strengthened mock-ups present similar behaviours in this direction. Furthermore, in the Earthquake 100% the gable walls of the mock-ups presents very low damage.

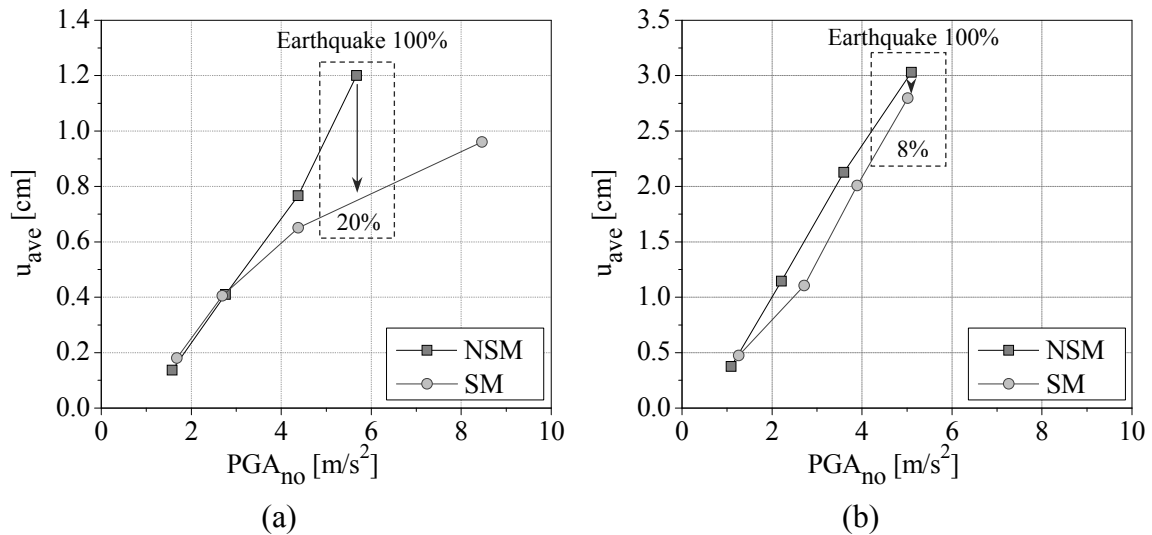


Figure 3.34 – Comparison of the average out-of-plane displacement at the: (a) 3rd floor of the facades; (b) 4th floor of the gable walls.

The displacement $u_{ave, corners}$ is a local parameter of the response of the masonry walls and allows evaluating the out-of-plane response with respect to the corners. What concerns to this parameter, in the Earthquake 100% the third floor of the facades of the strengthened mock-up presents a significant reduction of the local out-of-plane response (68%) with respect to the non-strengthened mock-up (Figure 3.35a). This reduction is according to the expected behaviour of the strengthened mock-up, i.e. it was expected that the steel angles, plates and cables limit the out-of-plane deformation of the facades. In the Earthquake 100%, the top of the gables walls of the strengthened mock-up (Figure 3.35b) also presents a significant reduction in the local out-of-plane deformation (48%). Thus, the strengthening of the connections of the timber floors, mainly the joists, with the gable walls and the steel angles improved also the local out-of-plane response of these masonry walls. Although the gable walls of the non-strengthened mock-up did not present damage, the seismic results shows that the connection of the strengthened mock-up between gable walls and timber floors are efficient.

Finally, the efficiency of the strengthening technique was also evaluated using the average maximum in-plane drift ($Drift_{in-plane, ave}$) at the third floor of the facades. In the Earthquake 100%, the $Drift_{in-plane, ave}$ of the non-strengthened mock-up presents a reduction of about 31% with respect to the non-strengthened mock-up (Figure 3.36). As expected, the steel angles and plates applied at the floor levels of the facades ensure that the masonry structural elements (spandrels and nodes spandrel/pier) remain connected, improving the in-plane response of the second and third floors, which resulted in a reduction of the in-plane relative displacements between these two floors.

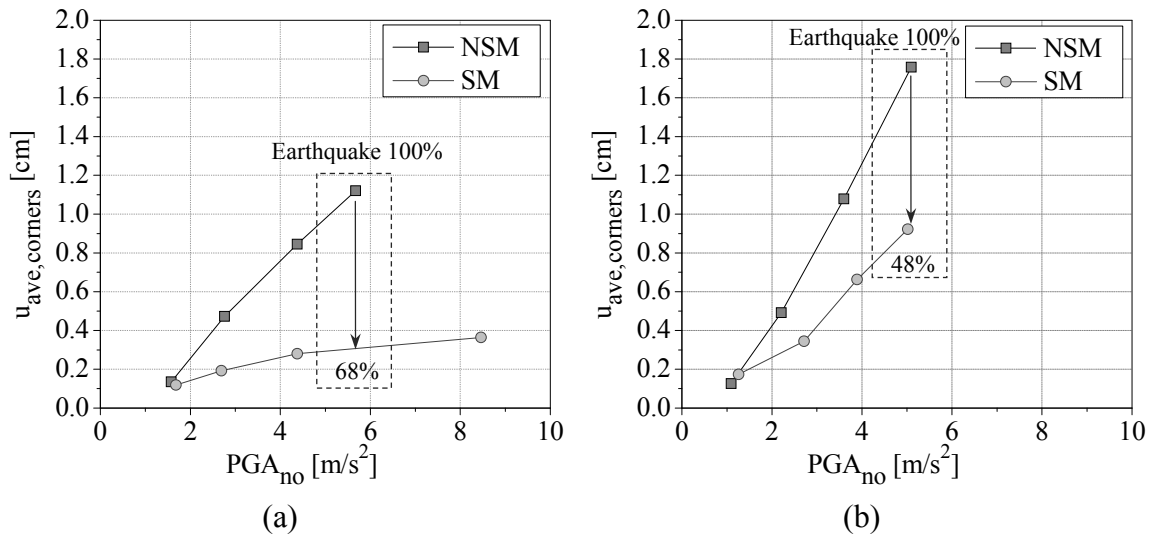


Figure 3.35 – Comparison of the average out-of-plane relative displacement with respect to the corners at the: (a) 3rd floor of the facades; (b) 4th floor of the gable walls.

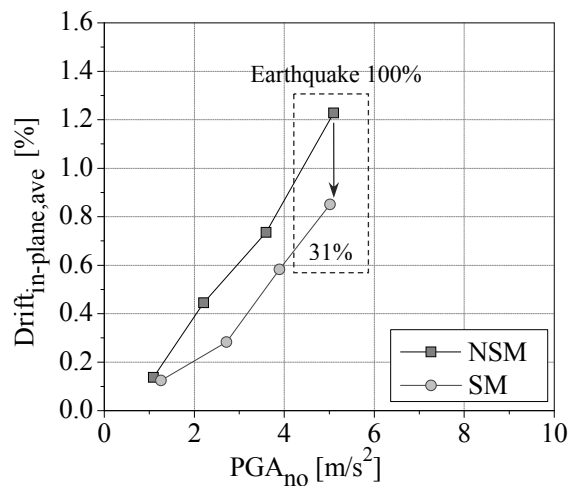


Figure 3.36 – Comparison of the average in-plane drift at the 3rd floor of the facades.

The comparison of the seismic performance of the mock-ups presents different levels of efficiency according to the parameters that are used to control the response. The non-linear multi-axial dynamic behaviour of this type of buildings is complex and depends of several variables that do not present the same evolution as a function of the seismic action applied or of the damage occurring. However, the results of the seismic tests show that the adopted strengthening techniques improved the seismic performance of the mock-up and can be considered in the reduction of the seismic vulnerability of the “gaioleiro” buildings.

3.6 Conclusions

In this Chapter the results of the dynamic identification and seismic tests at the 3D shaking table of LNEC are presented. The crack patterns shows that, in the Earthquake 100%, the non-strengthened mock-up presents a higher concentration of the damage at the facades, in which almost all spandrels have damage. Furthermore, almost all piers at the fourth level in the facade present horizontal cracks, related to in-plane rocking and out-of-plane bending. The gable walls, timber floors and corners do not present any damage. In general, the non-strengthened mock-up presents substantial damage, corresponding to a grade 3 for masonry buildings, according to the European Macroseismic Scale 1998 (Grünthal 1998). Although the collapse of the non-strengthened was not achieved, it is expected that with the increase of the seismic amplitude the damage concentrates at the spandrels and at the top piers, leading to the partial or global collapse of facades, which is common in buildings with flexible floors.

After the Earthquake 100% the non-strengthened mock-up was repaired, aiming at re-establishing the initial conditions, followed by the application of a strengthening technique. In the strengthened mock-up, steel angles and plates at the floor levels were used to provide better connection between floors and masonry walls. Additionally, steel cables at the two top floors were also applied. In the Earthquake 100%, the damage of the strengthened mock-up concentrates at the top floors, mainly at the facades. The gable walls of the strengthened mock-up present diagonal cracks, indicating that part of the out-of-plane inertial forces of the facades was transferred by the strengthening elements to the gable walls. In comparison to the non-strengthened mock-up, this mock-up presents moderate damage (grade 2), leading to the conclusion that strengthening elements improved the seismic performance of the mock-up.

The results of the dynamic identification were used to obtain the experimental seismic vulnerability curves of the mock-ups, based on relationship between a quantitative damage indicator and the seismic amplitude applied at the base. The damage indicator d is based on the decrease of the frequencies of the modes along the testing. In the Earthquake 100% and for the first transversal mode, the strengthened mock-up presents a reduction of the damage indicator d of about 46% with respect to the non-strengthened mock-up, leading to the conclusion that the strengthening technique was efficient in the reduction of the seismic vulnerability of the mock-up.

In the seismic tests the response of the mock-ups was evaluated through four parameters at the floor levels of the facades and gable walls. In the Earthquake 100% the parameters of the response of the strengthened mock-up present the following variation with respect to the strengthened mock-up:

- Average of the maximum acceleration amplification ($Amplification_{acc,ave}$) at the third floor of the facades and at the top of the gable walls: increase of 8% and 18%;

- Average of the maximum displacement (u_{ave}) at the third floor of the facades and at the top of the gable walls: reduction of 20% and 8%;
- Average of the maximum out-of-plane relative displacement with respect to the corners ($u_{ave, corners}$) at the third floor of the facades and at the top of the gable walls: reduction of 68% and 48%;
- Average of the maximum in-plane drift ($Drift_{in-plane, ave}$) at the third floor of the facades: reduction of 31%.

The results of the seismic tests show that the strengthening technique improved the seismic performance of the mock-up, mainly at the floor levels of the facades and gables that present the largest deformation in the non-strengthened mock-up.

Taking into account the results from the shaking table tests, it is concluded that the adopted strengthening technique improved significantly the seismic performance of the mock-ups, mainly the out-of-plane behaviour of the masonry walls, and is an effective solution for reducing of the seismic vulnerability of “gaioleiro” buildings.

Preparation and validation of the numerical model

4.1 Introduction

In this Chapter the calibration and validation of the numerical model of the non-strengthened mock-up at reduced scale is presented. Hereafter, only the non-strengthened model is considered, as much can be learned from this test and the addition of strengthening in a damaged and repaired model is likely to require significant effort in preparing a fine tuned numerical model. The calibration of the numerical model was based on the modal parameters (frequencies and mode shapes) estimated in the first dynamic identification test. In this calibration process, four numerical models with different variables to update and different number of modes were considered. After the modal updating, two non-linear dynamic analyses with time integration were carried out for validation of the numerical model in the non-linear range. In the first non-linear dynamic analysis the Earthquake 25% was applied and a comparison of the response, in terms of acceleration, displacements and crack patterns was done. A non-linear dynamic analysis with the Earthquake 100% was also done. Here, the main objective was to compare the elements with concentration of damage and the collapse mechanisms with respect to the ones observed in the experimental tests. Finally, a full size numerical

model was also prepared in order to discuss the scale effect, taking into account the modal parameters and the response for the Earthquakes 25% and 100%.

4.2 Preparation of the numerical model

The model of the non-strengthened mock-up is based on a macro-modelling strategy, in which the masonry is assumed as a composite and the units, the mortar and the interface are smeared out in the continuum (Lourenço 1996). The objective is to reduce the time and memory requirements of the analysis. Furthermore, this modelling strategy is more user-friendly to generate the mesh and provides a good compromise between accuracy and efficiency. The numerical model was prepared on a 1:3 reduced scale, using the Finite Element Method (FEM) and the non-linear analysis software DIANA (TNO 2009), aiming at comparing to the experimental results of the shaking table tests. The FEM will not be reviewed here as full details are given for example in Zienkiewicz and Taylor (2000) and Hutton (2004).

In the numerical model, quadratic shell elements with eight nodes (CQ40S) were used for simulating the masonry walls and beam elements with three nodes (CL18B) were used for simulating the MDF panels and the timber joists (TNO 2009). All the finite elements are based on the theory of Mindlin-Reissner, in which the shear deformation is taken into account. In the modeling of the floors, shell elements were used aiming at simulating the in-plane deformability (Figure 4.1). The adopted geometry properties are equal to the ones of the mock-up at 1:3 reduced scale, i.e. the thickness of the masonry walls and of the MDF panels is equal to 0.170 m and 0.012 m, respectively, and the dimensions of the cross section of the timber joists are equal to 0.100x0.075 m² (width and height), with spacing of 0.35 m. In plan, the numerical model has 3.15x4.15 m² and the interstory height is equal to 1.20 m. The translation and rotation degrees of freedom at the base were restrained.

The connection between masonry walls and floors is complex, making it difficult to numerically simulate it. Furthermore, the behaviour of the connections was not measured in the shaking table tests, taking as an example the relative displacements between the walls and floors. In the numerical model a joint between the nodes in the perimeter of the floors and the nodes of the masonry walls at the floor levels was made, i.e. the floors and the walls are physically separated. Here, the objective was to prepare a general numerical model in which different hypotheses to simulate the connections can be used (springs, interfaces elements, tyings, etc.). As a first attempt, tyings providing equal translation of degrees of freedom between walls and floors were assumed. The numerical model involves 5,816 elements (1,080 beam elements and 4,736 shell elements) with 15,176 nodes, resulting in 75,880 degrees of freedom.

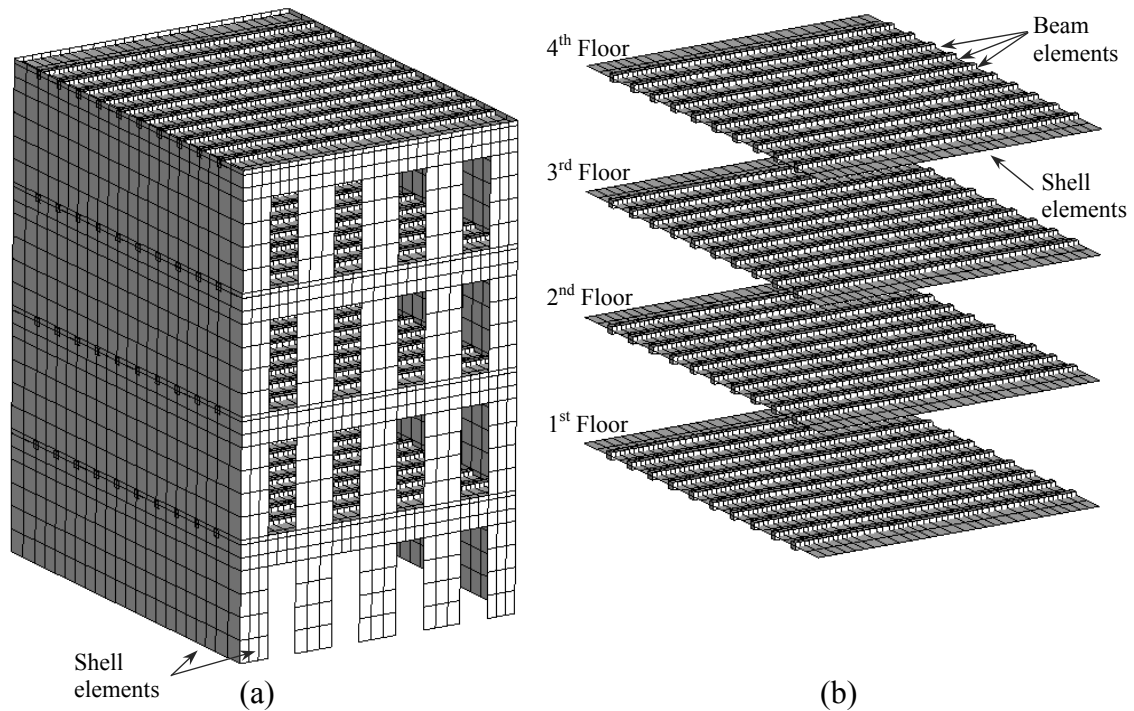


Figure 4.1 – Numerical model: (a) general view; (b) detail of the floors.

A linear static analysis, using the material properties presented in Table 4.1, was initially carried out. It is noted that the material properties of this model are not calibrated. The total self-weight of the numerical model is equal to 220 kN (equal to the measured weight of the mock-up). In this analysis, the numerical model presents very low deformation (3 mm of vertical deformation at the floors) and the maximum compressive principal stress is about 0.18 MPa at the base, leading to the expected observation that the numerical model presents linear behaviour under its self-weight. It is noted that the compressive strength obtained in the axial compression tests of the wallets is equal to 6.00 MPa.

Table 4.1 – Material properties of the first numerical model (not calibrated).

	Young's modulus [GPa]	Specific mass [kg/m ³]	Poisson ratio
Masonry walls	3.37	2162	0.2
MDF panels	0.15	760	0.3
Timber joists	12.00	580	0.3

4.3 Calibration of the dynamics properties

After the preparation of the numerical model, the modal parameters were calibrated based on the minimization of the difference between the experimental and the numerical dynamical properties. In this process, the frequencies and mode shapes of the numerical model were updated assuming the Young's modulus of the materials as variables to calibrate. Two methods for modal updating are briefly presented next, together with the results of the modal updating of the mock-up carried out.

4.3.1 Modal updating methods

The calibration of numerical frequencies can be accomplished with the method proposed by Douglas and Reid (1982), in which the frequency i of the numerical model f_i^N can be estimated by means of:

$$f_i^N(X_1, X_2, \dots, X_n) = C_i + \sum_{k=1}^n \left[A_{ik} X_k + B_{ik} (X_k)^2 \right] \quad (4.1)$$

where X_k ($k=1, 2, \dots, n$) are the variables to calibrate and A_{ik} , B_{ik} and C_i are constants.

The $(2n+1)$ constants can be obtained by the following system of equations:

$$\left\{ \begin{array}{l} f_i^N(X_1^B, X_2^B, \dots, X_n^B) = C_i + \sum_{k=1}^n \left[A_{ik} X_k^B + B_{ik} (X_k^B)^2 \right] \\ f_i^N(X_1^L, X_2^B, \dots, X_n^B) = C_i + \sum_{k=1}^n \left[A_{ik} X_k^L + B_{ik} (X_k^B)^2 \right] \\ f_i^N(X_1^U, X_2^B, \dots, X_n^B) = C_i + \sum_{k=1}^n \left[A_{ik} X_k^U + B_{ik} (X_k^B)^2 \right] \\ \dots \\ f_i^N(X_1^B, X_2^B, \dots, X_n^L) = C_i + \sum_{k=1}^n \left[A_{ik} X_k^L + B_{ik} (X_k^L)^2 \right] \\ f_i^N(X_1^B, X_2^B, \dots, X_n^U) = C_i + \sum_{k=1}^n \left[A_{ik} X_k^U + B_{ik} (X_k^U)^2 \right] \end{array} \right. \quad (4.2)$$

where X_k^B are the base values of the variables to calibrate (starting point or initial values), and X_k^L and X_k^U are their respective upper limit and lower limit values. Engineering judgment is necessary to define this set of values, as the result depends on this selection.

After calculating the constants, a least square minimization of the difference between the numerical frequencies f_i^N and the experimental ones f_i^E is carried out:

$$\pi = \sum_{i=1}^m w_i \varepsilon_i^2 \quad (4.3)$$

$$\varepsilon_i = \sum_{i=1}^m f_i^E - f_i^N (X_1, X_2, \dots, X_n) \quad (4.4)$$

where π is the objective function, ε is the residual function, w is the weight constants and m is the number of frequencies considered in the updating. For examples of the application of the Douglas Reid method see e.g. Gentile and Saisi (2004) and Mendes and Lourenço (2009).

A more robust updating method is used by Ramos (2007) and Teughels (2004), which is also used here to introduce directly in the objective function π the errors between the experimental and numerical natural frequencies ($\omega_{i,E}$ and $\omega_{i,N}$) and the differences between the experimental and numerical mode shapes ($\phi_{i,j,E}$ and $\phi_{i,j,N}$), resulting in:

$$\pi = \frac{1}{2} \left[W_\omega \sum_{i=1}^m \left(\frac{\omega_{i,N}^2 - \omega_{i,E}^2}{\omega_{i,E}^2} \right)^2 + W_\phi \sum_{i=1}^m \sum_{j=1}^n \left(\frac{\phi_{i,j,N}^2 - \phi_{i,j,E}^2}{\phi_{i,j,E}^2} \right)^2 \right] \quad (4.5)$$

where W_ω and W_ϕ are the weight constants of the natural frequencies and mode shapes, respectively, m is the number of modes and j is the number of modal displacements. The experimental and numerical mode shapes must be normalized such as the maximum real value of the modal displacement is equal to one.

The optimization can be carried out using the algorithms of the least squares problems, in which the Gradient $\nabla \pi(\theta)$ is constructed from the sensitivity matrix \underline{J} (Jacobian matrix with i rows and j columns) and is calculated from the first order partial derivatives of the residual functions:

$$\underline{J}(\theta)_{ji} = \frac{\partial \pi_i(\theta)}{\partial x_j} \quad (4.6)$$

and the Hessian $\nabla^2 \pi(\theta)$ matrix \underline{G} is calculated from the second order partial derivatives of the residual functions:

$$\underline{G}_i(\theta)_{jk} = \frac{\partial^2 \pi_i(\theta)}{\partial x_j \partial x_k} \quad (4.7)$$

where ε is the residual function and θ are the variables to calibrate.

The Gradient and the Hessian of the objective function have the following form:

$$\begin{aligned} \nabla \pi(\theta) &= \underline{J}(\theta)^T \pi(\theta) \\ \nabla^2 \pi(\theta) &= \underline{J}(\theta)^T \underline{J}(\theta) + \underline{Q}(\theta) \end{aligned} \quad (4.8)$$

where

$$\underline{Q}(\theta) = \sum_{i=1}^m \pi_i(\theta) \underline{G}_i(\theta) \quad (4.9)$$

The updated solution is obtained through using a least squares algorithm by minimization of the objective function until a given tolerance is achieved. It is noted that these methods can be unsuccessful when the objective function has several local minima. This aspect will be addressed in the discussions of the results of the modal updating of the numerical model.

In the case study, the nonlinear least square method implemented in MATLAB (2006) (function *lsqnonlin*) was used together with the software DIANA (TNO 2009) to calculate the numerical frequencies and mode shapes. A condition for stopping the iterative process of optimization was added, as the iterative process also stops if the difference between the values of the variables to calibrate in iteration n and $n-1$ is lower than the prescribed tolerance. A common tolerance of 10^{-6} for the difference between the iteration n and $n-1$ in the objective function and the variables to calibrate was assumed.

4.3.2 Results of the modal updating

In the modal updating four numerical models with different variables to calibrate were considered (Figure 4.2). In Model 1 the Young's modulus of the masonry walls and MDF panels were considered as variables to calibrate. Model 2 considers different Young's modulus for the masonry of the facades and gable walls, besides the Young's modulus of the MDF panels. Due to the dimensions of the piers and lintels, the facades presents stone units smaller than the ones used in the gables walls, causing different ratios of (mortar thickness)/(stone units' size). In Model 3 a different Young's modulus for the corners was also considered. Here, the objective was to simulate indirectly the

real stiffness between orthogonal masonry walls, because the usage of shells in FEM tends to under-predict the actual stiffness of the corners. Finally, Model 4 has four variables to calibrate, namely the Young's modulus of the facades, gables walls and MDF panels and the stiffness of the springs used to simulate the connection between facades and floors. The springs aim at improving the modal updating of the longitudinal modes, which are mainly related to the local behaviour (out-of-plane) of the facades.

In the modal updating, only the Young's modulus of the masonry and the stiffness of the springs between facades and floors were considered as variables to calibrate. The densities of the materials are well known, particularly the density of masonry, which represents the higher portion of mass in the mock-up. The Young's modulus of the timber joists does not have a relevant influence in the frequencies and modes shapes.

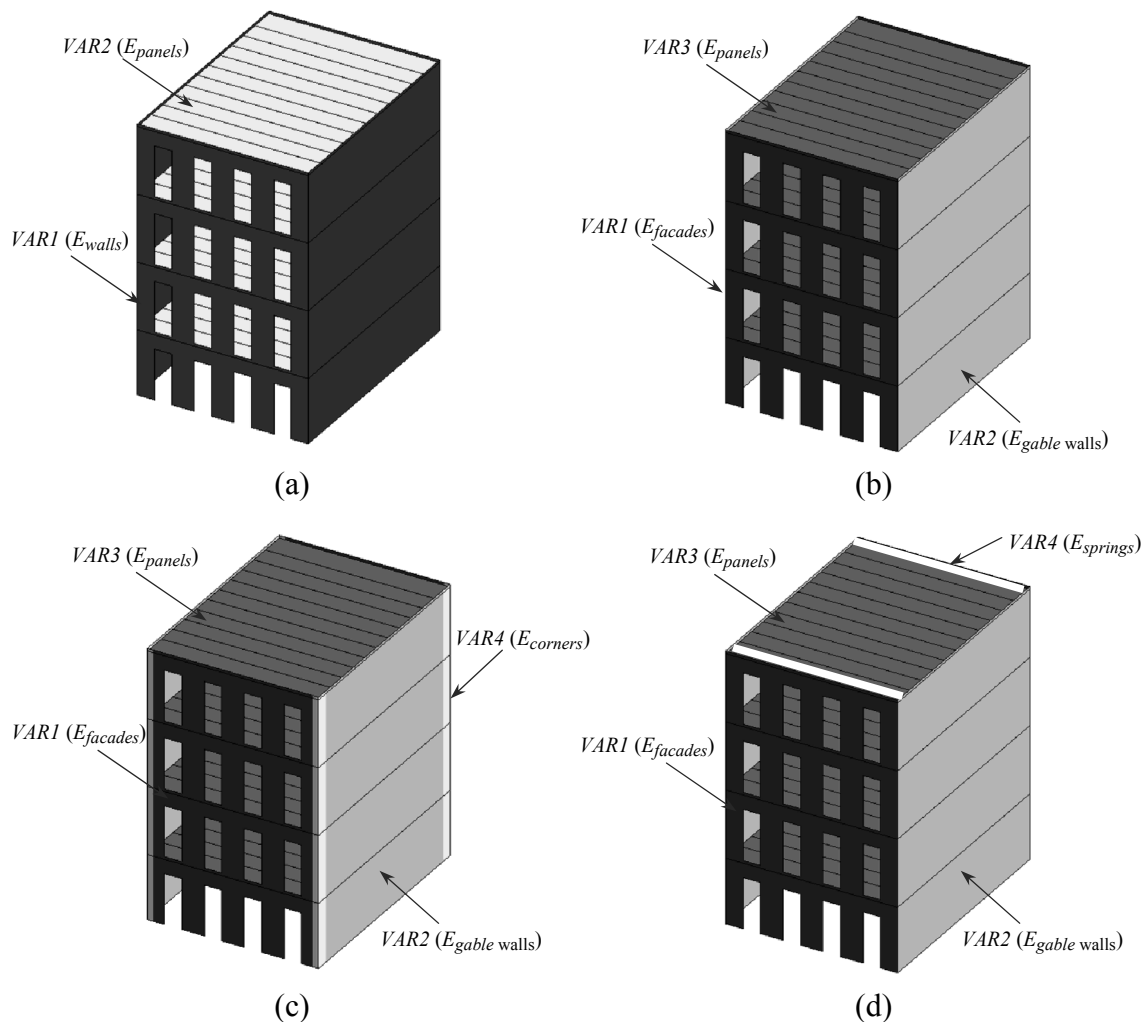


Figure 4.2 – Variables used in the modal updating: (a) Model 1; (b) Model 2; (c) Model 3; (d) Model 4.

As mentioned in the previous Section, the objective function for the modal updating method can present several local minima, i.e. the method is sensitive to the adopted

initial values. Thus, several optimization analyses were done for each numerical model, using different initial values for the variables to calibrate. In this procedure, the base values for each variable to calibrate were defined and the optimization was carried out. Afterwards, the initial values of all variables were increased and decreased 25% and 50% with respect to the base values and new optimization analyses were carried out. Finally, each variable was increased and decreased 25% and 50% with respect to its base value (while the other variables remained with their base values) and new optimization analysis were done. This procedure allowed to evaluate the influence of the initial values of the variables on the modal updating and to obtain more reliable values, resulting in $5+4n$ optimizations for each numerical model (n is the number of variables to calibrate).

The number of modes to calibrate is an important aspect to take into account in the modal updating. In the first dynamic identification of the non-strengthened mock-up eleven modes were identified (Figure 3.7). However, it is known that the greater the number of modes used, the more difficult is the modal updating. Thus, the modal updating was focused in the first modes, as they have higher contribution for the dynamic behaviour, assuming two hypotheses: (a) modal updating considering the first four modes (first transversal, first distortional and the two first longitudinal); (b) modal updating considering the first five modes (two first transversal, first distortional and the two first longitudinal). These hypotheses increased the number of optimizations and for each numerical model $2x(5+4n)$ optimizations were carried out, with exception of the Model 4, in which the modal updating was only done considering the first five modes, because the previous numerical models (Model 2 and 3) already presented very low frequency errors using the first four modes.

Figure 4.3 presents the average of the *MAC*'s (Equation (3.8)) and frequency errors for all optimizations carried out. In general, the results show that the average of *MAC*'s is almost insensitive to the type of numerical models and to the initial values of the variables. The *MAC* is, on average, equal to 0.90, which is a satisfactory result. Model 1 (Figure 4.3a), which has only two variables, is not sensitive to the initial values in the calibration of the first four modes (average of the frequency error is equal to 3.8%). In the calibration of the first five modes, the minimum average of the frequency errors is equal to 9.5% (*VAR2* with more 25%) and different from the results of other optimizations (11.1%), leading to the conclusions that Model 1 is sensitive to the initial values adopted in the calibration of the first five modes. In the modal updating of Model 2 (Figure 4.3b), the minimum frequency error, on average, is equal to 1.3% and 3.9% considering the four and five first modes, respectively, which is a significant improvement with respect to Model 1. Model 2 considers different variables in the facades and the gables walls, and the results show that the updated value of the Young's modulus of the facades (*VAR1*) is significantly lower than the Young's modulus of the gable walls (*VAR2*) (see Annex B). This aspect can be related to the different ratio of (mortar thickness)/(stone units' size) present in the masonry walls and also, indirectly,

to simulate the out-of-plane flexibility of the facades caused by the weak connections between facades and timber floors. Furthermore, modal updating of Model 2 is more sensitive to the adopted initial values, with an average frequency error ranging from 1.3% to 7.8% and from 3.9% to 17.5% considering the first four and five modes, respectively. The modal updating of Model 3 (Figure 4.3c), in which a different Young's modulus of the corners was also considered, presents a low decrease of the frequency errors (1.4% and 3.6% in the calibration of the first four and five modes, respectively) and a large scatter in the solutions of the optimization. Finally, Model 4 aims at simulating the weak connections between facades and gable walls through springs and, consequently, at increasing the Young's modulus of the facades obtained in the modal updating of Model 2. The average of the frequency errors increased with respect to previous models (4.6%) (Figure 4.3d) and the Young's modulus of the facades did not exhibit the expected behaviour.

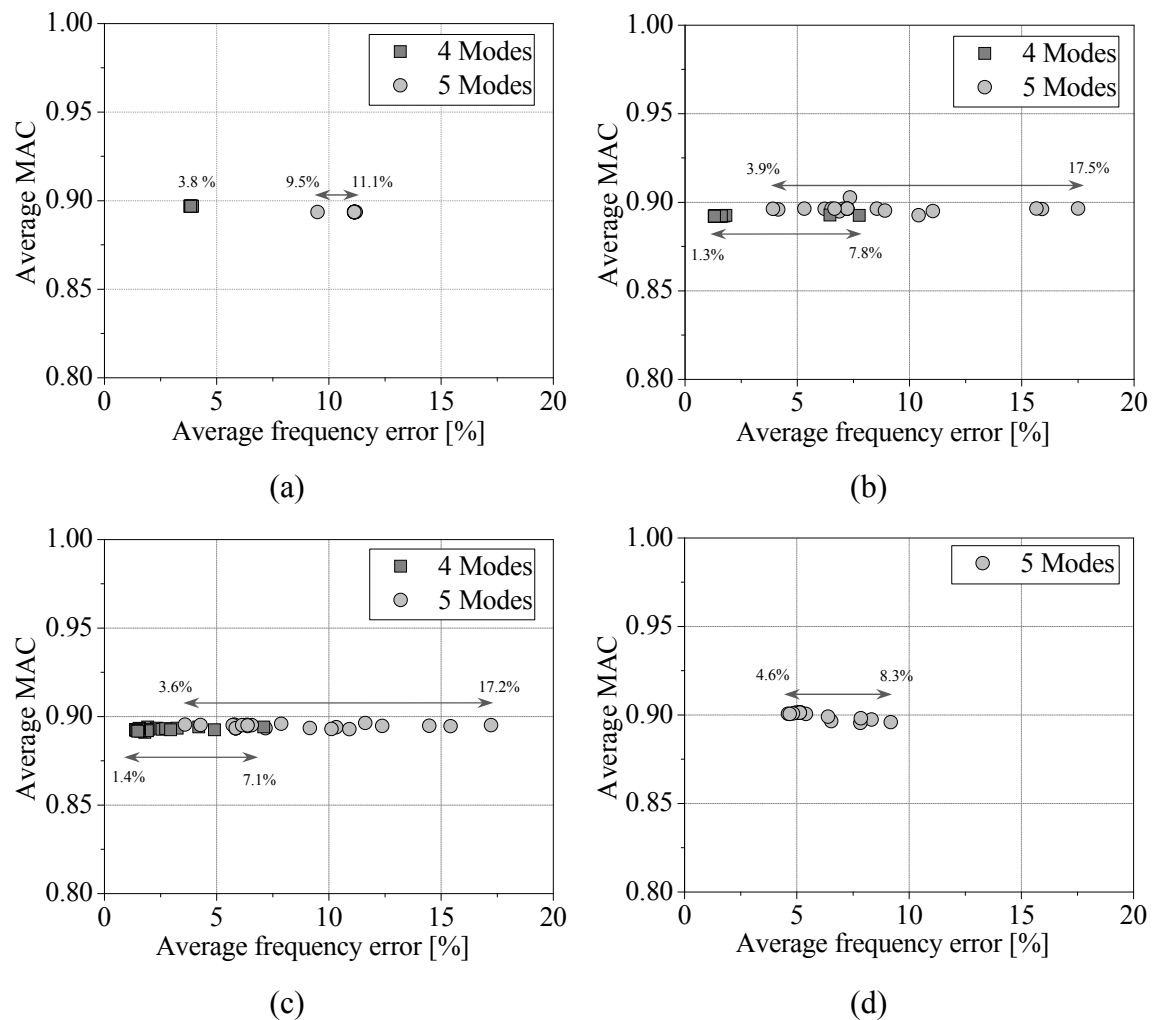


Figure 4.3 – Results of the modal updating for the: (a) Model 1; (b) Model 2; (c) Model 3; (d) Model 4.

After this large number of optimizations, a numerical model needs to be selected. The *MAC*'s do not present significant variations between the different models and, consequently, it is not a parameter that influences the decision of the numerical model to select. On the other hand, the average of the frequency errors ranges significantly and two numerical models present similar minima (Model 2 and 3). The difference between the minima of the frequency error considering the first four or the first five modes is small and the frequency average error using the first five modes is acceptable (3.6% and 3.9%). Thus, the modal updating of Model 3 considering the first five modes was selected. Model 3 presents the minimum of frequency error on average (3.6%) and the updated value of the Young's modulus of the gable walls (3.45 GPa) is the closest to the one obtained in the uniaxial compressive tests of the wallets (3.37 GPa) and the error of the frequency of the first mode is also lower. For more details on the modal updating of the numerical models see Annex B. Next, the results of the modal updating of Model 3 are presented in detail.

Table 4.2 presents the material properties of Model 3, including the updated values of the Young's modulus of the facades, gable walls, corners and MDF panels. As previously referred, an interesting aspect concerns the updated value of the gables walls, which is close to the one obtained in the uniaxial compressive tests of the wallets. In fact, the masonry used in the gable walls and in the wallets is the same and similar values of the material properties obtained from the uniaxial compressive tests and from the modal updating could be expected. The Young's modulus of the facades presents a value much lower than the one of the gable walls (0.64 GPa). This can be related to the higher percentage of mortar in the masonry and, indirectly, to the weak connection between facades and timber floors, i.e. the modal updating can decrease the Young's modulus of the facades to increase the out-of-plane modal components of the longitudinal mode shapes. The updated value of the Young's modulus in the corners presents an intermediate with respect to the facades and the gable walls (2.05 GPa). Finally, the updated Young's modulus of the MDF panels presents a very low value (0.16 GPa), as expected, simulating the flexible timber floors with joints.

Table 4.2 – Material properties of the Model 3 after modal updating.

	Young's modulus [GPa]	Specific mass [kg/m ³]	Poisson ratio
Facades	0.64*	2162	0.2
Gable walls	3.45*	2162	0.2
Corners	2.05*	2162	0.2
MDF panels	0.16*	760	0.3
Timber joists	12.00	580	0.3

(* updated value in the modal updating)

The results of the modal updating in terms of residuals of the objective function, frequency and *MAC* values are presented in the Figure 4.4. The history of the residuals of the objective function presents an instability related to the change of order of the last two modes, resulting in an alternation of high and low values of residuals. The frequency error, on average, is equal to 3.6%, in which the lowest and the highest errors of the frequency of the first and fifth modes (0.1% and 11.6%), respectively, are highlighted. Considering only the first four modes, the average frequency error is equal to 1.6% and approaches the value obtained in the modal updating using the first four modes (Figure 4.3c). However, in this modal updating the *MAC* of the fifth mode was also calibrated. The transversal modes (first and fifth modes) present the highest *MAC* values (0.99 and 0.91). The longitudinal modes (third and fourth modes) are more complex, due to the weak connection between facades and floors, and presents *MAC*'s equal to 0.89 and 0.88. The *MAC* of the distortional mode is equal to 0.81.

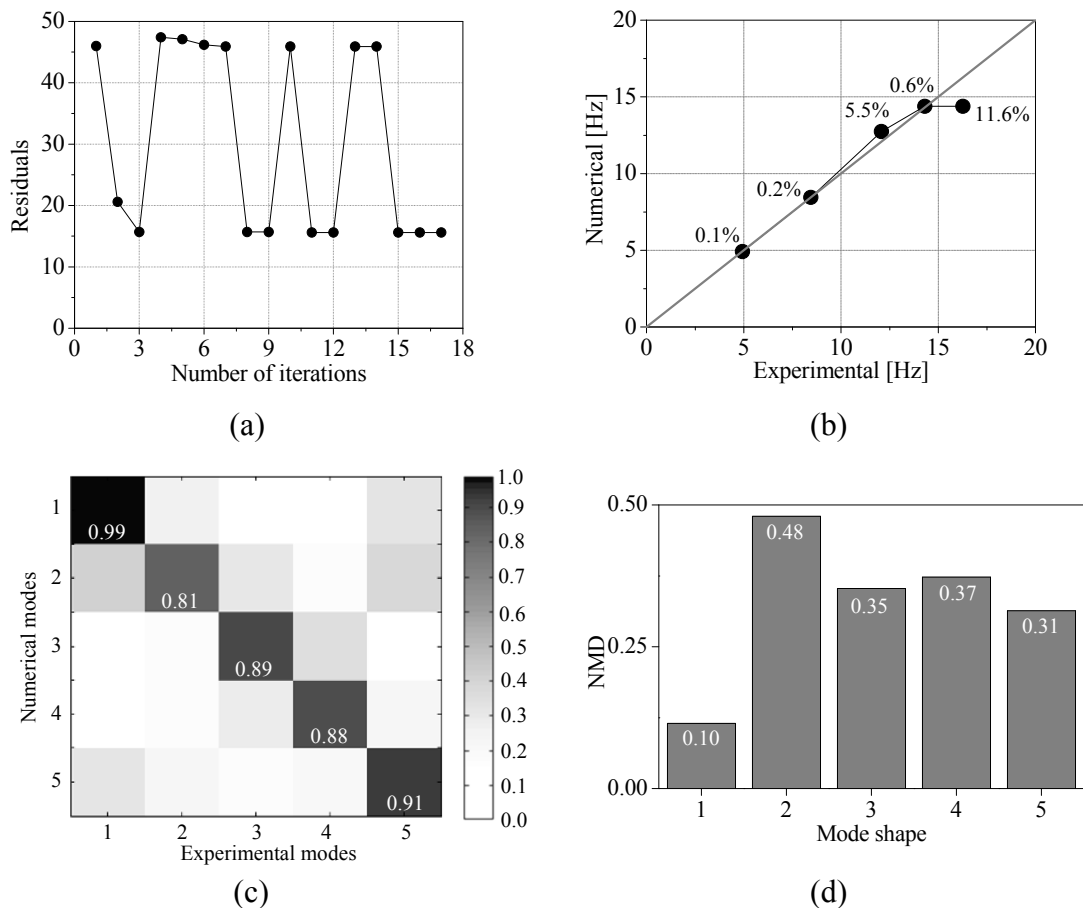


Figure 4.4 – Results of the optimization of the Model 3: (a) residuals of the objective function; (b) frequency comparison and errors; (c) *MAC* matrix; (d) *NMD* values.

In the modal evaluation, besides the frequency and MAC , the Normalised Modal Difference (NMD) was also used, which is more sensitive to the differences between the eigenvectors ϕ^u and ϕ^d and is calculated through the MAC as (Gentile and Cabrera 2001):

$$NMD_{u,d} = \sqrt{\frac{1 - MAC_{u,d}}{MAC_{u,d}}} \quad (4.10)$$

A NMD lower than 0.33 (MAC greater than 0.90) is, usually, assumed as an indicator of a good correlation between the two mode shapes. Using the NMD , it is concluded that the shapes of the numerical and experimental transversal modes present the highest correlations (Figure 4.4d). It is striking that the NMD is equal to 0.1 for the first transversal mode.

Finally, the Co-ordinate Modal Criterion ($COMAC$), which gives local information in the point i and considers the m mode shapes, was also calculated (Ewins 2000):

$$COMAC_{i,u,d} = \frac{\left| \sum_{j=1}^m \phi_{i,j}^u \phi_{i,j}^d \right|^2}{\sum_{j=1}^m (\phi_{i,j}^u)^2 \sum_{j=1}^m (\phi_{i,j}^d)^2} \quad (4.11)$$

A $COMAC$ equal to one means that modal displacements of two mode shapes in point i are equal. In the case study, the DOF's measured in the dynamic identification tests are represented by 64 points (16 points for the 4 corners with 4 floors and 48 points for the 3 central vertical alignments of each wall with 4 floors). The 64 modal displacements used in the modal updating for each direction correspond to the 40 modal displacements obtained from the dynamic identification tests in two of the walls (direct accelerometer reading of out-plane measurements orthogonal to the facades or gable walls) and 24 extrapolated modal displacement for the in-plane direction at the 3 central vertical alignments with 4 floors of the two perpendicular walls. It is noted that in the dynamic identification tests no accelerometers were used at the central vertical alignments measuring the in-plane response and these modal displacements were obtained by extrapolation, aiming at obtaining the complete mode shapes of the mock-ups. The average $COMAC$'s are equal to 0.85 and 0.62 in the transversal and longitudinal direction, respectively (Figure 4.5), showing that the correlation between the experimental and numerical modal displacements are very good in the transversal direction and acceptable in the longitudinal direction.

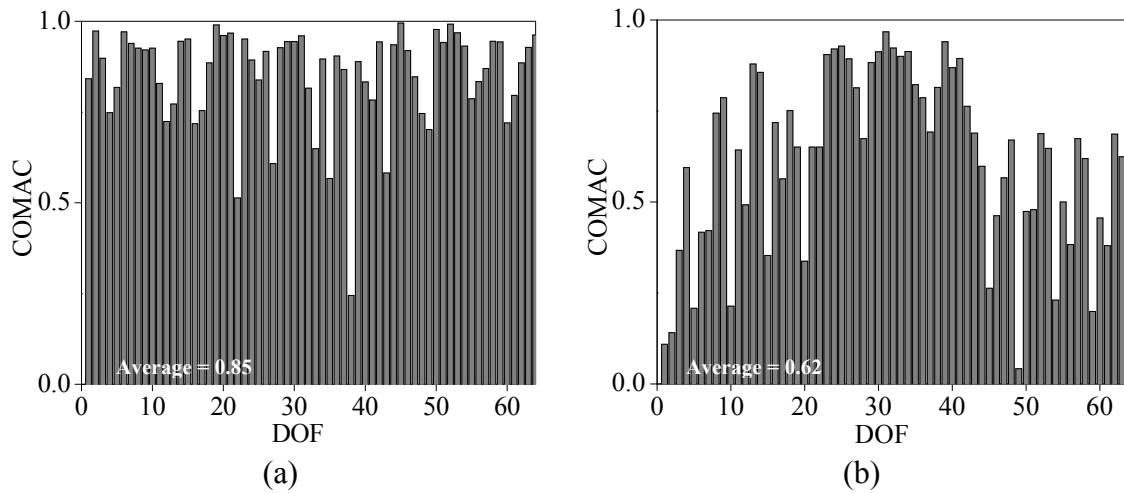


Figure 4.5 – *COMAC* values in the: (a) transversal direction; (b) longitudinal direction.

Figure 4.6 presents the numerical mode shapes and a comparison between the numerical and experimental modal displacements after updating. In general, a good correlation between numerical and experimental transversal modes is observed. The longitudinal and distortional modes are more complex and difficult to calibrate, as shown by the weaker, though acceptable, correspondence between the numerical and experimental modal displacements. It is noted that all the DOF's for each mode were used and the hypothesis of using only the DOF's in the direction of the modes (removing the modal displacements almost equal to zero) could artificially improve the modal updating.

In the modal updating only the first five modes were considered, which correspond to a contribution of about 82% and 33% of the total mass in the transversal and longitudinal direction, respectively (values of the updated numerical model). The cumulative effective mass in the transversal direction is close to the one required in the modal analysis (90%) presented in the Eurocode 8 (EN 1998-1 2004). However, in the longitudinal direction the cumulative effective mass is low due to the type of mode shapes obtained. In fact, the longitudinal modes are local modes of the facades, which mobilize mainly the mass of the facades and, consequently, provide a low contribution with respect to the total mass of the mock-up. Assuming a failure given by the local collapse of the facades, the contribution of the longitudinal modes increases significantly, because the effective mass is calculated considering the modal displacements of the facades and the total mass is equal to the mass of the facades and floors (7.80 ton). It is also noted that the modes with facades are in contra-phase (second and fourth modes), meaning that they present an effective mass equal to zero.

In the processing of the experimental results of the seismic tests, the signals were filtered with the highest frequency of cutting equal to 25 Hz. In this frequency range the cumulative effective mass of the modes is about 83% and 62%, with respect to total mass of the mock-up, in the transversal and longitudinal direction, respectively. Similarly, the lower contribution in longitudinal direction is related to the local modes estimated in this direction.

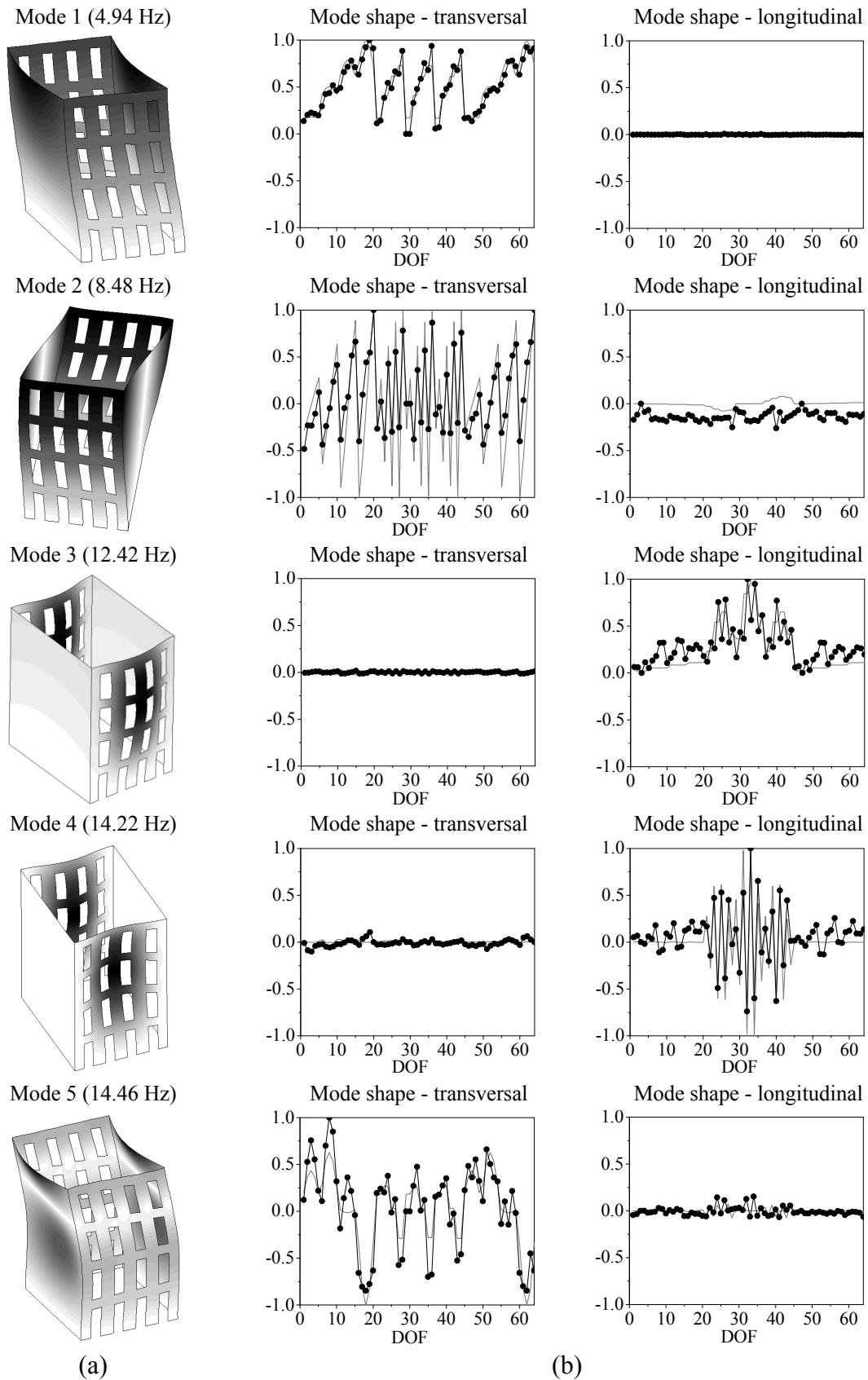


Figure 4.6 – Numerical mode shapes (Model 3): (a) general view; (b) comparison between the numerical (marker line) and experimental (grey line) DOF's in the transversal and longitudinal direction.

In conclusion, the updated modal parameters (frequencies and mode shapes) of the first five modes of the numerical model (Model 3) present a good and an acceptable correlation in the transversal and longitudinal direction, with respect to the modal parameters estimated in the first dynamic identification test (DI0) of the non-strengthened mock-up.

4.4 Non-linear dynamic analysis with time integration

The numerical model of the non-strengthened mock-up was updated in terms of modal properties estimated in dynamic identification tests, in which an acceleration signal with low amplitude is applied at the base of the mock-up, i.e. the numerical model is calibrated with respect to the linear dynamic properties. But non-linear dynamic analyses with time integration for the Earthquakes 25% and 100% were also carried out. Here, the objective is to discuss the response and to further validate the model by comparing the numerical results with the experimental response of the mock-up, including the damage and collapse mechanisms. Next, a description of the tools used in this type of analysis and the comparison between the numerical and experimental response of the mock-up are presented.

4.4.1 Analysis tools

Non-linear dynamic analysis with time integration for masonry structures is complex and takes considerable time to run and to process the results. In opposition to the typical reinforced concrete framed structures, where it is easy to identify the yielding hinges, masonry buildings have distributed cracking throughout the structure, which features opening, closing and reopening, due to the low value of the tensile strength.

The selection of an adequate material constitutive model was based on a compromise between accuracy of the results and computation time. The Total Strain Fixed Crack Model (TNO 2009), which corresponds to a model of distributed and fixed cracks based on total strains, was selected due to its robustness and simplicity. In this model, the cracks are fixed according the principal directions of the strains and remain invariant during the loading of the structure. Furthermore, in each integration point a maximum of two orthogonal cracks can open (Figueiras 1983, Damjamic and Owen 1984, Póvoas 1991). Experimental research showed that the cracks can rotate during the loading of the structure (Vecchio 1981) and material models with fixed cracks can have a strength capacity slightly higher than the real ones in shear dominated applications.

Multi-fixed crack models allow the development of more than two cracks per integration point, not necessarily orthogonal. This type of material model provides

lower strength capacity than the real ones, since the deterioration of the stiffness increases due to the possibility of the cracks to rotate according to the directions of the principal strains. But rotational crack models are not recommended for the application sought and they are less stable, due to the difficulty of controlling, simultaneously, the opening, the closing and the reopening of the cracks. Consequently, the fixed crack model was adopted. It is noted that more complex anisotropic models are available for masonry, but these are not justified for this particular stone masonry type.

After selecting of the non-linear material model, the next step is the definition of the stress-strains relationships to be used in the different types of behaviour. Here, and taking into account that only the non-linear behaviour of the masonry was considered, exponential tension-softening for the tensile behaviour and parabolic hardening and softening for the compressive behaviour were adopted. The shear behaviour was simulated by a linear relationship between stress and strains, in which the shear stiffness is reduced after cracking according to the following equation:

$$G^{cr} = \beta G \quad (4.12)$$

where G^{cr} is the shear modulus after cracking, G is shear modulus without damage and β is the shear retention factor (ranging from zero to one).

The crack bandwidth h for the shell elements was estimated as function of the area of the element A , making the analysis results independent of the size of the finite element mesh:

$$h = \sqrt{A} \quad (4.13)$$

During an earthquake with high amplitude the materials are subjected to tensile and compressive stresses, resulting in cracking and crushing. In the adopted hysteretic behaviour for the masonry (Figure 4.7), the degradation of the material is monitored by the vector of the strains of internal damage ε_{damage} , which in a three-dimensional application takes the following form:

$$\varepsilon_{damage} = [\varepsilon_1^d, \varepsilon_2^d, \varepsilon_3^d, \varepsilon_4^d, \varepsilon_5^d, \varepsilon_6^d]^T \quad (4.14)$$

where ε_1^d to ε_3^d monitor the maximum tensile strains and ε_4^d to ε_6^d monitor the maximum compressive strains, in the principal directions of the strains. In the adopted hysteretic behaviour it is assumed that damage recovery is not possible, which implies that the absolute strains of internal damage cannot assume values lower than the ones obtained in the previous time step.

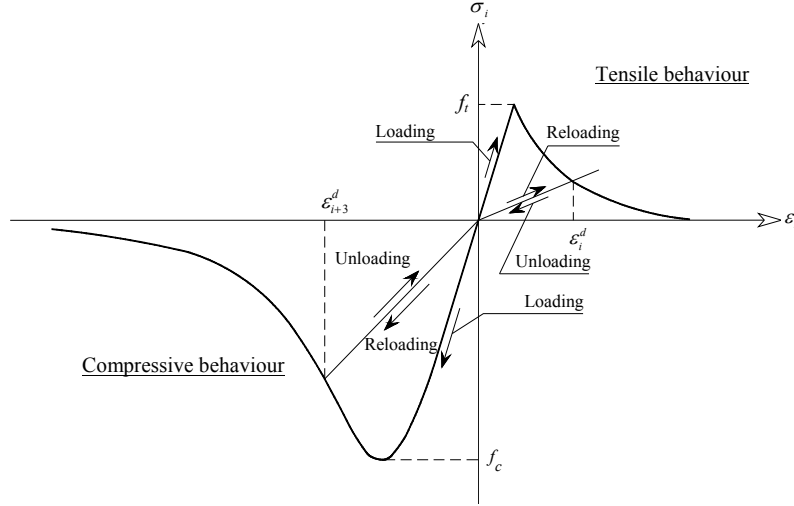


Figure 4.7 – Adopted hysteretic behaviour.

The loading-unloading-reloading condition is controlled by additional unloading constraints r_i (i correspond to the directions of the principal strains) allowing to monitor the stiffness degradation in tension and in compression. In tension the unloading constraints are given by:

$$r_i = \begin{cases} 0 & \text{if } {}^{t+\Delta t}\varepsilon_i > {}^t\varepsilon_i^d \\ 1 & \text{if } {}^{t+\Delta t}\varepsilon_i \leq {}^t\varepsilon_i^d \end{cases} \quad i=1,2,3 \quad (4.15)$$

and in compression by:

$$r_i = \begin{cases} 0 & \text{if } {}^{t+\Delta t}\varepsilon_i < {}^t\varepsilon_i^d \\ 1 & \text{if } {}^{t+\Delta t}\varepsilon_i \geq {}^t\varepsilon_i^d \end{cases} \quad i=4,5,6 \quad (4.16)$$

The update of the strains of internal damage is done according to the following equation:

$${}^{t+\Delta t}\varepsilon_i^d = {}^t\varepsilon_i^d + w_i \Delta\varepsilon_i \quad (4.17)$$

where w_i is given by:

$$w_i = 1 - r_i \quad i=1, \dots, 6 \quad (4.18)$$

Assuming that the damage is not recoverable, the stress σ in the direction i is given by:

$$\sigma_i = f_i(\varepsilon_{damage}, \varepsilon^{pr}) R_i^{UR}(\varepsilon_{damage}, \varepsilon^{pr}) \quad (4.19)$$

where ε^{pr} is the principal strain, f_i is the uniaxial stress-strain relationship and R_i^{UR} is the function controlling the unloading and reloading.

The uniaxial stress-strain relationship f_i is not only a function of the strain of internal damage in the direction i , but also a function of the strains of internal damage and strains in the other directions. However, in this case study the lateral confinement and cracking were not considered.

Finally, if the unloading and reloading is simulated by a secant approach, which means that unloading is a function passing through the origin (Figure 4.7), the function controlling unloading and reloading is given by (ranging from zero to one):

$$R_i^{UR} = 1 - \frac{\varepsilon_i^d - \varepsilon_i}{\varepsilon_i^d} \quad i=1, \dots, 6 \quad (4.20)$$

In what concerns damping, the \underline{C} viscous damping (proportional to the velocity) of Rayleigh was adopted, which is a linear combination between the mass and stiffness matrix in the form (Chopra 2001):

$$\underline{C} = \alpha \underline{M} + \beta \underline{K} \quad (4.21)$$

where α and β are the coefficients that weigh the contribution of the mass \underline{M} and \underline{K} matrices, respectively. The damping ratio ζ_i for the natural frequency ω_i is calculated by the following equation:

$$\zeta_i = \frac{1}{2} \left(\beta \omega_i + \frac{\alpha}{\omega_i} \right) \quad (4.22)$$

In general, the α and β coefficients are determined through the application of the Equation (4.22) for two frequencies with known damping ratios in the linear range (without damage). It is known that under high dynamic loading the damage increases during the analysis, changing the values of the frequencies and of the damping ratios. Furthermore, in the non-linear dynamic analysis an integration point totally damaged contributes to the damping forces. Thus, the update of the damping at the end of each

time step would allow better simulating the non-linear dynamic behaviour of the structures. However, this procedure is not usual and would increase the computing time, particularly in analysis with large numerical models.

Another important aspect of the non-linear dynamic analysis with time integration concerns the type of integration method to use. The quasi-brittle masonry behaviour in tension introduces numerical noise, due to the fast transition from the linear elastic behaviour to the fully cracked state involving almost zero stiffness. The quasi-instantaneous changes in the displacement field tend to originate the propagation of high frequency spurious vibrations (Cervera et al. 1995). Therefore, it is important to adopt the Hilber-Hughes-Taylor (HHT) time integration method (also called the α method), in which it is possible to introduce numerical dissipation without degrading the accuracy (Faria 1994). The HHT method uses the same finite difference equations as the Newmark method, i.e.:

$$\underline{\dot{u}}^{t+\Delta t} = \underline{\dot{u}}^t + [(1-\gamma)\underline{\ddot{u}}^t + \gamma \underline{\ddot{u}}^{t+\Delta t}] \Delta t \quad (4.23)$$

$$\underline{u}^{t+\Delta t} = \underline{u}^t + \underline{\dot{u}}^t \Delta t + \left[\left(\frac{1}{2} - \beta \right) \underline{\ddot{u}}^t + \beta \underline{\ddot{u}}^{t+\Delta t} \right] \Delta t^2 \quad (4.24)$$

where

$$\gamma = \frac{1}{2}(1-2\alpha) \quad (4.25)$$

$$\beta = \frac{1}{4}(1-\alpha)^2 \quad (4.26)$$

and $\underline{\ddot{u}}$, $\underline{\dot{u}}$, \underline{u} are the acceleration, velocity and displacement vectors, respectively, γ and β are the parameters associated to the Newmark method, α is the parameter associated to the HHT method and Δt is the time step.

Using the HHT method, the typical equation of motion for a multi-degree-of-freedom system in the time $t+\Delta t$:

$$\underline{M} \underline{\ddot{u}}^{t+\Delta t} + \underline{C} \underline{\dot{u}}^{t+\Delta t} + \underline{K} \underline{u}^{t+\Delta t} = \underline{f}_{ext}^{t+\Delta t} \quad (4.27)$$

assumes the following form:

$$\underline{M} \ddot{\underline{u}}^{t+\Delta t} + (I+\alpha)\underline{C} \dot{\underline{u}}^{t+\Delta t} - \alpha \underline{C} \dot{\underline{u}}^t + (I+\alpha)\underline{f}_{int}^{t+\Delta t} - \alpha \underline{f}_{int}^t = (I+\alpha)\underline{f}_{ext}^{t+\Delta t} + \alpha \underline{f}_{ext}^t \quad (4.28)$$

where

$$\underline{f}_{int} = \underline{K} \underline{u} \quad (4.29)$$

and \underline{f}_{ext} and \underline{f}_{int} are the vectors of the restoring and external loads, respectively.

The method is second-order accurate and unconditionally stable, and, in general, the α parameter assumes values between $-1/3$ and $1/2$. For α equal to zero the HHT method reduces to the Newmark method. Decreasing α means increasing the numerical damping, and the adopted damping is usually low for the low frequency modes and high for the high frequency modes. Here, the parameter α was assumed equal to -0.1 .

The time step Δt is an important parameter to take into account in the non-linear dynamic analysis with time integration. Here, two criteria to define the time step were used (TNO 2009):

- The time step Δt must be sufficiently small in comparison to the total duration of the analysis t_d :

$$\Delta t \ll t_d \quad (4.30)$$

- In order to take into account the contribution of mode with lowest frequency T_i with an error lower than 5%, the time step Δt must be defined by:

$$\Delta t = \frac{1}{20} T_i \quad (4.31)$$

Finally, the equilibrium of the equations in each step of the non-linear analysis is obtained through iterative solution methods, such as the Linear Stiffness, the Regular and Modified Newton-Raphson and the Secant methods. Here, several methods were tested and the Linear Stiffness method, which uses the linear stiffness matrix the entire analysis, presented the best results in terms of convergence. It is noted that this is not usually the case for static non-linear analysis. In the iterative method, a convergence criterion based on the internal energy with tolerance equal to 10^{-3} was used.

4.4.2 Non-linear dynamic analysis for Earthquake 25%

In the first non-linear dynamic analysis with time integration the Earthquake 25% used in the seismic shaking table test was applied (Annex A). The non-linear material properties of the masonry in tension and in compression (Table 4.3) were defined based on the experimental tests and the recommendations proposed by Lourenço (2008) and Eurocode 6 (EN 1996-1-1 2005). As the updated Young's modulus of the gable walls is close to the one obtained in the uniaxial compressive tests of the wallets, the experimental values of the compressive and tensile strength of the wallets were used for these walls. For the compressive strength of the facades and corners the approximation $f_c = E/1000$, proposed by Eurocode 6, was adopted. The tensile properties of the facades and of the corners were assumed equal to the gable walls. For all the masonry walls, a shear retention factor equal to 0.1 was assumed.

Table 4.3 – Material properties of the masonry walls.

	Young's modulus E [GPa]	Compressive strength f_c [MPa]	Compressive fracture energy G_c [N/mm]	Tensile strength f_t [MPa]	Mode I- tensile fracture energy G_t [N/mm]
Facades	0.64	0.64	1.03	0.10	0.05
Gable walls	3.45	6.00	9.60	0.10	0.05
Corners	2.05	2.05	3.28	0.10	0.05

In what concerns damping, the modal properties of the two first transversal (frequencies and damping ratios) estimated in the first dynamic identification of the non-strengthened mock-up (Table 3.1) were used to calculate the α and β parameters. Applying Equation (4.22) for each mode, a $\alpha=1.48218$ and $\beta=0.00052$ were obtained. Figure 4.8 presents the viscous damping used in the non-linear dynamic analysis with time integration.

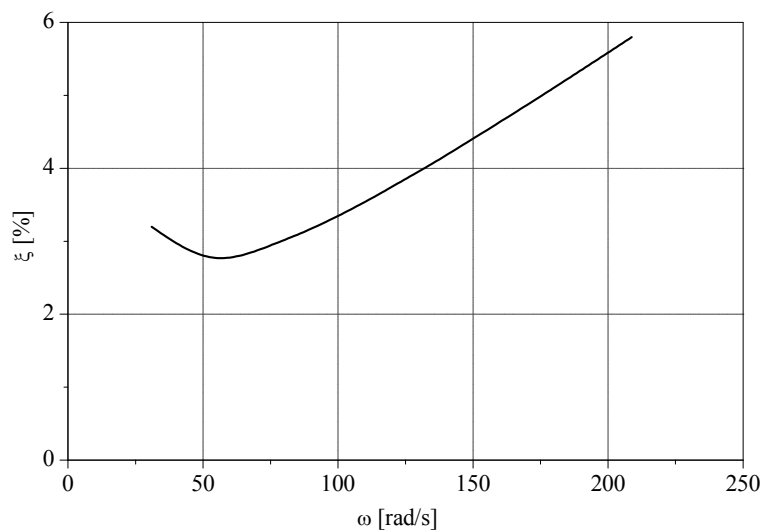


Figure 4.8 – Viscous damping of the numerical model.

The response of the numerical model was compared to the results obtained in the shaking table test at floor levels and in both directions, using the same parameters as in the analysis of the experimental behaviour of the mock-ups, namely: the maximum out-of-plane acceleration amplification, the average maximum out-of-plane displacement, the average maximum out-of-plane relative displacement with respect to the corners and the average maximum in-plane drift of the facades. As the behaviour of the two facades and of the two gable walls are similar in the numerical model, the comparison of the responses, at each floor level, was carried out in terms of global average in the longitudinal direction (average of the North and South facades) and in the transversal direction (average of the East and West gable walls).

Figure 4.9 presents the comparison between the average maximum out-of-plane amplification of acceleration of the mock-up and the numerical model. The acceleration amplification of the numerical model is significantly higher than the experimental, with exception of the gable walls at the first floor, in which the numerical model does not present any acceleration amplification. The average error between numerical and experimental acceleration amplification is equal to 47% (the experimental results are used as reference).

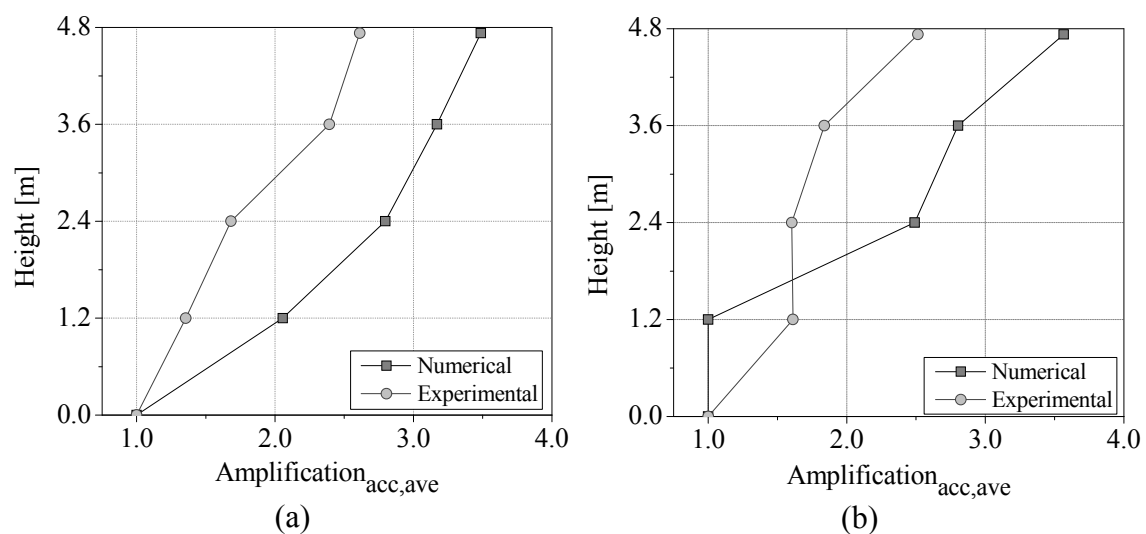


Figure 4.9 – Comparison of the average maximum out-of-plane acceleration amplification at floors levels: (a) facades; (b) gable walls.

The average maximum out-of-plane displacement of the numerical model also presents some differences with respect to the experimental results (Figure 4.10), mainly in the longitudinal direction, in which the average error is about 60%. In the longitudinal direction the out-of-plane displacements obtained from the experimental tests are significantly higher than the ones obtained from the non-linear dynamic analysis, which may be related with differences in the connections between facades and timber floors. In the transversal direction, out-of-plane displacements of the numerical model are closer to the experimental results and, consequently, the average error decreased (28%). In the gable walls the error decreases in elevation, with a low error at the top (5%).

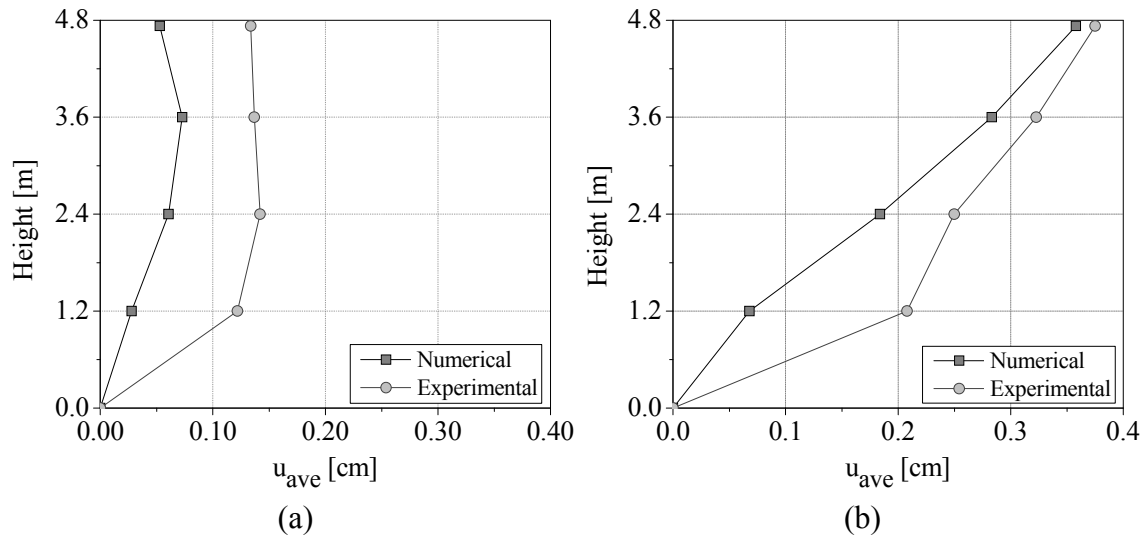


Figure 4.10 – Comparison of the average maximum out-of-plane displacement at floors levels: (a) facades; (b) gable walls.

The average maximum out-of-plane displacement relative to the corners of the numerical model and mock-up (Figure 4.11), which is a local parameter of the out-of-plane response of the masonry walls, also presents significant differences in the longitudinal direction (average error equal to 77%). In this direction the experimental results are higher than the numerical ones, which lead to the conclusions that the numerical model presents better connection between facades and floors than the mock-up. On the other hand, in the transversal direction the differences between the numerical and experimental responses are acceptable. The error in the transversal direction is, on average, equal to 14%, in which the error equal to 4% at the top is highlighted.

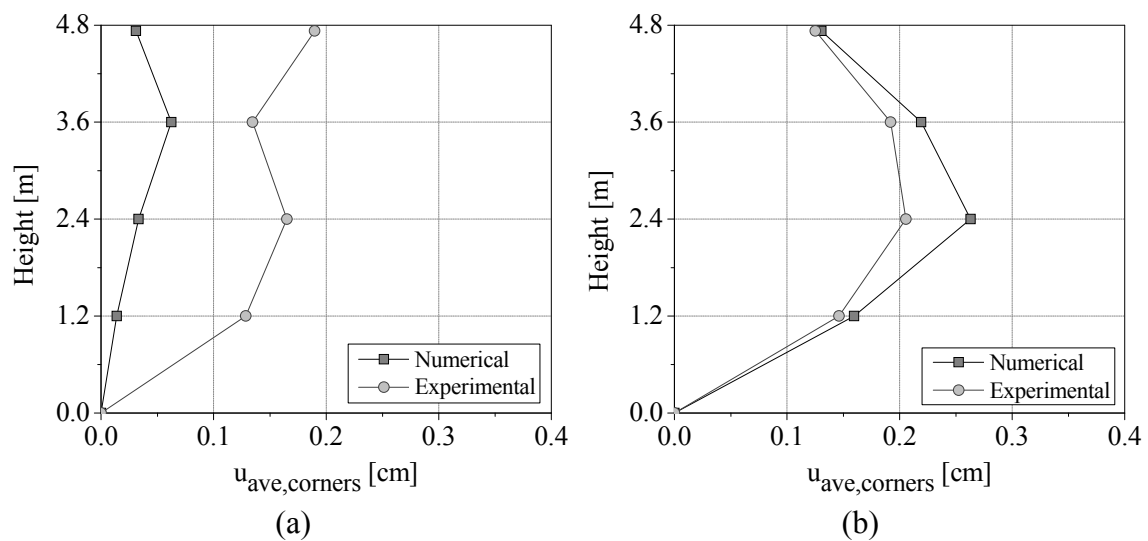


Figure 4.11 – Comparison of the average maximum out-of-plane relative displacement with respect to the corners at floors levels: (a) facades; (b) gable walls.

The average maximum in-plane drift of the facades of the numerical model presents an error, on average, of about 30% with respect to the experimental results (Figure 4.12). The in-elevation shape of the drifts of the numeral model and mock-up are similar, with maxima at the second and third floors. However, the experimental in-plane drifts of facades are higher than the ones obtained from the non-linear dynamic analysis, mainly at the top of walls. This means that in the in-plane of the facades (response in the transversal direction), the mock-up is more flexible than the numerical model. However, local out-of-plane response shows that the gable walls (response in the transversal direction) of the non-strengthened mock-up are slightly stiffer than the numerical model ones (Figure 4.11b). Thus, the in-plane stiffness of the facades and the out-of-plane stiffness of the gables walls of the numerical model should decrease and increase, respectively.

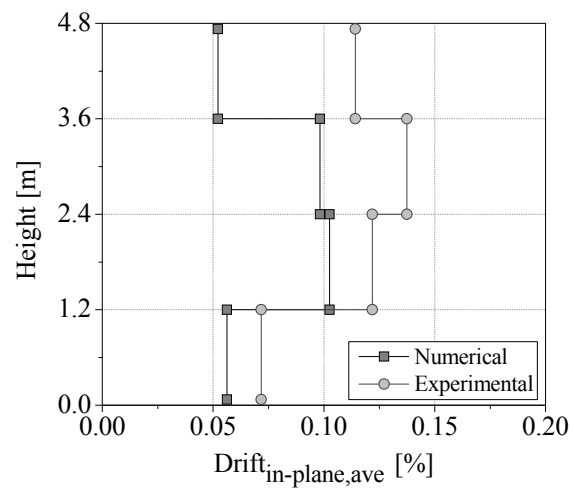


Figure 4.12 – Comparison of the average of the maximum in-plane drifts of the facades.

In the comparison between the numerical and experimental responses the adopted parameters are based on peak values, i.e. on the maximum values of the response occurring in the earthquake. Different parameters can be used to compare the time histories of the response, namely integral parameters, which take into account the history of amplitudes occurring. The Root Mean Square of Displacement (RMS_D) (Equation (2.6)), which is a statistical measure of the displacement amplitudes, is used next for this purpose on selected walls. In the longitudinal direction, the numerical and experimental responses in terms of RMS_D at the middle of the South facade present the same shape in-elevation, with the maximum at the third floor and an average error equal to 28% (Figure 4.13a). In the transversal direction, the RMS_D at the middle of the East gable wall of the numerical and experimental responses presents the same shape, increasing in-elevation and an average error equal to 24% (Figure 4.13b).

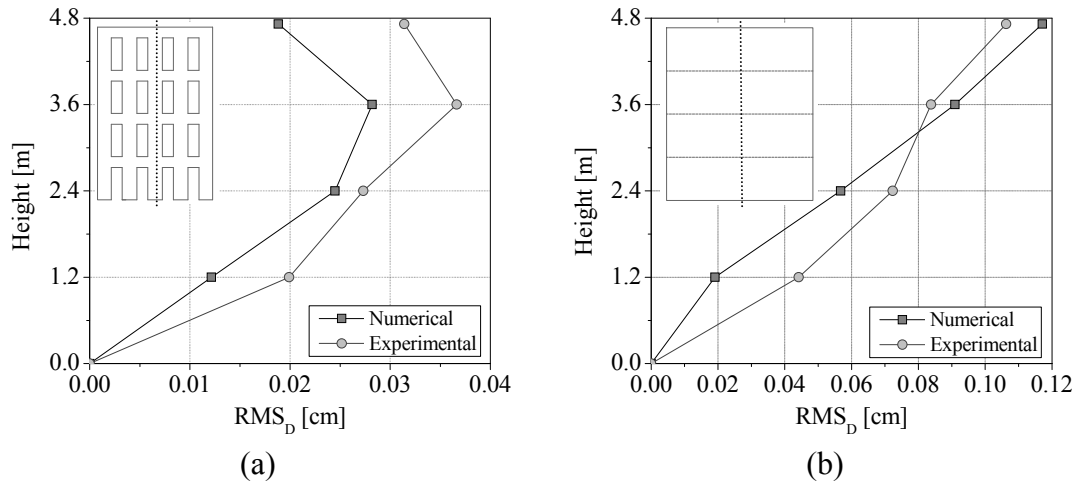


Figure 4.13 – Comparison of the Root Mean Square of displacement at the central vertical alignment of the: (a) South facade; (b) East gable wall.

Finally, a qualitative comparison of damage after Earthquake 25% was also done (Figure 4.14). Here, the maximum tensile principal strain, which is an indicator of the cracking of the numerical model, was used. The crack pattern of the non-strengthened mock-up shows that the damage is rather low and only a few small cracks were observed. The numerical model also presents low damage, namely at the spandrels of the facades due to concentration of stresses and strains at the corners of the openings. The maximum width of the cracks at the spandrels is about 0.3 mm (calculated by integration of the principal strains), showing that the damage is rather low and difficult to observe in the experimental tests. Thus, in the Earthquake 25% the damage of the numerical model is according to the crack pattern of the mock-up, in which the behaviour is, basically, linear.

The comparison of the results shows that in the transversal direction the response in terms of peak values of the numerical model is acceptable with respect to the shaking table test of the mock-up, mainly in terms of displacements. In the longitudinal direction the maximum response of the numerical model presents significant differences, which may be related to the difficulty to simulate correctly the connections between the facades and timber floors. In the numerical model the relative displacement between the facades and floors is not allowed and the out-of-plane deformation of the facades is significantly lower than the experimental one. This is according to the results of the modal updating, in which the *MAC*'s between the numerical and experimental mode shapes are higher in the transversal direction. It is noted that the dynamic identification tests were carried out using acceleration signals with low amplitude and, consequently, the behaviour of the connections does not present significant relative displacements. In the shaking table tests, in which the amplitude of the input is higher, the connections can present relative displacements between facades and floors. However, analysing the results in terms of RMS_D , which provides a better analysis of the time history response, it is concluded that the numerical response is acceptable in both directions.

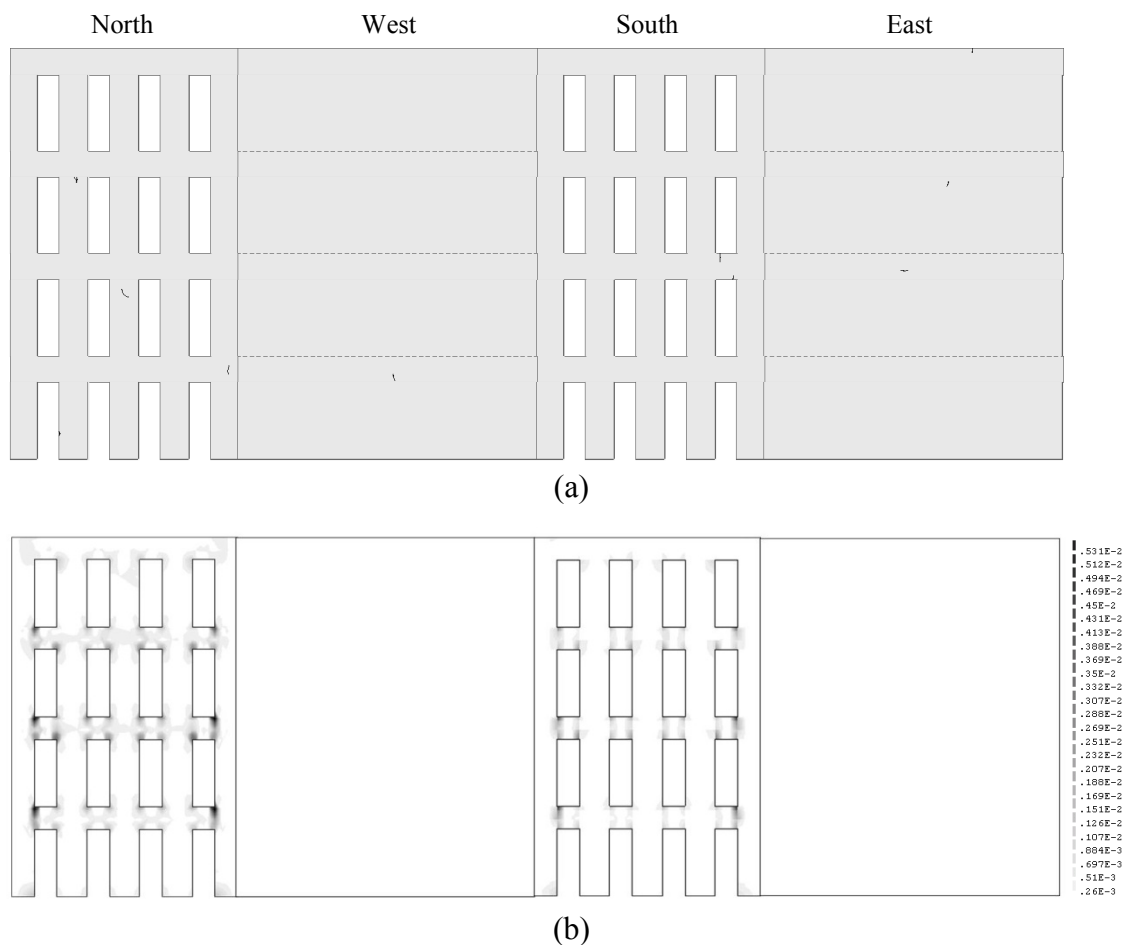


Figure 4.14 – Comparison of the damage for the Earthquake 25%: (a) experimental crack pattern; (b) maximum tensile principal strains at the external surface.

4.4.3 Non-linear dynamic analysis with Earthquake 100%

The non-linear dynamic analyses with time integration require rather large computational efforts and, for this reason, the analysis with Earthquake 50% and 75% were not carried out here. Another non-linear dynamic analysis with Earthquake 100% (Annex A) was carried out, aiming at comparing the damage and the on-set of collapse mechanisms of the structure. It is noted that at the beginning of this new analysis the numerical model does not present any damage while the mock-up presents damage due the previous seismic shaking table tests. Therefore, the initial conditions of the numerical model are not equal to the ones of the non-strengthened mock-up. Thus, the quantitative comparison of the parameters of the response, as previously done in the non-linear dynamic analysis with Earthquake 25%, is not presented here, focusing the analysis of the results only in a qualitative comparison of damage.

In the Earthquake 100%, the non-strengthened mock-up (Figure 4.15a) presents high concentration of damage at the facades, namely at the spandrels, caused by diagonal

tension, and at the piers of the fourth floor, caused by the in-plane rocking and out-of-plane bending. The gable walls do not present any significant damage. The numerical model (Figure 4.15b) presents a high concentration of tensile principal strains (cracking) at the facades, in which the diagonal cracks at the spandrels of the first three floors, associated to in-plane behaviour, as observed in the experimental tests. At the top of the facades, the numerical model presents damage at the corners of the openings and at the piers. The damage at the ends of the piers is associated to the in-plane rocking and is according to the horizontal cracks observed in the experimental test. The numerical model also presents damage within the height of the central piers of the fourth floor. This damage is related to the out-of-plane bending of the piers and was also observed in the shaking table test. Furthermore, the base of the numerical model (facades and gable walls) presents cracking, which was not observed in the experimental tests, and are related to the adopted boundary conditions. In general, the numerical model of the non-strengthened mock-up simulates correctly the main collapse mechanisms and the concentration of damage (cracking) observed in the shaking table tests with Earthquake 100%.

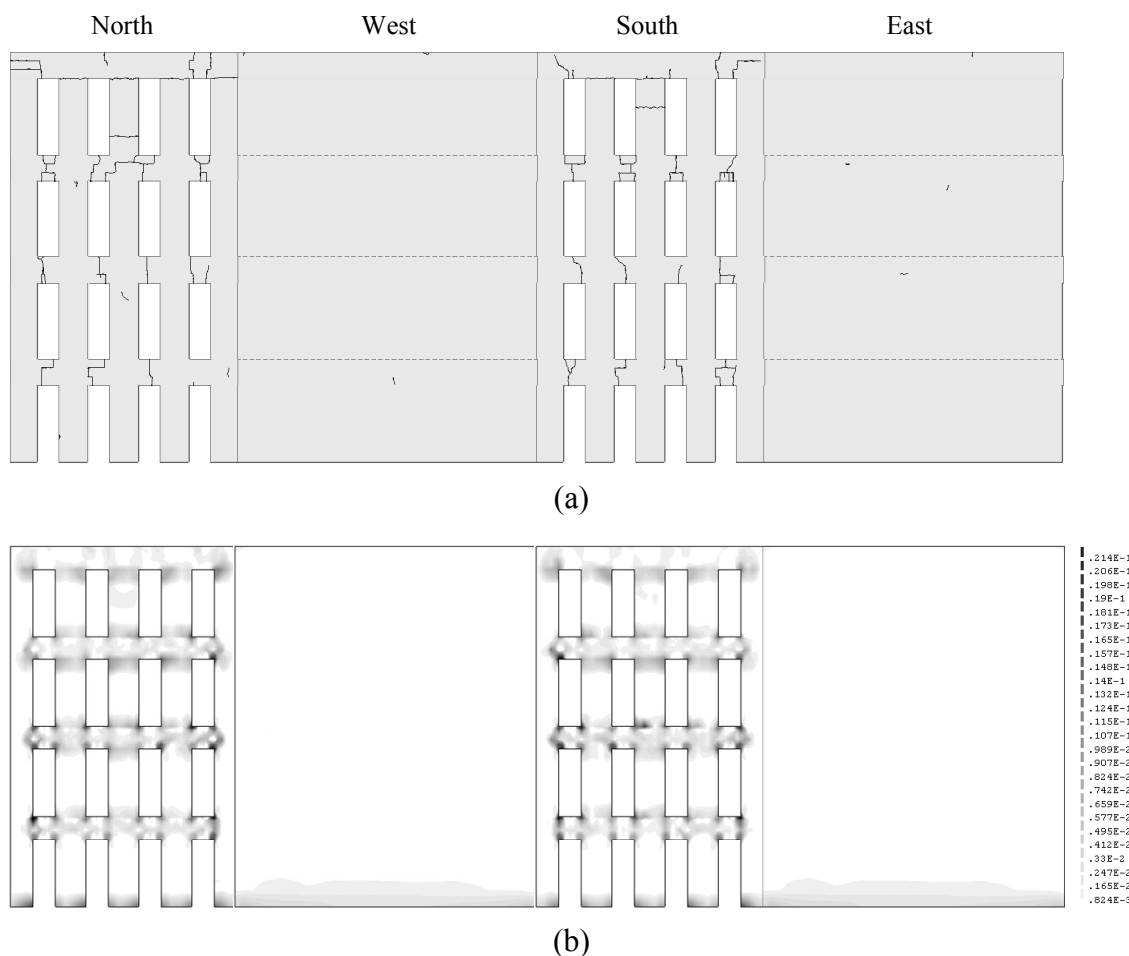


Figure 4.15 – Comparison of the damage for the Earthquake 100%: (a) experimental crack pattern; (b) maximum tensile principal strains at the external surface.

4.5 Scale effect discussion

The mock-ups are built at 1:3 reduced scale, taking into account the Cauchy law of similitude, which corresponds to a similitude between the inertial forces and the restoring forces. Although testing full mock-ups at the 3D shaking table is not possible due to its maximum load capacity, the numerical modelling does not present this limitation and the discussion between the results at reduced and full scale can be done. This is a subject that receives considerable attention in the earthquake community and the full numerical model of the mock-up was also prepared according the relationships presented in the Table 2.1.

The total mass of the mock-ups was the first parameter evaluated. The mass of the reduced and full models are about 22.4 ton and 604.0 ton, respectively. This means that the mass of the full model is equal to 27 times (scale factor = 3^3) the mass of the reduced model, which is according to the relationship of mass defined in the Cauchy law of similitude. Furthermore, the frequencies of the full model were also calculated. The comparisons between the frequencies of the reduced model and the frequencies of the full models are in agreement with the law of similitude, in which the frequencies of the reduced model are equal to 3 times (scale factor = 3) the frequencies of the full model (Table 4.4). This means that the models comply with the similitude of distribution of mass and stiffness, as expected.

Table 4.4 – Frequencies of the reduced and full numerical models.

	Reduced model [Hz]	Full model [Hz]
1 st Transversal	4.94	1.65
1 st Distortional	8.48	2.83
1 st Longitudinal	12.42	4.14
2 nd Longitudinal	14.22	4.74
2 nd Transversal	14.46	4.82

The modal parameters are calculated with linear properties of the materials (without damage). However, under non-linear behaviour the size effect must be taking into account, as it can influence the load capacity of structures. The size effect is simply explained by the variation of the ultimate load capacity as function of the dimensions of the structure. In addition: (a) the response of brittle structures to random motions have chaotic features and the time compression in the Cauchy law of similitude might have an influence on the results; (b) in Cauchy law of similitude, it is not possible to increase the vertical acceleration, meaning that the vertical stresses are lower than expected, which again might influence the results. Therefore, non-linear dynamic analysis with the full model, for the Earthquakes 25% and 100%, were also carried out, aiming at comparing its response with the response of the reduced model. As the frequencies of the full model are different from the reduce model (Table 4.4), the α and β parameters of the viscous damping of Rayleigh were updated assuming the same damping ratios used in the reduced model ($\alpha=0.49324$ and $\beta=0.00157$). It is noted that the comparisons

were done based on the results at real scale. Thus, the response of the reduced model was updated taking into account the relationships defined in the Table 2.1.

In non-linear dynamic analysis with the Earthquake 25% the reduced model presents acceleration amplification higher than the full model at all floor levels (Figure 4.16). The variation of maximum acceleration amplification of the reduced model is, on average, equal to 9% and 24% at the middle of the North facades and East gable wall, respectively, with respect to the full model. In what concerns the maximum out-of-plane displacements, the reduced model presents also higher displacements than the full model (Figure 4.17). At the middle of the North facade the variation of displacements is lower (8%), in comparison to the variation of displacements at the middle of the East gable (22%). It is noted that in this analysis the model presents slight non-linear behaviour, which is enough to cause differences in the responses of the reduced and full models.

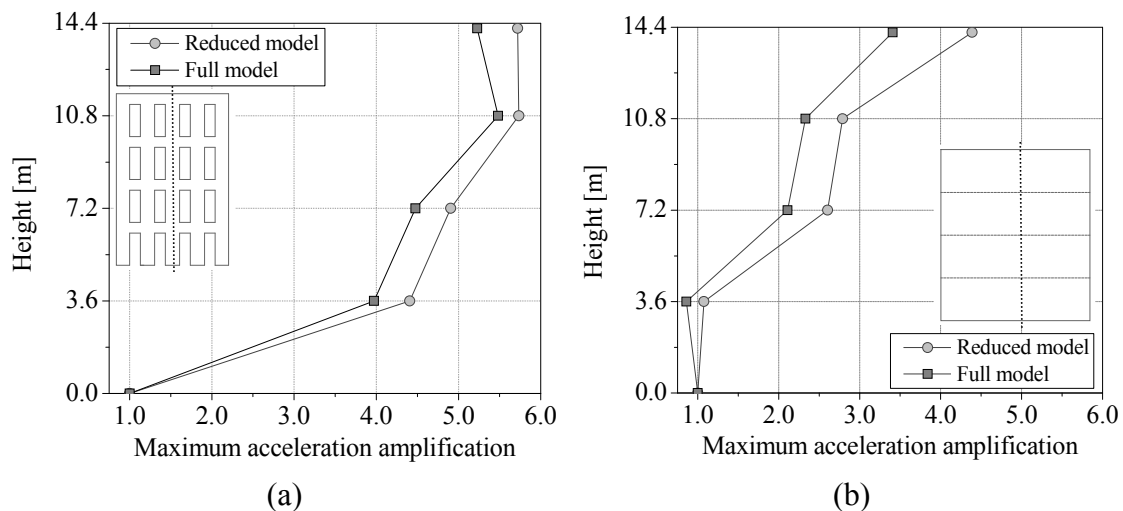


Figure 4.16 – Maximum acceleration amplifications of the Earthquake 25% for the reduced and full models at the middle of the: (a) North facade; (b) East gable wall.

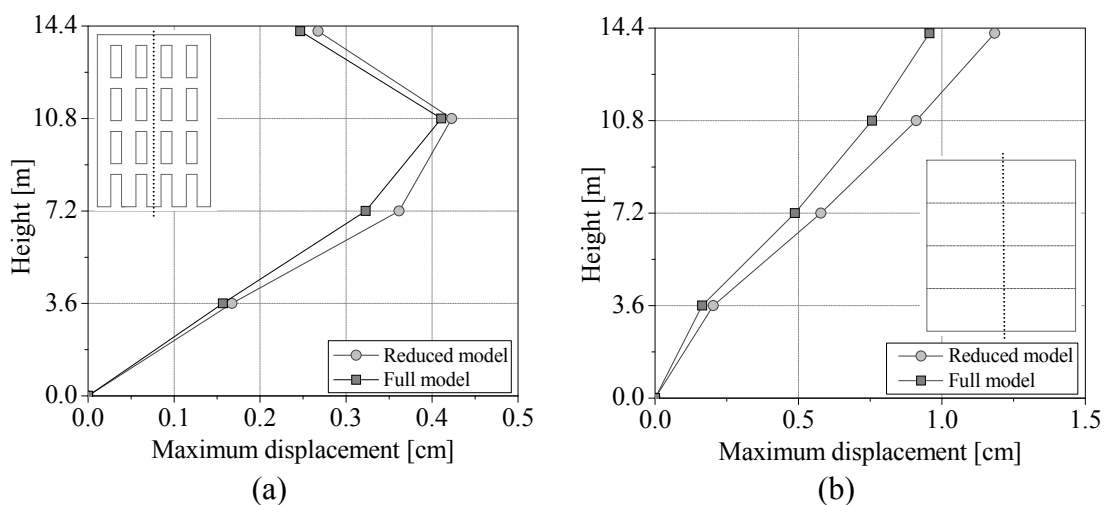


Figure 4.17 – Maximum displacements of the Earthquake 25% for the reduced and full models at the middle of the: (a) North facade; (b) East gable wall.

In the non-linear dynamic analysis with Earthquake 100% the deformation of the structure is also higher using the reduced model. As an example, the variation of out-of-plane displacements at the middle of the North facade using the reduced model is, on average, 24% larger than the full model, with an increase of 56% at the third floor (Figure 4.18a). At the middle of the East gable wall (Figure 4.18b), the results are rather similar, with displacements in the reduced model slightly higher than the full model from the base to the third floor. However, the maximum out-of-plane displacement at the top in the reduced model is slightly lower when using the full model for this wall. It is noted that the non-linear behaviour of the structure is rather complex, mainly due to the fact that two strong horizontal accelerograms are applied simultaneously, inducing in-plane and out-of-plane non-linear behaviour of the walls, that flexible floors are present with linear behaviour, and that significant distributed cracking occurs in the masonry walls.

In general and taking into account mainly the response of the facades, the results of the reduced model are conservative in comparison to the full scale model, as it presents larger deformation than the full model.

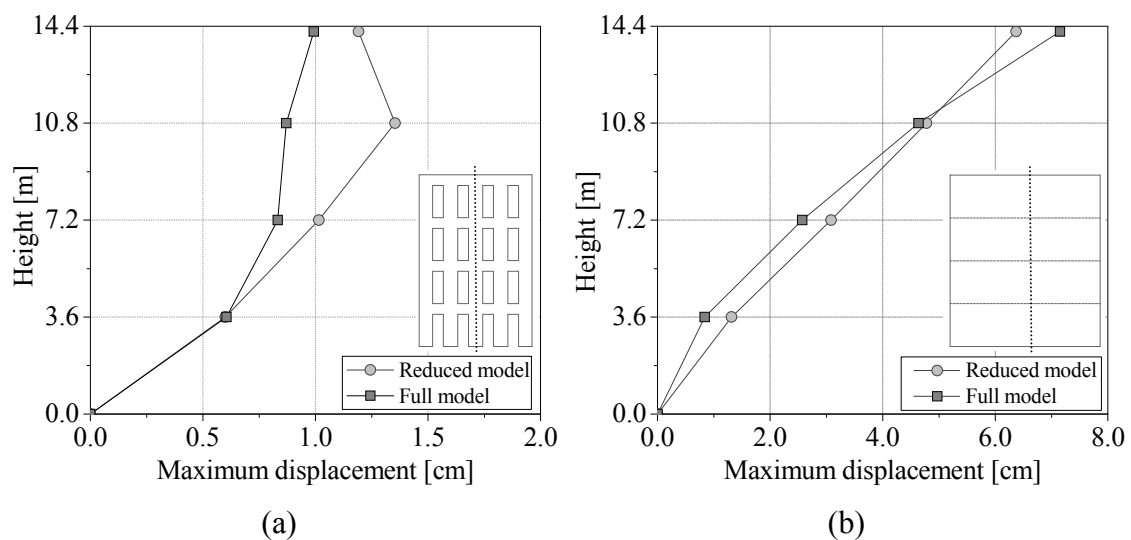


Figure 4.18 – Maximum displacements of the Earthquake 100% for the reduced and full models at the middle of the: (a) North facade; (b) East gable wall.

Finally, it was mentioned that the differences between the responses of reduced and full models are related to the scale effect, i.e. the response in non-linear behaviour depends on the dimensions of the structure, and the combination of similitude laws with non-linear behaviour. The linear dynamic response must be the same for both models. A linear dynamic analysis with the Earthquake 25% for both models was also carried out. The results show that the response of the models is exactly same, as expected. As an example, Figure 4.19 presents the maximum out-of-plane displacements at the middle

of the North facade and the East gable wall, in which it is observed that the results are equal, further demonstrating that the differences found above are related to the non-linear behaviour of models with different dimensions.

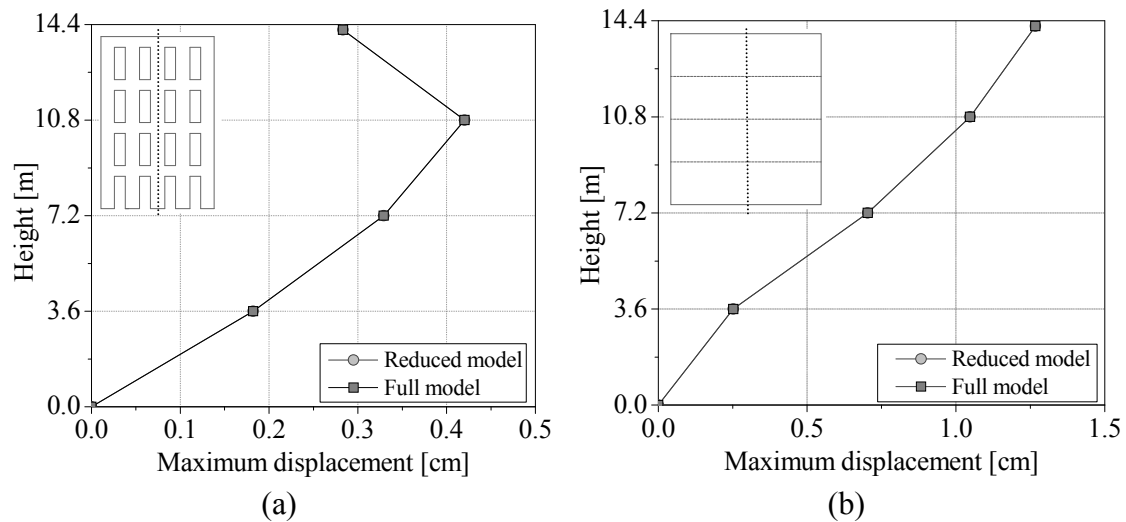


Figure 4.19 – Maximum displacements of the Earthquake 25% with linear behaviour for the reduced and full models at the middle of the: (a) North facade; (b) East gable wall. (The responses of the models are equal)

4.6 Conclusions

The numerical model of the non-strengthened mock-up was prepared, at 1:3 reduced scale, calibrated and validated. The numerical model was calibrated with respect to modal parameters (frequencies and mode shapes) identified in the first dynamic identification test. Four numerical models with different variables to calibrate were used in the modal updating, considering the first four or first five modes. Furthermore, as the objective function of the modal updating method is sensitive to the initial values, several modal updating analyses changing the initial values were carried out. The results show that the modal updating method is more sensitive in models with higher number of variables and for the calibrations with more number of modes. The numerical model that considers as variables the Young's modulus of the facades, gables walls, corners and MDF panels presented the minimum average frequency error and was adopted in subsequent analysis. In the modal updating considering the first five modes, the adopted numerical model presents an error, on average, equal to 3.6%. In what concerns the mode shapes, the *MAC*, *NMD* and *COMAC* values show that the correlation between the experimental and numerical modal displacements is good in the transversal direction and acceptable in the longitudinal direction.

Non-linear dynamic analyses with time integration were also carried out. In the first analysis, the Earthquake 25% was applied and the response of the numerical was compared with the experimental results. The results show that the numerical response is

acceptable in comparison to the response obtained from the seismic shaking table test, mainly in the transversal direction. In the longitudinal direction the response of numerical model presents larger differences with respect to the experimental results, due to the difficulty in correctly simulating the connections between the facades and timber floors, which possibly require the inclusion of non-linear effects. In the dynamic analysis with Earthquake 100%, only a qualitative comparison of the damage was done. In general, the numerical model simulates correctly the onset of the collapse mechanisms and the concentration of cracking observed in the seismic shaking table test. The quality of the numerical results of the non-linear dynamic analyses is in agreement with the conclusions of the modal updating, in which the response in the transversal direction is the one that best fits the experimental results. Furthermore, it is noted that the dynamic identification tests were carried with low amplitude, in which the mock-up presents linear behaviour. However, in the seismic shaking table tests, which present higher amplitudes, the mock-up can present non-linear behaviour and relative displacements between the facades and floors can occur, increasing the differences between the numerical and experimental response in the longitudinal direction. Therefore, this work also allows concluding the following: (a) complex structures as the one presented are difficult to replicate numerically in detail, even if the global response can be adequately replicated; (b) dynamic identification tests should be used with caution in existing masonry structures, as adequate tuning of the model for low level excitation is hardly a guarantee of adequate performance of the model for significant seismic inputs.

A numerical model at real scale was also prepared, aiming at evaluating the differences between its response and the response of the reduced model due to the scale effect. As expected, in the linear range both models present the same results. However, under non-linear behaviour the responses of the models exhibit some differences. The out-of-plane displacements of the reduced model are higher than the ones obtained using the full models, leading to the conclusion that the experimental tests with reduced models provide conservative results for the adopted 1:3 scale and the differences are acceptable from an engineering perspective.

The dynamic behaviour of the mock-up is rather complex, mainly due to the type of material (masonry), flexible floors and weak connections between walls and floors. This complex behaviour, observed in the shaking table tests, is quite difficult to reproduce by a numerical model, mainly due to the use of macro-modelling and the difficulties in characterizing the connections. Macro-modelling was used due to high dimensions and type of numerical model, and the time requirement of the analyses. However, the updated numerical model response is acceptable in comparison with the experimental results. Furthermore, in the next Chapter a sensitivity analysis is presented, aiming at evaluating the influence of the main parameters on the seismic performance of the numerical model and improving the conclusions.

Chapter 5

Sensitivity analysis

5.1 Introduction

In the previous Chapter the numerical model of the non-strengthened mock-up was prepared and calibrated. However, this model was prepared at reduced scale and is representative only of the features attributed to the “gaioleiro” building typology. In this Chapter a sensitivity analysis taking into account a deviation in the mechanical characteristics of the “gaioleiro” buildings was done. Furthermore, the full model was used, aiming at eliminating any influence in the results due to the scale effect. The sensitivity of the dynamic behaviour of the “gaioleiro” buildings with respect to changes in its properties was evaluated through two types of structural analysis: (a) pushover analysis; (b) non-linear dynamic analysis with time integration. Basically, the values of the properties were changed, and the obtained responses were compared to the response of the reference model.

In the pushover analyses, the distribution of lateral loads applied to the structure and the changes in the stiffness of the masonry walls, stiffness of the floors, compressive and tensile strength, and compressive and tensile failure energy, were evaluated for each direction. Besides these parameters, in the non-linear dynamic analyses the influences of the damping and of the vertical component of the earthquake were also evaluated.

5.2 Results for the reference numerical model

The definition of a reference numerical model was the first step of the sensitivity analysis. Here, it was thought that the initial approach should be the updated full model. This numerical model has three different Young's modulus for the masonry walls (facades, gable walls and corners). Furthermore, the Young's modulus and compressive strength of the gable walls (3.45 GPa and 6.00 MPa, respectively) are high with respect to the expected values for ancient masonry, which is explained by the larger size stone units and higher strength mortar. On the other hand, the updated value of the Young's modulus of the facades (0.64 GPa) is lower than the value expected for this type of masonry, possibly due to the indirect way to simulate the weak connection between facades and floors. Finally, it was decided to change the updated numerical model and use only one Young's modulus for the masonry walls (1.00 GPa). The idea was to simplify the number of parameters in the sensitivity analysis and to use values of the properties of masonry more usual in the ancient buildings. Tables 5.1 and 5.2 present the linear and non-linear properties of the materials used in the sensitive analysis presented next, respectively.

Table 5.1 – Linear material properties of the reference model.

	Young's modulus [GPa]	Specific mass [kg/m ³]	Poisson ratio
Masonry walls	1.00	2162	0.2
MDF panels	0.16	760	0.3
Timber joists	12.00	580	0.3

Table 5.2 – Non-linear material properties of the masonry walls of the reference model.

	Compressive strength f_c [MPa]	Compressive fracture energy G_c [N/mm]	Tensile strength f_t [MPa]	Mode I- tensile fracture energy G_t [N/mm]
Masonry walls	1.00	1.60	0.10	0.05

Once the Young's modulus of the masonry walls was changed, new modes were calculated for the structure (Table 5.3). The frequency of the first mode of the reference model is equal to 1.69 Hz, which corresponds to a variation of about 2% with respect to the updated model (1.65 Hz). The frequency of the distortional mode also presents an increase of about 3% (2.91 Hz). However, the frequency of the first longitudinal mode is equal to 3.65 Hz, decreasing about 12% with respect to the updated model (4.14 Hz), which is related to the decrease of the stiffness contribution of the gables walls. The second mode presents an increase of about 4%, which is related to the increase of the Young's modulus of the facades. Finally, the second transversal mode of the reference model presents significant differences in comparison with the second transversal mode of the updated model. The reference model presents two modes with similar mode

shape to the second transversal mode of the updated model. The mode shape of the first mode (3.59 Hz) is mainly a second curvature in-elevation of the gable walls and the facades present low modal displacements. Thus, in this mode, the displacements of the gable walls are the ones that better fit the mode shape of the second transversal mode of the updated model. On the other hand, the second mode (8.53 Hz) is mainly a mode shape with second curvature in-elevation of the facades and, consequently, the modal displacements of the facades are the ones that better fit the mode shape of the second transversal mode of the updated model. This is according to the changes in the reference numerical model, in which the stiffness of the facades and of the gables walls increased and decreased, respectively, with respect to the updated model.

Table 5.3 – Frequencies of the updated and reference full numerical models.

	Updated model [Hz]	Reference model [Hz]
1 st Transversal	1.65	1.69
1 st Distortional	2.83	2.91
1 st Longitudinal	4.14	3.65
2 nd Longitudinal	4.74	4.93
2 nd Transversal	4.82	3.59; 8.53

Non-linear dynamic analysis with time integration and pushover analyses for the reference numerical model were carried out. The dynamic analysis was done according to the methodology presented in the Section 4.4. The pushover analysis is a non-linear static analysis that aims at simulating the structural response during an earthquake, through application of incremental horizontal forces (forced based) or displacements (displacement based) until collapse. The response of the structure is given by the so-called capacity curve, which represents the value of the base shear or seismic coefficient (Equation (5.1)) versus the displacement at a control point (usually at the top of the structure). Two vertical distributions of lateral forces, defined by the Eurocode 8 (EN 1998-1 2004), are commonly used: (a) uniform pattern, in which the lateral forces are proportional to the mass regardless of elevation (uniform response acceleration); (b) modal pattern, in which the lateral forces are proportional to the mode shape of the first mode in the applied direction. Here, lateral forces proportional to the mass was adopted and a pushover analysis for each direction was done, as the use of the modal pattern can provide excessively conservative responses for masonry structures (Lourenço et al. 2011). In these analyses, the Regular Newton-Raphson iterative method with a convergence criterion based on the internal energy with tolerance equal to 10^{-3} was used. The Arc Length Control method (Lu et al. 2005, Bashir-Ahmed and Xiao-zu 2004), which is an indirect displacement control and is useful in case of local snap-through or snap-back behaviour and allows to obtain the response of the structure in the post-peak range, was used. The Line Search algorithm (TNO 2009), which scales the incremental displacements in the iteration process automatically and stabilizes the convergence process, was also used.

$$\alpha_b = \frac{\sum \text{Horizontal forces at the base}}{\text{Self-weight of the structure}} \quad (5.1)$$

In the non-linear dynamic analysis with Earthquake 100%, the maximum seismic coefficient at the base is equal to 0.10 and 0.25 in the transversal and longitudinal direction, respectively (Figure 5.1). According to the pushover analyses, the force based capacity reaches its limit in the transversal direction ($\alpha_b=0.10$). However, in the longitudinal direction the seismic coefficient obtained from the non-linear dynamic analysis ($\alpha_b=0.25$) is significantly lower than the force based capacity obtained from the pushover analysis ($\alpha_b=0.46$). Furthermore, in the non-linear dynamic analysis the displacement is significantly lower than the value obtained from the pushover analysis. As an example, in the transversal direction the maximum displacement at the top obtained from the non-linear dynamic analysis (Earthquake 100%) and from the pushover analysis is about 4.4 cm and 20.0 cm, respectively, which corresponds a difference of about 355%. Thus, the seismic action was increased and a non-linear dynamic analysis with Earthquake 300% was carried out, aiming at exploring the deformation capacity of the structure and obtaining serious damage that allows identifying clearly the collapse mechanism. In the non-linear dynamic analysis of the Earthquake 300% (Figure 5.1), the force based capacity approaches the one obtained from the pushover analyses. In terms of deformation, in the transversal direction the non-linear dynamic analysis of the Earthquake 300% presents similar maximum displacement at the top. However, in the longitudinal direction the analyses present significant differences.

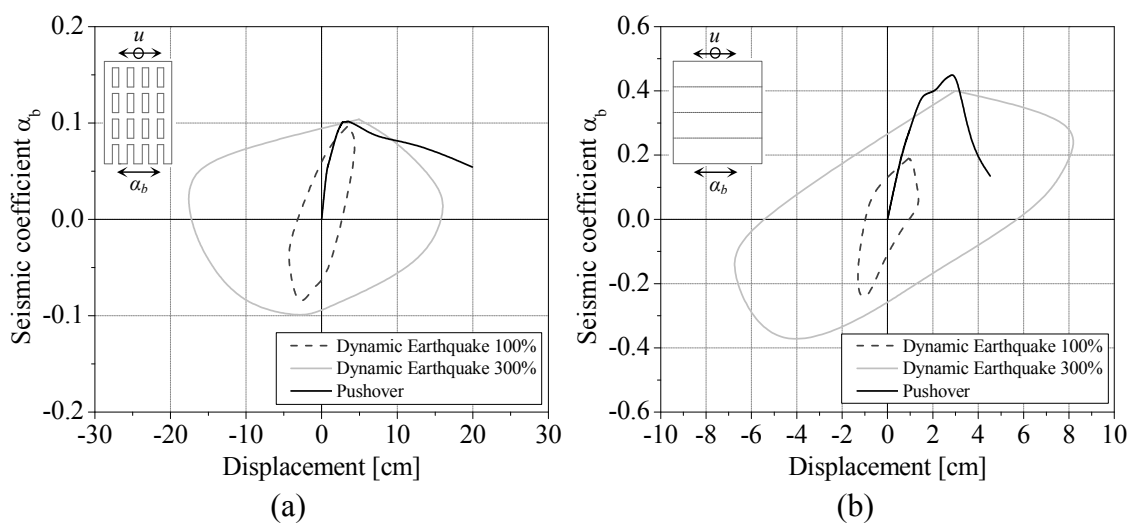


Figure 5.1 – Envelope of the response obtained from the non-linear dynamic analysis with time integration and capacity curve obtained from the pushover analysis of the reference model in the: (a) transversal direction; (b) longitudinal direction.

Besides the quantitative parameters of the capacity of the structure, the analysis of the damage and collapse mechanisms are fundamental for the assessment of the seismic performance of masonry structures. Figure 5.2a presents the distribution of the maximum principal tensile strains, which is an indicator of the cracking, for the non-linear dynamic analysis of the Earthquake 100%. It is observed that damage concentrates at the spandrels, due to the diagonal cracking, and at the piers of the top floor, due to in-plane rocking and out-of-plane bending. The gable walls do not present significant damage. The damage found is again in agreement with the crack patterns obtained in the shaking table tests. In the Earthquake 300% (Figure 5.2b) the structure presents serious damage, with several spandrels totally damaged and piers at the top floor presenting significant cracks due to in-plane rocking and out-of-plane bending. Furthermore, the piers of the first floor also present severe damage. This damage is related to the damage of the spandrels, which present significant deformations and do not adequately restrict the relative displacements of the piers, causing damage mainly due to in-plane forces. The gables walls also present damage, with shear cracks, which have origin at the floor levels and progress to the middle of the walls, and vertical cracks at the top of the walls. Furthermore, local damage at the base and at the connections between the gable walls and the joists of the first floor is observed.

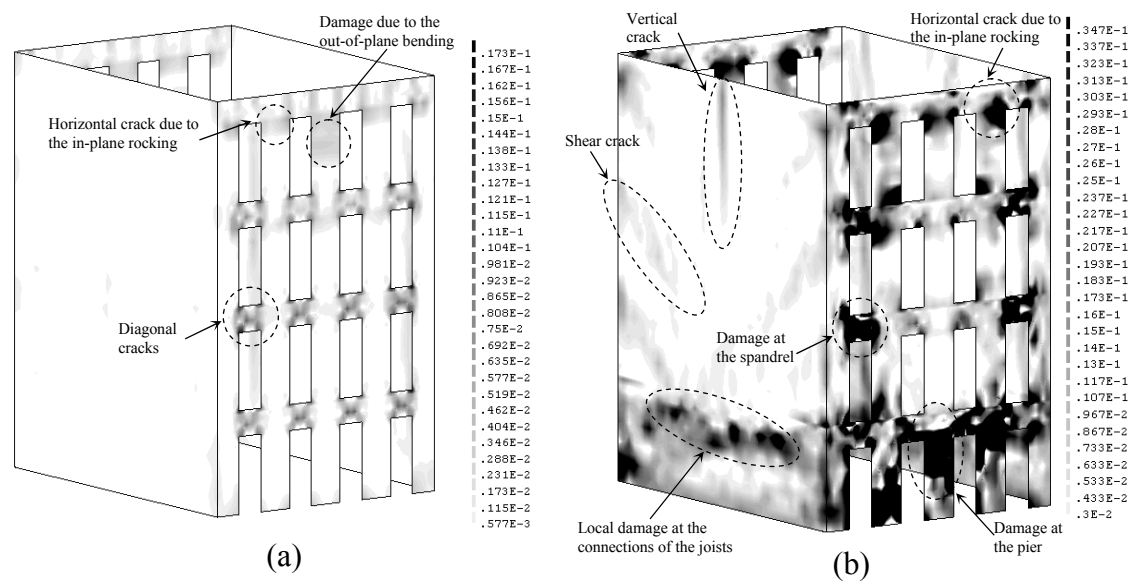


Figure 5.2 – Maximum tensile principal strains at the external surface of the non-linear dynamic analyses of the reference model: (a) Earthquake 100%; (b) Earthquake 300%.

Figure 5.3 presents the maximum principal strains obtained in the pushover analysis in the transversal and longitudinal direction. The transverse damage (Figure 5.3a) is according to the one observed in the non-linear dynamic analysis caused by the in-plane forces (Figure 5.2b), mainly with damage concentration at the piers and horizontal cracks at the piers of the top floor. The piers of the first floor and the base also present damage, but less severe in comparison to the damage observed in the non-linear

dynamic analysis. In the pushover analysis in the longitudinal direction (Figure 5.3b) the piers of the top floor do not present significant damage caused by the out-of-plane bending as observed in the non-linear dynamic analyses (Figure 5.2). The damage concentrates mainly in the gable walls, with two vertical shear cracks that have origin at the floor levels and progress to the middle of the base, and one vertical crack. According to this analysis, the numerical model presents a typical collapse mechanism, in which the facades collapse with the vertical cracks occurring at the top floors of the gable walls (near to first joist of the timber floors) and at the corner of the first floor. The MDF panels are rather flexible and are not able to transfer the inertial forces of the facades to the gables, resulting in out-of-plane collapse of the facades. This collapse mechanism is not observed in the non-linear dynamic analysis, because the model reaches its strength capacity firstly in the transversal direction.

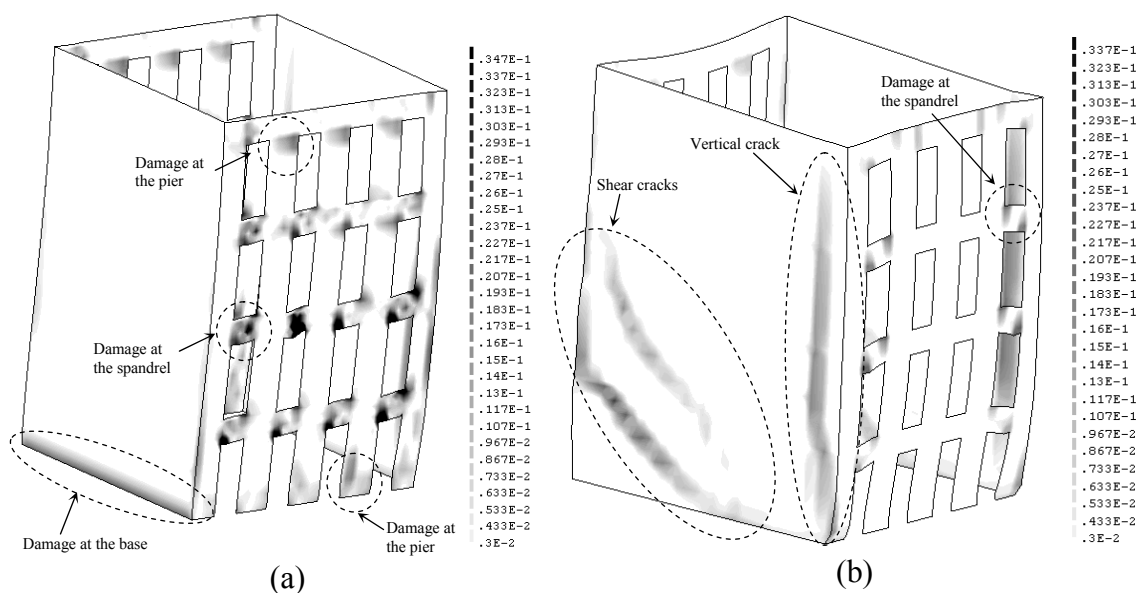


Figure 5.3 – Maximum tensile principal strains at the external surface of the pushover analysis of the reference model in the: (a) transversal direction;
(b) longitudinal direction.

Finally, the out-of-plane and in-plane behavior of the masonry walls was also evaluated, through the absolute maximum out-of-plane displacement at the middle of the walls and the absolute maximum in-plane drift at the corners. In the non-linear dynamic analysis of the Earthquake 100% the maximum out-of-plane displacement in the North facade is equal to 1.9 cm and occurs at the third floor. In the analysis of the Earthquake 300%, and due to serious damage at the piers of the top floor, the maximum out-of-plane displacement occurs at the top of structure and is equal to 8.2 cm (Figure 5.4a). At the middle of the East gable wall the out-of-plane displacement of the Earthquake 300% is equal to 18.0 cm and represents an increase of about 300% with respect to the analysis of the Earthquake 100% (Figure 5.4b). In what concerns the pushover analyses, the dynamic analysis of the Earthquake 300% presents out-of-plane displacements higher

than the pushover analysis at the middle of the North facade, which is related to the damage concentration at the facades. On the other hand, in the pushover analysis in the longitudinal direction the facades collapse from vertical cracks at the gable walls (Figure 5.3b). The dynamic analysis of the Earthquake 300% presents the maximum in-plane drift of the North facade at the first floor (1.7%), due to serious damage at the spandrels and piers, and the drift distribution along the height is very different from the pushover analysis (Figure 5.5a). At the middle of the East gable wall (Figure 5.5b), the maximum in-plane drifts of the dynamic analysis with Earthquake 300% occur at the second and third floors (about 0.7%), being very different from the pushover analysis. In this analysis, the maximum in-plane drift is equal to 0.6% and occurs at the first floor, which is related to the damage at the corners of this floor (Figure 5.3b).

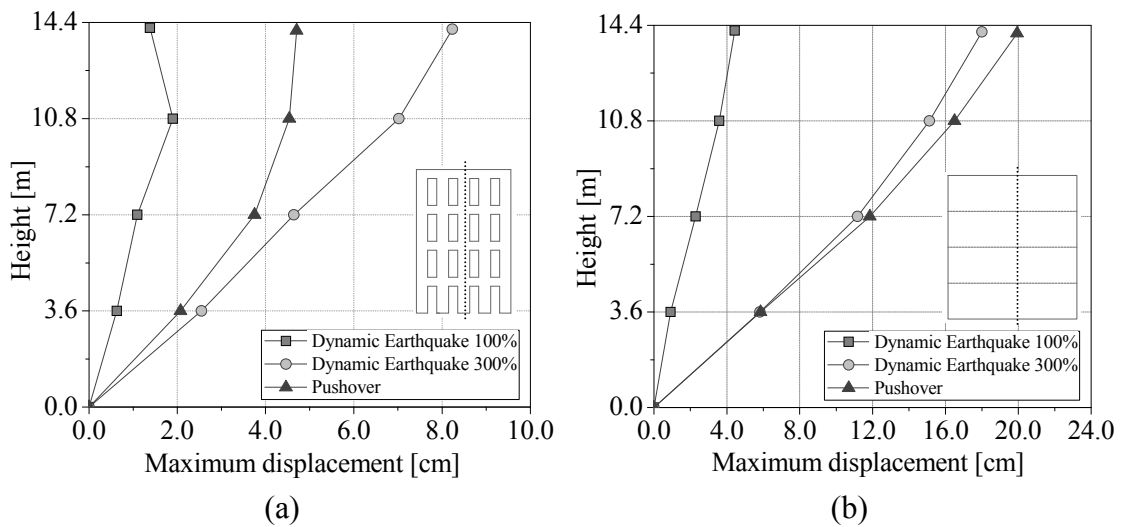


Figure 5.4 – Maximum out-of-plane displacement of the reference model at the middle of the: (a) North facade; (b) East gable wall.

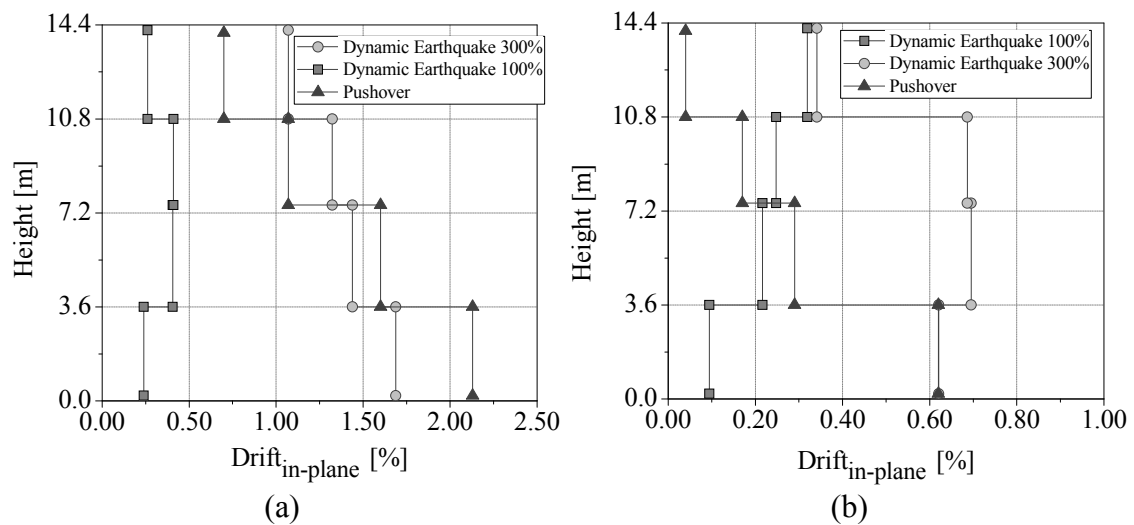


Figure 5.5 – Maximum in-plane drift of the reference model of the: (a) North facade; (b) East gable wall.

5.3 Non-linear dynamic parametric analysis

The non-linear dynamic analysis with time integration involves several parameters that influence the response in a different way and, consequently, the conclusions about the seismic performance of the structures. Thus, a sensitivity analysis taking into account the main parameters that can influence the seismic behaviour of the “gaioleiro” buildings was carried out. Here, the objective is to evaluate the variation of response of the structure, with respect to the reference model, varying the value of each parameter, taking into account the dispersion in the features of the “gaioleiro” building typology. The considered parameters (Table 5.4) aim at evaluating the response of the numerical models with respect to the variation on stiffness of the masonry walls, on stiffness of the floors, on non-linear properties of the masonry in compression and tension, and on damping ratio. Furthermore, the influence in the response of the vertical component of the earthquake was also studied. Next, the analysis of the response of the numerical model for each parameter is briefly presented.

Table 5.4 – Parameters considered in the non-linear dynamic sensitivity analysis.

	Lower value	Reference value	Upper value
Young's modulus of the walls	$0.5 \times E_{walls,ref}$	$E_{walls,ref} = 1.00 \text{ GPa}$	$2.0 \times E_{walls,ref}$
Young's modulus of the floors	$0.1 \times E_{floors,ref}$	$E_{floors,ref} = 0.16 \text{ GPa}$	$10 \times E_{floors,ref}$
Compressive strength	$0.5 \times f_{c,ref}$	$f_{c,ref} = 1.00 \text{ MPa}$	$2.0 \times f_{c,ref}$
Compressive fracture energy	$0.5 \times G_{c,ref}$	$G_{c,ref} = 1.00 \text{ N/mm}$	$2.0 \times G_{c,ref}$
Tensile strength	$0.5 \times f_{t,ref}$	$f_{t,ref} = 0.10 \text{ MPa}$	$2.0 \times f_{t,ref}$
Tensile fracture energy	$0.5 \times G_{t,ref}$	$G_{t,ref} = 0.05 \text{ N/mm}$	$2.0 \times G_{t,ref}$
Damping ratio	$\zeta_{Lower} = 2.0\%$	$\zeta_{ref} = 3.3\%^*$	$\zeta_{Upper} = 5.0\%$
Vertical earthquake	vertical component of the earthquake		

(* average of the damping ratios of the two modes considered)

5.3.1 Stiffness of the masonry walls

The analysis of the response with respect to the stiffness of the masonry walls was carried out decreasing ($0.5 \times E_{walls,ref}$) and increasing ($2.0 \times E_{walls,ref}$) the Young's modulus of the walls, which involves alterations in the modes. The frequency of the first mode in the transversal direction is equal to 1.25 Hz and 2.26 Hz for the numerical model with $0.5 \times E_{walls,ref}$ and $2.0 \times E_{walls,ref}$, respectively. The mode shape also presents differences. The mode shape of the numerical with $0.5 \times E_{walls,ref}$ presents different curvature in elevation with less interstory relative modal displacement at the top of the structure. The frequency of the first longitudinal mode is equal to 2.78 Hz and 4.72 Hz for the numerical with $0.5 \times E_{walls,ref}$ and $2.0 \times E_{walls,ref}$ respectively. In this direction, the

numerical model with $0.5x E_{walls,ref}$ presents modal displacements at the gable walls significantly higher than the numerical model with $2.0x E_{walls,ref}$.

Figure 5.6 presents the envelopes of the dynamic response (seismic coefficient at the base versus displacement at the top of the structure). In general, the responses of the numerical models with $0.5x E_{walls,ref}$ present a decrease of the seismic coefficient together with an increase of the displacement in comparison to the reference model, while the inverse occurs for $2.0x E_{walls,ref}$. However, in the transversal direction the maximum displacement at the top of the numerical model with $0.5x E_{walls,ref}$ is slightly lower than the maximum displacement of the reference model. This is related to the alteration in the mode shape of the first transversal mode previously mentioned. However, at other floor levels the maximum displacements of the numerical model with $0.5x E_{walls,ref}$ are higher than the displacements of the reference model (Figure 5.7).

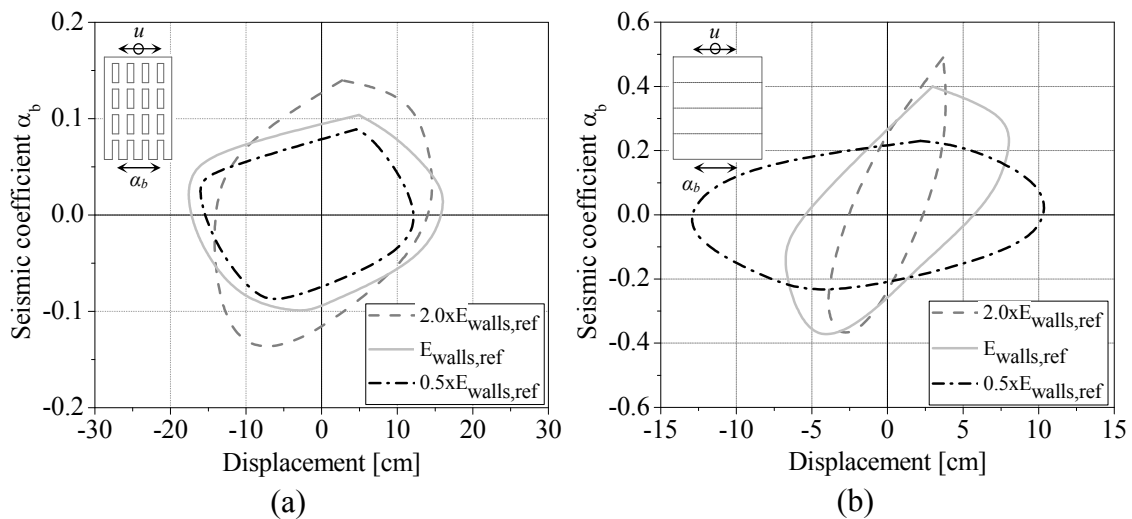


Figure 5.6 – Envelope of the response varying the Young's modulus of the masonry walls in the: (a) transversal direction; (b) longitudinal direction.

The most significant differences occur in the longitudinal direction, in which an increase of about 60% of the out-of-plane displacement at the top of the facades is obtained (Figure 5.6b and Figure 5.7a). The maximum in-plane drifts present a significant increase in the gable walls and at the base of the facades for the numerical model $0.5x E_{walls,ref}$. As expected, the damage increases and decreases significantly for the numerical model with $0.5x E_{walls,ref}$ and $2.0x E_{walls,ref}$, respectively, which is due to the different deformation of the models. The numerical model with $2.0x E_{walls,ref}$ presents very low damage in the gable walls. Furthermore, the collapse mechanisms are similar to the reference model (see Annex C).

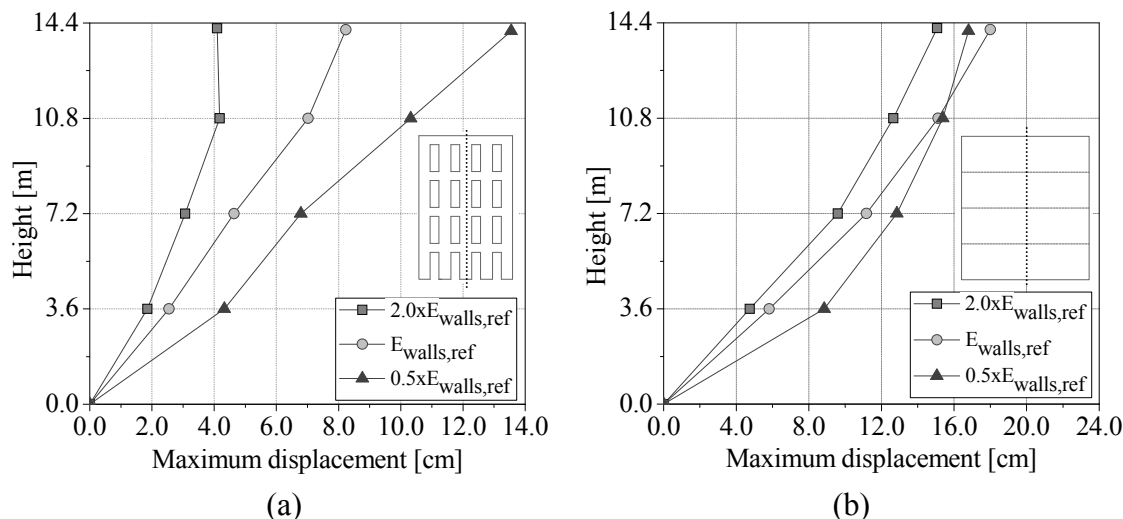


Figure 5.7 – Maximum out-of-plane displacement, obtained from the dynamic analysis, varying the Young's modulus of the masonry walls at the middle of the: (a) North facade; (b) East gable wall.

5.3.2 Stiffness of the timber floors

The influence of the stiffness of the timber floors on the response of the structure was evaluated decreasing ($0.1 \times E_{\text{floors,ref}}$) and increasing ($10 \times E_{\text{floors,ref}}$) ten times the Young's modulus of the MDF panels, with respect to the reference model. The average of the frequency variation of the first transversal and longitudinal modes of the numerical models, with respect to reference model, is equal to 12% and 16%, respectively. The modes present significant differences in their shape. In the mode shapes of the numerical model with $0.1 \times E_{\text{floors,ref}}$ the masonry walls presents significant relative modal displacements with respect to corners. On the other hand, in the numerical model with $10 \times E_{\text{floors,ref}}$ the relative modal displacements of the walls with respect to the corners are very low, because the floors prevent the out-of-plane deformation of the masonry walls.

The response in the transversal direction presents only minor variations. While the maximum seismic coefficient remains constant, the displacement at the top of the numerical model with $0.1 \times E_{\text{floors,ref}}$ presents an increase of about 24% (Figure 5.8a). In the longitudinal direction the maximum seismic coefficients present variations of about -18% and 15% for the numerical model with $0.1 \times E_{\text{floors,ref}}$ and $10 \times E_{\text{floors,ref}}$, respectively. The displacements in the longitudinal direction of the numerical model with $0.1 \times E_{\text{floors,ref}}$ and $10 \times E_{\text{floors,ref}}$ present an increase of about 60% and a decrease of about 10%, with respect to the reference model, respectively (Figure 5.8b).

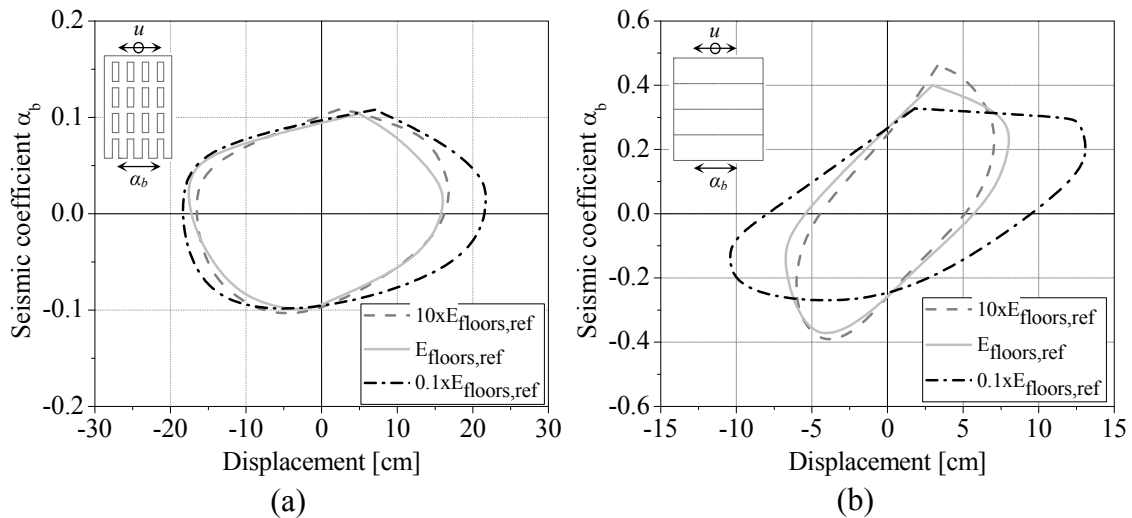


Figure 5.8 – Envelope of the response varying the Young's modulus of the floors in the: (a) transversal direction; (b) longitudinal direction.

The numerical models present significant differences in terms of damage and collapse mechanisms. In the numerical model with $0.1x E_{floors,ref}$ (Figure 5.9a) the facades present damage at the spandrels at the piers of the top floors due to the in-plane forces. Furthermore, the piers of the top floor also present damage due to the out-of-plane bending. The gable walls present vertical cracks associated to a typical collapse mechanism of the masonry buildings with flexible floors – collapse of the facades involving a portion of the orthogonal walls. In the numerical model with $0.1x E_{floors,ref}$ the flexible floors are not able to transfer the inertial forces between orthogonal walls and, consequently, the inertial forces have to be transferred from the corners, causing damage in this part of the structure. Furthermore, the flexible floors do not provide a box behaviour, leading to contra-phase movements and high relative displacements between facades. This behaviour, combined with the out-of-plane bending, causes high tensile stress in the gables, resulting in the out-of-plane collapse of the facades involving a portion of the gables walls. On the other hand, the numerical model with $10x E_{floors,ref}$ (Figure 5.9b) presents serious damage at the facades mainly associated to the in-plane forces (serious damage at the spandrels and piers). The increased stiffness of the floors improves the performance of the building, in which the gable walls present moderate damage (shear cracks) and do not present vertical cracks at the middle of the walls.

The maximum out-of-plane displacements of the numerical model with $10x E_{floors,ref}$ do not present a significant decrease with respect to the reference model, mainly in the gable walls due to the timber joists (Figure 5.10). The numerical model with $0.1x E_{floors,ref}$ presents significant increases of the out-of-plane displacements, in which an increase of about 100% at the third floor of the North facade is highlighted (Figure 5.10a). The in-plane drifts present a significant increase at the three top floors of the gable walls due to the vertical cracks found in the walls (see Annex C).

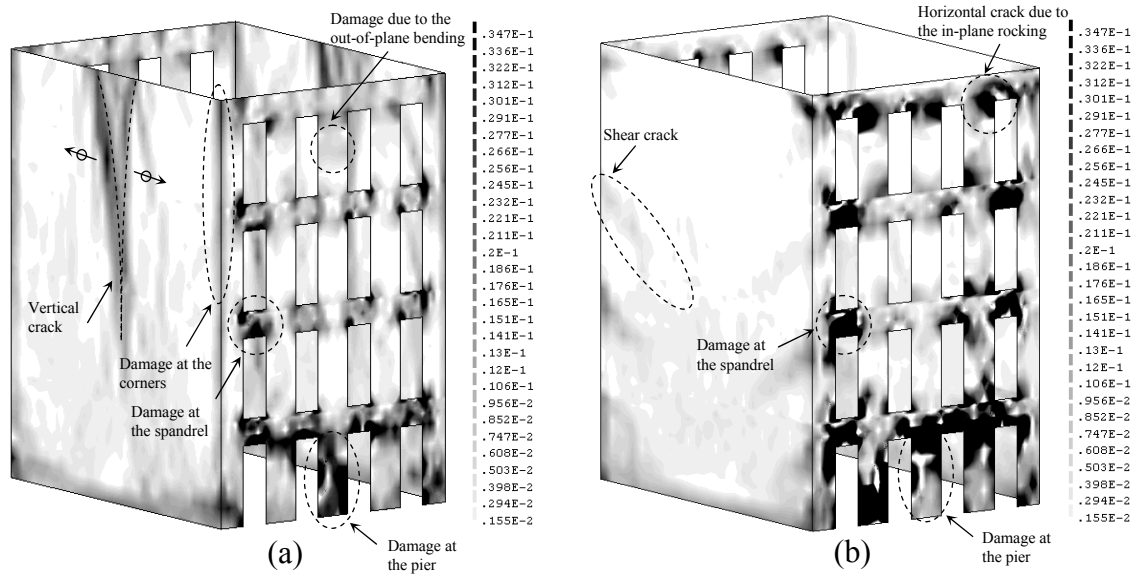


Figure 5.9 – Maximum tensile principal strains at the external surface, obtained from the dynamic analysis, varying the Young’s modulus of the floors: (a) $0.1 \times E_{floors,ref}$; (b) $10 \times E_{floors,ref}$.

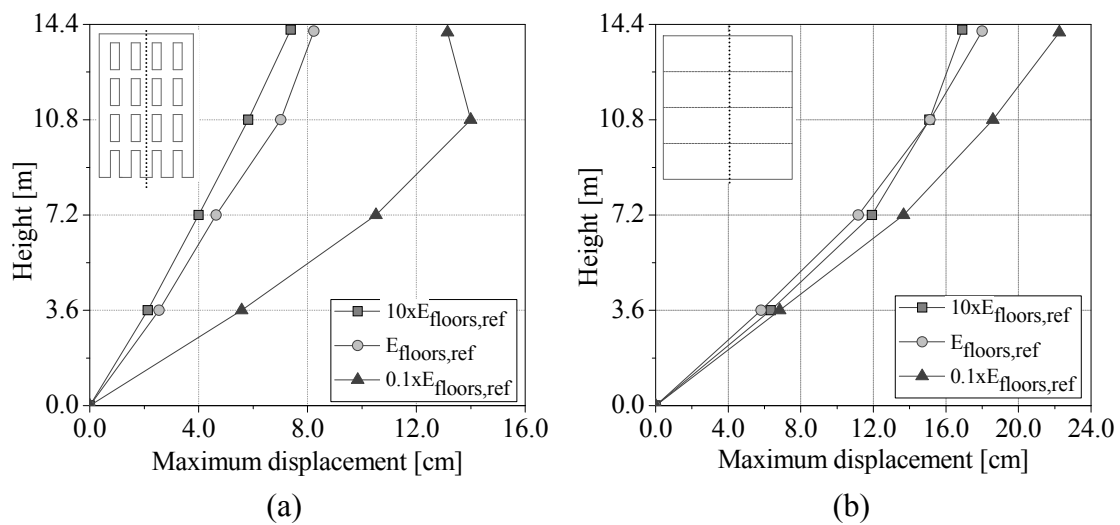


Figure 5.10 – Maximum out-of-plane displacement, obtained from the dynamic analysis, varying the Young’s modulus of the floors at the middle of the: (a) North facade; (b) East gable wall.

5.3.3 Compressive non-linear properties of the masonry

In the sensitivity analysis of the compressive non-linear properties of the masonry, two parameters were considered: (a) compressive strength; (b) compressive fracture energy. Each parameter was decreased ($0.5 \times f_{c,ref}$, $0.5 \times G_{c,ref}$) and increased ($2.0 \times f_{c,ref}$, $2.0 \times G_{c,ref}$) two times with respect to the reference value. It is noted that the alterations on the

compressive strength also change the shape of the compression function and, consequently, the ultimate strains.

In the transversal direction (Figure 5.11a), the maximum seismic coefficients of the numerical models with $0.5x f_{c,ref}$ and $2.0x f_{c,ref}$ present a decrease and an increase of about 20% and 70%, respectively. In the longitudinal direction (Figure 5.11b) the variation is similar for both numerical models (about 47%). In terms of deformation, the models do not present large variations of displacements in the transversal direction, mainly at the two first floors (Figures 5.11a and 5.12b). In the longitudinal direction the highest variation of displacement is equal to 50% and occurs at the top of the numerical model with $0.5x f_{c,ref}$ (Figures 5.11b and 5.12a).

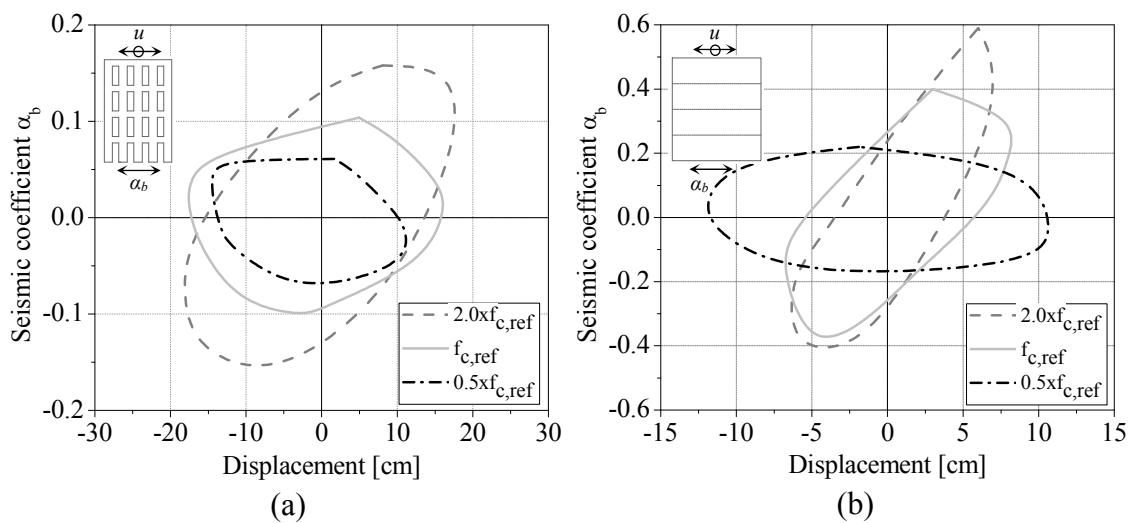


Figure 5.11 – Envelope of the response varying the compressive strength in the: (a) transversal direction; (b) longitudinal direction.

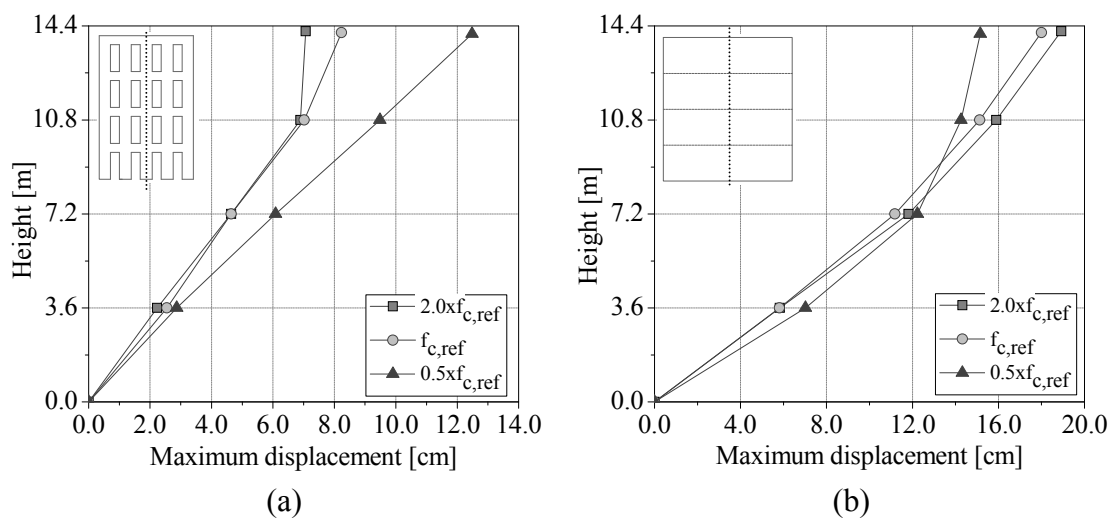


Figure 5.12 – Maximum out-of-plane displacement, obtained from the dynamic analysis, varying the compressive strength at the middle of the: (a) North facade; (b) East gable wall.

The crack patterns of the numerical models varying the compressive strength present some changes. The numerical model with $0.5x f_{c,ref}$ presents a concentration of the damage at facades (spandrels and piers at the top and at the base) and at the base of the gable walls (Figure 5.13a). However, increasing the compressive strength ($2.0x f_{c,ref}$) the damage is significant lower in comparison to the damage of the reference model, in which generalized cracking (low damage concentration), diagonal cracks at the spandrels and small vertical cracks at the top of the gable are observed (Figure 5.13b). The generalized cracking is related to the increase of the compressive strength while keeping the fracture energy, which causes the decrease of the ultimate strain.

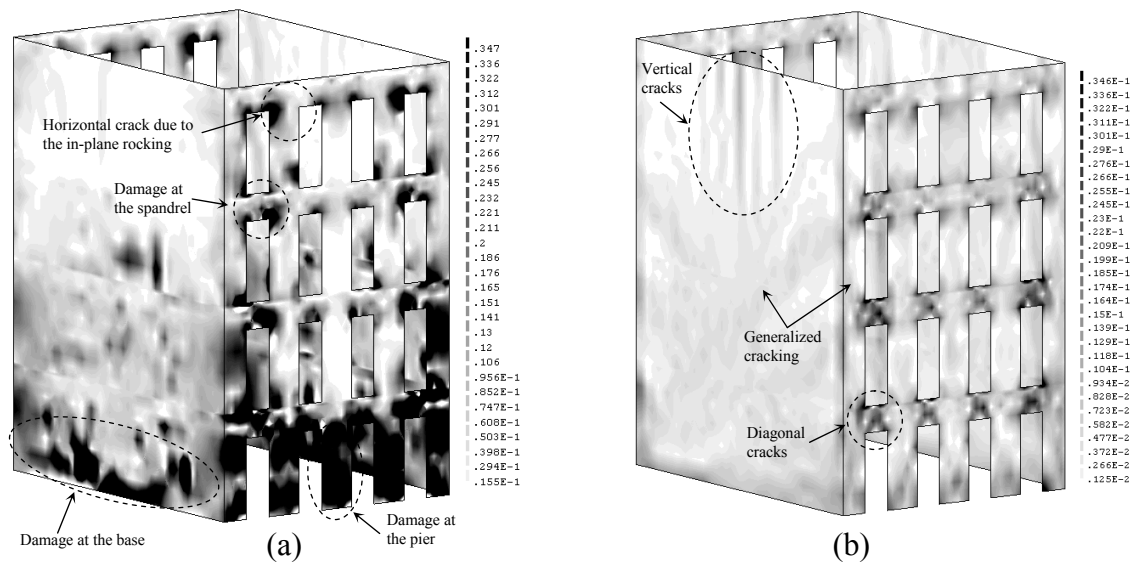


Figure 5.13 – Maximum tensile principal strains at the external surface, obtained from the dynamic analysis, varying the compressive strength: (a) $0.5x f_{c,ref}$, (b) $2.0x f_{c,ref}$.

In what concerns the variation of the compressive fracture energy, in the transversal direction the maximum seismic coefficient increases about 20% and remain equal, with respect to reference model, for the numerical model with $2.0x G_{c,ref}$ and $0.5x G_{c,ref}$, respectively (Figure 5.14a). In the longitudinal direction (Figure 5.14b), the numerical models with $0.5x G_{c,ref}$ and $2.0x G_{c,ref}$ present variations of the maximum seismic coefficient of about -38% and +33%, respectively. The numerical model with the maximum compressive fracture energy presents a low variation of the maximum displacement at the top in both directions (about 5% on average). In terms of deformation, the maximum variation of the displacement at the top is equal to 32% and occurs for the numerical with $0.5x G_{c,ref}$ in the longitudinal direction (Figure 5.14).

In terms of in-plane behavior, the maximum variation of the in-plane drift occurs at the gable walls of the numerical model with $0.5x G_{c,ref}$, in which an increase of the in-plane drift at the top of about 129% is highlighted. The numerical models present the same collapse mechanisms of the reference model and, as expected, higher damage and lower damage concentration for the numerical model with $0.5x G_{c,ref}$ and $2.0x G_{c,ref}$, respectively (see Annex C).

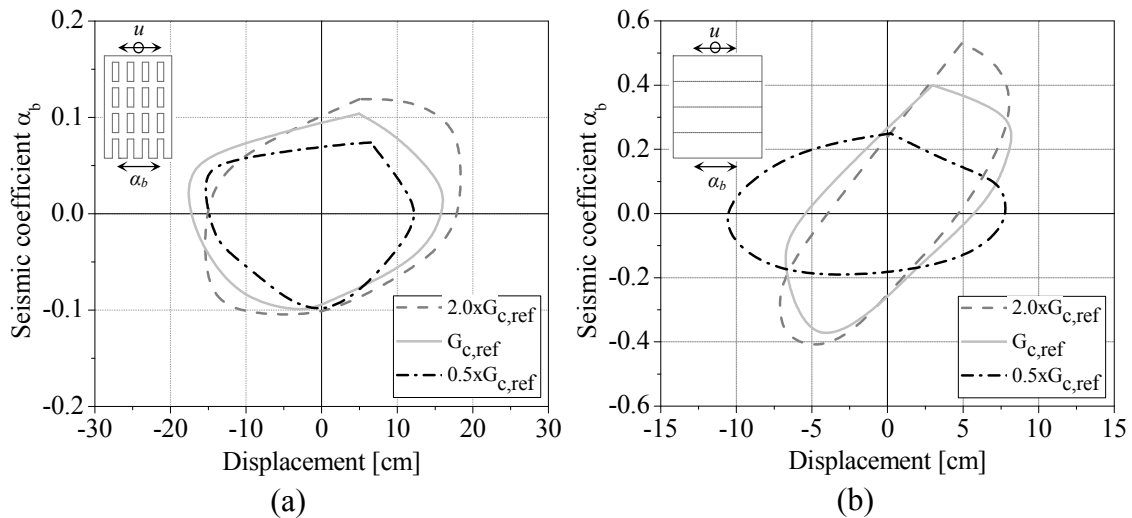


Figure 5.14 – Envelope of the response varying the compressive fracture energy in the: (a) transversal direction; (b) longitudinal direction.

The reference value of the compressive strength is low (1.00 MPa) and the building is relatively high, with four storeys. The adopted lower and upper limits form a range of values of the compressive non-linear properties ($0.5 \text{ MPa} \leq f_c \leq 2.0 \text{ MPa}$; $0.5 \text{ N/mm} \leq G_c \leq 2.0 \text{ N/mm}$) where it is found that the compressive strength changes significantly the bending moment resistance and, consequently, the dynamic behaviour of the structure.

5.3.4 Tensile non-linear properties of the masonry

The variations in the response of the structure decreasing ($0.5 \times f_{t,ref}$, $0.5 \times G_{t,ref}$) and increasing ($2.0 \times f_{t,ref}$, $2.0 \times G_{t,ref}$) two times the tensile non-linear properties were also evaluated, namely the tensile strength and the tensile fracture energy.

In what concerns the tensile strength, the maximum seismic coefficient in the transversal direction presents very low variation (-2%) for the numerical model with $0.5 \times f_{t,ref}$ and about +20% for the numerical model with $2.0 \times f_{t,ref}$. The maximum seismic coefficient in the longitudinal direction presents a variation of about 10% for both numerical models (Figure 5.15). The maximum displacements at the top also present low variations in both directions of the numerical model with $0.5 \times f_{t,ref}$. The highest variation of the displacement at the top is equal to -28% and occurs in the longitudinal direction of the numerical model with $2.0 \times f_{t,ref}$ (Figure 5.15b). The numerical model with $2.0 \times f_{t,ref}$ presents more damage than the numerical model with $0.5 \times f_{t,ref}$, namely at the spandrels and at the piers of the top and first floors (see Annex C). The increase of the tensile strength involves a decrease of the ultimate strain, causing a higher damage concentration in the numerical model with $2.0 \times f_{t,ref}$ under high seismic amplitude.

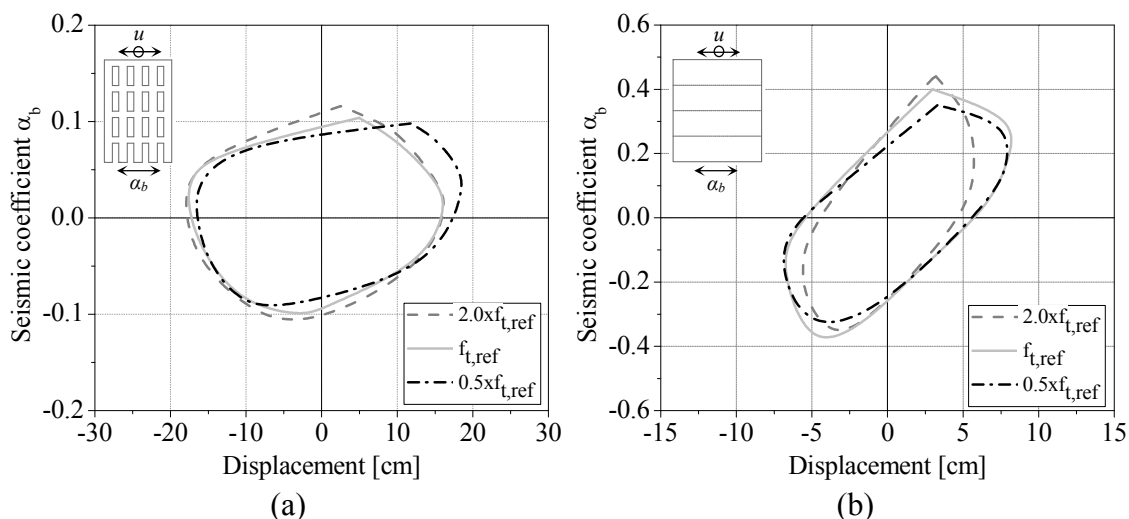


Figure 5.15 – Envelope of the response varying the tensile strength in the: (a) transversal direction; (b) longitudinal direction.

The variations of the maximum seismic coefficients and maximum displacements varying the tensile fracture are very low (Figure 5.16). The maximum variation occurs for the maximum seismic coefficient in the longitudinal direction of the numerical model with $2.0 \times G_{t,ref}$ (+13%). The damage presented is according to what it could be expected and without different collapse mechanisms from the reference model, in which an increase and decrease of the damage for the numerical model with $0.5 \times G_{t,ref}$ and $2.0 \times G_{t,ref}$, respectively, is observed (see Annex C).

It is noted that the low variation of the response when the tensile properties are changed is also associated to the low range of the adopted values ($0.05 \text{ MPa} \leq f_t \leq 0.20 \text{ MPa}$; $0.025 \text{ N/mm} \leq G_t \leq 0.100 \text{ N/mm}$). However, these limits correspond to a common feature of masonry – low tensile strength, meaning that the non-linear tensile properties seem not to affect significantly the response under high seismic amplitude.

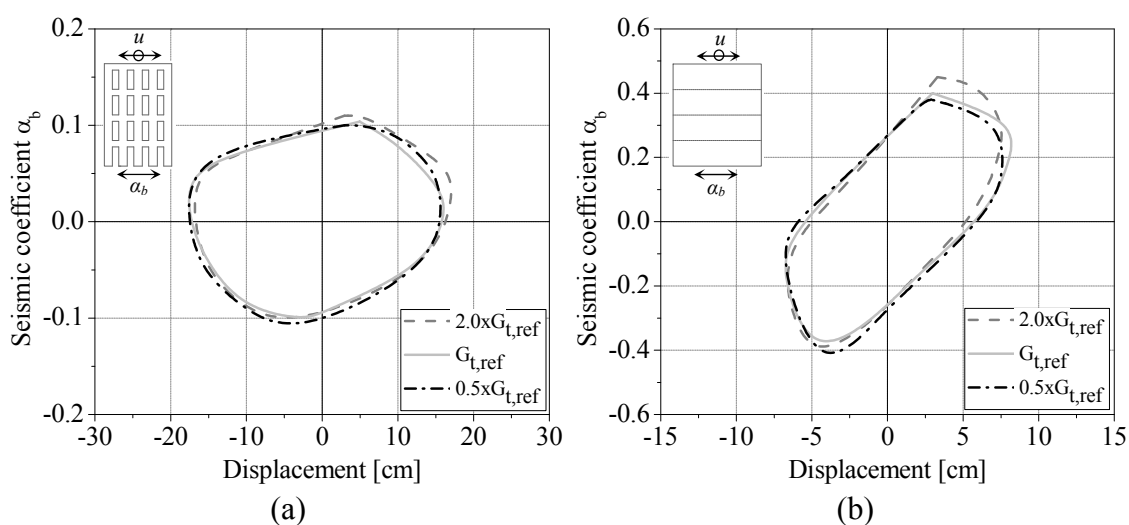


Figure 5.16 – Envelope of the response varying the tensile fracture energy in the: (a) transversal direction; (b) longitudinal direction.

5.3.5 Damping

The reference viscous damping was defined assuming the damping ratio of the first (3.20%) and second (3.39%) transversal modes estimated in the first dynamic identification test (Table 3.1) and with the frequencies updated to the full model. In order to evaluate the sensitivity of the response to the damping, two non-linear dynamic analyses with 2% and 5% for the damping ratios of the first and second transversal modes were carried out. The response of the structure in the transversal direction does not change significantly decreasing the ratio damping of about 1% ($\zeta_{Lower}=2.0\%$). The maximum variation of the response in the longitudinal direction for the numerical model with $\zeta_{Lower}=2.0\%$ is equal to -8% (displacement at the top). In the transversal direction of the numerical model with $\zeta_{Upper}=5.0\%$ the maximum seismic coefficient increases about 10% and the maximum displacement at the top decreases about 17%. In the longitudinal direction the response ($\zeta_{Upper}=5.0\%$) presents a variation of about 20% for both parameters (Figure 5.17). The numerical model with $\zeta_{Lower}=2.0\%$ presents serious damage at the spandrels, piers at the top floor and at the base, and at the first floor of the gable walls. On the other hand, when increasing the damping ($\zeta_{Upper}=5.0\%$) the numerical model presents, as expected, a damage reduction. The numerical model with $\zeta_{Lower}=2.0\%$ also presents a significant increase of the in-plane drift at the base of the facades and at the top of the gable walls (see Annex C).

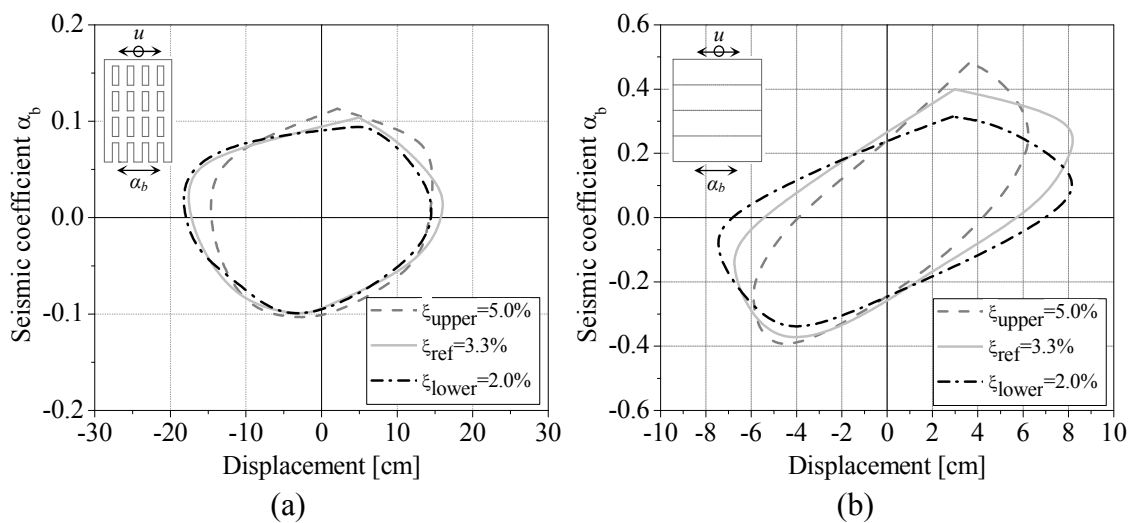


Figure 5.17 – Envelope of the response varying the damping ratio in the: (a) transversal direction; (b) longitudinal direction.

5.3.6 Vertical component of the earthquake

The effect of the vertical component of the earthquake on masonry structures has not been much studied. It is known that masonry structures present low tensile strength and were built to resist compressive stresses, i.e. in general a state of compressive stresses is favourable to their seismic performance. Under an earthquake, the vertical component

may reduce the compressive stress in some instance of time and decrease the strength capacity of the structure (e.g. a masonry wall under shear and normal forces). Thus, an artificial accelerogram compatible with the vertical elastic response spectrum defined by Eurocode 8 (EN 1998-1 2004) and Portuguese National Annex for Lisbon ($a_{vg} = 1.125 \text{ m/s}^2$), with a damping ratio equal to 5% and a type *A* soil (rock, $S = 1$) was generated, increased three times (amplitude according the Earthquake 300%) and applied in the vertical direction of the model.

The results of the non-linear dynamic analysis of the earthquake show that the vertical component does not change significantly the behaviour of the structure with respect to the reference model (Figure 5.18). The out-of-plane displacements at the middle of the walls, the in-plane drifts and the damage present very low variations (see Annex C). The numerical model is very stiff in the vertical direction and the maximum variation of vertical displacement at the top of the gable walls, with respect to the vertical displacement caused by the self-weight, is lower than 0.2 cm. The structure has four storeys and a large mass, which causes high compressive stresses due to the self-weight. The vertical component of the earthquake is not enough to change significantly the state of stress and, consequently, to reduce its strength capacity. A non-linear dynamic analysis with the Earthquake 100% and including the vertical component of the earthquake, aiming to evaluate its influence in the response under lower seismic amplitude, was also carried out. The results also show that in the Earthquake 100% the variation in the response of the numerical model is very low.

It is noted that the numerical model was prepared according to a macro-modelling strategy, in which the mortar and interfaces unit/mortar are not simulated. In real cases, the vertical component of the earthquake can reduce the normal compressive stress in the mortar and in the interfaces, provoking some cracking. This might be become particularly relevant in rubble masonry and mortar with low cohesion.

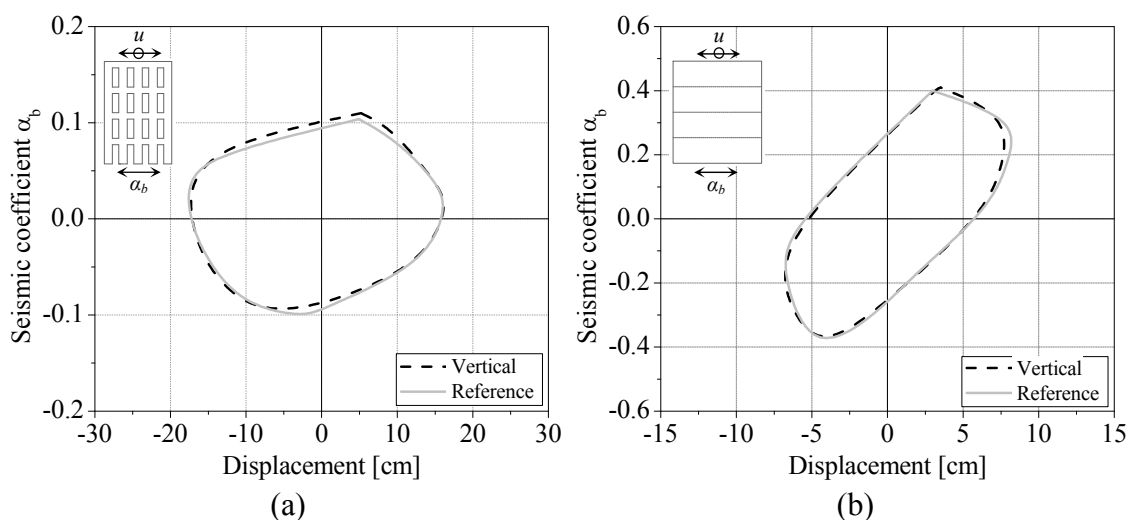


Figure 5.18 – Envelope of the response including the vertical component of the earthquake in the: (a) transversal direction; (b) longitudinal direction.

5.4 Pushover parametric analysis

Pushover analysis is much used for evaluating the seismic performance of structures, particularly for reinforced concrete and steel structures. Its application to ancient masonry buildings (structures with flexible floors, distributed stiffness and mass) is still a challenge. The results of the pushover analysis of the reference model in the transversal direction is according to the response obtained from the non-linear dynamic analysis, in which similar damage occurred in the facades associated to the in-plane forces and similar maximum out-of-plane displacements of the gables wall were found. It is noted that, according to the non-linear dynamic analysis and experimental tests, the facades are the most vulnerable masonry walls to an earthquake, presenting the higher concentration of damage.

As previously done in the dynamic sensitivity analysis, in the pushover analysis presented next the values of the Young' modulus of the masonry walls, the Young' modulus of the timber floors and the compressive and tensile non-linear properties of the masonry were changed (lower and upper limits) and the variations on the response were analyzed. Furthermore, the type of load pattern applied horizontally to the structure was also discussed and a pushover analysis proportional to the modal displacements of the first mode in the applied direction was carried out besides a standard uniform load distribution (Table 5.5). Here, the objective is to evaluate the variation of the response of the structure under a seismic action based on displacement (first mode proportional) with respect to a loading based in force (proportional to the mass). The pushover analysis proportional to the first mode based on force, as defined in the Eurocode 8, was not carried out, due to the difficulties of obtaining the mass matrix.

Next the most relevant variations of the response are presented. For more detail about the results of the pushover analysis, see Annex D.

Table 5.5 – Parameters considered in pushover sensitivity analysis.

	Lower value	Reference value	Upper value
Young's modulus of the walls	$0.5 \times E_{walls,ref}$	$E_{walls,ref} = 1.00 \text{ GPa}$	$2.0 \times E_{walls,ref}$
Young's modulus of the floors	$0.1 \times E_{floors,ref}$	$E_{floors,ref} = 0.16 \text{ GPa}$	$10 \times E_{floors,ref}$
Compressive strength	$0.5 \times f_{c,ref}$	$f_{c,ref} = 1.00 \text{ MPa}$	$2.0 \times f_{c,ref}$
Compressive fracture energy	$0.5 \times G_{c,ref}$	$G_{c,ref} = 1.00 \text{ N/mm}$	$2.0 \times G_{c,ref}$
Tensile strength	$0.5 \times f_{t,ref}$	$f_{t,ref} = 0.10 \text{ MPa}$	$2.0 \times f_{t,ref}$
Tensile fracture energy	$0.5 \times G_{t,ref}$	$G_{t,ref} = 0.05 \text{ N/mm}$	$2.0 \times G_{t,ref}$
Load pattern	displacement proportional to the first mode		

5.4.1 Stiffness of the masonry walls

According to the pushover analysis when varying the Young's modulus of the masonry walls the seismic coefficient presents a decrease of about 2% and 9% for the numerical model with $0.5x E_{walls,ref}$ in the transversal and longitudinal direction, respectively. A slightly larger variation occurs for the numerical model with $2.0x E_{walls,ref}$, in which the seismic coefficient increases about 25% and 11% in the transversal and longitudinal direction, respectively (Figure 5.19). As expected, when decreasing the Young's modulus of the masonry walls the initial stiffness decreases and the maximum seismic coefficient occurs for a larger displacement at the top, i.e. the response is more flexible. In comparison to the dynamic analysis, the maximum seismic coefficient in the transversal direction of the pushover analysis is about 11% higher and 9% lower for the numerical model with $0.5x E_{walls,ref}$ and $2.0x E_{walls,ref}$, respectively. However, it is noted that in the dynamic analysis the seismic amplitude was not increased.

The collapse mechanisms are equal to the reference model, with failure of the spandrels and piers in the pushover analysis in the transversal direction and out-of-plane collapse of the facades and shear cracks at the gables walls in the pushover analysis in the longitudinal direction (see Annex D).

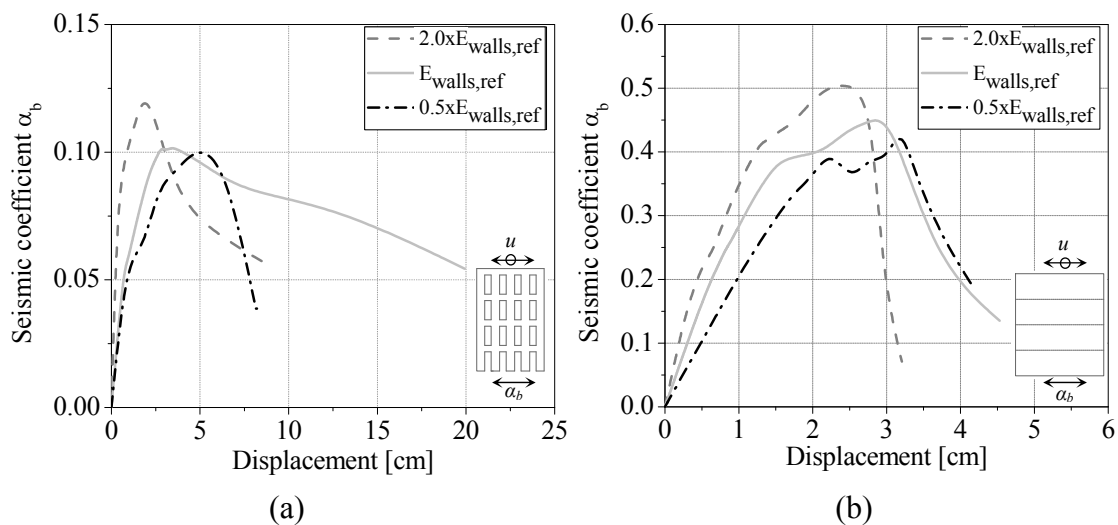


Figure 5.19 – Capacity curves varying the Young's modulus of the masonry walls in the: (a) transversal direction; (b) longitudinal direction.

5.4.2 Stiffness of the timber floors

In the pushover analysis when varying the Young's modulus of the timber floors, the maximum seismic coefficient presents on average variations of about 11% and 13% in the transversal and longitudinal direction, respectively (Figure 5.20). The major differences occur in the pushover analysis in the longitudinal direction, which is more dependent of the stiffness of the timber floors. The numerical model with $10x E_{floors,ref}$

presents a response stiffer than the reference model and with a high reduction of the lateral forces after post-peak for low deformation (more brittle behaviour). On the other hand, the response of the numerical model with $0.1 \times E_{floors,ref}$ presents several losses of stiffness until the maximum seismic coefficient and high deformation (Figure 5.20b). In the end of the pushover analyses in the longitudinal direction the numerical models with $0.1 \times E_{floors,ref}$ and $10 \times E_{floors,ref}$ present similar seismic coefficient and significant different displacements. This is related to the serious damage present in the numerical model with $0.1 \times E_{floors,ref}$, mainly due to the vertical crack near the corners that cause the out-of-plane collapse of the facades (Figure 5.21a). In the numerical model with $10 \times E_{floors,ref}$ the collapse occurs due to shear failure of the gable walls (Figure 5.21b).

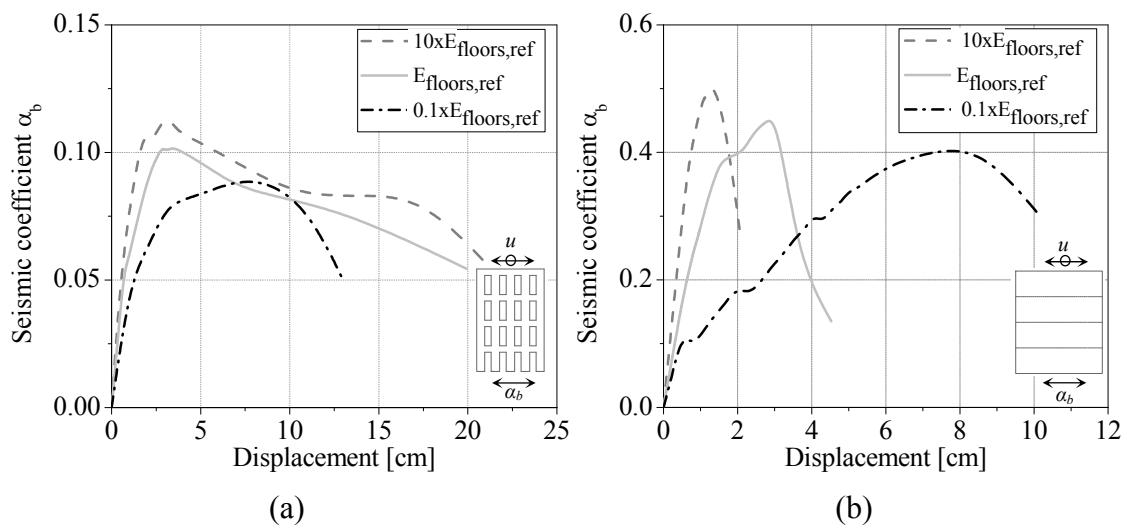


Figure 5.20 – Capacity curves varying the Young’s modulus of the timber floors in the: (a) transversal direction; (b) longitudinal direction.

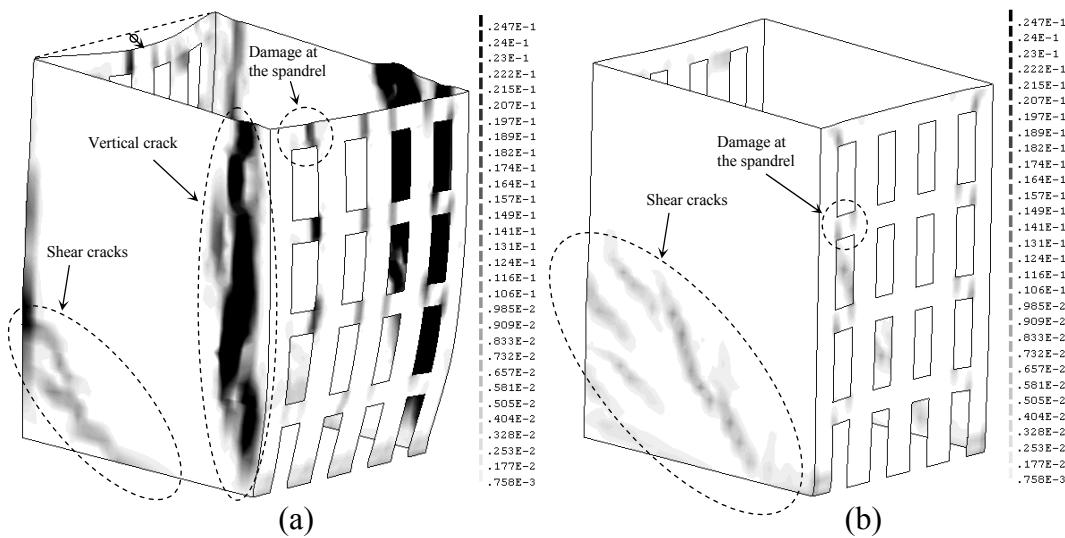


Figure 5.21 – Maximum tensile principal strains at the external surface, obtained from the pushover analysis in the longitudinal direction, varying the Young’s modulus of the floors: (a) $0.1 \times E_{floors,ref}$; (b) $10 \times E_{floors,ref}$.

5.4.3 Compressive non-linear properties of the masonry

The pushover analyses varying the values of the compressive strength present a high variation of the maximum seismic coefficient, mainly in the transversal direction as occurred in the dynamic analysis. In the transversal direction the maximum seismic coefficient increases about 34% and decreases about 32% for the numerical model with $0.5x f_{c,ref}$ and $2.0x f_{c,ref}$, respectively, with respect to the reference model (Figure 5.22a). In the pushover analysis in the longitudinal direction the maximum seismic coefficients present a variation of about -37% and 8% for the numerical model with $0.5x f_{c,ref}$ and $2.0x f_{c,ref}$, respectively, with respect to the reference model (Figure 5.22b).

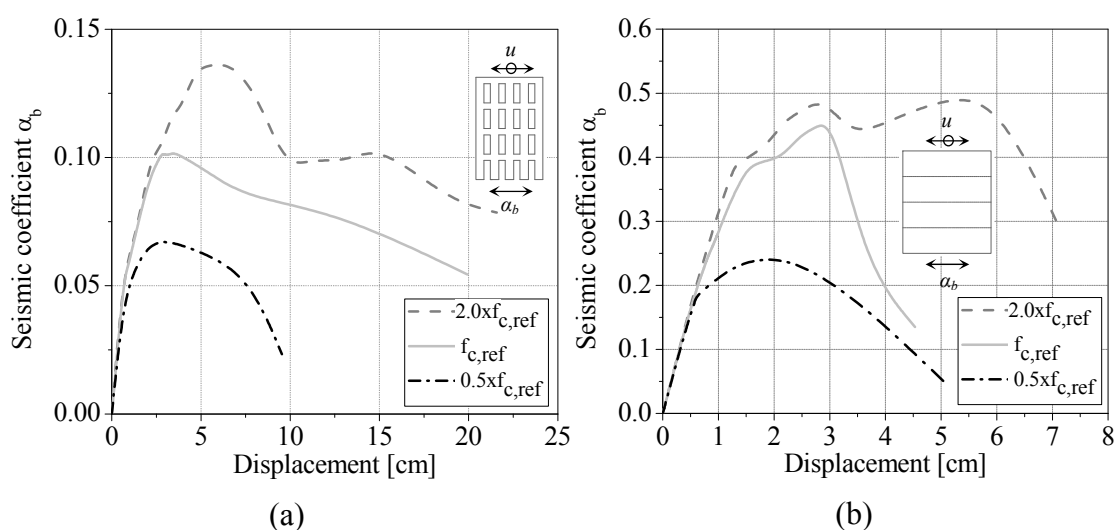


Figure 5.22 – Capacity curves varying the compressive strength in the: (a) transversal direction; (b) longitudinal direction.

In the pushover analysis varying the compressive fracture energy the variations of the maximum seismic coefficient are lower. In the pushover analysis of the numerical model with $0.5x G_{c,ref}$ the maximum seismic coefficient decreases about 3% and 7% in the transversal and longitudinal direction, respectively. In the numerical model with $2.0x G_{c,ref}$ the maximum seismic coefficient increases 13% and 1% in the transversal and longitudinal direction, respectively (Figure 5.23). Here, the major differences are related to the deformation of the structure. For the same seismic post-peak coefficient the structure presents higher displacement at the top increasing the compressive fracture energy, i.e. the response becomes more ductile as expected. The response is more ductile in the transversal direction, as it is associated to the progressive damage at the spandrels and piers of the facades. On the other hand, in the longitudinal direction the response is more brittle and the collapse is associated to the vertical cracks near the corners and shear failure of the gable walls (see Annex D).

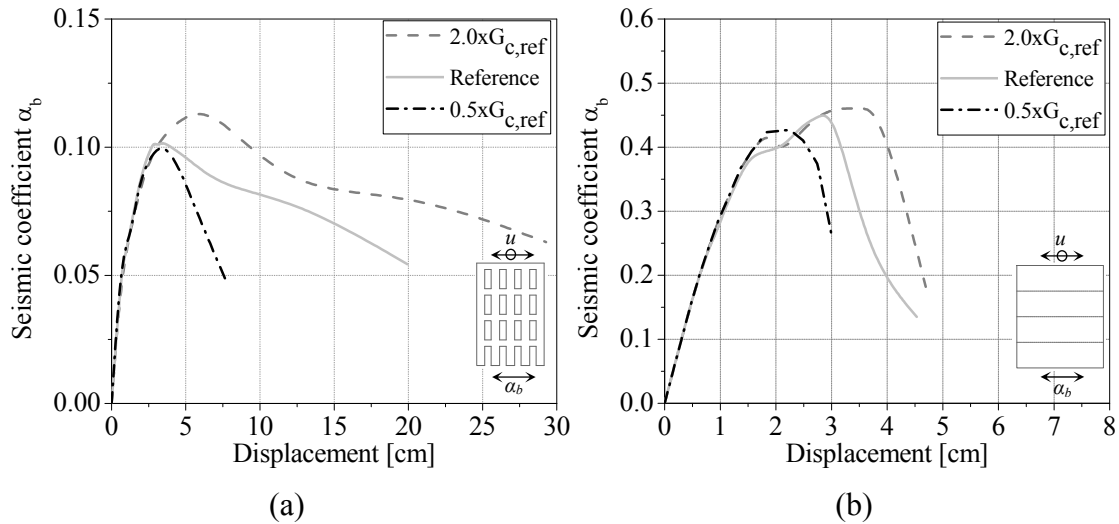


Figure 5.23 – Capacity curves varying the compressive fracture energy in the: (a) transversal direction; (b) longitudinal direction.

5.4.4 Tensile non-linear properties of the masonry

The pushover analysis when varying the tensile strength present variations of the maximum seismic coefficient of about -2% and 11% in the transversal direction for the numerical model with $0.5x f_{t,ref}$ and $2.0x f_{t,ref}$, respectively, with respect to the reference model (Figure 5.24a). In the longitudinal direction the variation of the seismic coefficient decreases about 20% and increase about 8% for the model with $0.5x f_{t,ref}$ and $2.0x f_{t,ref}$, respectively (Figure 5.24b). In general, the variations of the strength capacity are more sensitive to the compressive strength for the building under analysis.

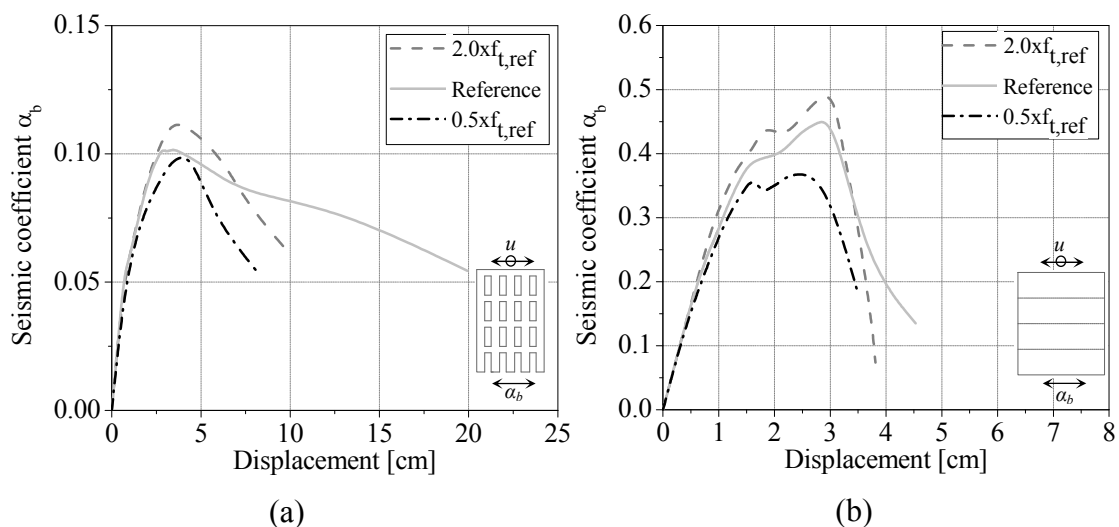


Figure 5.24 – Capacity curves varying the tensile strength in the: (a) transversal direction; (b) longitudinal direction.

The numerical model with $0.5x_{f_{t,ref}}$ presents serious damage at the spandrels of the facades and in the gable walls. The gable walls present a vertical crack near the corners and two diagonal cracks that start at the top of the structure and propagate towards the base (Figure 5.25a). In the numerical model with $2.0x_{f_{t,ref}}$ the gable walls present different crack pattern, in which the damage at the base and the diagonal cracks that start from the base are highlighted (Figure 5.25b). It is noted that increasing tensile strength, means that the ultimate strain decreases, and vice versa.

In the pushover analysis when varying the tensile fracture energy, the maximum seismic coefficient decreases 6% for the numerical model with $0.5x_{G_{t,ref}}$ in both direction. The maximum seismic coefficient of the numerical model with $2.0x_{G_{t,ref}}$ increases about 8% and 11% in the transversal and longitudinal direction, respectively (Figure 5.26).

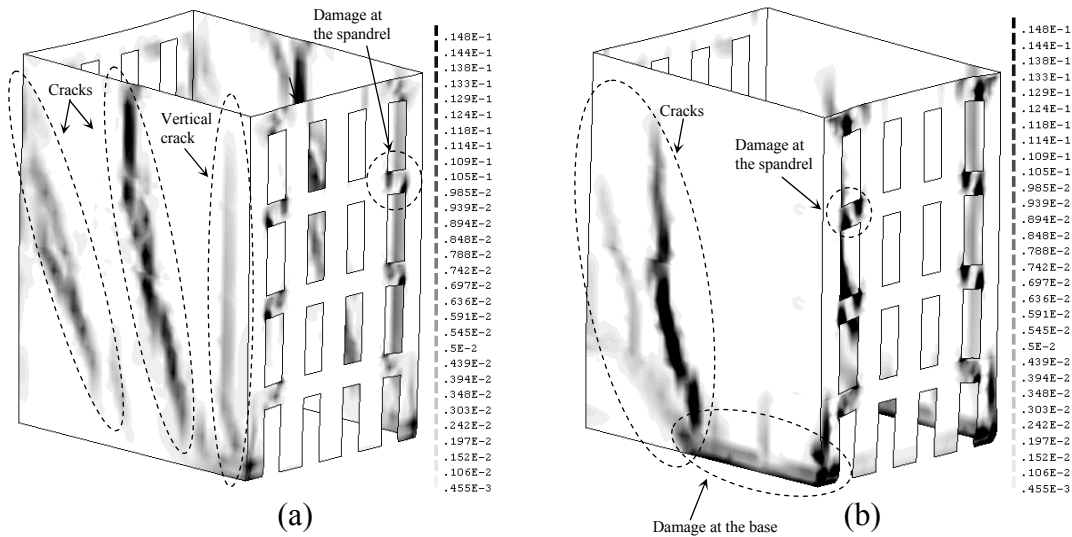


Figure 5.25 – Maximum tensile principal strains at the external surface, obtained from the pushover analysis in the longitudinal direction, varying the tensile strength: (a) $0.5x_{f_{t,ref}}$; (b) $2.0x_{f_{t,ref}}$.

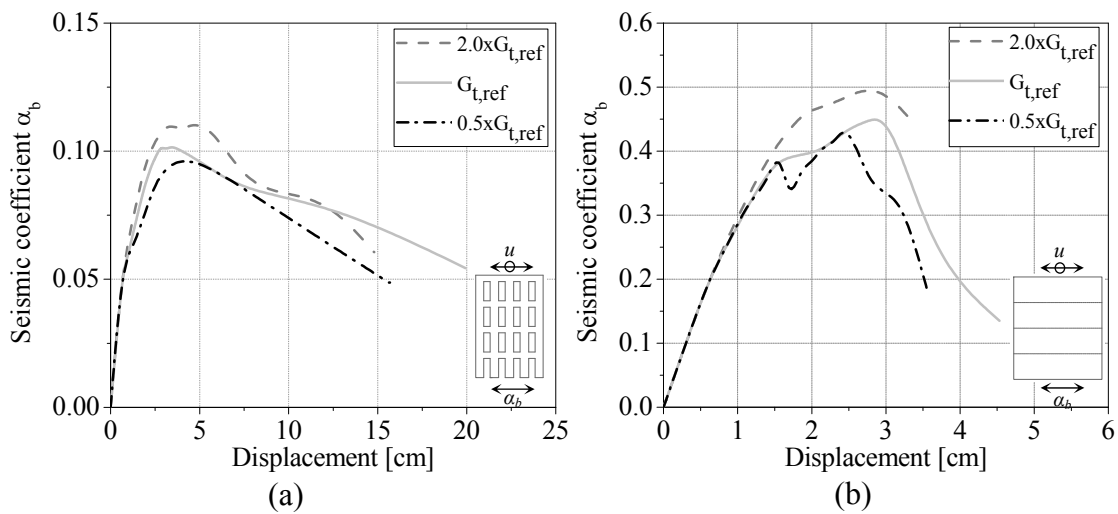


Figure 5.26 – Capacity curves varying the tensile fracture energy in the: (a) transversal direction; (b) longitudinal direction.

5.4.5 Pushover analysis proportional to the first mode

In the pushover analysis proportional to the first mode, the horizontal forces proportional to the mass were replaced by the modal displacements of the first mode in the direction of application. Here, the objective is to evaluate the response of the structure as function of the incremental action based on displacements, which takes into account the relationship between the distribution of mass and stiffness of the first mode of each horizontal direction.

The pushover analysis proportional to the first mode in the transversal direction presents a decrease of the maximum seismic coefficient of about 12% with respect to the reference model (Figure 5.27a). In the longitudinal direction the response is rather different from the one of the reference model and the maximum seismic coefficient presents a decrease of about 27% (Figure 5.27b). The response of the pushover analysis proportional to the first mode in the longitudinal direction is considerably more ductile than the response of the reference model, presenting nearly the double of the deformation for the same seismic coefficient.

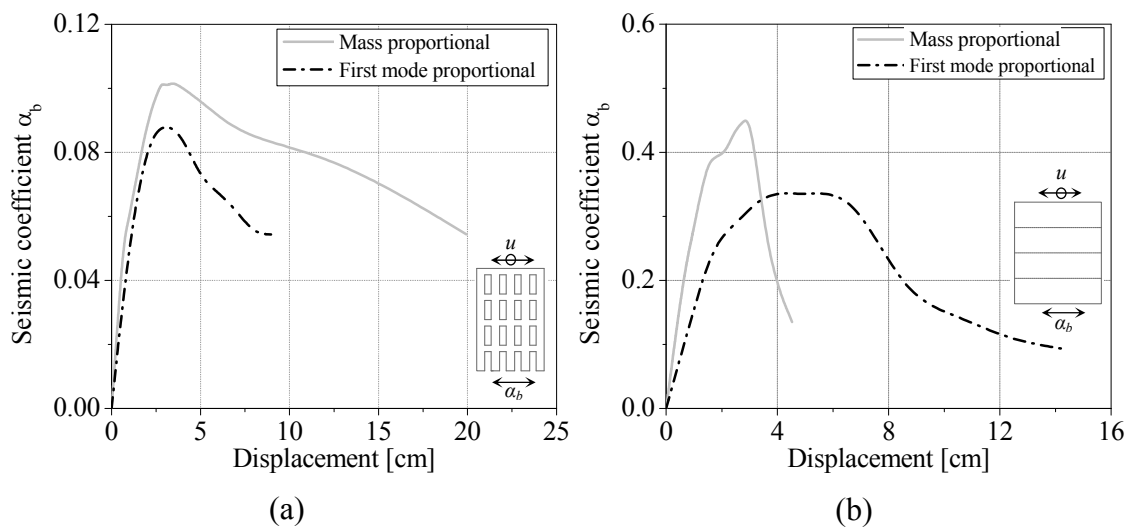


Figure 5.27 – Capacity curves of the pushover analysis proportional to the first mode in the: (a) transversal direction; (b) longitudinal direction.

The damage also presents significant differences with respect to the reference model. In the pushover analysis proportional to first mode in the transversal direction the structure presents damage at the piers of the two top floors, diagonal cracks at the spandrels of the facades and severe vertical cracks at the middle of the gable walls (Figure 5.28a). The vertical cracks are related to out-of-plane bending of the gable walls. It is noted that in the pushover analysis of the reference model in the transversal direction the damage occurs at the spandrels of the facades (Figure 5.3a). In the pushover analysis proportional to the first mode in the longitudinal direction, the gable walls present several diagonal cracks, damage at the base with damage concentration at the corners

and the facades presents damage at the spandrels, mainly at the middle (Figure 5.28b). This crack pattern is not according to the damage obtained in the pushover analysis of the reference model, in which the gable walls present shear cracks and vertical cracks near the corners that may lead to the out-of-plane collapse of the facades (Figure 5.3b).

In conclusion, the pushover analysis with incrementing displacements proportional to the mode shape of the first mode in each direction lead to lower capacity strength in comparison to the pushover analysis proportional to the mass, and the collapse mechanism is not according to the damage obtained from the non-linear dynamic analysis with time integration, mainly in the transversal direction (direction with lower seismic coefficient). For more examples of pushover analyses with different load and displacement patterns in masonry structures see Mendes and Lourenço (2009) and Peña et al. (2010).

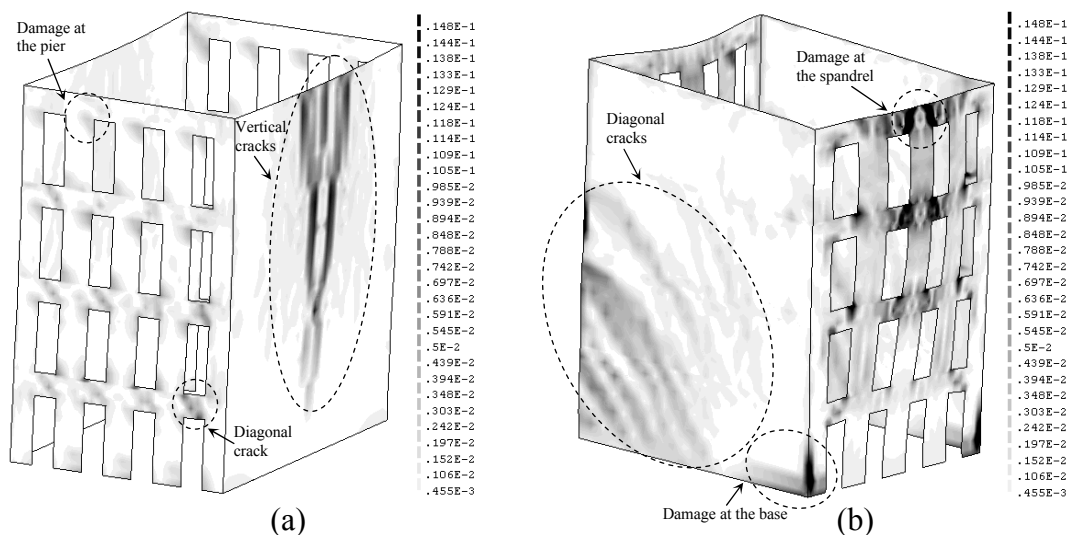


Figure 5.28 – Maximum tensile principal strains at the external surface, obtained from the pushover analysis proportional to the mode shape of the first mode in the: (a) transversal direction; (b) longitudinal direction.

5.5 Conclusions

In this chapter the sensitivity of the response to variations of the properties of the numerical model was evaluated with respect to the reference model. Here, two types of structural analysis were considered – non-linear dynamic analysis with time integration and pushover analysis proportional to the mass. The Young's modulus of the masonry walls, Young's modulus of the timber floors, the compressive and tensile non-linear properties (strength and fracture energy) were the parameters varied in both types of analysis. Furthermore, in the dynamic analysis the influence of the variation of the viscous damping and of the vertical component of the earthquake were also evaluated.

Finally, a pushover analysis proportional to the modal displacement of the first mode in each direction was also carried out.

The results of the non-linear dynamic analysis with time integration of the reference model with the Earthquake 100% shows that the structure reaches its force capacity in the transversal direction for a seismic coefficient equal to 0.10, which is according to the results obtained from the pushover analysis in the transversal direction. However, in the Earthquake 100% the deformation is moderate and the seismic amplitude was increased three times (Earthquake 300%) for the sensitivity analysis through non-linear dynamic analysis, aiming at exploring the deformation capacity of the structure and at clearly identifying the collapse mechanisms. In the analysis with the Earthquake 300% the structure presents serious damage at the spandrels due to diagonal cracking and at the piers of the top floors due to the in-plane rocking and out-of-plane bending, indicating that collapse has been found. Furthermore, the piers of the first floor also present serious damage associated to the failure of the spandrels due to the in-plane forces. The gable walls presents shear cracks, a vertical crack at the top and local damage at the connections between masonry wall and timber floor of the first floor. The pushover analysis in the transversal direction is able to simulate the damage at the facades caused by in-plane forces, namely the damage at the spandrels and at the piers.

The sensitivity analysis carried out through non-linear dynamic analysis with time integration shows that the Young's modulus of the masonry walls, the Young's modulus of the timber floors and the compressive non-linear properties are the parameters that most influence the seismic performance of the structure. The range of variation of the maximum seismic coefficient assuming 0.50 GPa as lower limit (very poor ancient masonry) and 2.00 GPa as upper limit for the Young's modulus of the masonry walls is about 54% of the reference value. The stiffness of the floors has also an important role on the seismic performance of the structure. The numerical model with very flexible floor presents the typical out-of-plane collapse of the facades with portion of the gable walls and damage at the corners. On the other hand, when increasing the stiffness of the floors the damage concentrates at the facades and the gable walls do not present serious damage. Furthermore, the damage is mainly associated to the in-plane forces. Thus, the connections between floors and masonry walls, and the timber floors with stiffness that allows the transference of inertial forces between orthogonal walls, are fundamental to prevent the out-of-plane collapse mechanism and to improve the seismic performance of the "gaioleiro" buildings. It is expected that the variation of compressive non-linear properties has limited influence in the response of masonry structures, but here a relevant influence in the strength capacity of the structure has been found. This aspect is related to the low reference value of the compressive strength (1.00 MPa - ancient masonry), the range of the adopted values (0.50 MPa to 2.00 MPa) and the type of failure mode obtained. It is noted that the maximum compressive stress due to the self-weight is about 20% of the compressive strength, which would seem reasonable for the stability against vertical loading. The vertical component of the earthquake does not

have influence on the response, which is due to the dimensions of the structure and high compressive stresses present, minimizing the effect of the vertical acceleration. Furthermore, the structure is very stiff in the vertical direction and, consequently, presented very small deformation in this direction. Finally, the increment of the damping ratio presents a significant decrease of the displacement at the top of the structure. Tables 5.6 and 5.7 present the variation of the maximum seismic coefficient and displacement at the top of the structure obtained from the non-linear dynamic parametric analysis for the transversal direction (direction with the lowest strength capacity).

Table 5.6 – Variation of the response in the transversal direction obtained from the non-linear dynamic parametric analysis for the lower limits of the parameters.

	$0.5x E_{walls,ref}$	$0.1x E_{floors,ref}$	$0.5x f_{c,ref}$	$0.5x G_{c,ref}$	$0.5x f_{t,ref}$	$0.5x G_{t,ref}$	$\zeta=2\%$
Seismic coefficient	-10%	10%	-20%	0%	-2%	10%	0%
Displacement	-7%	24%	-16%	-11%	4%	-1%	0%

Table 5.7 – Variation of the response in the transversal direction obtained from the non-linear dynamic parametric analysis for the upper limits of the parameters and earthquake vertical component.

	$2.0x E_{walls,ref}$	$10x E_{floors,ref}$	$2.0x f_{c,ref}$	$2.0x G_{c,ref}$	$2.0x f_{t,ref}$	$2.0x G_{t,ref}$	$\zeta=5\%$	Vertical earthquake
Seismic coefficient	39%	20%	70%	20%	20%	10%	10%	10%
Displacement	-17%	-6%	3%	3%	0%	-4%	-17%	-3%

The sensitivity analysis based on the pushover proportional to the mass shows that the Young's modulus of the masonry walls, the stiffness of the timber floors and the compressive strength are the properties that present the highest influence on the strength capacity of the structure. Furthermore, the decrease of the tensile strength causes a significant decrease of the strength capacity in the longitudinal direction (-20%). In the pushover analysis in the transversal direction (direction with the lowest strength capacity) the damage is caused by in-plane forces and is similar to the one obtained from the non-linear dynamic analysis, in which severe damage at the spandrels and piers is found. Finally, the pushover analysis proportional to the modal displacements of the first mode presents lower strength capacity with respect to the pushover analysis proportional to mass and does not provide any improvement in the simulation of the local damage at the piers of the top floor caused by the out-of-plane bending. Tables 5.8 and 5.9 present the variations of the maximum seismic coefficient obtained from the pushover parametric analysis for the transversal and longitudinal directions.

Table 5.8 – Variation of the maximum seismic coefficient obtained from the pushover parametric analysis for the lower limits of the parameters.

Direction	$0.5x E_{walls,ref}$	$0.1x E_{floors,ref}$	$0.5x f_{c,ref}$	$0.5x G_{c,ref}$	$0.5x f_{t,ref}$	$0.5x G_{t,ref}$
Transversal	-2%	-10%	-32%	-3%	-2%	-6%
Longitudinal	-9%	-14%	-37%	-7%	-20%	-6%

Table 5.9 – Variation of the maximum seismic coefficient obtained from the pushover parametric analysis for the upper limits of the parameters and pushover analysis proportional to the first mode.

Direction	$2.0x E_{walls,ref}$	$10x E_{floors,ref}$	$2.0x f_{c,ref}$	$2.0x G_{c,ref}$	$2.0x f_{t,ref}$	$2.0x G_{t,ref}$	1 st Mode
Transversal	25%	11%	34%	13%	11%	8%	-12%
Longitudinal	11%	12%	8%	1%	8%	11%	-27%

Conclusions and future work

6.1 Conclusions

This thesis aims at evaluating and improving the seismic behaviour of the building typology that is believed to present the highest seismic vulnerability of the Portuguese housing stock – “gaioleiro” buildings. The main features of this type of buildings are the presence of masonry load-bearing walls and flexible floors. Although the thesis is focused in a Portuguese building typology, this type of buildings is also present in other countries with seismic hazard, as in the Mediterranean region.

The thesis can be divided in two main parts: (a) experimental research; (b) numerical study. In the experimental research, a non-strengthened mock-up representative of the main features of the “gaioleiro” building was built at 1:3 reduced scale and was tested at the shaking table. After the last seismic test the non-strengthened mock-up was repaired, strengthened and tested again. The mock-up was strengthened using steel angles and plates at the floors levels, improving the connections between masonry walls and floors. Furthermore, in the two top floors steel cables were also installed, aiming at improving the transference of the inertial forces among the load-bearing walls. Here, the main objective was to improve the seismic behaviour of “gaioleiro” buildings using simple strengthening techniques that are easily applied in large scale, are economic feasible in comparison to build new buildings, are only slightly intrusive and that were shown to be able to improve the seismic behaviour of similar buildings subjected to earthquakes in the past (Calderoni et al. 2009) [2]. This experimental research provided

an assessment of the seismic performance of “gaioleiro” buildings through tests in the shaking table and a direct comparison (structure with the same properties and geometry) of the efficiency of the strengthening technique adopted. The experimental planning involved seismic tests and dynamic identification tests at the shaking table. The dynamic identification tests aimed at evaluating the decrease of the frequencies of the modes of the mock-ups along the testing, which was used to define a damage indicator and seismic vulnerability curves. In the numerical study, a model of the non-strengthened mock-up was prepared and validated with to the results obtained from the shaking table tests. Furthermore, a real scale numerical model was prepared aiming at discussing the scale effect. Finally, a sensitivity analysis was carried out, aiming at evaluating the variations on the response due to changes in the values of the properties of the model. The sensitivity analysis was carried out for two types of structural analysis, namely: (a) non-linear dynamic analysis with time integration; (b) pushover analysis proportional to the mass of the structure. Next, the main conclusions of each part of the work are presented.

6.1.1 Experimental research

The seismic tests at the shaking table were carried out by imposing accelerograms in the two orthogonal directions with increasing amplitude at the base of the mock-ups. Furthermore, dynamic identification tests before the first and after each seismic test were carried out, aiming at obtaining a damage indicator based on the decrease of the frequencies of the modes. The damage indicator was related to the amplitude of the seismic action applied at the base of the mock-ups, defining thus the seismic vulnerability curves.

The results of the dynamic identification show that after the Earthquake 100%, corresponding to the design spectrum in Lisbon, the strengthened mock-up presents a reduction of the damage indicator, obtained from the frequency of the first mode, of about 46% with respect to the non-strengthened mock-up. This shows that the strengthening technique improved the seismic performance of the structure.

The crack pattern obtained from the seismic shaking table test with Earthquake 100% shows that the non-strengthened mock-up presents a higher damage concentration at the facades, in which almost all spandrels have damage and most piers at the top floor present horizontal cracks related to the in-plane rocking and out-of-plane bending. The gable walls, timber floors and corners do not present any damage. Although collapse was not achieved, it is expected that the non-strengthened mock-up presents a partial or global collapse of facades, common in buildings with flexible floors. The crack pattern of the strengthened mock-up presents damage concentration at the top floors for the seismic tests with the same amplitude, mainly at the facades. Furthermore, the gable walls present diagonal cracks, indicating that part of the out-of-plane inertial forces of the facades were transferred to the in-plane of the gable walls by the strengthening

elements. Several quantitative parameters of measuring the response of the mock-ups were compared. In the Earthquake 100%, the analysis of the quantitative parameters shows that the strengthening technique improved the seismic behaviour of the mock-up, reducing significantly the out-of-plane response of the masonry walls, which remained connected to the lintels at floor levels. Here, a reduction of the average maximum out-of-plane displacement relative to the corners of about 68% at the third floor of the facades is highlighted.

As final conclusions on the experimental research, it is referred that the strengthening technique improved significantly the seismic behaviour of the mock-up, mainly the out-of-plane response of the masonry walls, and it is an effective solution for reducing the seismic vulnerability of the “gaioleiro” buildings. The seismic vulnerability of the “gaioleiro” buildings also depends on the foundation, connection between roof and walls as well as of the partition walls. For examples of strengthening of foundation and connections between roof and walls see e.g. Bothara and Brzev (2011), Costa (2008) and Roque (2002).

6.1.2 Numerical study

The numerical model of the non-strengthened mock-up was prepared at 1:3 reduced scale using a masonry macro-modelling strategy and was validated taking into account the dynamic properties estimated from the dynamic identification tests and the results of the seismic tests at the shaking table. The modal updating of the numerical model presents good results, with an average error of frequency for the five first modes of about 3.6%. The *MAC*, *NMD* and *COMAC* values show that the correlation between the experimental and numerical modal displacements is good in the transversal direction and acceptable in the longitudinal direction. The comparison of the results obtained for the non-linear dynamic analyses and the seismic shaking table tests of the Earthquake 25% (low amplitude) shows that the response of the numerical model is acceptable. In the longitudinal direction the response of numerical model presents larger differences with respect to the experimental results, due to the difficulty in correctly simulating the connections between the facades and timber floors, which possibly requires the inclusion of non-linear effects. For high seismic amplitude (Earthquake 100%) only a qualitative comparison of the damage was carried out. Here, the results show that the numerical model is able to correctly simulate the onset of the collapse mechanisms and the concentration of cracking observed in the seismic shaking table test. Furthermore, the preparation and validation of the numerical model allows concluding the following: (a) complex structures as the one presented are difficult to represent numerically in detail, even if the global response can be adequately replicated; (b) dynamic identification tests should be used with caution in existing masonry structures, as adequate tuning of the model for low level excitation is hardly a guarantee of adequate performance of the model for high seismic inputs.

A real scale numerical model was also prepared and the differences between its response and the response of the reduced model were analysed. In the linear dynamic range the models present the same results. However, in the non-linear dynamic range the responses of the models present some differences, in which the experimental tests with reduced models provide conservative results. For the adopted 1:3 scale the differences are acceptable from an engineering perspective.

A sensitivity analysis using the numerical model at real scale was also carried out. Here, two parametric analysis using different techniques of structural modelling were done, namely: (a) non-linear dynamic analysis with time integration; (b) pushover analysis proportional to the mass. The objective was to evaluate the variation of the response taking into account the deviations in the main features of the numerical model. The Young's modulus of the masonry walls, Young's modulus of the timber floors, the compressive and tensile non-linear properties (strength and fracture energy) were the parameters considered in both type of parametric analysis. Furthermore, in the non-linear dynamic analysis the influence of the variation of the viscous damping and of the vertical component of the earthquake was also evaluated. Finally, a pushover analysis proportional to the modal displacement of the first mode in each direction was carried out. The results of the sensitivity analysis shows that the Young's modulus of the masonry walls, the Young's modulus of the timber floors and the compressive non-linear properties are the parameters that most influence the seismic performance of the structure for both parametric analyses. The vertical component of the earthquake does not have influence on the response of the numerical model, which is related to the dimensions of the structure, high compressive stresses caused by self-weight and high stiffness in the vertical direction. The pushover analysis proportional to the modal displacements of the first mode presents lower strength capacity with respect to the pushover analysis proportional to the mass and does not provide any improvement in terms of failure mode.

Finally, it is concluded that the stiffness of the floors influences significantly the strength capacity and the collapse mechanism of the numerical model. Strengthening timber floors such that they can be considered as rigid diaphragms, with good connection between floors and masonry walls, is a solution to reduce the seismic vulnerability of "gaioleiro" buildings, namely preventing the global collapse of the facades. Here, the strengthening of the floors using timber or steel elements are preferable when compared for example to a solution with concrete slabs, as it allows an increase of the in-plane stiffness of floors without increasing significantly the inertial forces at floor levels. For examples of strengthening of floors with timber or steel elements see e.g. Modena et al. (2009), Valluzzi et al. (2010) and Valluzzi and Modena (2006).

6.2 Future work

This work does not close the issue of assessing and reducing the seismic vulnerability of “gaioleiro” buildings, or similar buildings with masonry load-bearing walls with flexible floors. Further research on the seismic performance of this type of buildings should be conducted. Next, a set of future work is presented:

- Definition of a seismic vulnerability curve for each mock-up considering the contribution of several modes. For this purpose the experimental modal contribution of each mode has to be computed, where the final damage indicator corresponds to the weighting sum of the damage indicators obtained for each mode considered;
- Definition of the experimental capacity curves (seismic coefficient at the base versus displacement at the top of the structure) of the mock-ups. In this task the total horizontal forces can be computed assuming only the sum of the inertial forces at each accelerometer position. The capacity curves are obtained from the maximum seismic coefficient of each seismic shaking table test;
- Preparation of a numerical model of the strengthened mock-up, aiming at validating numerically the efficiency of the strengthening technique adopted;
- Numerical evaluation of different strengthening techniques and conclusion on the best solution to apply to “gaioleiro” buildings;
- The increase of the number of floors, the type of soil, the roof and the different relationship of the dimensions of the piers and spandrels should be also considered in the sensitivity analysis;
- Modern numerical analysis, namely the hybrid frequency time domain analysis, which is a combination of a modal frequency response analysis and a transient non-linear analysis, should be tested for this type of buildings;
- The application of the new versions of pushover analysis, for instance the modal pushover analysis introduced by Chopra and Goel (2002), and the adaptive capacity spectrum method proposed by Casarotti and Pinho (2007), which include the effects of higher modes contribution, should be tested for masonry structures with flexible floors.

References

- Andrade H. (2011). “Characterization of ancient buildings. “Gaioleiro” buildings”. Master Thesis. Nova University of Lisbon, Portugal. (In Portuguese).
- Appleton J. (2003). “Rehabilitation of ancient buildings – Pathologies and intervention technologies”. Orion edition. ISBN: 9728620039. (In Portuguese).
- Appleton J. (2005). “Rehabilitation of “gaioleiros” buildings – a block in Lisbon”. Orion edition. ISBN: 9728620055 (In Portuguese).
- ASTM Standard D2938-95 (2002). “Standard test method for unconfined compressive Strength of Intact Rock Core Specimens”. American Society for Testing and Materials. (doi:10.1520/D2938-95R02)
- ASTM Standard E178-02 (2002). “Standard practice for dealing with outlying observations”. American Society for Testing and Materials. (doi:10.1520/E0178-02)
- ATC-40 (1996). “Seismic evaluation and retrofit of concrete buildings.” Applied Technology Council, California.
- Bairrão R. and Falcão M. (2009). “Shaking table tests of two different reinforcement techniques using polymeric grids on an asymmetric limestone full-scaled structure”. *Engineering Structures*, Volume 31, Issue 6, 1312-1330. (doi:10.1016/j.engstruct.2008.04.039)
- Barbat A. and Pujades L. (2004). “Vulnerability and risk seismic assessment in urban areas. Case study: Barcelona.” 6th National Congress on Seismology and Earthquake Engineering (Sísmica 2004). Guimarães, Portugal, 229-252. (In Spanish)
- Bashir-Ahmed M. and Xiao-zu S. (2004). “S Arc-length technique for nonlinear finite element analysis ”. *Journal of Zhejiang University SCIENCE*, Volume 5, Issue 5, 618-628. (doi:10.1016/j.engstruct.2008.04.039)
- Bendat J. and Piersol A. (2000). “Random data: Analysis and measurement Procedures”. 2nd Edition, John Wiley & Sons.
- Binda L., Pina-Henriques J., Anzani A. and Lourenço P. (2006). “A contribution for the understanding of load-transfer mechanisms in multi-leaf masonry walls: Testing and modeling”. *Engineering Structures*, Volume 28, Issue 8, 1132-1148. (doi:10.1016/j.engstruct.2005.12.004)

- Bothara J. and Brzev S. (2011). "A tutorial: Improving the seismic performance of stone masonry buildings". 1st Edition, Publication number WHE-2011-01, Earthquake Engineering Research Institute, Oakland, California.
- Braga F., Dolce M. and Liberatore D. (1982). "A statistical study on damaged buildings and ensuing review of the MSK76 scale". 7th European Conference on Earthquake Engineering. Athens, Greece, 431-450.
- Branco M. and Guerreiro L. (2011). "Seismic rehabilitation of historical masonry buildings". *Engineering Structures*, Volume 33, Issue 5, 1626-1634. (doi:10.1016/j.engstruct.2011.01.033)
- Brignola A., Podestá S. and Pampanin S. (2008). "In-plane stiffness of wooden floor". New Zealand Society for Earthquake Engineering Conference, paper number 49.
- Bruneau M. (1994) [1]. "Seismic performance of unreinforced masonry buildings – a state-of-art report". *Canadian Journal of Civil Engineering*, Volume 21, Number 3, 512-539. (doi: 10.1139/194-054)
- Bruneau M. (1994) [2]. "State-of-art report on seismic performance of unreinforced masonry buildings". *Journal of Structural Engineering*, Volume 120, Number 1, 230-251. (doi:http://dx.doi.org/10.1061/(ASCE)0733-9445(1994)120:1(230))
- Cabrita A., J. Aguiar J., Appleton J. (1993) "Manual of support rehabilitation of buildings in the "Bairro Alto"". Lisbon City Hall and National Laboratory for Civil Engineering, Portugal. ISBN: 9729583404. (In Portuguese)
- Caetano E. (2000). "Dynamic of cable-stayed bridges: Experimental assessment of cable-structure interaction". PhD Thesis. Engineering Faculty of University of Porto, Portugal.
- Calderini C., Cattari S. and Lagomarsino S. (2009) [1]. "Identification of the shear mechanical parameters of masonry piers from diagonal compression test". 11th Canadian Masonry Symposium, Toronto, Ontario, Canada.
- Calderoni B., Cordasco E., Giubileo C. and Migliaccio L. (2009) [2]. "Preliminary report on damages suffered by masonry buildings in consequence of the L'Aquila earthquake of 6th April 2009". ReLIUS.
- Candeias P. (2008). "Seismic vulnerability assessment of ancient buildings". PhD Thesis. University of Minho, Portugal. (<http://hdl.handle.net/1822/9057>) (In Portuguese)
- Carocci C. (2001). "Guidelines for the safety and preservation of historical centres in seismic areas". *Historical Constructions: Possibilities of numerical and experimental techniques*. Guimarães, Portugal, 145-166.
- Carvalho A. (2007). "Stochastic modelling of the seismic action in Mainland Portugal". PhD Thesis. Technical University of Lisbon, Portugal. (In Portuguese).

- Carvalho E. (1998). "Seismic testing of structures". 11th European Conference on Earthquake, Paris, France. Rotterdam: AA Balkema, 53-64.
- Casarotti C. and Pinho R. (2007). "An adaptive capacity spectrum method for assessment of bridges to earthquake action". *Bulletin of Earthquake Engineering*, Volume 5, Issue 3, 337-390. (doi:10.1007/s10518-007-9031-8)
- Census (1991). "General census of population and housing". Statistics Portugal. (In Portuguese)
- Cervera M., Oliver J. and Faria R. (1995). "Seismic evaluation of concrete dams via continuum damage models". *Earthquake Engineering & Structural Dynamics*, Volume 24, Issue 9, 1225-1245. (doi: 10.1002/eqe.4290240905)
- Chopra A. (2001). "Dynamics of Structures: Theory and applications to earthquake engineering". 3rd Edition, Prentice Hall.
- Chopra A. and Goel R. (2002). "A modal pushover analysis procedure for estimating seismic demands for buildings". *Earthquake Engineering and Structural Dynamics*, Volume 31, Issue 3, 561-582. (doi:10.1002/eqe.144)
- Coelho E., Campos-Costa A., Sousa M. and Carvalho E. (1999). "Assessment of the vulnerability of the structures and seismic tests". 4th National Congress on Seismology and Earthquake Engineering, Faro, Portugal. (In Portuguese)
- Coelho E. and Carvalhal F. (2005). "Seismic tests – Facilities of LNEC". *Engenharia e Vida*, nº10, 51- 55. (In Portuguese)
- Corsanego A. and Gavarini C. (1993). "Ten years of research into the seismic vulnerability of constructions in Italy", 149-156. (<http://hdl.handle.net/2122/3596>)
- Cosenza E. and Manfredi G. (2000). "Damage indices and damage measures". *Progress in Structural Engineering and Materials*, Volume 2, Issue 2, 50-59. (doi:10.1002/(SICI)1528-2716(200001/03)2:1<50::AID-PSE7>3.0.CO;2-S)
- Costa A. (2008). "Repair and reinforcement of buildings". *Earthquakes and Buildings*. 1st Edition, Orion Editions, Editorial manager: Mário Lopes, Chapter 11, 469-529. (In Portuguese)
- Damjamic F. and Owen D. (1984). "Practical considerations for modelling of post-cracking concrete behaviour for finite element analysis of reinforced concrete structures". *International Conference on Computer Aided Analysis and Design of Concrete Structures*, 693-706.
- D'Ayala D. and Speranza E. (2002). "An integrated procedure for the assessment of seismic vulnerability of historic buildings". 12th European Conference on Earthquake Engineering. London, United Kingdom, paper 561.

- Dazio A. and Beyer K. (2010). "Seismic behaviour of different types of masonry spandrels". 14th European Conference on Earthquake Engineering. Ohrid, Republic of Macedonia, paper 468.
- Degée H., Denoël V., Candeias P., Campos-Costa A. and Coelho E. (2007). "Experimental investigation on the seismic behaviour of North European masonry houses". 7th National Congress on Seismology and Earthquake Engineering (Sísmica 2007), Porto, Portugal. (In Portuguese)
- Douglas B. and Reid W. (1982). "Dynamic tests and system identification of bridges". Journal of the Structural Division, Volume 108, Number 10, 2295-2312.
- EN 1996-1-1 (2005). "Eurocode 6: Design of masonry structures – Part 1-1: General rules for reinforced and unreinforced masonry structures". European Committee for Standardization.
- EN 1998-1 (2004). "Eurocode 8: Design of structures for earthquake resistance – General rules, seismic actions and rules for building". European Committee for Standardization.
- ENDEVCO (2010). <http://www.endevco.com>
- Ewing R., Johnson A. and Kariotis J. (1981). "Methodology for mitigation of seismic hazards in existing unreinforced masonry buildings (ABK methodology): diaphragm testing". ABK-TR-03, ABK, El Segundo, California.
- Ewins D. (2000). "Modal testing: theory, practice and application". 2nd Edition, Research Studies Press LTD, Baldock, Hertfordshire, England.
- Faria R. (1994). "Evaluation of the seismic behaviour of concrete dams via continuum damage model". PhD Thesis. Engineering Faculty of University of Porto, Portugal. (In Portuguese)
- FEMA 306 (1998). "Evaluation of earthquake damaged concrete and masonry wall buildings". Applied Technology Council (ATC-43 Project). The Partnership for Response and Recovery, Federal Emergency Management Agency, Washington D.C.
- FEMA 440 (2005). "Improvement of nonlinear static seismic analysis procedures". Applied Technology Council (ATC-55 Project). Department of Homeland Security, Federal Emergency Management Agency, Washington D.C.
- Figueiras J. (1983). "Ultimate load analysis of anisotropic and reinforced concrete plates and shells". PhD Thesis. University of Wales.
- Frocht M. (1931). "Recent advances in photoelasticity: And an investigation of the stress distribution in square blocks subjected to diagonal compression". American Society of Mechanical Engineers, 135-153.

- Gelfi P. (2006). "SIMQKE_GR – Software for generating artificial accelerograms compatible with the response spectrum". University of Brescia, Italy. Available from: http://dicata.ing.unibs.it/gelfi/software/programmi_studenti
- Gentile C. and Cabrera F. (2001). "Dynamic assessment of a curved cable-stayed bridge at the Malpensa 2000 Airport, Milan, Italy". *Structural Engineering International*, Volume 11, Number 1, 52–58.
- Gentile C. and Saisi A. (2004). "Dynamic-based F.E. model updating to evaluate damage in masonry towers". 4th International Seminar on Structural analysis of Historical Constructions, Padova, Italy, Volume 1, 439-449.
- Giovinazzi S. (2005). "The vulnerability assessment and the damage scenario in seismic risk analysis." PhD Thesis, Technical University Carolo-Wilhelmina, Braunschweig, and University of Florence, Italy.
- Giovinazzi S. and Lagomarsino S. (2003). "Seismic risk analysis: A method for the vulnerability assessment of built-up areas." European Safety and Reliability International Conference. Maastricht, Netherlands.
- Griffith M., Vaculik J., Lam N., Wilson J. and Lumantarna E. (2007). "Cyclic testing of unreinforced masonry walls in two-way bending". *Earthquake Engineering and Structural Dynamics*, Volume 36, Issue 6, 801-821. (doi:10.1002/eqe.654)
- Grünthal G. (1998). "European Macroseismic Scale 1998: EMS-98". European Seismological Commission, Subcommittee on Engineering Seismology, Working Group Macroseismic Scales, Volume 15.
- Gulkan P., Aschheim M. and Spence R. (2002). "Reinforced concrete frame buildings with masonry infills." *World Housing Encyclopedia*, Housing report: 64. Available from: www.world-housing.net.
- Hough S. and Bilham R. (2006). "After the earth quakes – Elastic rebound on an urban planet". Oxford University Press, Inc.
- Hutton D. (2004). "Fundamentals of finite element analysis". 1st Edition, McGraw-Hill, New York.
- Ingham J., Biggs D. and Moon L. (2011). "How did unreinforced masonry buildings perform in the February 2011 Christchurch earthquake?". *The Structural Engineer* Volume 89, Issue 6, 14-18.
- International Correspondence Schools (2008). "A Treatise on architecture and building construction V3: Prepared for students of the international correspondence schools (1899)". Kessinger.
- Kramer S. (1996). "Geotechnical earthquake engineering". Prentice-Hall International Series in Civil Engineering and Engineering Mechanics.

- Lagomarsino S. (2012). “Seismic performance of masonry buildings after the 2009 L’Aquila earthquake”. Learning from the past to protect the future. 2012 EERI Annual Meeting & National Earthquake Conference, United States of America.
- Lemaitre J. and Desmorat R. (2005). “Engineering damage mechanics: Ductile, creep, fatigue and brittle failures”. Springer.
- Lindt J., Pryor S. and Pei S. (2011). “Shake table testing of a full-scale seven-story steel–wood apartment building”. *Earthquake Structures*, Volume 33, Issue 3, 757-766. (doi:10.1016/j.engstruct.2010.11.031)
- LNEC (2010). <http://www.lnec.pt/organizacao/de/nesde>
- Lourenço P.B. (1996). “Computational strategies for masonry structures”. PhD Thesis. Delft University of Technology, Netherlands. Available from: <http://www.civil.uminho.pt/masonry>
- Lourenço P.B. (2008). “Modelling of masonry and homogenization”. Slides of the Advanced Master in Structural Analysis of Monuments and Historical Constructions.
- Lourenço P.B., Mendes N., Ramos L. and Oliveira D. (2011). “Analysis of masonry structures without box behaviour”. *International Journal of Architectural Heritage*, Volume 5, Issue 4-5, 369-382. (doi:10.1080/15583058.2010.528824)
- Lu M., Schultz A. and Stolarski H. (2005). “Application of the arc-length method for the stability of solid unreinforced masonry walls under lateral loads”. *Engineering Structures*, Volume 27, Issue 6, 909-919. (doi:10.1016/j.engstruct.2004.11.018)
- NP EN 196-1 (1996). “Methods of testing cement - Part 1: Determination of strength”. Portuguese standard of the EN 196-1, European Committee for Standardization, Portuguese Institute for Quality. (In Portuguese)
- Magenes G., Bolognini D. and Braggio C. (2000). “Simplified methods for non-linear seismic of masonry buildings”. National Group for Earthquakes Protection (GNDT). (In Italian)
- Magenes G. and Calvi G. (1997). “In-plane seismic response of brick masonry walls”. *Earthquake Engineering and Structural Dynamics*, Volume 26, Issue 11, 1091-1112. (doi:10.1002/(SICI)1096-9845(199711)26:11<1091::AID-EQE693>3.0.CO;2-6).
- Maia N. and Silva J. (1997). “Theoretical and experimental modal analysis”. Research Studies Press LTD, England.
- Mascarenhas J. (2003). “Construction systems - III: Walls and basic materials”. *Livros Horizonte, Técnicas de Construção*. (In Portuguese)
- MATLAB (2006). “MATLAB: The language of technical computing”. The MathWorks, Release 7.2, USA.

- Mendes L. (2008). “LNEC-SPA: Signal Processing and Analysis Tools for Civil Engineers”. Earthquake Engineering and Structural Dynamics Division, National Laboratory for Civil Engineering, Lisbon, Portugal.
- Mendes N. and Lourenço P.B. (2009). “Seismic assessment of masonry “gaioleiro” buildings in Lisbon, Portugal”. *Journal of Earthquake Engineering*, Volume 14, Issue 1, 80-101. (doi:10.1080/13632460902977474)
- Mendes N., Lourenço P.B. and Campos-Costa A. (2010) [1]. “Characterization tests of the dynamic properties of a masonry mock-up”. 8th National Congress of Experimental Mechanics. (<http://hdl.handle.net/1822/17630>) (In Portuguese)
- Mendes N., Lourenço P.B. and Campos-Costa A. (2010) [2]. “Shaking table tests of stone masonry buildings”. *Structural Faults & Repair 2010*, 13th International Conference, Edinburgh, Scotland. (<http://hdl.handle.net/1822/19037>)
- Moaveni B., He X., Conte J. and Restrepo J. (2010). “Damage identification study of a seven-story full-scale building slice tested on the UCSD-NEES shake table”. *Structural Safety*, Volume 32, Issue 5, 397-409. (doi:10.1016/j.strusafe.2010.03.006)
- Modena C., Casarin F., Porto F., Garbin E., Mazzon N. Munari M., Panizza M. and Valluzzi M. (2009). “Structural interventions on historical masonry buildings: Review of Eurocode 8 provisions in the light of Italian experience”. *Eurocode 8 Perspectives from the Italian Standpoint Workshop*, Napoli, Italy, 225-236.
- Oliveira D. (2003). “Experimental and numerical analysis of block masonry structures under cyclic loading”. PhD Thesis. University of Minho, Portugal. Available from: www.civil.uminho.pt/masonry
- Oliveira C., Cabrita A. (1985). “Typification of the housing stock of Lisbon – Introductory document of the theme”. 1st Meeting on Conservation and Rehabilitation of housing buildings, National Laboratory for Civil Engineering, Lisbon, Portugal. (In Portuguese).
- OPCM 3274 (2003). “First elements on general criteria for seismic classification of the national territory and technical standards for construction in seismic areas”. Ordinance of the President of the Council of Ministers. (In Italian)
- Palacios S. (2004). “State of the art in seismic vulnerability.” Institutional repository of Alicante University. (<http://hdl.handle.net/10045/2626>)
- Paquette J. and Bruneau M. (2006). “Pseudo-dynamic testing of unreinforced masonry building with flexible diaphragm and comparison with existing procedures”. *Construction and Building Materials*, Volume 20, Issue 4, 220-228. (doi:10.1016/j.conbuildmat.2005.08.025)
- Paulay T. and Priestley M. (1992). “Seismic design of reinforced concrete and masonry buildings”. John Wiley & Sons, Inc.

PCB (2010). <http://www.pcb.com>

Peña F., Lourenço P.B., Mendes N. and Oliveira D. (2010). "Numerical models for seismic assessment of an old masonry tower". *Engineering Structures*, Volume 32, 1466-1478. (doi: 10.1016/j.engstruct.2010.01.027)

Penna A. (2008). "Vulnerability assessment of masonry structures using experimental data and simplified models". Short course and post-earthquake buildings safety and damage assessment, Eucentre, Pavia.

Pinho F. (2000). "Walls from ancient Portuguese buildings." "Edifícios", N°8, National Laboratory for Civil Engineering, Lisbon, Portugal. (In Portuguese).

Pinto A., Pegon P., Magonette G., Molina J., Buchet P. and Tsionis G. (2002). "Pseudodynamic tests on large-scale model of an existing RC bridge using non-linear substructuring and asynchronous motion". Institute for the Protection and Security of the Citizen. European Laboratory for Structural Assessment (ELSA).

Póvoas R. (1991). "Non-linear models of analysis and design". PhD Thesis. Engineering Faculty of University of Porto, Portugal. (In Portuguese)

Ramos L. (2007). "Damage identification on masonry structures based on vibration signatures". PhD Thesis. University of Minho, Portugal. (<http://hdl.handle.net/1822/7380>)

Ramos L. and Lourenço P. (2004). "Advanced numerical analysis of historical centers: A case study in Lisbon." *Engineering Structures*, Volume 26, Issue 9, 1295-1310. (doi:10.1016/j.engstruct.2004.04.008)

Rodrigues J. (2004). "Stochastic modal identification – Analysis methods and applications in civil engineering structures". PhD Thesis. Engineering Faculty of University of Porto, Portugal.

Roque J. (2002). "Structural rehabilitation of ancient masonry walls". Master Thesis. University of Minho, Portugal. (<https://bibliotecadigital.ipb.pt/handle/10198/1724>) (In Portuguese)

SEAOC (1986). "Earthquake hazard mitigation of unreinforced pre-1933 masonry buildings: Construction notes for contractors, building officials, owners/developers, architects, engineers". Structural Engineers Association of Southern California.

Silva V. (2001). "Technical feasibility of the national programme for reducing the seismic vulnerability of the building stock". Reducing the Seismic Vulnerability of the Building Stock. Lisbon, Portugal.

Silva V. and Soares I. (1997). "Seismic vulnerability of the "gaioleiros" buildings of Lisbon and possible measures to reduce it". 3rd Meeting on Seismology and Seismic Engineering. Technical University of Lisbon, Portugal. (In Portuguese)

- Sonin A. (2001). "The physical basis of dimensional analysis". 2nd Edition, Department of Mechanical Engineering, Massachusetts Institute of Technology (MIT), Cambridge.
- Sousa M. (2006). "Seismic risk in Mainland Portugal." PhD Thesis. Technical University of Lisbon, Portugal. (In Portuguese).
- Teughels A. (2004). "Inverse modelling of civil engineering structures based on operational modal data". PhD Thesis. Catholic University of Leuven, Belgium.
- TNO (2009). "DISplacement method ANALyser". User's Manual, Release 9.4, Netherlands.
- Tomažević M. (1999). "Earthquake-resistance design of masonry buildings". Series on Innovation in Structures and Construction, Volume 1, Imperial College Press.
- Tomažević M. (2000). "Some aspects of experimental testing of seismic behaviour of masonry walls and models of masonry buildings". Journal of Earthquake Technology, Volume 37, No. 4, 101-117.
- Tomažević M., Lutman P. and Weiss P. (1996). "Seismic upgrading of old brick-masonry urban houses: Tying of walls with steel ties". Earthquake Spectra, Volume 12, No. 3, 599-622.
- Toumbakari E. (2002). "Lime-pozzolan-cement grouts and their structural effects on composite masonry walls". PhD Thesis, Katholieke Universiteit Leuven, Belgium.
- USGS (2012). "U. S. Geological Survey: Science for a changing the world". Available from: www.usgs.gov/default.asp
- Valluzzi M., Porto F. and Modena C. (2004). "Behaviour and modelling of strengthened three-leaf stone masonry walls". Materials and Structures, Volume 37, No. 3, 184-192. (doi:10.1007/BF02481618)
- Valluzzi R. and Modena C. (2006). "Mechanical behaviour of masonry structures strengthened with different improvement techniques". Fracture and Failure of Natural Building Stones, Part I, Chapter 3.2, 137-156. (doi: 10.1007/978-1-4020-5077-0_9)
- Valluzzi R., Garbin E., Benetta M. and Modena C. (2010). "In-plane strengthened of timber floors for the seismic improvement of masonry buildings". 11th World Conference on Timber Engineering, Trentino, Italy, paper 241.
- Vasconcelos G. (2005). "Experimental investigations on the mechanics of stone masonry: Characterization of granites and behaviour of ancient masonry shear walls". PhD Thesis. University of Minho, Portugal. Available from: www.civil.uminho.pt/masonry
- Vecchio F. (1981). "The response of reinforced concrete to in-plane shear and normal stresses". PhD Thesis, University of Toronto.

Viviane W. (2007). "Mitigation of pounding between adjacent buildings in earthquake situations". LESSLOSS final workshop, Sub-project 7 - Vulnerability reduction in structures.

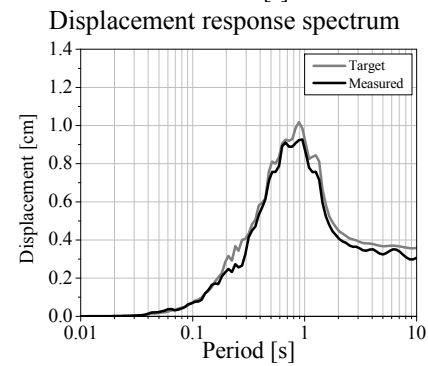
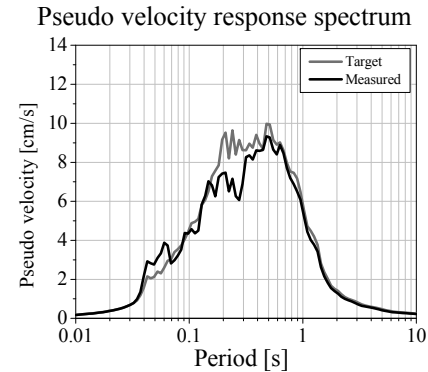
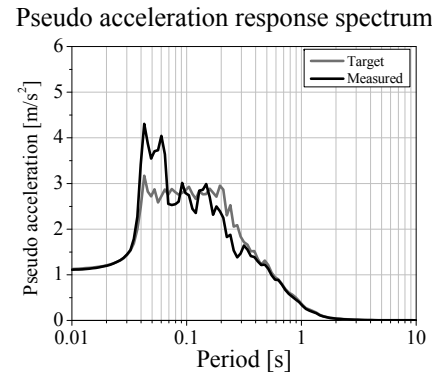
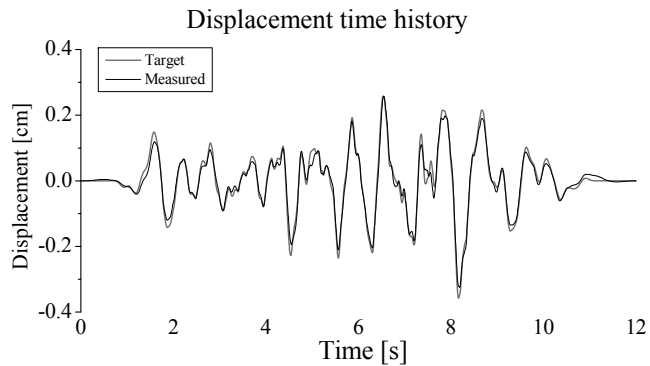
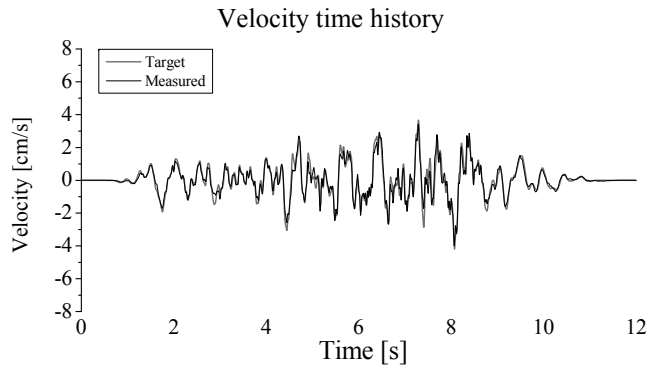
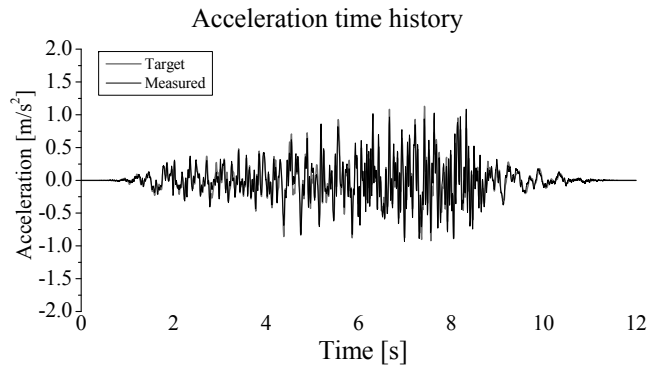
Yi T. (2004). "Experimental investigations and numerical simulation of an unreinforced Masonry structure with flexible diaphragms". PhD Thesis. Georgia Institute of Technology.

Zienkiewicz O. and Taylor R. (2000). "The finite element method". 5th Edition, Bitterworth-Heinemann, Oxford.

Annex A

Input signals

A.1 Transversal input signal of the non-strengthened mock-up: Earthquake 25%

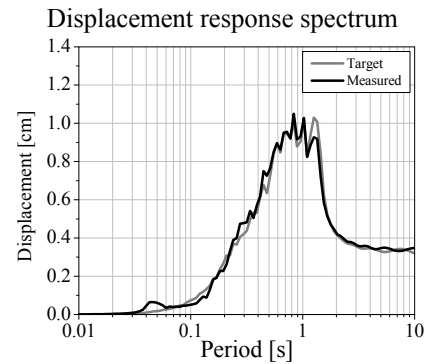
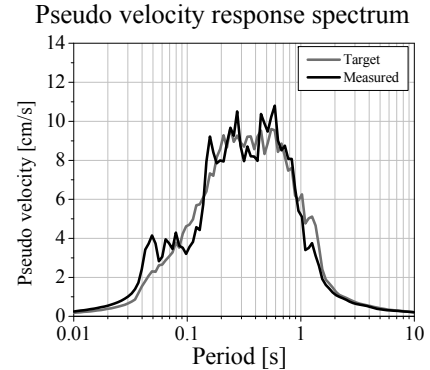
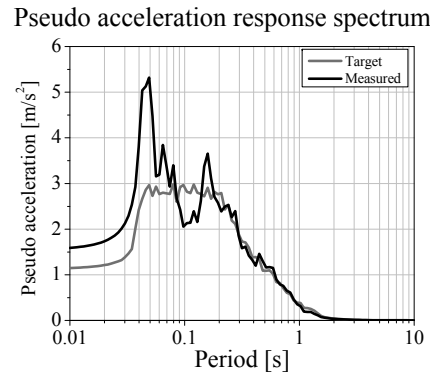
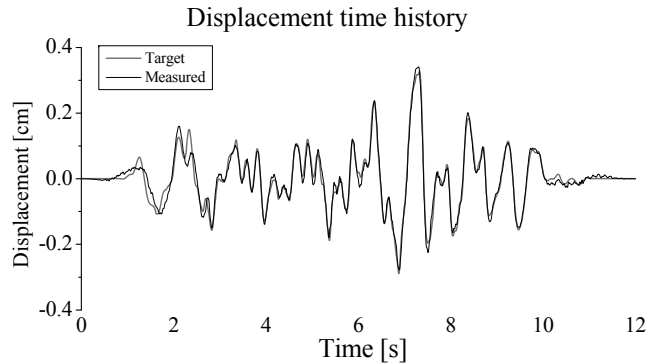
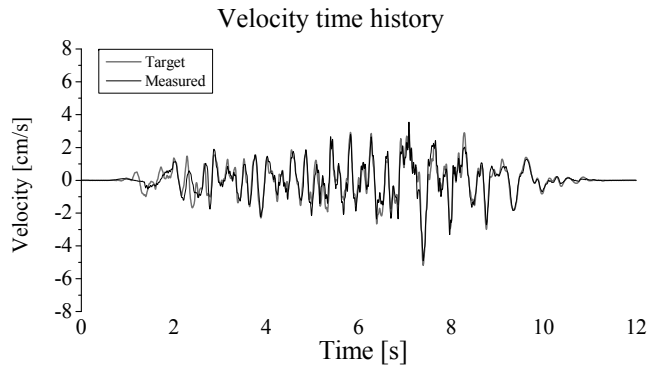
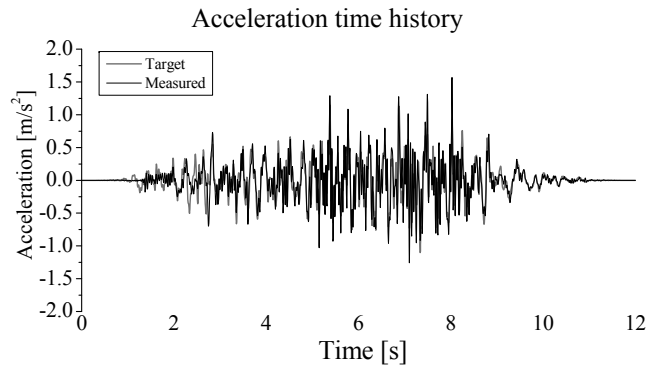


Parameter	Target	Measured	Variation [%]
PGA [m/s^2]	1.129	1.083	-4.1
PGV [cm/s]	4.187	3.986	-4.8
PGD [cm]	0.358	0.325	-9.2
PGV/PGA [s^{-1}]	0.037	0.037	-0.8
PGD/PGA [s^{-2}]	0.003	0.003	-5.3
IA [m/s]	0.117	0.119	1.3
E [$kg\ m^2/s^2$]	416	396	-4.9
CAV [m/s]	1.906	1.901	-0.3
SED [m^2/s]	0.001	0.001	-14.6
RMS_A [m/s^2]	0.247	0.248	0.6
RMS_V [cm/s]	0.993	0.917	-7.6
RMS_D [cm]	0.092	0.085	-7.3

PGA	Peak Ground Acceleration
PGV	Peak Ground Velocity
PGD	Peak Ground Displacement
IA	Arias Intensity
E	Input Energy
CAV	Cumulative Absolute Velocity
SED	Specific Energy Density
RMS_A	Root Mean Square of Acceleration
RMS_V	Root Mean Square of Velocity
RMS_D	Root Mean Square of Displacement

Filter: Fourier 0.7 – 25 Hz

A.2 Longitudinal input signal of the non-strengthened mock-up: Earthquake 25%

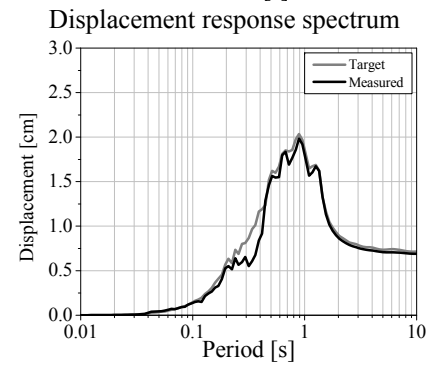
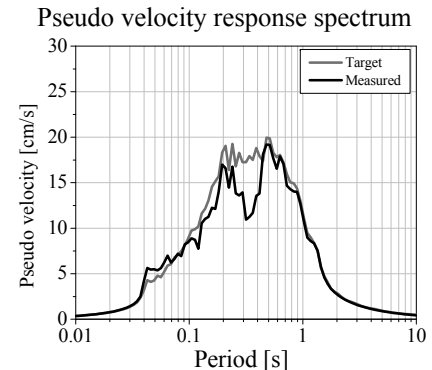
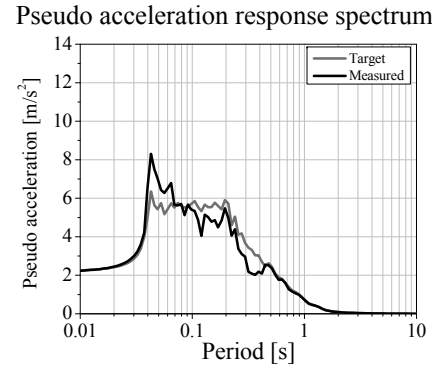
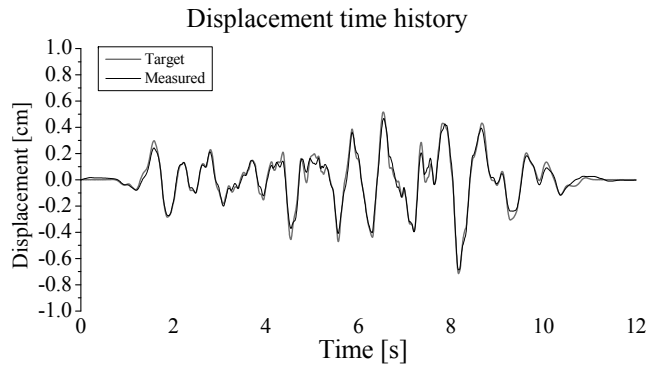
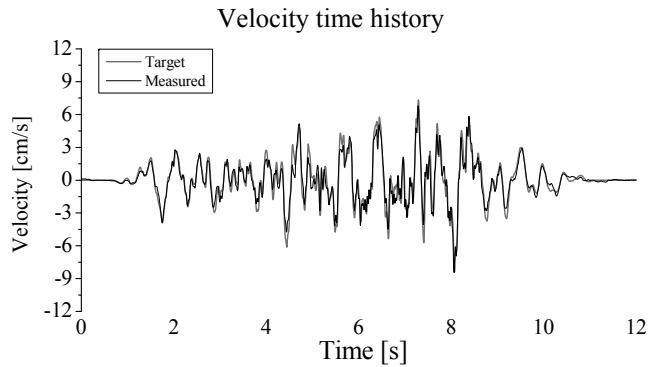
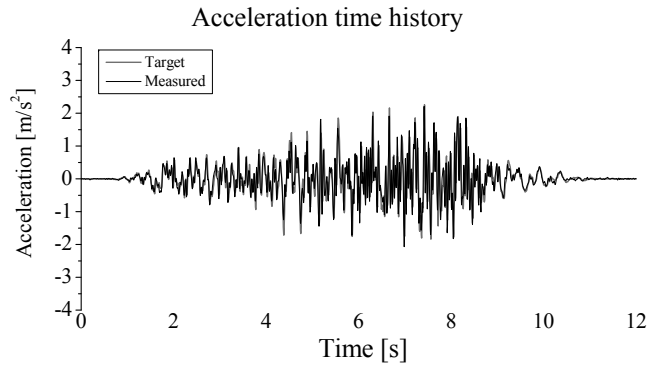


Parameter	Target	Measured	Variation [%]
PGA [m/s^2]	1.149	1.569	36.5
PGV [cm/s]	5.185	4.909	-5.3
PGD [cm]	0.328	0.341	4.1
PGV/PGA [s^{-1}]	0.045	0.031	-30.7
PGD/PGA [s^{-2}]	0.003	0.002	-23.7
IA [m/s]	0.124	0.149	19.8
E [$kg\ m^2/s^2$]	446	467	4.7
CAV [m/s]	2.041	2.081	1.9
SED [m^2/s]	0.001	0.001	-5.5
RMS_A [m/s^2]	0.254	0.278	9.4
RMS_V [cm/s]	1.004	0.976	-2.8
RMS_D [cm]	0.088	0.088	-0.5

- PGA Peak Ground Acceleration
- PGV Peak Ground Velocity
- PGD Peak Ground Displacement
- IA Arias Intensity
- E Input Energy
- CAV Cumulative Absolute Velocity
- SED Specific Energy Density
- RMS_A Root Mean Square of Acceleration
- RMS_V Root Mean Square of Velocity
- RMS_D Root Mean Square of Displacement

Filter: Fourier 0.7 – 25 Hz

A.3 Transversal input signal of the non-strengthened mock-up: Earthquake 50%

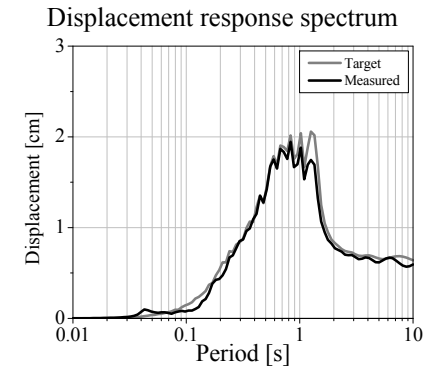
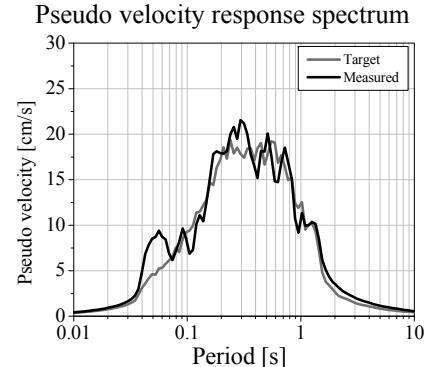
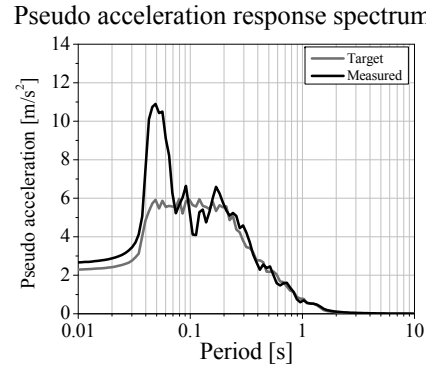
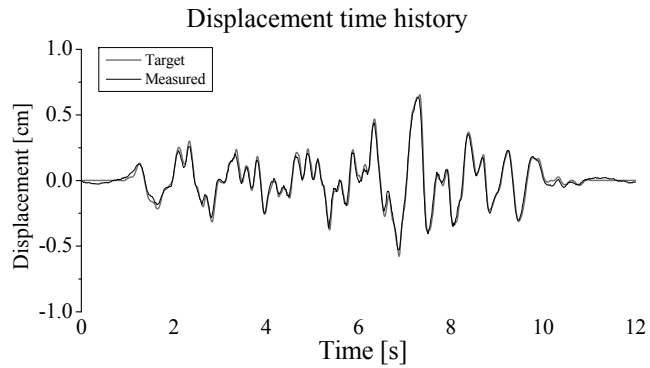
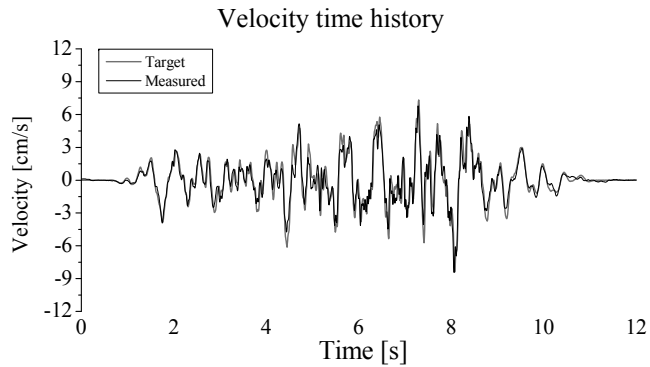
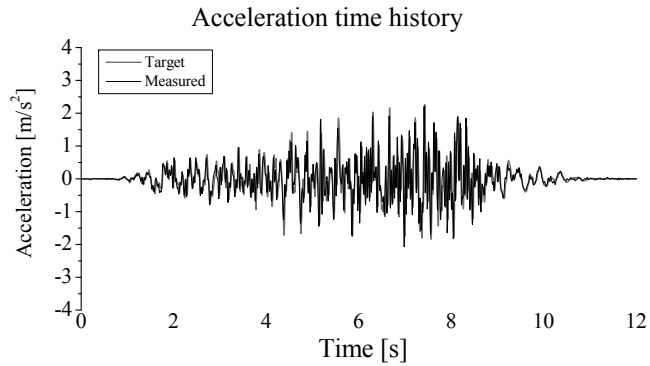


Parameter	Target	Measured	Variation [%]
PGA [m/s ²]	2.259	2.208	-2.2
PGV [cm/s]	8.374	8.435	0.7
PGD [cm]	0.715	0.687	-4.0
PGV/PGA [s ⁻¹]	0.037	0.038	3.0
PGD/PGA [s ⁻²]	0.003	0.003	-1.9
IA [m/s]	0.469	0.440	-6.2
E [kg m ² /s ²]	1664	1479	-11.1
CAV [m/s]	3.812	3.691	-3.2
SED [m ² /s]	0.005	0.004	-18.6
RMS_A [m/s ²]	0.494	0.478	-3.1
RMS_V [cm/s]	1.985	1.791	-9.8
RMS_D [cm]	0.184	0.175	-5.1

PGA	Peak Ground Acceleration
PGV	Peak Ground Velocity
PGD	Peak Ground Displacement
IA	Arias Intensity
E	Input Energy
CAV	Cumulative Absolute Velocity
SED	Specific Energy Density
RMS_A	Root Mean Square of Acceleration
RMS_V	Root Mean Square of Velocity
RMS_D	Root Mean Square of Displacement

Filter: Fourier 0.7 – 25 Hz

A.4 Longitudinal input signal of the non-strengthened mock-up: Earthquake 50%

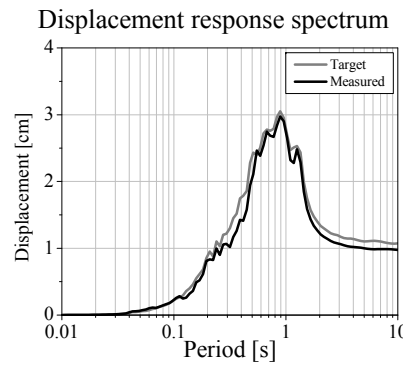
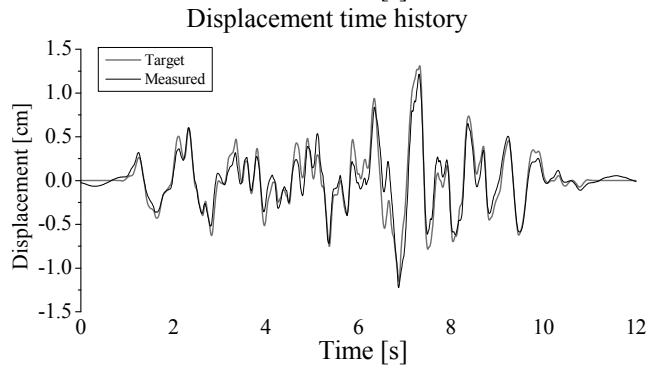
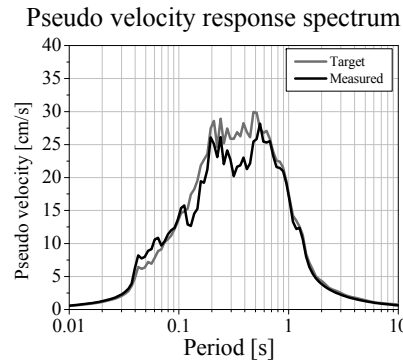
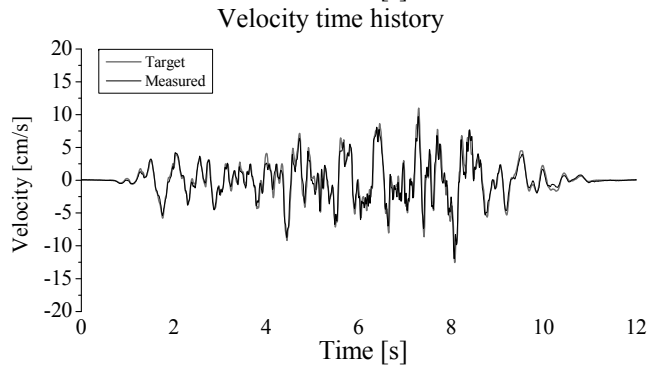
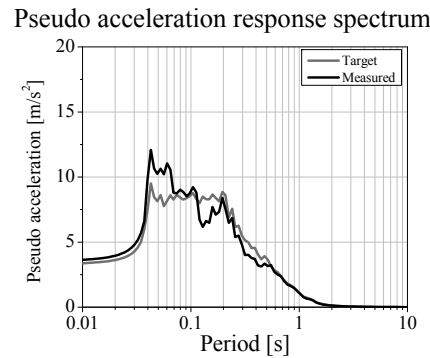
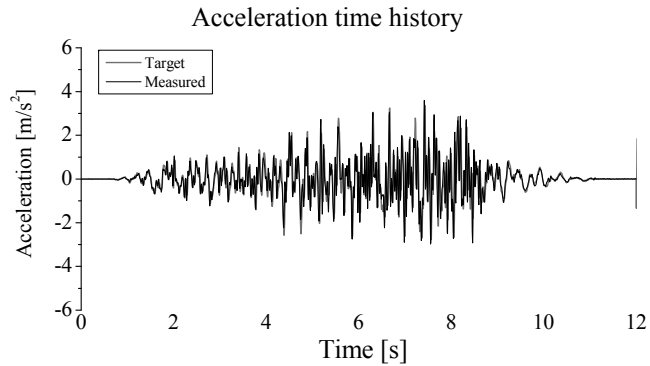


Parameter	Target	Measured	Variation [%]
PGA [m/s^2]	2.298	2.639	14.8
PGV [cm/s]	10.371	10.920	5.3
PGD [cm]	0.655	0.632	-3.6
PGV/PGA [s^{-1}]	0.045	0.041	-8.3
PGD/PGA [s^{-2}]	0.003	0.002	-16.1
IA [m/s]	0.498	0.609	22.4
E [$kg\ m^2/s^2$]	1784	1945	9.0
CAV [m/s]	4.082	4.433	8.6
SED [m^2/s]	0.005	0.005	1.0
RMS_A [m/s^2]	0.509	0.563	10.6
RMS_V [cm/s]	2.008	2.018	0.5
RMS_D [cm]	0.176	0.164	-7.0

- PGA Peak Ground Acceleration
- PGV Peak Ground Velocity
- PGD Peak Ground Displacement
- IA Arias Intensity
- E Input Energy
- CAV Cumulative Absolute Velocity
- SED Specific Energy Density
- RMS_A Root Mean Square of Acceleration
- RMS_V Root Mean Square of Velocity
- RMS_D Root Mean Square of Displacement

Filter: Fourier 0.7 – 25 Hz

A.5 Transversal input signal of the non-strengthened mock-up: Earthquake 75%

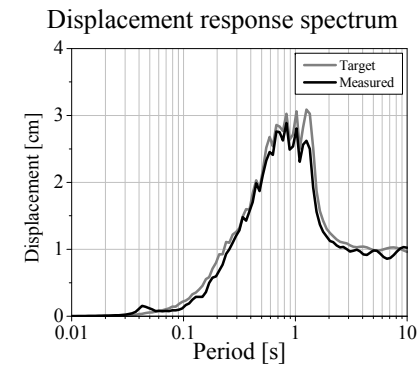
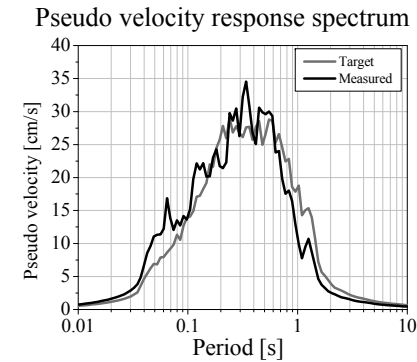
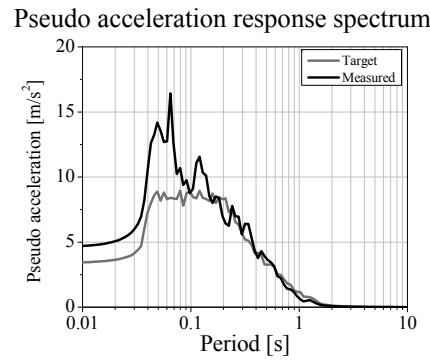
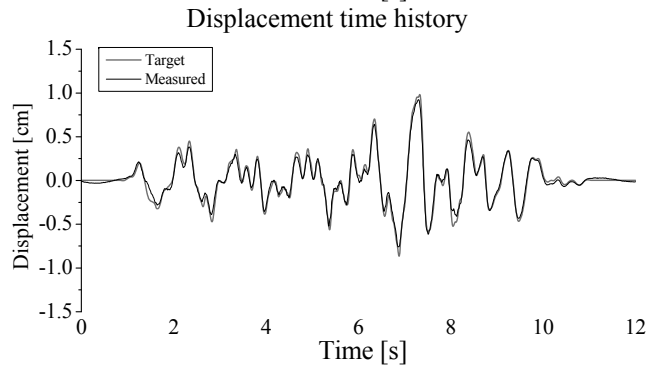
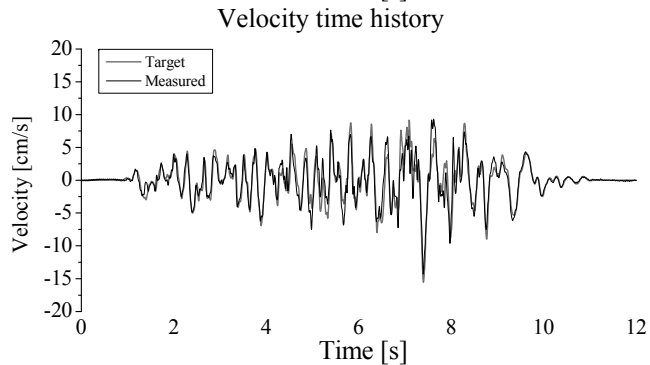
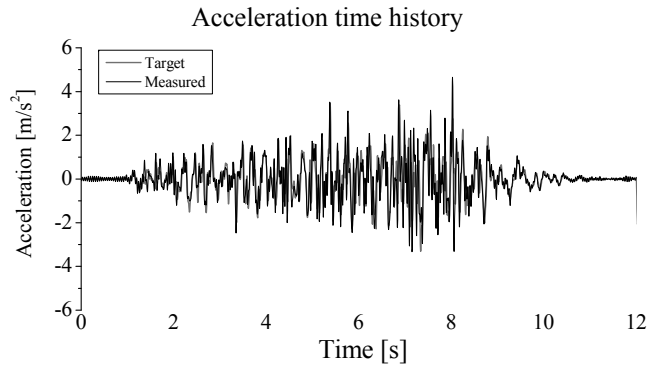


Parameter	Target	Measured	Variation [%]
PGA [m/s^2]	3.388	3.598	6.2
PGV [cm/s]	12.562	11.955	-4.8
PGD [cm]	1.073	0.966	-10.0
PGV/PGA [s^{-1}]	0.037	0.033	-10.4
PGD/PGA [s^{-2}]	0.003	0.003	-15.2
IA [m/s]	1.055	1.057	0.2
E [$kg\ m^2/s^2$]	3744	3465	-7.5
CAV [m/s]	5.719	5.661	-1.0
SED [m^2/s]	0.011	0.009	-15.6
RMS_A [m/s^2]	0.741	0.741	0.1
RMS_V [cm/s]	2.978	2.736	-8.1
RMS_D [cm]	0.276	0.261	-5.7

- PGA Peak Ground Acceleration
- PGV Peak Ground Velocity
- PGD Peak Ground Displacement
- IA Arias Intensity
- E Input Energy
- CAV Cumulative Absolute Velocity
- SED Specific Energy Density
- RMS_A Root Mean Square of Acceleration
- RMS_V Root Mean Square of Velocity
- RMS_D Root Mean Square of Displacement

Filter: Fourier 0.7 – 25 Hz

A.6 Longitudinal input signal of the non-strengthened mock-up: Earthquake 75%

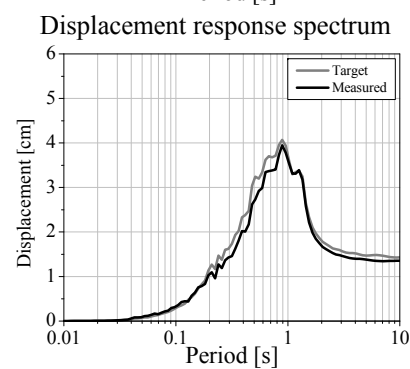
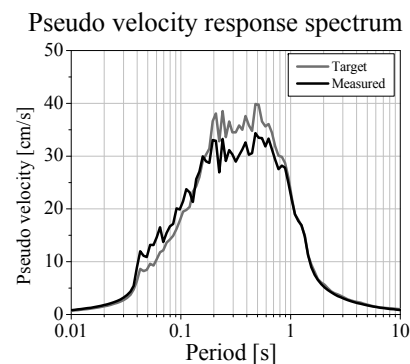
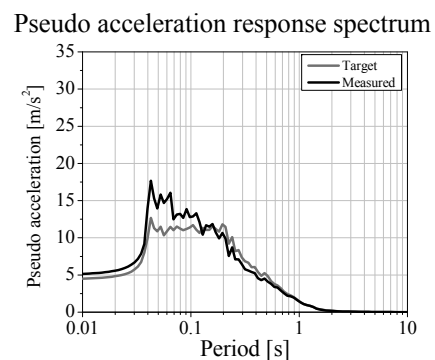
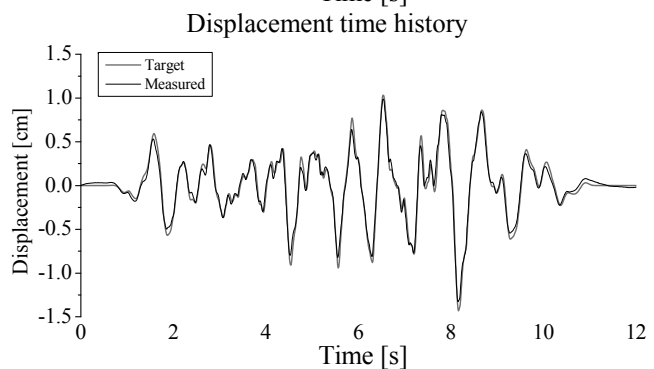
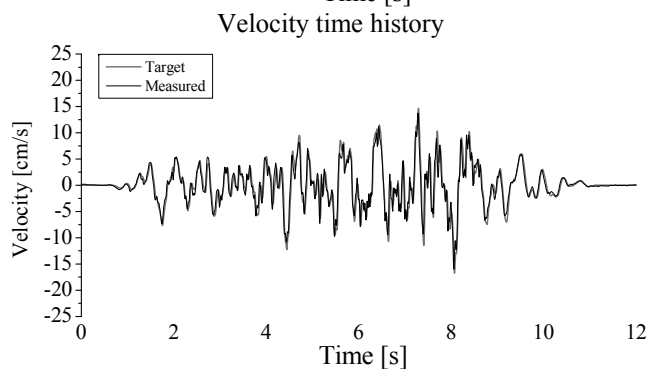
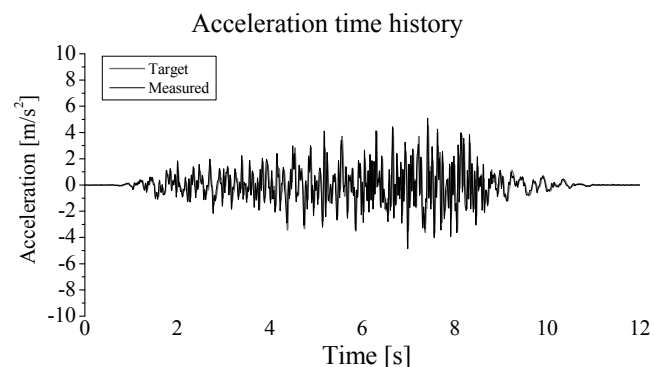


Parameter	Target	Measured	Variation [%]
PGA [m/s^2]	3.448	4.654	35.0
PGV [cm/s]	15.556	14.304	-8.0
PGD [cm]	0.983	0.929	-5.5
PGV/PGA [s^{-1}]	0.045	0.031	-31.9
PGD/PGA [s^{-2}]	0.003	0.002	-30
IA [m/s]	1.120	1.397	24.7
E [$kg\ m^2/s^2$]	4015	4141	3.1
CAV [m/s]	6.123	6.796	11.0
SED [m^2/s]	0.011	0.010	-7.4
RMS_A [m/s^2]	0.763	0.853	11.7
RMS_V [cm/s]	3.012	2.899	-3.8
RMS_D [cm]	0.264	0.239	-9.4

- PGA Peak Ground Acceleration
- PGV Peak Ground Velocity
- PGD Peak Ground Displacement
- IA Arias Intensity
- E Input Energy
- CAV Cumulative Absolute Velocity
- SED Specific Energy Density
- RMS_A Root Mean Square of Acceleration
- RMS_V Root Mean Square of Velocity
- RMS_D Root Mean Square of Displacement

Filter: Fourier 0.7 – 25 Hz

A.7. Transversal input signal of the non-strengthened mock-up: Earthquake 100%

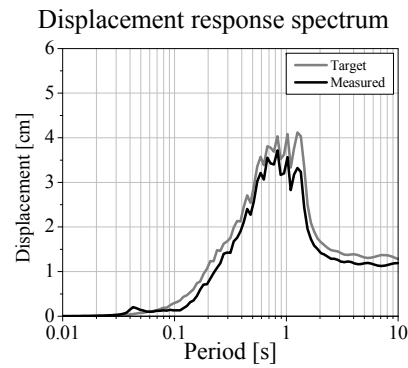
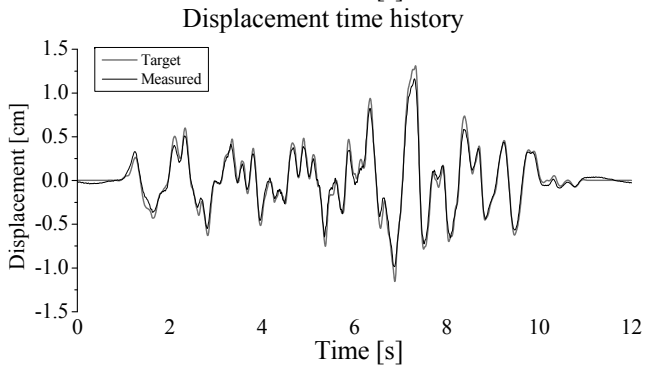
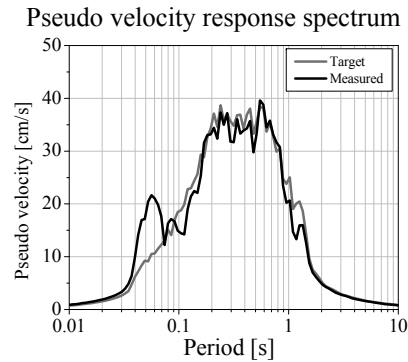
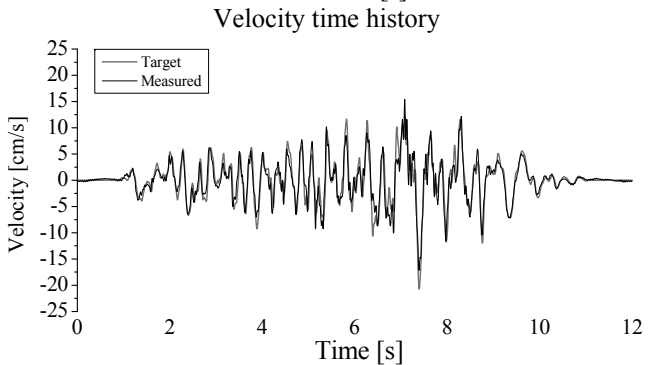
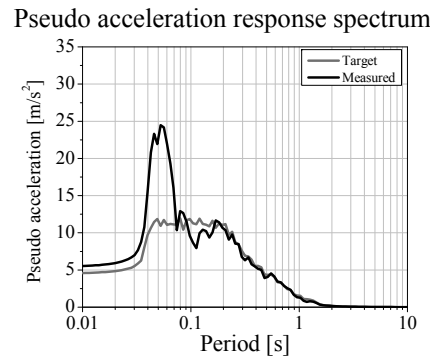
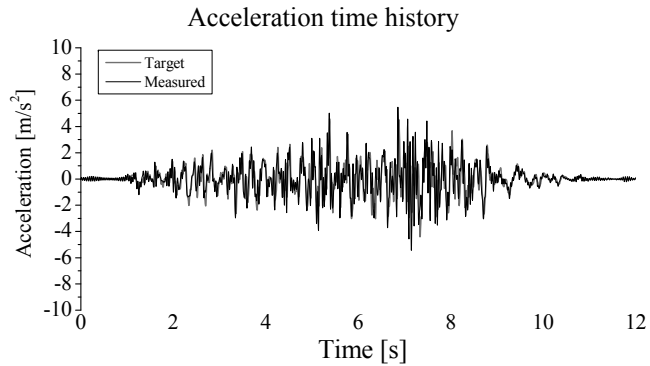


Parameter	Target	Measured	Variation [%]
PGA [m/s^2]	4.518	5.097	12.8
PGV [cm/s]	16.749	15.991	-4.5
PGD [cm]	1.431	1.327	-7.3
PGV/PGA [s^{-1}]	0.037	0.031	-15.4
PGD/PGA [s^{-2}]	0.003	0.003	-17.8
IA [m/s]	1.875	2.331	24.3
E [$kg\ m^2/s^2$]	6657	6863	3.1
CAV [m/s]	7.625	8.604	12.8
SED [m^2/s]	0.019	0.016	-14.5
RMS_A [m/s^2]	0.988	1.101	11.5
RMS_V [cm/s]	3.970	3.671	-7.5
RMS_D [cm]	0.368	0.344	-6.7

PGA	Peak Ground Acceleration
PGV	Peak Ground Velocity
PGD	Peak Ground Displacement
IA	Arias Intensity
E	Input Energy
CAV	Cumulative Absolute Velocity
SED	Specific Energy Density
RMS_A	Root Mean Square of Acceleration
RMS_V	Root Mean Square of Velocity
RMS_D	Root Mean Square of Displacement

Filter: Fourier 0.7 – 25 Hz

A.8. Longitudinal input signal of the non-strengthened mock-up: Earthquake 100%

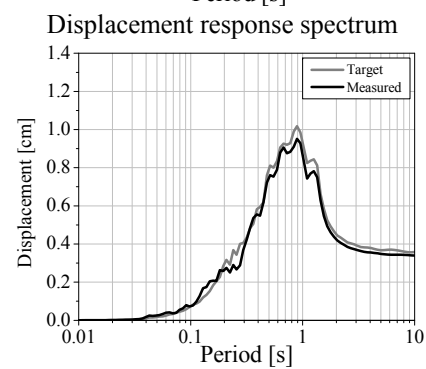
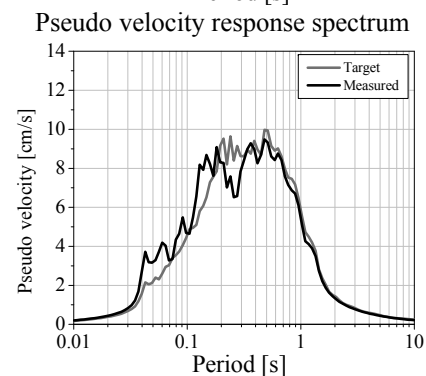
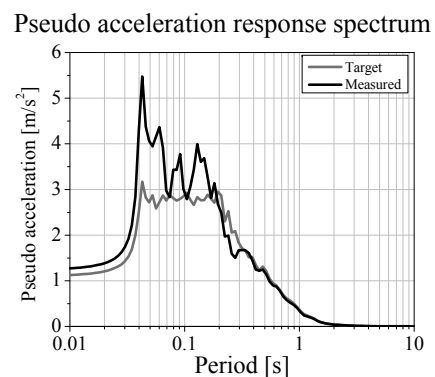
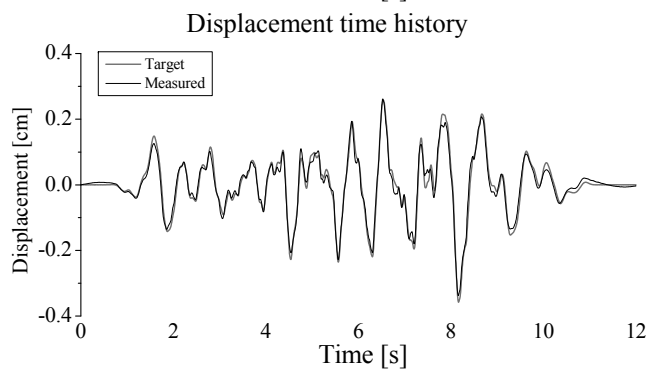
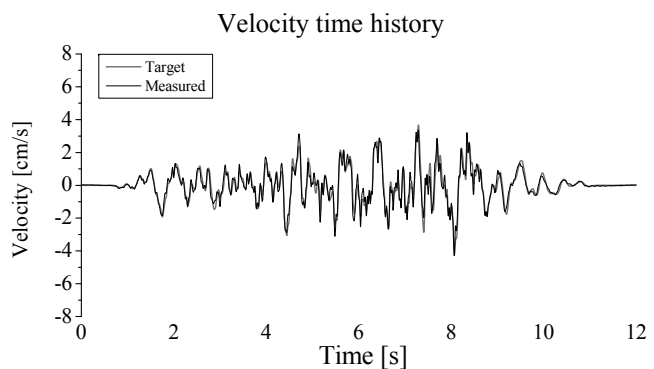
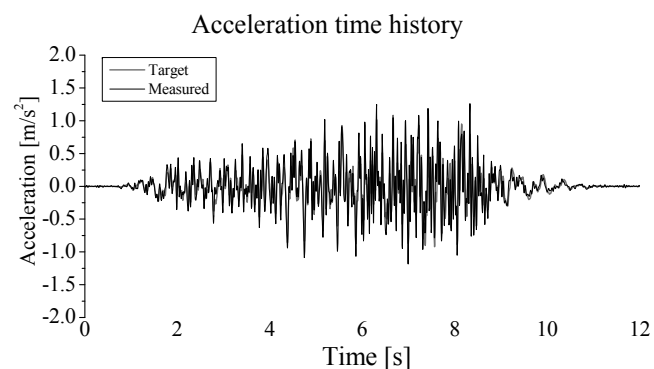


Parameter	Target	Measured	Variation [%]
PGA [m/s^2]	4.597	5.484	19.3
PGV [cm/s]	20.742	17.171	-17.2
PGD [cm]	1.311	1.161	-11.4
PGV/PGA [s^{-1}]	0.045	0.031	-30.6
PGD/PGA [s^{-2}]	0.003	0.002	-25.8
IA [m/s]	1.991	2.352	18.1
E [$kg\ m^2/s^2$]	7138	7235	1.4
CAV [m/s]	8.164	8.692	6.5
SED [m^2/s]	0.019	0.017	-11.7
RMS_A [m/s^2]	1.018	1.106	8.7
RMS_V [cm/s]	4.016	3.775	-6.0
RMS_D [cm]	0.352	0.309	-12.3

- PGA Peak Ground Acceleration
- PGV Peak Ground Velocity
- PGD Peak Ground Displacement
- IA Arias Intensity
- E Input Energy
- CAV Cumulative Absolute Velocity
- SED Specific Energy Density
- RMS_A Root Mean Square of Acceleration
- RMS_V Root Mean Square of Velocity
- RMS_D Root Mean Square of Displacement

Filter: Fourier 0.7 – 25 Hz

A.9. Transversal input signal of the strengthened mock-up: Earthquake 25%

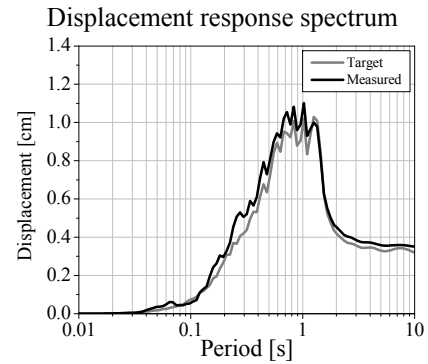
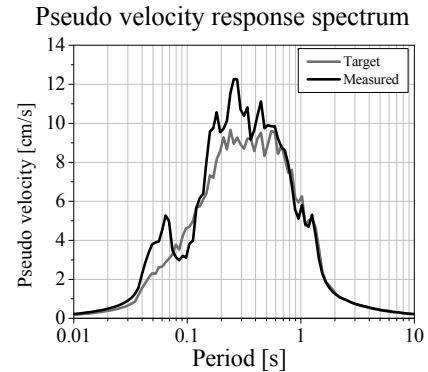
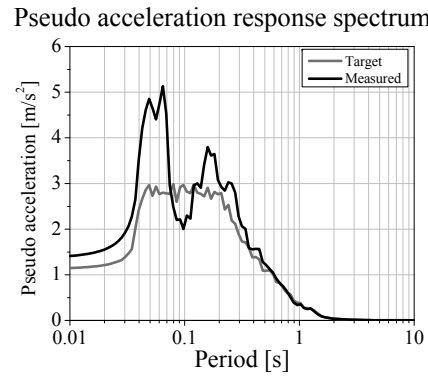
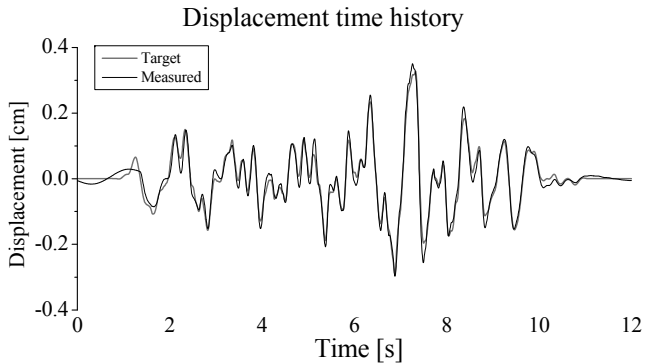
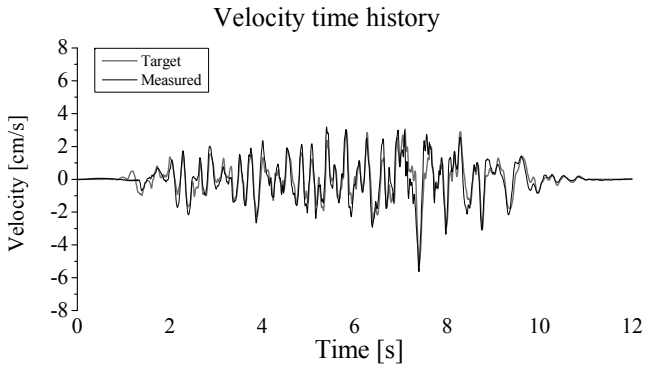
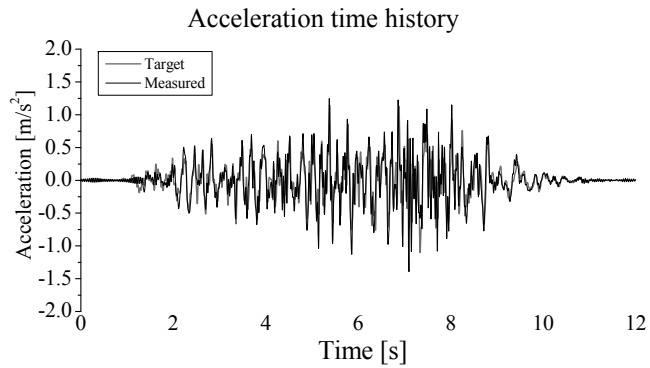


Parameter	Target	Measured	Variation [%]
PGA [m/s^2]	1.129	1.261	11.7
PGV [cm/s]	4.187	4.286	2.4
PGD [cm]	0.358	0.337	-5.7
PGV/PGA [s^{-1}]	0.037	0.034	-8.3
PGD/PGA [s^{-2}]	0.003	0.003	-15.6
IA [m/s]	0.117	0.174	48.5
E [$kg\ m^2/s^2$]	416	513	23.3
CAV [m/s]	1.906	2.320	21.7
SED [m^2/s]	0.001	0.001	-2.8
RMS_A [m/s^2]	0.247	0.301	21.9
RMS_V [cm/s]	0.993	0.979	-1.4
RMS_D [cm]	0.092	0.087	-5.9

PGA	Peak Ground Acceleration
PGV	Peak Ground Velocity
PGD	Peak Ground Displacement
IA	Arias Intensity
E	Input Energy
CAV	Cumulative Absolute Velocity
SED	Specific Energy Density
RMS_A	Root Mean Square of Acceleration
RMS_V	Root Mean Square of Velocity
RMS_D	Root Mean Square of Displacement

Filter: Fourier 0.7 – 25 Hz

A.10. Longitudinal input signal of the strengthened mock-up: Earthquake 25%

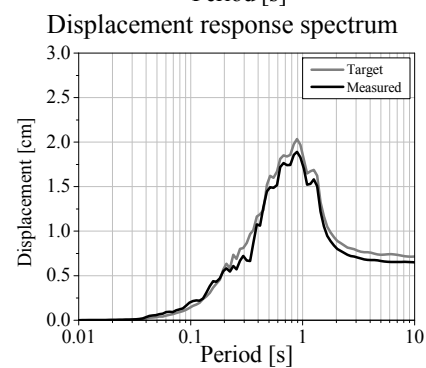
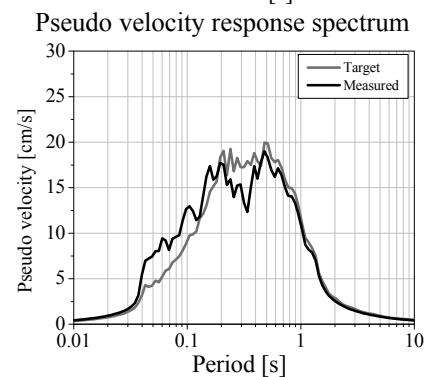
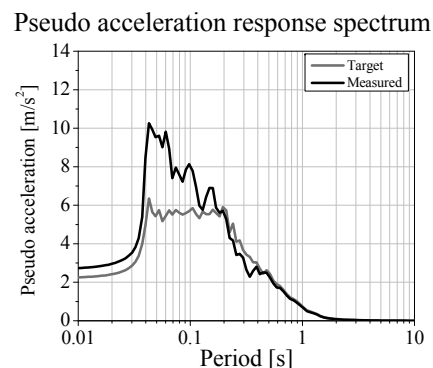
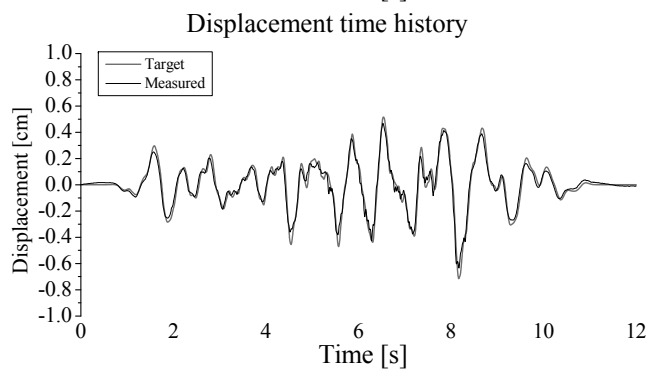
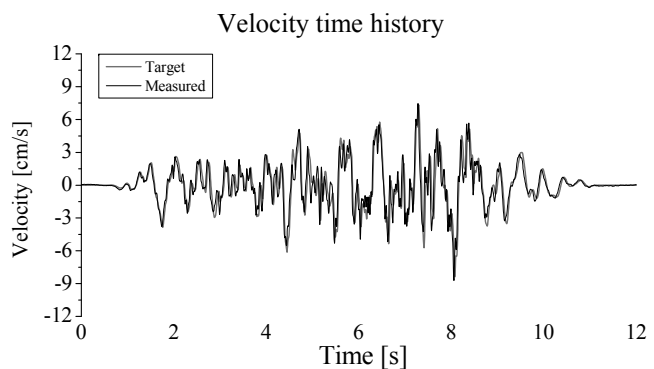
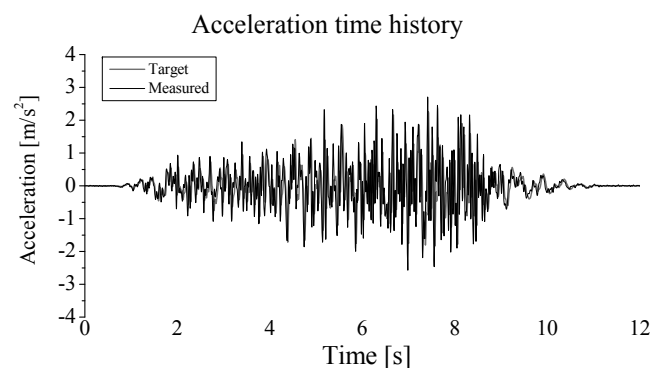


Parameter	Target	Measured	Variation [%]
PGA [m/s ²]	1.149	1.536	33.7
PGV [cm/s]	5.185	5.998	15.7
PGD [cm]	0.328	0.351	7.0
PGV/PGA [s ⁻¹]	0.045	0.039	-13.5
PGD/PGA [s ⁻²]	0.003	0.002	-20.0
IA [m/s]	0.124	0.193	55.1
E [kg m ² /s ²]	446	632	41.7
CAV [m/s]	2.041	2.462	20.6
SED [m ² /s]	0.001	0.002	30.2
RMS_A [m/s ²]	0.254	0.317	24.6
RMS_V [cm/s]	1.004	1.146	14.1
RMS_D [cm]	0.088	0.091	3.4

- PGA Peak Ground Acceleration
- PGV Peak Ground Velocity
- PGD Peak Ground Displacement
- IA Arias Intensity
- E Input Energy
- CAV Cumulative Absolute Velocity
- SED Specific Energy Density
- RMS_A Root Mean Square of Acceleration
- RMS_V Root Mean Square of Velocity
- RMS_D Root Mean Square of Displacement

Filter: Fourier 0.7 – 25 Hz

A.11. Transversal input signal of the strengthened mock-up: Earthquake 50%

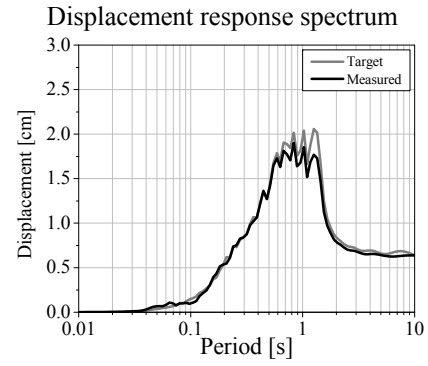
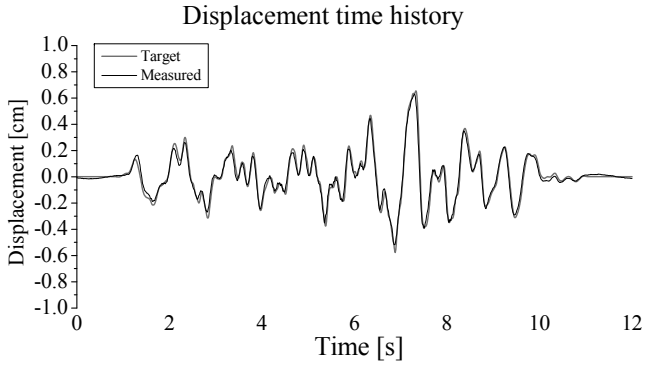
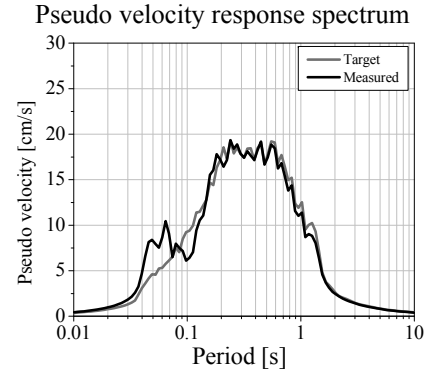
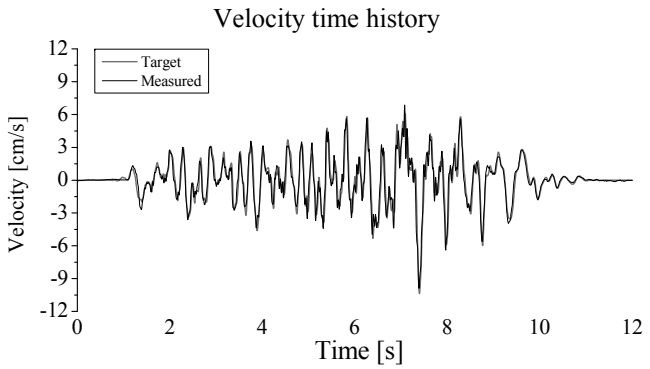
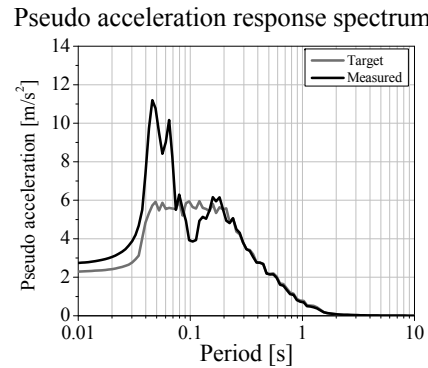
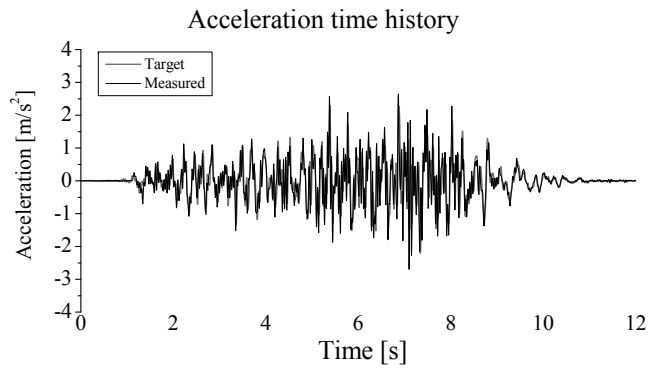


Parameter	Target	Measured	Variation [%]
PGA [m/s^2]	2.259	2.710	20.0
PGV [cm/s]	8.374	8.715	4.1
PGD [cm]	0.715	0.641	-10.4
PGV/PGA [s^{-1}]	0.037	0.032	-13.3
PGD/PGA [s^{-2}]	0.003	0.002	-25.3
IA [m/s]	0.469	0.736	57.1
E [$kg\ m^2/s^2$]	1664	2026	21.7
CAV [m/s]	3.812	4.779	25.3
SED [m^2/s]	0.005	0.004	-7.9
RMS_A [m/s^2]	0.494	0.619	25.3
RMS_V [cm/s]	1.985	1.905	-4.0
RMS_D [cm]	0.184	0.171	-7.1

PGA	Peak Ground Acceleration
PGV	Peak Ground Velocity
PGD	Peak Ground Displacement
IA	Arias Intensity
E	Input Energy
CAV	Cumulative Absolute Velocity
SED	Specific Energy Density
RMS_A	Root Mean Square of Acceleration
RMS_V	Root Mean Square of Velocity
RMS_D	Root Mean Square of Displacement

Filter: Fourier 0.7 – 25 Hz

A.12. Longitudinal input signal of the strengthened mock-up: Earthquake 50%

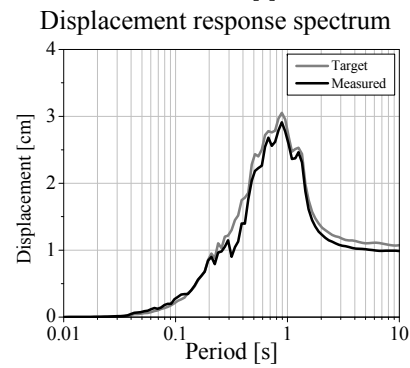
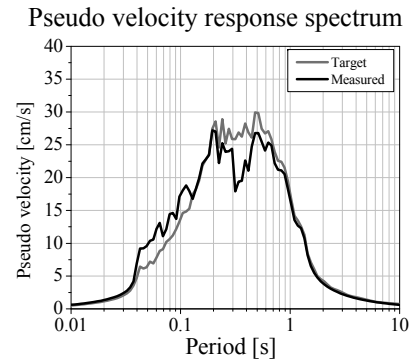
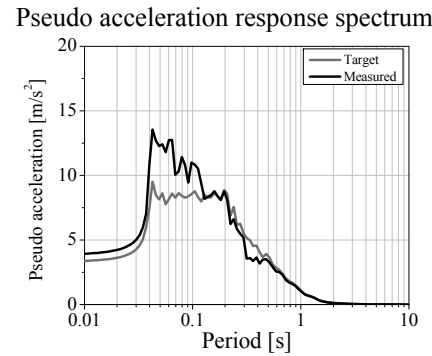
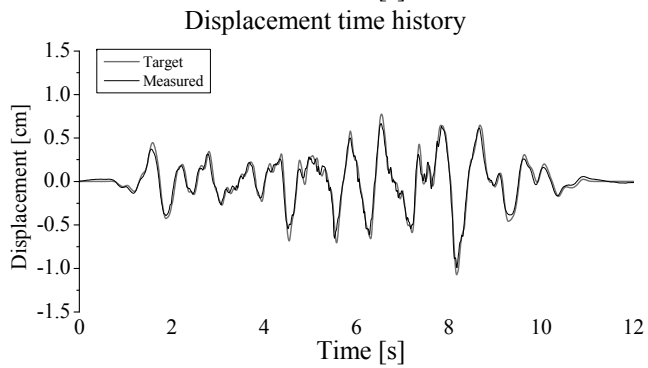
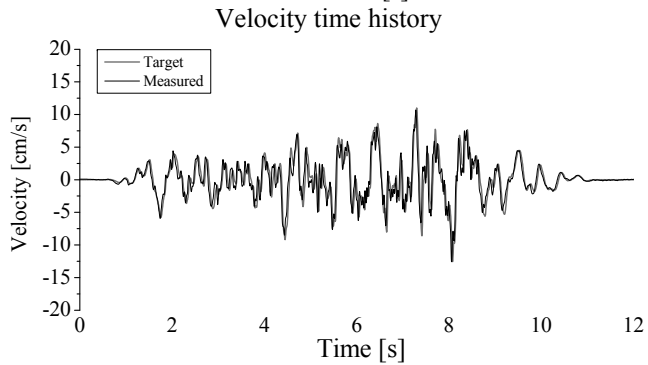
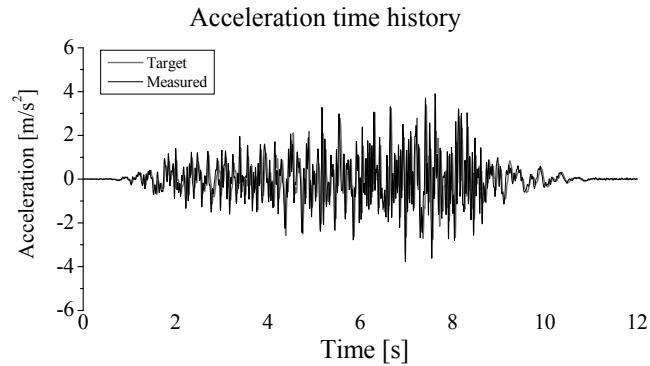


Parameter	Target	Measured	Variation [%]
$PGA [m/s^2]$	2.298	2.697	17.4
$PGV [cm/s]$	10.371	9.894	-4.6
$PGD [cm]$	0.655	0.624	-4.8
$PGV/PGA [s^{-1}]$	0.045	0.037	-18.7
$PGD/PGA [s^{-2}]$	0.003	0.002	-18.8
$IA [m/s]$	0.498	0.611	22.8
$E [kg m^2/s^2]$	1784	1923	7.8
$CAV [m/s]$	4.082	4.406	7.9
$SED [m^2/s]$	0.005	0.005	-4.0
$RMS_A [m/s^2]$	0.509	0.564	10.8
$RMS_V [cm/s]$	2.008	1.967	-2.0
$RMS_D [cm]$	0.176	0.162	-7.9

- PGA Peak Ground Acceleration
- PGV Peak Ground Velocity
- PGD Peak Ground Displacement
- IA Arias Intensity
- E Input Energy
- CAV Cumulative Absolute Velocity
- SED Specific Energy Density
- RMS_A Root Mean Square of Acceleration
- RMS_V Root Mean Square of Velocity
- RMS_D Root Mean Square of Displacement

Filter: Fourier 0.7 – 25 Hz

A.13. Transversal input signal of the strengthened mock-up: Earthquake 75%

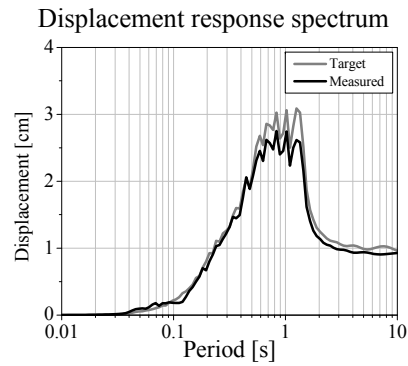
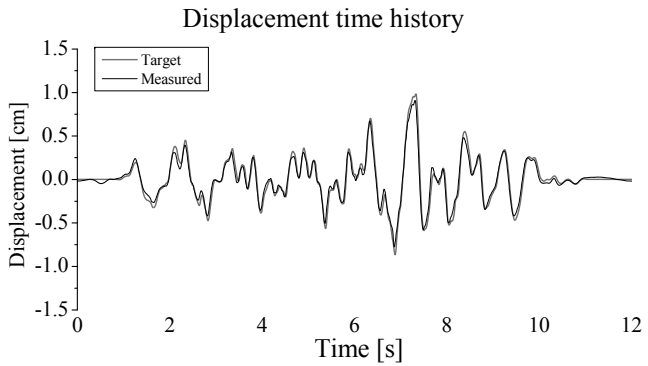
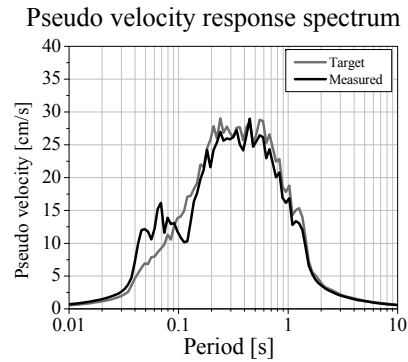
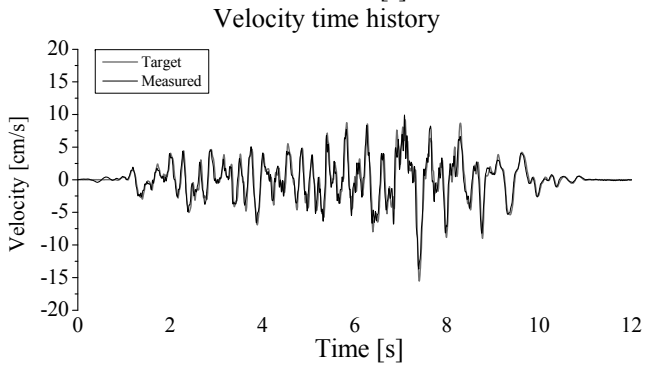
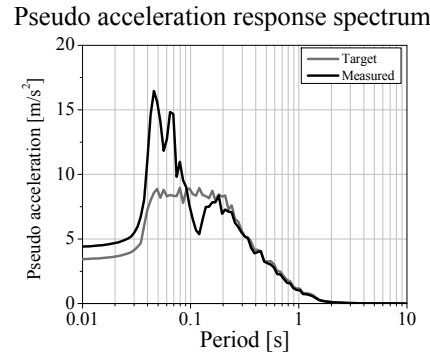
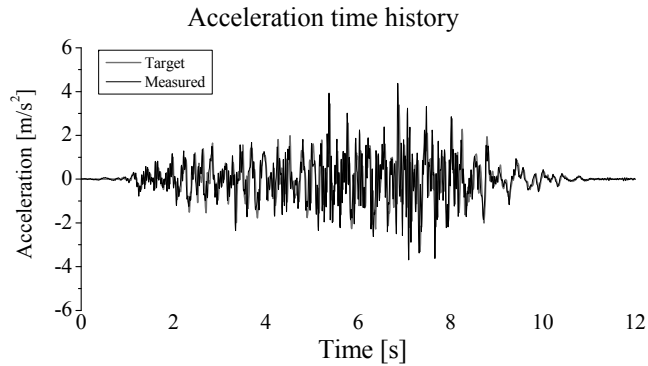


Parameter	Target	Measured	Variation [%]
PGA [m/s^2]	3.388	3.901	15.1
PGV [cm/s]	12.562	12.574	0.1
PGD [cm]	1.073	0.975	-9.1
PGV/PGA [s^{-1}]	0.037	0.032	-13.1
PGD/PGA [s^{-2}]	0.003	0.003	-21.1
IA [m/s]	1.055	1.425	35.1
E [$kg\ m^2/s^2$]	3744	4092	9.3
CAV [m/s]	5.719	6.755	18.1
SED [m^2/s]	0.011	0.009	-12.7
RMS_A [m/s^2]	0.741	0.861	16.2
RMS_V [cm/s]	2.978	2.783	-6.5
RMS_D [cm]	0.276	0.258	-6.7

PGA	Peak Ground Acceleration
PGV	Peak Ground Velocity
PGD	Peak Ground Displacement
IA	Arias Intensity
E	Input Energy
CAV	Cumulative Absolute Velocity
SED	Specific Energy Density
RMS_A	Root Mean Square of Acceleration
RMS_V	Root Mean Square of Velocity
RMS_D	Root Mean Square of Displacement

Filter: Fourier 0.7 – 25 Hz

A.14. Longitudinal input signal of the strengthened mock-up: Earthquake 75%

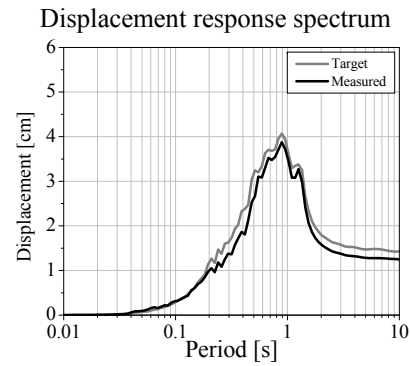
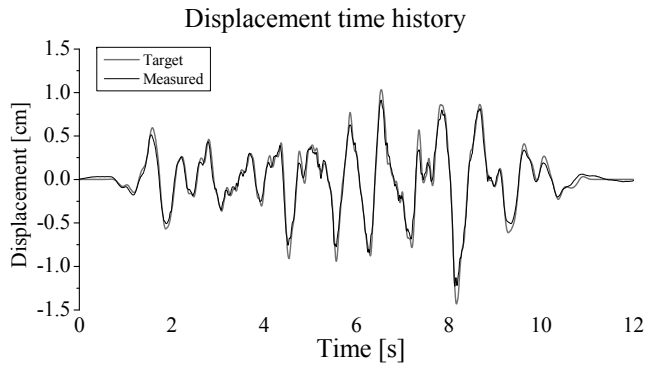
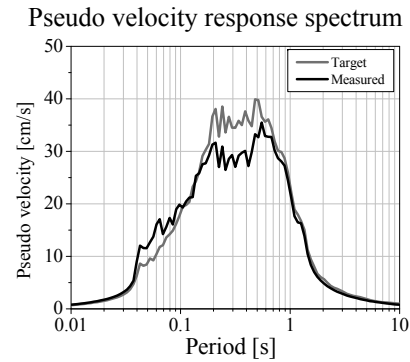
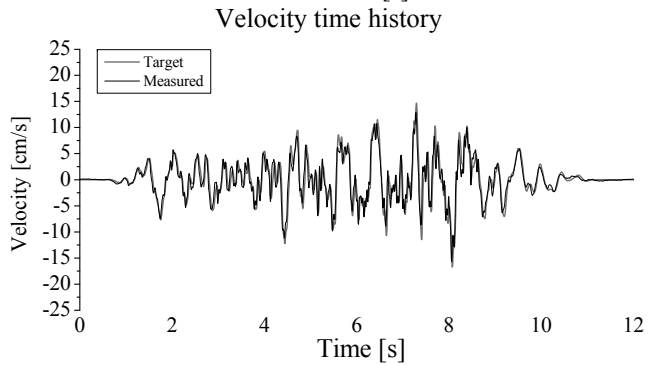
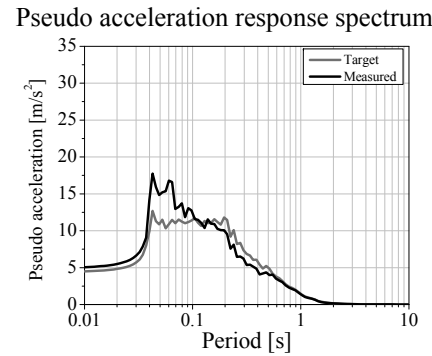
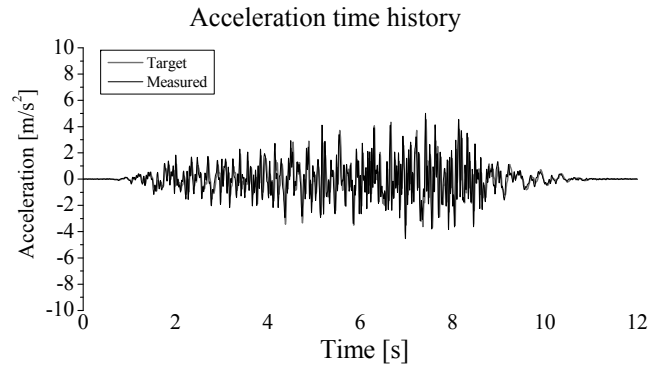


Parameter	Target	Measured	Variation [%]
PGA [m/s^2]	3.448	4.381	27.1
PGV [cm/s]	15.556	13.696	-12.0
PGD [cm]	0.983	0.907	-7.7
PGV/PGA [s^{-1}]	0.045	0.031	-30.7
PGD/PGA [s^{-2}]	0.003	0.002	-27.4
IA [m/s]	1.120	1.289	15.1
E [$kg\ m^2/s^2$]	4015	3966	-1.2
CAV [m/s]	6.123	6.423	4.9
SED [m^2/s]	0.011	0.009	-13.2
RMS_A [m/s^2]	0.763	0.819	7.3
RMS_V [cm/s]	3.012	2.806	-6.9
RMS_D [cm]	0.264	0.236	-10.9

- PGA Peak Ground Acceleration
- PGV Peak Ground Velocity
- PGD Peak Ground Displacement
- IA Arias Intensity
- E Input Energy
- CAV Cumulative Absolute Velocity
- SED Specific Energy Density
- RMS_A Root Mean Square of Acceleration
- RMS_V Root Mean Square of Velocity
- RMS_D Root Mean Square of Displacement

Filter: Fourier 0.7 – 25 Hz

A.15. Transversal input signal of the strengthened mock-up: Earthquake 100%

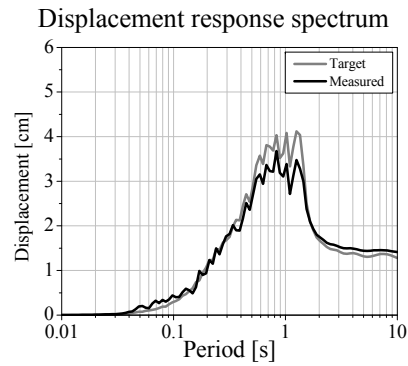
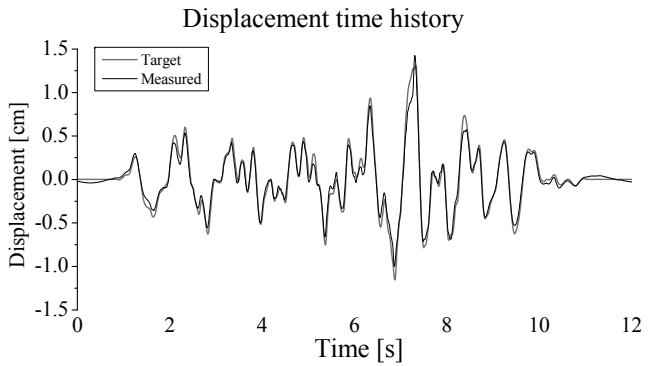
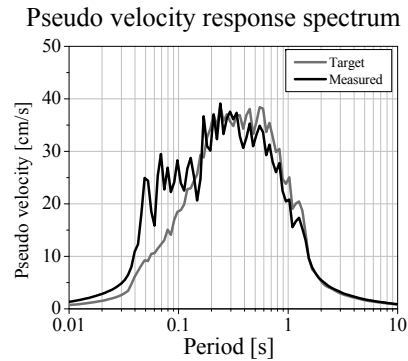
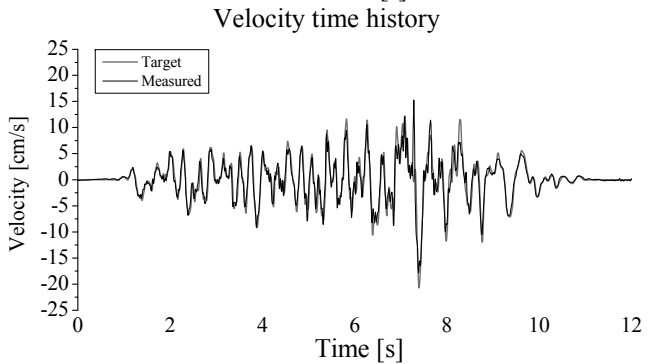
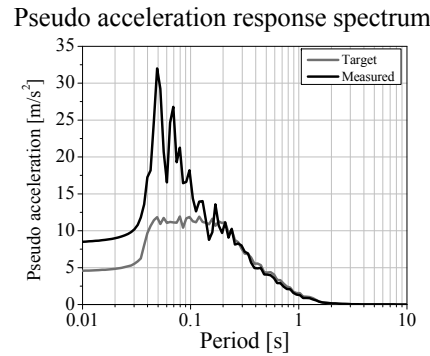
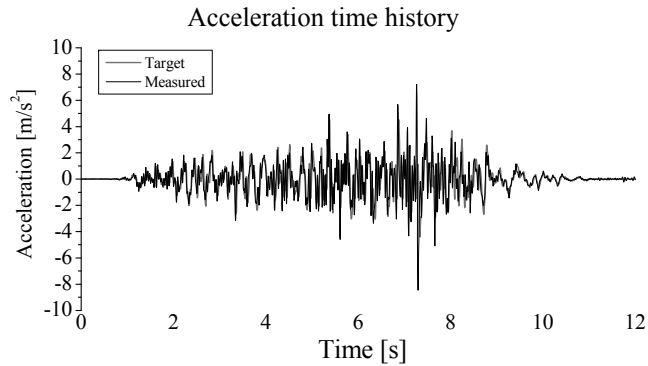


Parameter	Target	Measured	Variation [%]
<i>PGA</i> [m/s ²]	4.518	5.008	10.9
<i>PGV</i> [cm/s]	16.749	15.704	-6.2
<i>PGD</i> [cm]	1.431	1.243	-13.1
<i>PGV/PGA</i> [s ⁻¹]	0.037	0.031	-15.4
<i>PGD/PGA</i> [s ⁻²]	0.003	0.002	-21.6
<i>IA</i> [m/s]	1.875	2.330	24.3
<i>E</i> [kg m ² /s ²]	6657	6767	1.7
<i>CAV</i> [m/s]	7.625	8.710	14.2
<i>SED</i> [m ² /s]	0.019	0.016	-16.0
<i>RMS_A</i> [m/s ²]	0.988	1.101	11.5
<i>RMS_V</i> [cm/s]	3.970	3.639	-8.3
<i>RMS_D</i> [cm]	0.368	0.341	-7.4

- PGA* Peak Ground Acceleration
- PGV* Peak Ground Velocity
- PGD* Peak Ground Displacement
- IA* Arias Intensity
- E* Input Energy
- CAV* Cumulative Absolute Velocity
- SED* Specific Energy Density
- RMS_A* Root Mean Square of Acceleration
- RMS_V* Root Mean Square of Velocity
- RMS_D* Root Mean Square of Displacement

Filter: Fourier 0.7 – 25 Hz

A.16. Longitudinal input signal of the strengthened mock-up: Earthquake 100%

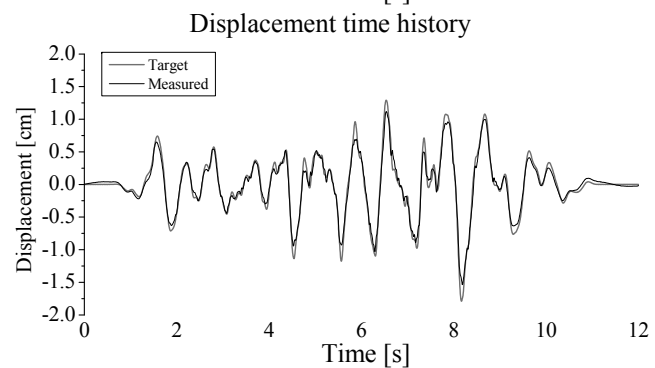
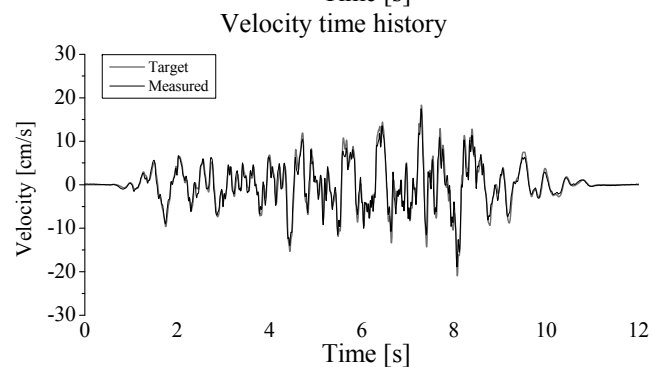
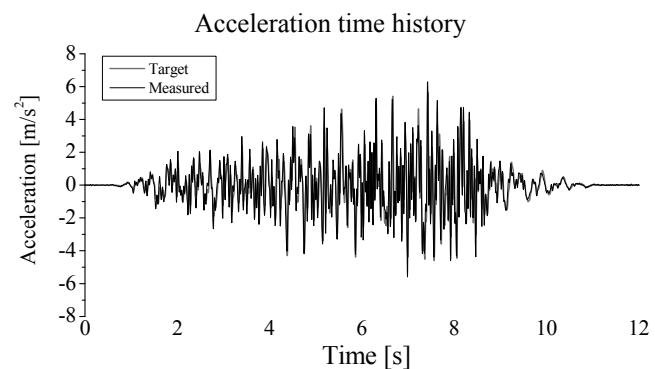


Parameter	Target	Measured	Variation [%]
PGA [m/s^2]	4.597	8.460	84.0
PGV [cm/s]	20.742	17.868	-13.9
PGD [cm]	1.311	1.426	8.8
PGV/PGA [s^{-1}]	0.045	0.021	-53.2
PGD/PGA [s^{-2}]	0.003	0.002	-40.9
IA [m/s]	1.991	2.504	25.8
E [$kg\ m^2/s^2$]	7138	7182	0.6
CAV [m/s]	8.164	8.671	6.2
SED [m^2/s]	0.019	0.017	-14.8
RMS_A [m/s^2]	1.018	1.141	12.2
RMS_V [cm/s]	4.016	3.708	-7.7
RMS_D [cm]	0.352	0.308	-12.6

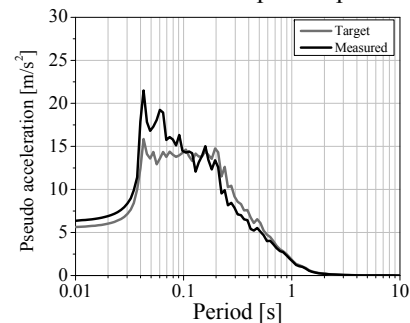
- PGA Peak Ground Acceleration
- PGV Peak Ground Velocity
- PGD Peak Ground Displacement
- IA Arias Intensity
- E Input Energy
- CAV Cumulative Absolute Velocity
- SED Specific Energy Density
- RMS_A Root Mean Square of Acceleration
- RMS_V Root Mean Square of Velocity
- RMS_D Root Mean Square of Displacement

Filter: Fourier 0.7 – 25 Hz

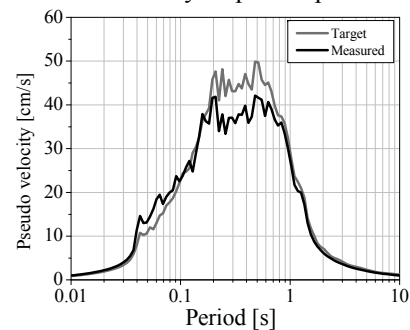
A.17. Transversal input signal of the strengthened mock-up: Earthquake 125%



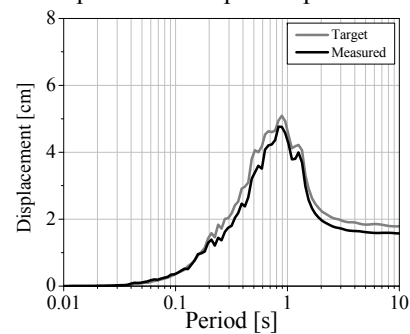
Pseudo acceleration response spectrum



Pseudo velocity response spectrum



Displacement response spectrum

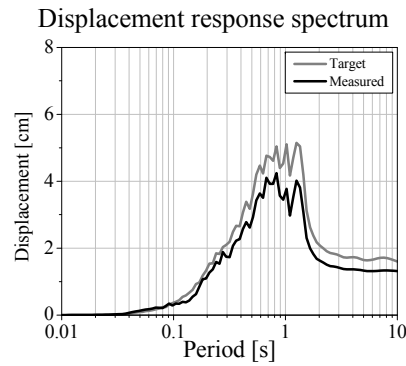
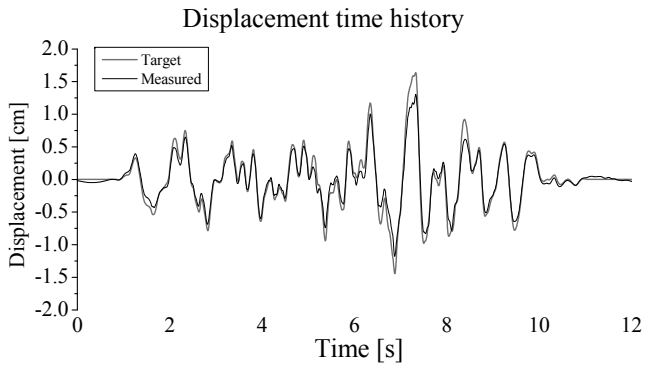
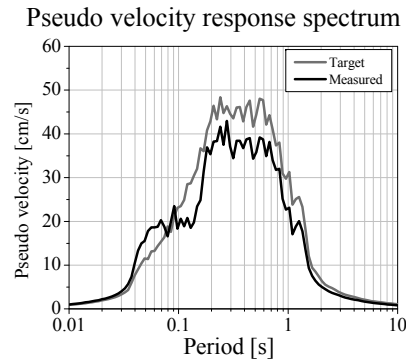
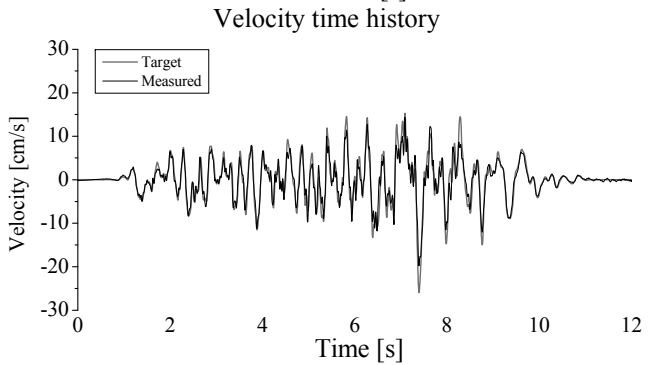
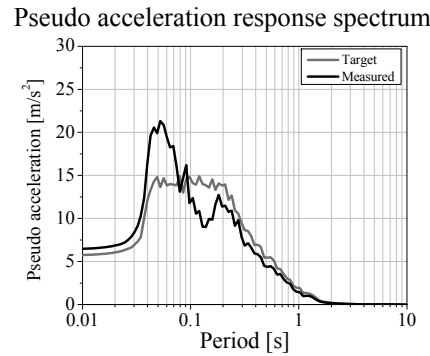
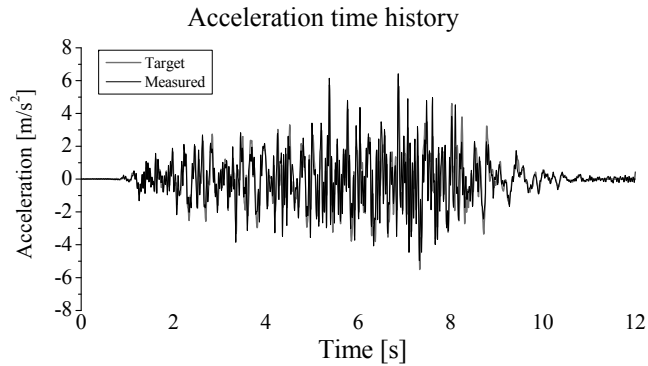


Parameter	Target	Measured	Variation [%]
PGA [m/s^2]	5.647	6.293	11.4
PGV [cm/s]	20.936	18.920	-9.6
PGD [cm]	1.789	1.559	-12.9
PGV/PGA [s^{-1}]	0.037	0.030	-18.9
PGD/PGA [s^{-2}]	0.003	0.002	-21.8
IA [m/s]	2.344	3.392	44.7
E [$kg\ m^2/s^2$]	8321	10053	20.8
CAV [m/s]	9.531	10.378	8.9
SED [m^2/s]	0.024	0.024	2.4
RMS_A [m/s^2]	1.235	1.328	7.6
RMS_V [cm/s]	4.963	4.493	-9.5
RMS_D [cm]	0.460	0.421	-8.6

PGA	Peak Ground Acceleration
PGV	Peak Ground Velocity
PGD	Peak Ground Displacement
IA	Arias Intensity
E	Input Energy
CAV	Cumulative Absolute Velocity
SED	Specific Energy Density
RMS_A	Root Mean Square of Acceleration
RMS_V	Root Mean Square of Velocity
RMS_D	Root Mean Square of Displacement

Filter: Fourier 0.7 – 25 Hz

A.18. Longitudinal input signal of the strengthened mock-up: Earthquake 125%

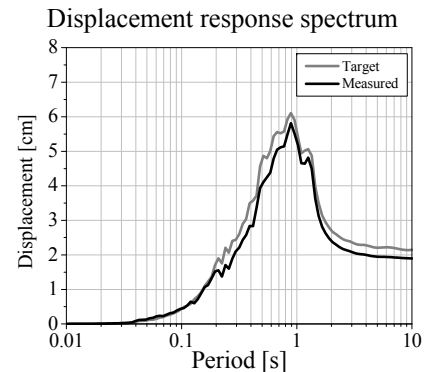
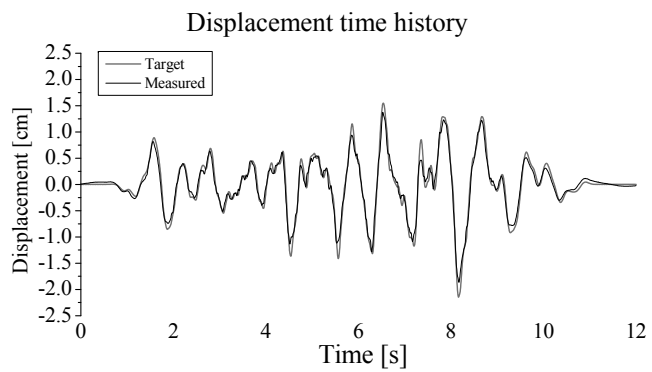
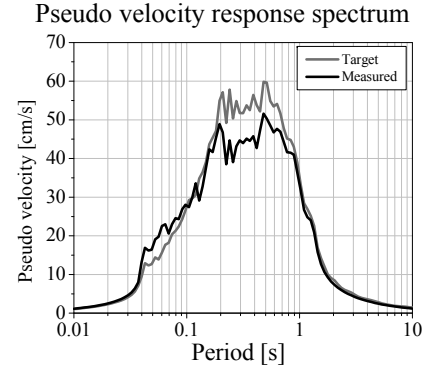
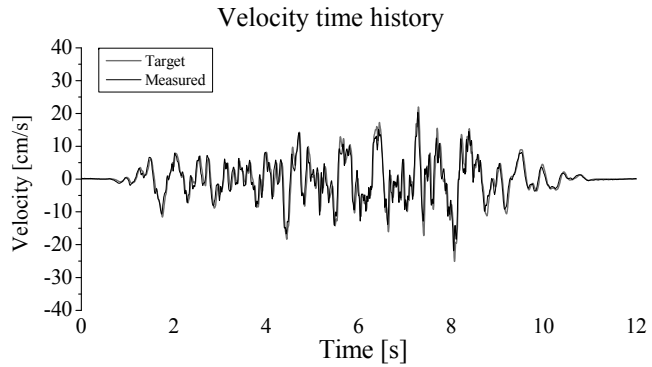
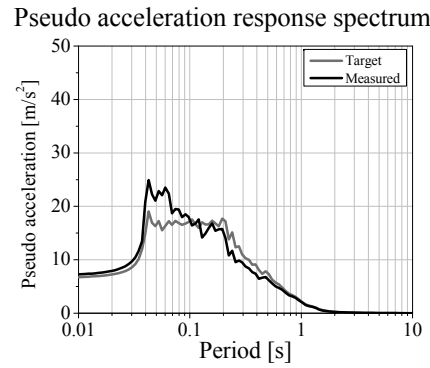
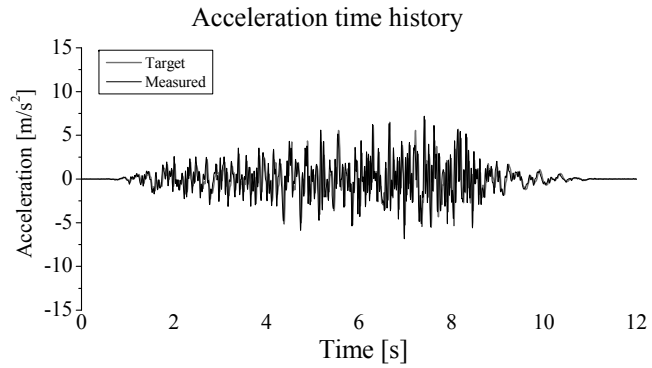


Parameter	Target	Measured	Variation [%]
PGA [m/s^2]	5.746	6.426	11.8
PGV [cm/s]	25.927	19.802	-23.6
PGD [cm]	1.638	1.304	-20.4
PGV/PGA [s^{-1}]	0.045	0.031	-31.7
PGD/PGA [s^{-2}]	0.003	0.002	-28.8
IA [m/s]	2.489	3.248	30.5
E [$kg\ m^2/s^2$]	8922	9546	7.0
CAV [m/s]	10.205	10.445	2.3
SED [m^2/s]	0.024	0.022	-10.0
RMS_A [m/s^2]	1.272	1.300	2.2
RMS_V [cm/s]	5.020	4.260	-15.2
RMS_D [cm]	0.441	0.356	-19.2

- PGA Peak Ground Acceleration
- PGV Peak Ground Velocity
- PGD Peak Ground Displacement
- IA Arias Intensity
- E Input Energy
- CAV Cumulative Absolute Velocity
- SED Specific Energy Density
- RMS_A Root Mean Square of Acceleration
- RMS_V Root Mean Square of Velocity
- RMS_D Root Mean Square of Displacement

Filter: Fourier 0.7 – 25 Hz

A.19. Transversal input signal of the strengthened mock-up: Earthquake 150%

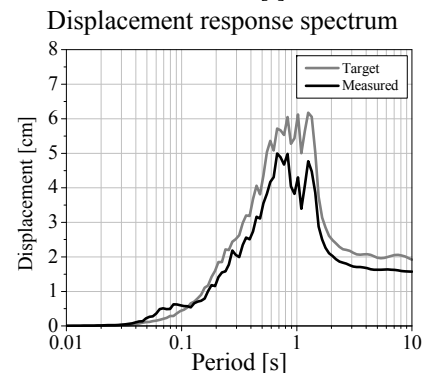
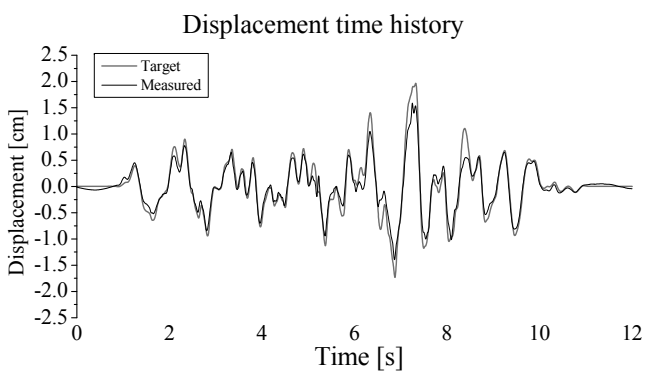
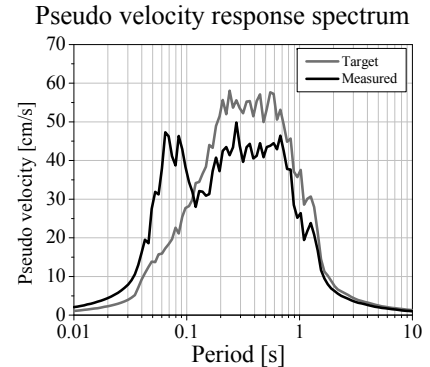
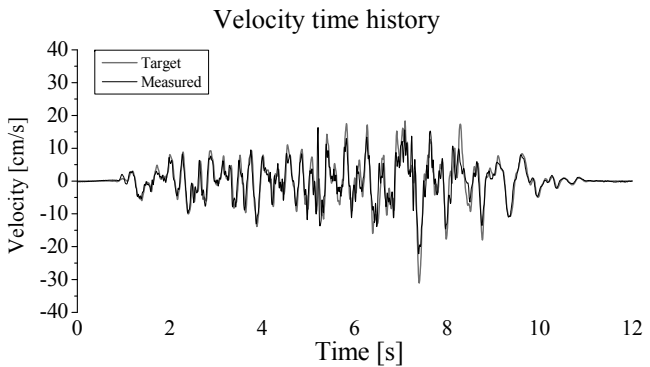
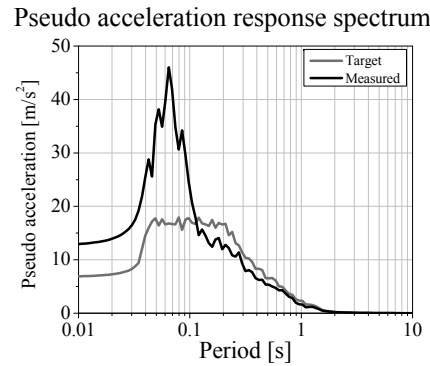
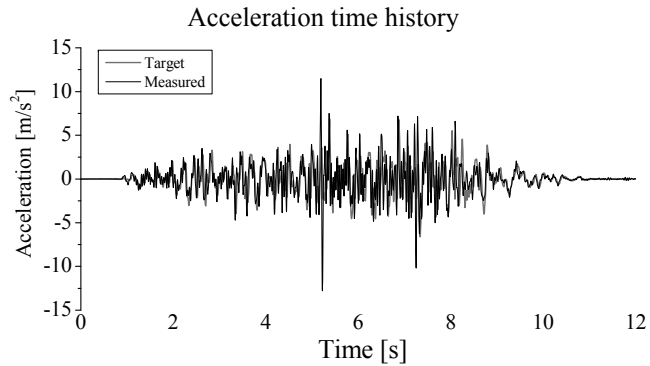


Parameter	Target	Measured	Variation [%]
<i>PGA</i> [m/s ²]	6.776	7.180	6.0
<i>PGV</i> [cm/s]	25.123	21.878	-12.9
<i>PGD</i> [cm]	2.146	1.888	-12.0
<i>PGV/PGA</i> [s ⁻¹]	0.037	0.030	-17.8
<i>PGD/PGA</i> [s ⁻²]	0.003	0.003	-17.0
<i>IA</i> [m/s]	2.812	5.045	79.4
<i>E</i> [kg m ² /s ²]	9985	14732	47.5
<i>CAV</i> [m/s]	11.437	12.719	11.2
<i>SED</i> [m ² /s]	0.028	0.035	24.3
<i>RMS_A</i> [m/s ²]	1.481	1.620	9.4
<i>RMS_V</i> [cm/s]	5.956	5.423	-8.9
<i>RMS_D</i> [cm]	0.553	0.507	-8.3

- PGA* Peak Ground Acceleration
- PGV* Peak Ground Velocity
- PGD* Peak Ground Displacement
- IA* Arias Intensity
- E* Input Energy
- CAV* Cumulative Absolute Velocity
- SED* Specific Energy Density
- RMS_A* Root Mean Square of Acceleration
- RMS_V* Root Mean Square of Velocity
- RMS_D* Root Mean Square of Displacement

Filter: Fourier 0.7 – 25 Hz

A.20. Longitudinal input signal of the strengthened mock-up: Earthquake 150%



Parameter	Target	Measured	Variation [%]
PGA [m/s^2]	6.895	12.800	85.6
PGV [cm/s]	31.113	22.153	-28.8
PGD [cm]	1.966	1.586	-19.3
PGV/PGA [s^{-1}]	0.045	0.017	-61.6
PGD/PGA [s^{-2}]	0.003	0.001	-56.5
IA [m/s]	2.987	5.927	98.5
E [$kg\ m^2/s^2$]	10706	14681	37.1
CAV [m/s]	12.246	13.196	7.8
SED [m^2/s]	0.029	0.031	5.7
RMS_A [m/s^2]	1.527	1.756	15.0
RMS_V [cm/s]	6.025	5.057	-16.1
RMS_D [cm]	0.529	0.420	-20.5

- PGA Peak Ground Acceleration
- PGV Peak Ground Velocity
- PGD Peak Ground Displacement
- IA Arias Intensity
- E Input Energy
- CAV Cumulative Absolute Velocity
- SED Specific Energy Density
- RMS_A Root Mean Square of Acceleration
- RMS_V Root Mean Square of Velocity
- RMS_D Root Mean Square of Displacement

Filter: Fourier 0.7 – 25 Hz

Annex B

Modal updating

B.1 Model 1

	4 Modes					5 Modes				
	-50%	-25%	Base value	+25%	+50%	-50%	-25%	Base value	+25%	+50%
<i>VAR1</i>	Young's modulus of the facades					Young's modulus of the MDF panels				
<i>VAR2</i>	2.50					0.20				
	GPa					GPa				

	4 Modes					5 Modes				
	<i>VAR1</i> -50%	<i>VAR1</i> -25%	Base value	<i>VAR1</i> +25%	<i>VAR1</i> +50%	<i>VAR1</i> -50%	<i>VAR1</i> -25%	Base value	<i>VAR1</i> +25%	<i>VAR1</i> +50%
Average frequency error [%]	3.88	3.85	3.82	3.82	3.84	11.14	11.16	11.13	11.14	11.16
Average <i>MAC</i>	0.897	0.897	0.897	0.897	0.897	0.894	0.894	0.894	0.894	0.894
Updated <i>VAR1</i>	1.05	1.04	1.04	1.04	1.04	1.06	1.06	1.06	1.06	1.06
Updated <i>VAR2</i>	0.14	0.14	0.14	0.14	0.14	0.17	0.16	0.17	0.17	0.17

	4 Modes					5 Modes				
	<i>VAR2</i> -50%	<i>VAR2</i> -25%	Base value	<i>VAR2</i> +25%	<i>VAR2</i> +50%	<i>VAR2</i> -50%	<i>VAR2</i> -25%	Base value	<i>VAR2</i> +25%	<i>VAR2</i> +50%
Average frequency error [%]	3.89	3.93	3.82	3.83	3.85	11.17	11.20	11.13	9.50	11.14
Average <i>MAC</i>	0.897	0.897	0.897	0.897	0.897	0.894	0.894	0.894	0.894	0.894
Updated <i>VAR1</i>	1.04	1.05	1.04	1.04	1.04	1.06	1.06	1.06	1.06	1.06
Updated <i>VAR2</i>	0.14	0.14	0.14	0.14	0.14	0.17	0.17	0.17	0.16	0.17

B.2 Model 2

		Base value		Unit
<i>VAR1</i>	Young's modulus of the facades	1.00		GPa
<i>VAR2</i>	Young's modulus of the gable walls	3.50		GPa
<i>VAR3</i>	Young's modulus of the MDF panels	0.20		GPa

	4 Modes					5 Modes				
	-50%	-25%	Base value	+25%	+50%	-50%	-25%	Base value	+25%	+50%
Average frequency error [%]	1.38	1.34	1.31	1.62	1.39	7.04	5.32	7.23	6.22	15.91
Average <i>MAC</i>	0.892	0.892	0.892	0.892	0.892	0.896	0.896	0.896	0.896	0.896
Updated <i>VAR1</i>	0.67	0.67	0.67	0.69	0.68	0.60	0.71	0.73	0.67	1.01
Updated <i>VAR2</i>	3.09	3.15	3.17	3.17	3.17	2.88	3.43	3.78	3.88	4.18
Updated <i>VAR3</i>	0.15	0.15	0.15	0.15	0.15	0.14	0.17	0.19	0.19	0.20

	4 Modes					5 Modes				
	<i>VAR1</i> -50%	<i>VAR1</i> -25%	Base value	<i>VAR1</i> +25%	<i>VAR1</i> +50%	<i>VAR1</i> -50%	<i>VAR1</i> -25%	Base value	<i>VAR1</i> +25%	<i>VAR1</i> +50%
Average frequency error [%]	1.34	1.64	1.31	1.58	7.76	7.35	8.55	7.23	4.15	10.41
Average <i>MAC</i>	0.892	0.892	0.892	0.892	0.893	0.903	0.896	0.896	0.896	0.893
Updated <i>VAR1</i>	0.67	0.66	0.67	0.66	0.95	0.57	0.76	0.73	0.60	1.04
Updated <i>VAR2</i>	3.14	3.11	3.17	3.18	3.06	2.82	3.89	3.78	3.49	3.18
Updated <i>VAR3</i>	0.15	0.15	0.15	0.15	0.14	0.21	0.19	0.19	0.17	0.14

	4 Modes					5 Modes				
	<i>VAR2</i> -50%	<i>VAR2</i> -25%	Base value	<i>VAR2</i> +25%	<i>VAR2</i> +50%	<i>VAR2</i> -50%	<i>VAR2</i> -25%	Base value	<i>VAR2</i> +25%	<i>VAR2</i> +50%
Average frequency error [%]	1.33	1.73	1.31	1.51	1.40	6.87	6.53	7.23	15.66	17.51
Average <i>MAC</i>	0.892	0.892	0.892	0.892	0.892	0.895	0.896	0.896	0.897	0.897
Updated <i>VAR1</i>	0.67	0.66	0.67	0.66	0.66	0.87	0.74	0.73	0.98	0.92
Updated <i>VAR2</i>	3.17	3.10	3.17	3.18	3.18	3.06	3.53	3.78	4.27	4.76
Updated <i>VAR3</i>	0.15	0.15	0.15	0.15	0.15	0.14	0.17	0.19	0.21	0.24

	4 Modes					5 Modes				
	<i>VAR3</i> -50%	<i>VAR3</i> -25%	Base value	<i>VAR3</i> +25%	<i>VAR3</i> +50%	<i>VAR3</i> -50%	<i>VAR3</i> -25%	Base value	<i>VAR3</i> +25%	<i>VAR3</i> +50%
Average frequency error [%]	1.83	1.62	1.31	6.46	1.32	3.92	11.04	7.23	8.91	6.67
Average <i>MAC</i>	0.893	0.892	0.892	0.893	0.892	0.896	0.895	0.896	0.895	0.896
Updated <i>VAR1</i>	0.71	0.69	0.67	0.86	0.67	0.69	0.99	0.73	0.91	0.72
Updated <i>VAR2</i>	3.08	3.16	3.17	3.17	3.19	3.17	3.45	3.78	3.33	3.66
Updated <i>VAR3</i>	0.15	0.15	0.15	0.15	0.15	0.15	0.16	0.19	0.16	0.18

B.3 Model 3

	Base value		Unit
<i>VAR1</i>	Young's modulus of the facades		GPa
<i>VAR2</i>	Young's modulus of the gable walls		GPa
<i>VAR3</i>	Young's modulus of the MDF panels		GPa
<i>VAR4</i>	Young's modulus of the corners		GPa

	4 Modes					5 Modes				
	-50%	-25%	Base value	+25%	+50%	-50%	-25%	Base value	+25%	+50%
Average frequency error [%]	1.93	2.32	1.40	1.79	1.80	7.88	3.59	5.86	12.38	15.43
Average <i>MAC</i>	0.894	0.893	0.892	0.892	0.891	0.896	0.895	0.894	0.895	0.895
Updated <i>VAR1</i>	0.75	0.67	0.67	0.68	0.69	0.56	0.64	0.69	0.95	1.03
Updated <i>VAR2</i>	2.97	3.27	3.27	3.21	3.15	2.87	3.45	3.80	4.21	4.38
Updated <i>VAR3</i>	0.14	0.15	0.15	0.15	0.15	0.13	0.16	0.18	0.20	0.21
Updated <i>VAR4</i>	0.68	1.79	1.79	2.49	3.16	2.39	2.05	1.91	1.32	1.51

	4 Modes					5 Modes				
	<i>VAR1</i> -50%	<i>VAR1</i> -25%	Base value	<i>VAR1</i> +25%	<i>VAR1</i> +50%	<i>VAR1</i> -50%	<i>VAR1</i> -25%	Base value	<i>VAR1</i> +25%	<i>VAR1</i> +50%
Average frequency error [%]	1.59	2.57	1.40	1.95	2.73	5.79	6.38	5.86	10.33	10.92
Average <i>MAC</i>	0.893	0.893	0.892	0.893	0.893	0.896	0.895	0.894	0.894	0.893
Updated <i>VAR1</i>	0.69	0.73	0.67	0.70	0.74	0.67	0.72	0.69	0.94	1.02
Updated <i>VAR2</i>	3.27	3.23	3.27	3.31	3.34	3.78	3.93	3.80	3.84	3.64
Updated <i>VAR3</i>	0.15	0.15	0.15	0.15	0.15	0.18	0.18	0.18	0.18	0.17
Updated <i>VAR4</i>	1.67	1.78	1.79	1.66	1.32	2.40	1.27	1.91	1.17	1.15

	4 Modes					5 Modes				
	<i>VAR2</i> -50%	<i>VAR2</i> -25%	Base value	<i>VAR2</i> +25%	<i>VAR2</i> +50%	<i>VAR2</i> -50%	<i>VAR2</i> -25%	Base value	<i>VAR2</i> +25%	<i>VAR2</i> +50%
Average frequency error [%]	3.24	4.21	1.40	1.63	1.92	7.18	11.62	5.86	14.47	17.23
Average <i>MAC</i>	0.893	0.894	0.892	0.892	0.892	0.893	0.896	0.894	0.895	0.895
Updated <i>VAR1</i>	0.76	0.94	0.67	0.64	0.68	0.89	0.74	0.69	0.99	0.95
Updated <i>VAR2</i>	3.32	3.16	3.27	3.23	3.29	3.25	3.53	3.80	4.34	4.92
Updated <i>VAR3</i>	0.15	0.15	0.15	0.15	0.15	0.14	0.17	0.18	0.20	0.23
Updated <i>VAR4</i>	1.27	0.50	1.79	2.28	2.33	1.48	1.50	1.91	1.51	1.55

	4 Modes					5 Modes				
	<i>VAR3</i> -50%	<i>VAR3</i> -25%	Base value	<i>VAR3</i> +25%	<i>VAR3</i> +50%	<i>VAR3</i> -50%	<i>VAR3</i> -25%	Base value	<i>VAR3</i> +25%	<i>VAR3</i> +50%
Average frequency error [%]	1.57	2.95	1.40	4.90	7.10	4.29	10.12	5.86	9.15	6.57
Average <i>MAC</i>	0.892	0.893	0.892	0.893	0.894	0.895	0.893	0.894	0.894	0.895
Updated <i>VAR1</i>	0.67	0.73	0.67	0.73	1.00	0.65	0.99	0.69	0.94	0.72
Updated <i>VAR2</i>	3.17	3.30	3.27	3.30	3.35	3.23	3.47	3.80	3.63	3.91
Updated <i>VAR3</i>	0.15	0.15	0.15	0.15	0.16	0.15	0.15	0.18	0.17	0.18
Updated <i>VAR4</i>	2.32	1.68	1.79	1.68	0.51	1.70	1.56	1.91	0.99	1.39

	4 Modes					5 Modes				
	<i>VAR4</i> -50%	<i>VAR4</i> -25%	Base value	<i>VAR4</i> +25%	<i>VAR4</i> +50%	<i>VAR4</i> -50%	<i>VAR4</i> -25%	Base value	<i>VAR4</i> +25%	<i>VAR4</i> +50%
Average frequency error [%]	1.56	1.52	1.40	1.44	1.49	6.36	5.72	5.86	6.14	6.38
Average <i>MAC</i>	0.893	0.893	0.892	0.892	0.892	0.895	0.895	0.894	0.895	0.895
Updated <i>VAR1</i>	0.71	0.69	0.67	0.66	0.65	0.71	0.69	0.69	0.70	0.71
Updated <i>VAR2</i>	3.34	3.31	3.27	3.24	3.23	3.80	3.79	3.80	3.86	3.91
Updated <i>VAR3</i>	0.15	0.15	0.15	0.15	0.15	0.18	0.18	0.18	0.18	0.18
Updated <i>VAR4</i>	1.10	1.46	1.79	2.12	2.42	1.91	1.82	1.91	1.56	1.44

B.4 Model 4

	Base value		Unit
<i>VAR1</i>	Young's modulus of the facades		1.00 GPa
<i>VAR2</i>	Young's modulus of the gable walls		3.50 GPa
<i>VAR3</i>	Young's modulus of the MDF panels		0.20 GPa
<i>VAR4</i>	Stiffness of the springs		100 kN/m

	5 Modes					5 Modes				
	-50%	-25%	Base value	+25%	+50%	<i>VAR1</i> -50%	<i>VAR1</i> -25%	Base value	<i>VAR1</i> +25%	<i>VAR1</i> +50%
Average frequency error [%]	5.19	5.14	5.13	5.08	4.61	8.33	7.83	5.13	5.14	4.95
Average <i>MAC</i>	0.901	0.901	0.901	0.901	0.901	0.897	0.896	0.901	0.901	0.901
Updated <i>VAR1</i>	0.62	0.62	0.62	0.63	0.65	0.58	0.75	0.62	0.62	0.64
Updated <i>VAR2</i>	3.00	3.03	3.04	3.07	3.09	3.39	3.50	3.04	3.03	3.05
Updated <i>VAR3</i>	0.24	0.24	0.24	0.24	0.22	0.23	0.20	0.24	0.24	0.24
Updated <i>VAR4</i>	300.00	305.51	306.64	310.31	372.54	110.24	99.98	306.64	305.89	311.10

	5 Modes					5 Modes				
	<i>VAR2</i> -50%	<i>VAR2</i> -25%	Base value	<i>VAR2</i> +25%	<i>VAR2</i> +50%	<i>VAR3</i> -50%	<i>VAR3</i> -25%	Base value	<i>VAR3</i> +25%	<i>VAR3</i> +50%
Average frequency error [%]	5.41	5.11	5.13	9.19	6.53	5.13	5.18	5.13	5.11	4.87
Average <i>MAC</i>	0.901	0.901	0.901	0.896	0.896	0.901	0.902	0.901	0.901	0.901
Updated <i>VAR1</i>	0.72	0.62	0.62	0.92	0.71	0.62	0.64	0.62	0.63	0.62
Updated <i>VAR2</i>	2.84	3.04	3.04	4.06	4.44	3.01	2.94	3.04	3.03	3.07
Updated <i>VAR3</i>	0.20	0.24	0.24	0.25	0.27	0.24	0.24	0.24	0.24	0.22
Updated <i>VAR4</i>	330.16	309.61	306.64	107.66	158.03	307.99	276.57	306.64	304.33	367.15

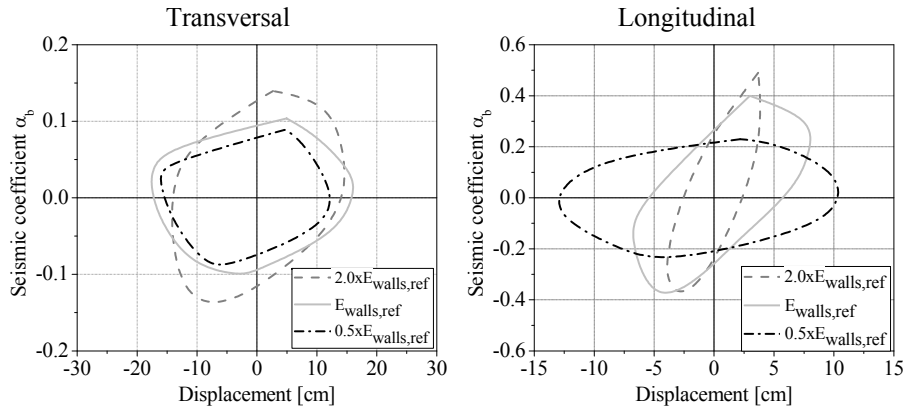
	5 Modes				
	<i>VAR4</i> -50%	<i>VAR4</i> -25%	Base value	<i>VAR4</i> +25%	<i>VAR4</i> +50%
Average frequency error [%]	7.85	6.39	5.13	4.83	4.69
Average <i>MAC</i>	0.898	0.899	0.901	0.901	0.901
Updated <i>VAR1</i>	0.68	0.67	0.62	0.63	0.64
Updated <i>VAR2</i>	3.41	3.35	3.04	3.08	3.08
Updated <i>VAR3</i>	0.26	0.00	0.24	0.23	0.22
Updated <i>VAR4</i>	96.33	129.06	306.64	345.95	380.67

Annex C

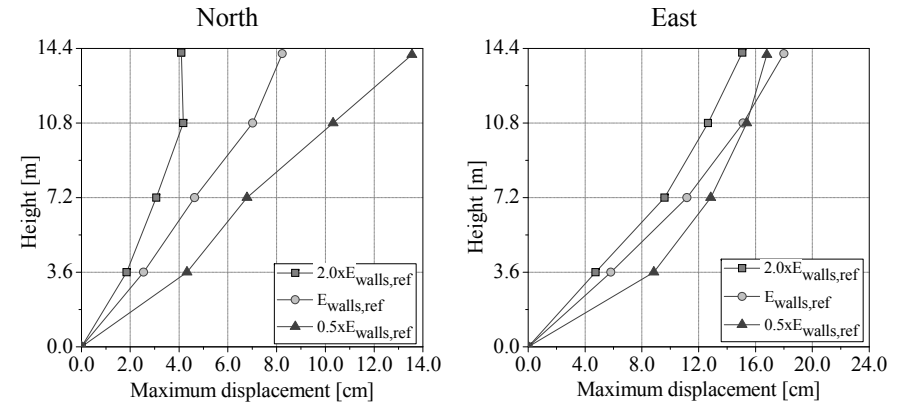
Non-linear dynamic parametric analysis

C.1 Stiffness of the masonry walls

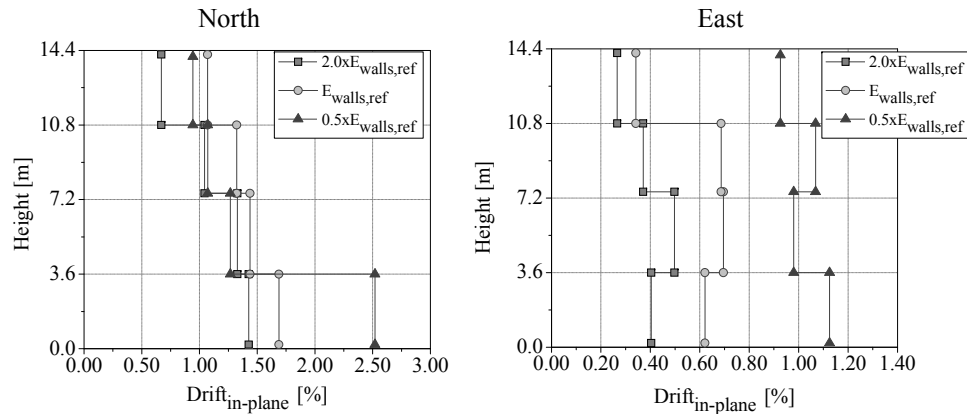
Envelope of the response in each direction:



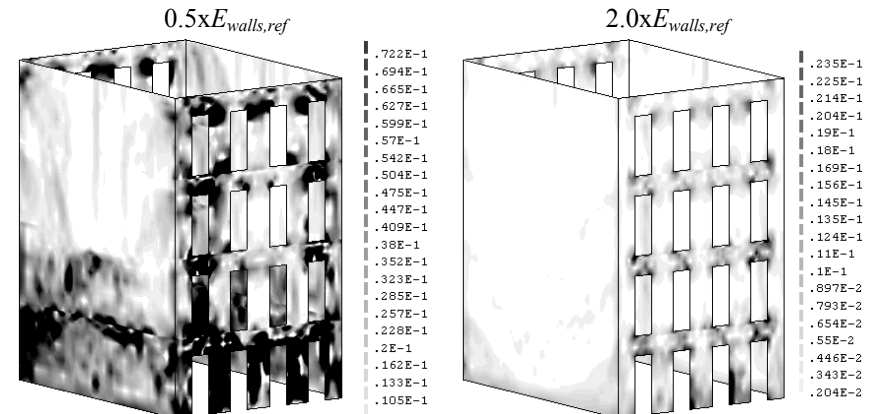
Maximum out-of-plane displacement at the middle of the wall:



Maximum in-plane drift of the wall:

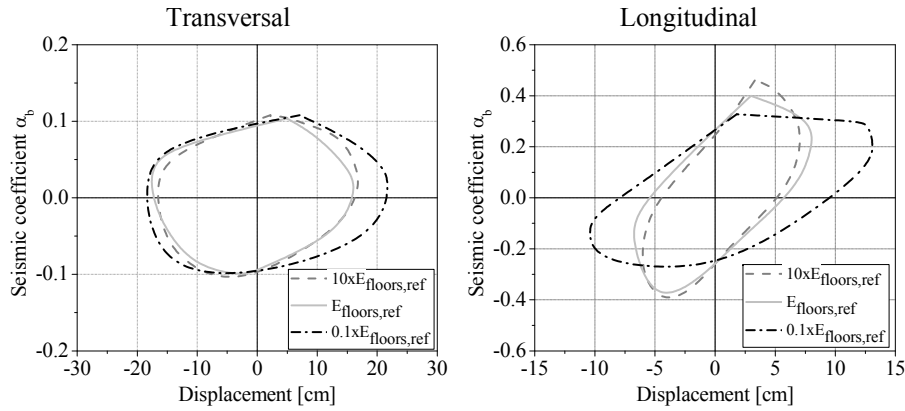


Maximum tensile principal strains at the external surface:

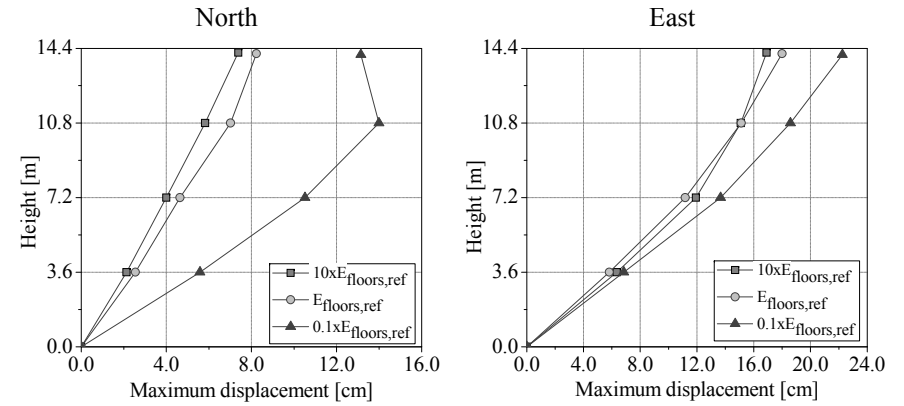


C.2 Stiffness of the timber floors

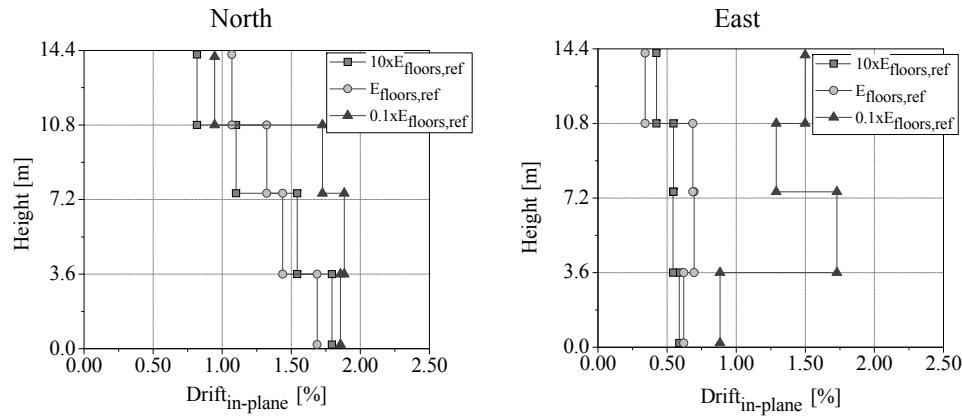
Envelope of the response in each direction:



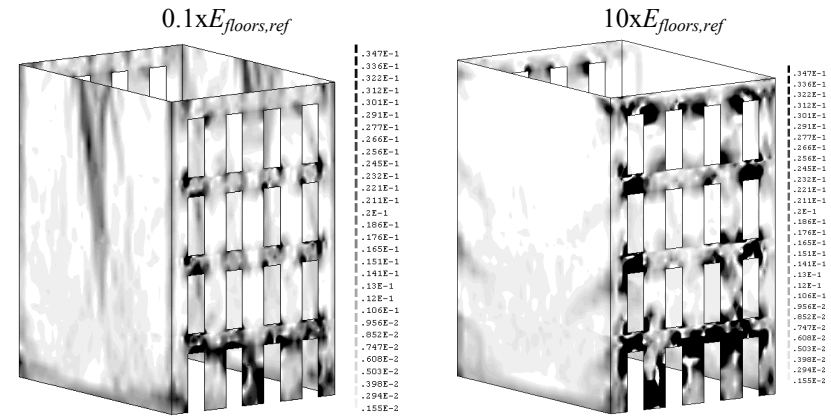
Maximum out-of-plane displacement at the middle of the wall:



Maximum in-plane drift of the wall:

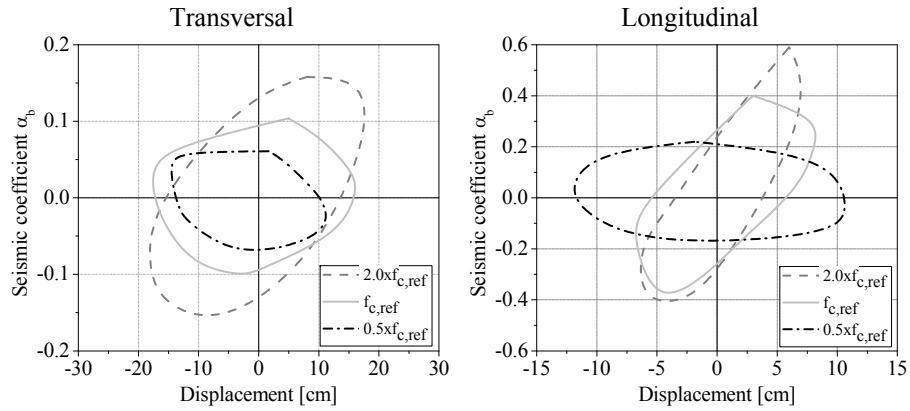


Maximum tensile principal strains at the external surface:

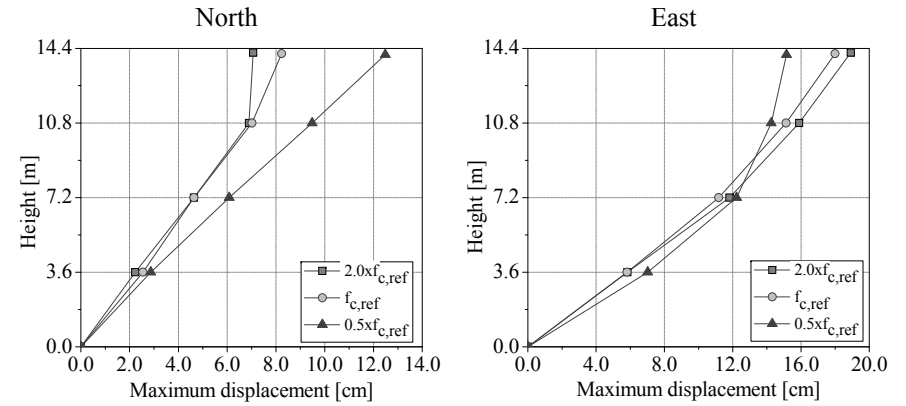


C.3 Compressive strength

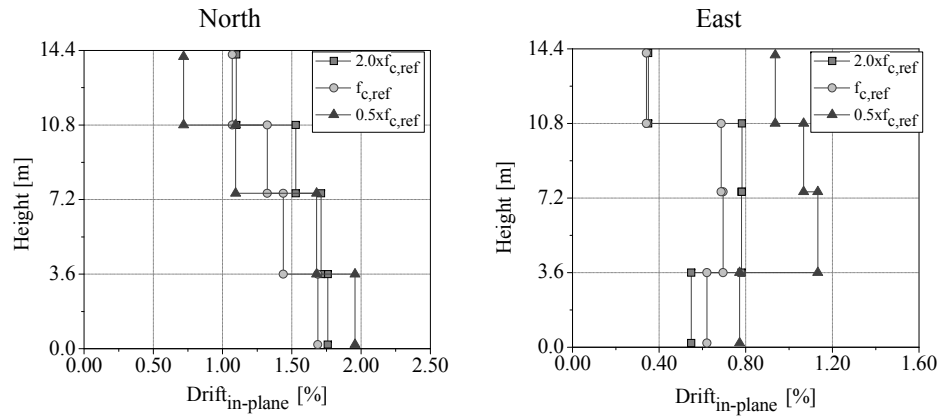
Envelope of the response in each direction:



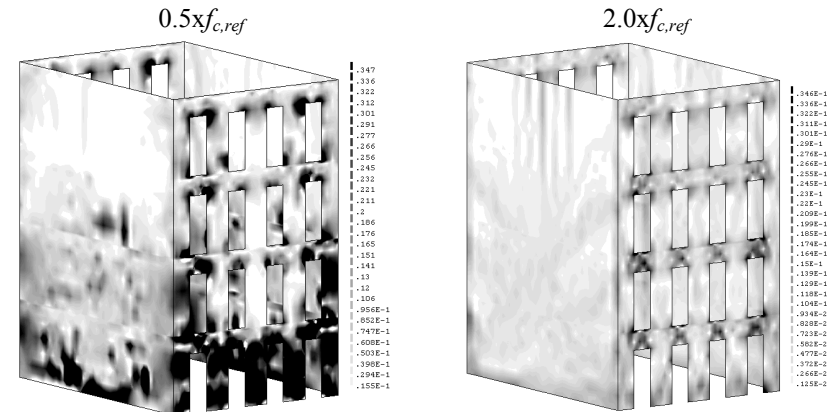
Maximum out-of-plane displacement at the middle of the wall:



Maximum in-plane drift of the wall:

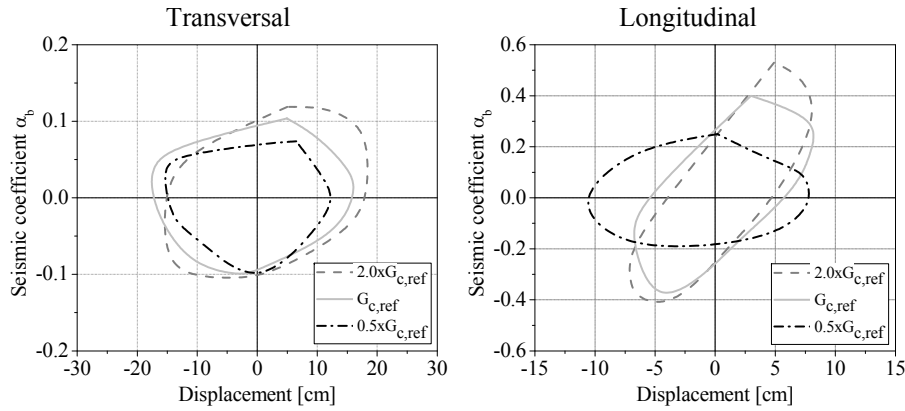


Maximum tensile principal strains at the external surface:

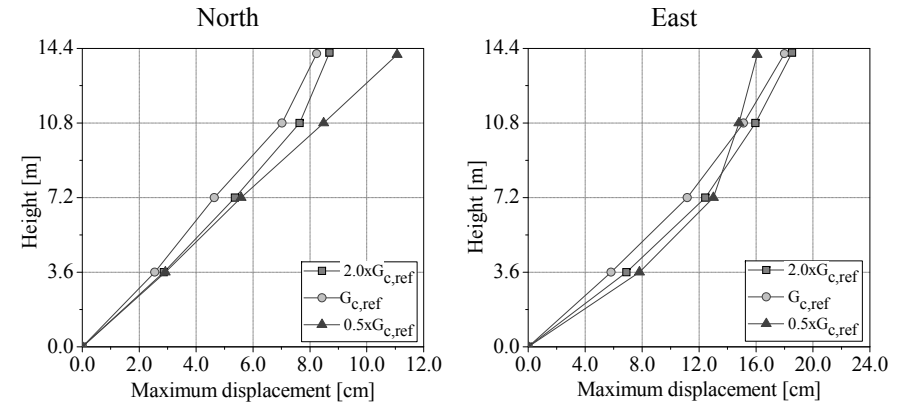


C.4 Compressive fracture energy

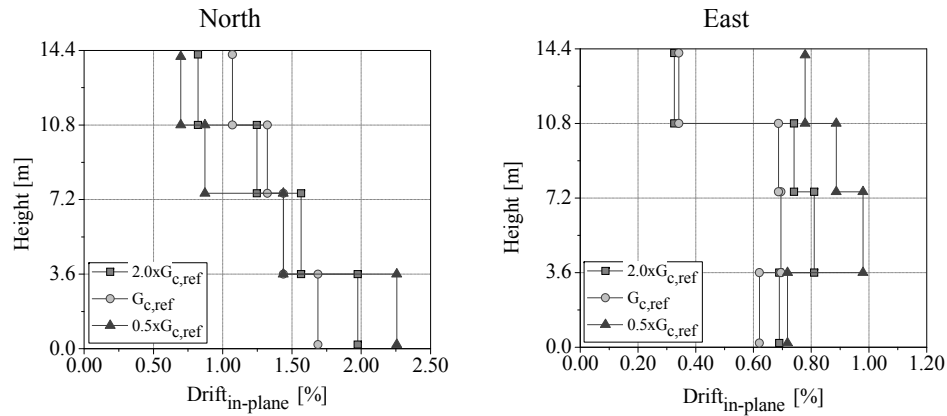
Envelope of the response in each direction:



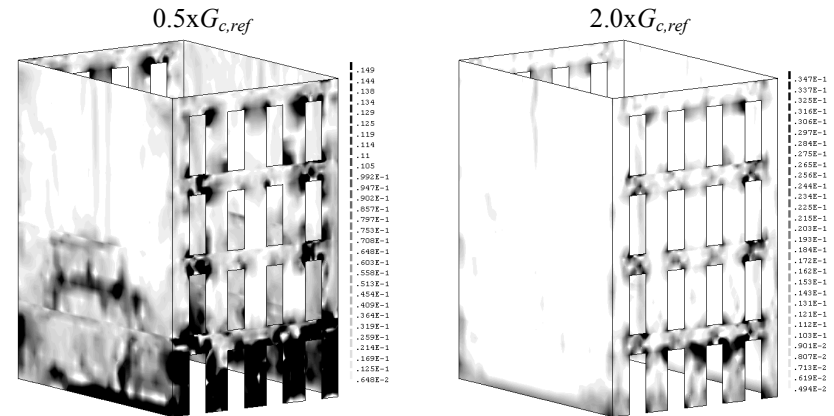
Maximum out-of-plane displacement at the middle of the wall:



Maximum in-plane drift of the wall:

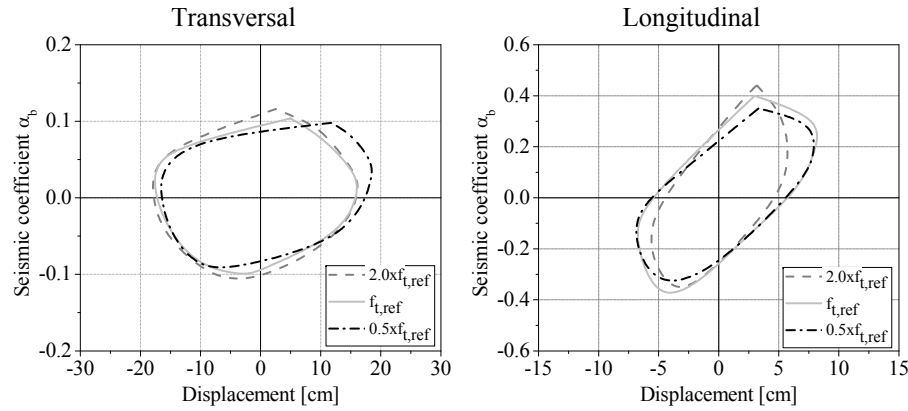


Maximum tensile principal strains at the external surface:

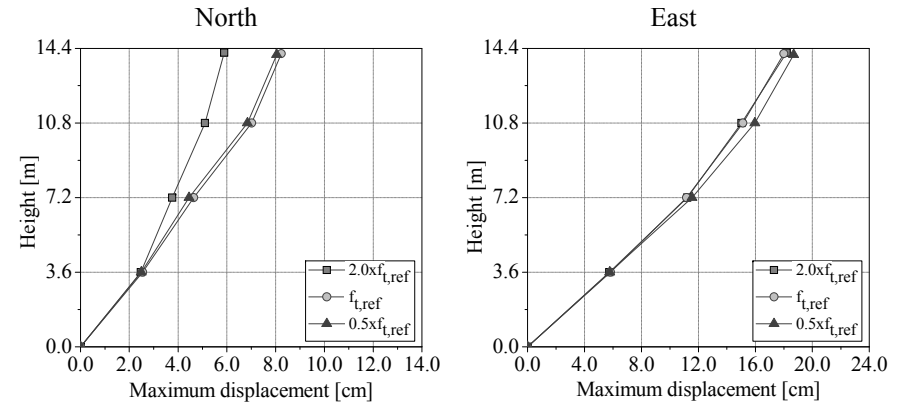


C.5 Tensile strength

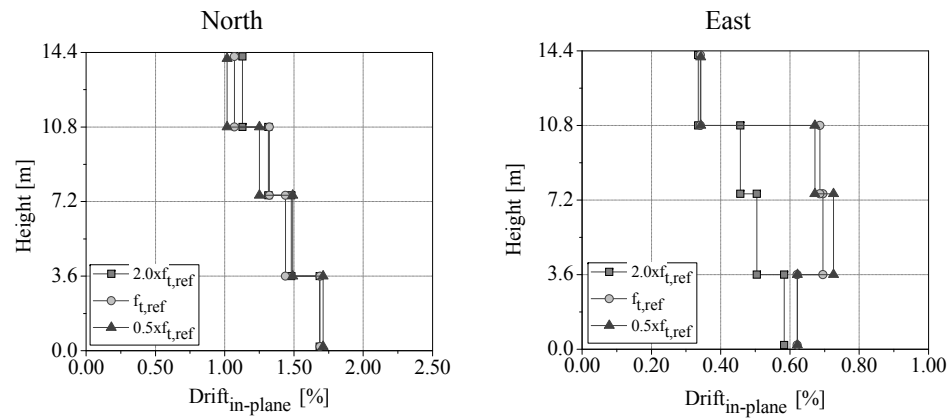
Envelope of the response in each direction:



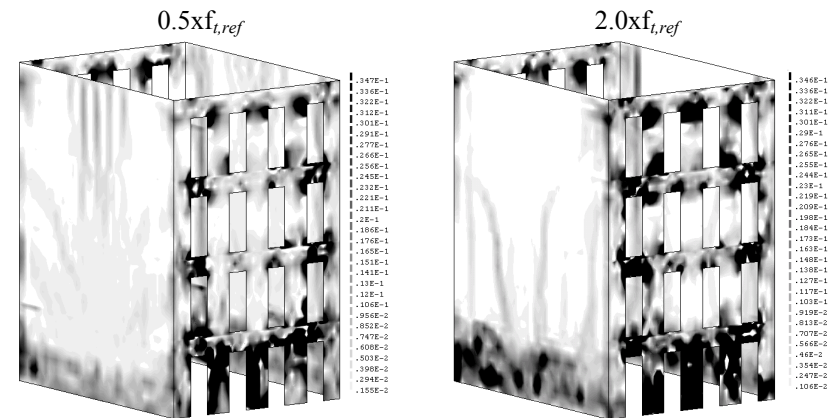
Maximum out-of-plane displacement at the middle of the wall:



Maximum in-plane drift of the wall:

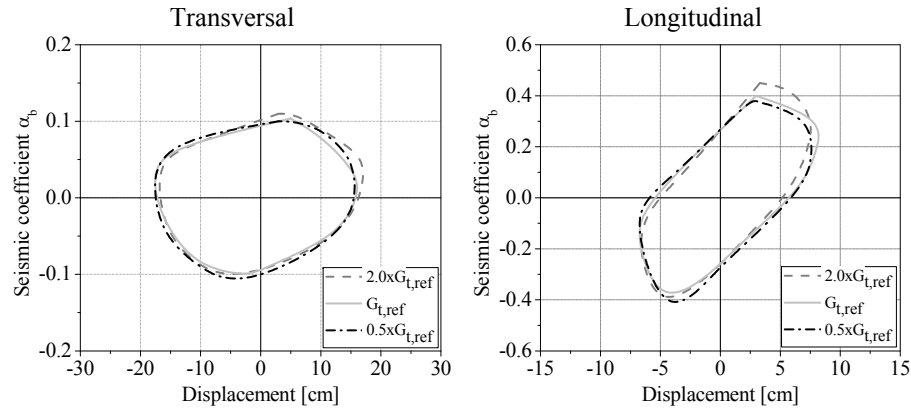


Maximum tensile principal strains at the external surface:

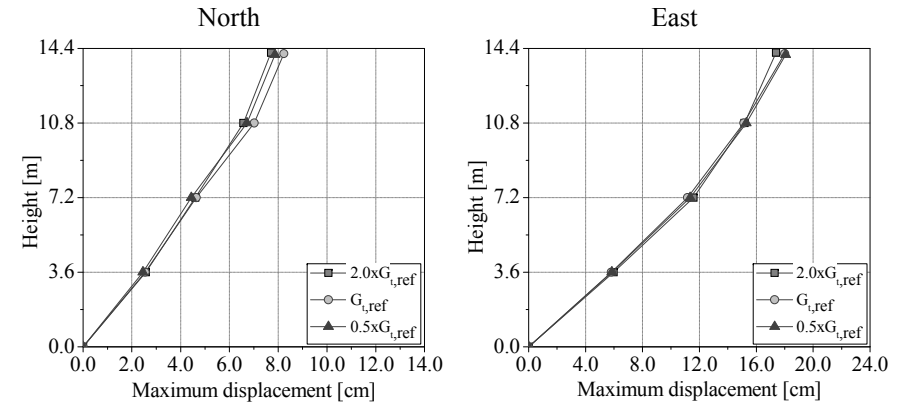


C.6 Tensile fracture energy

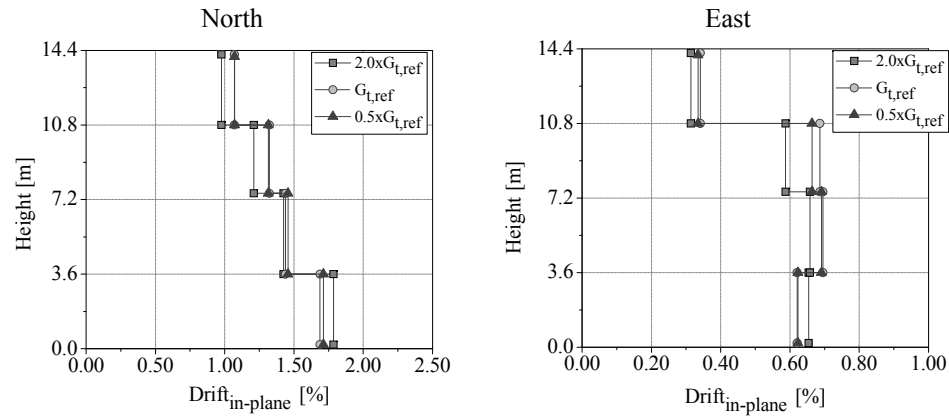
Envelope of the response in each direction:



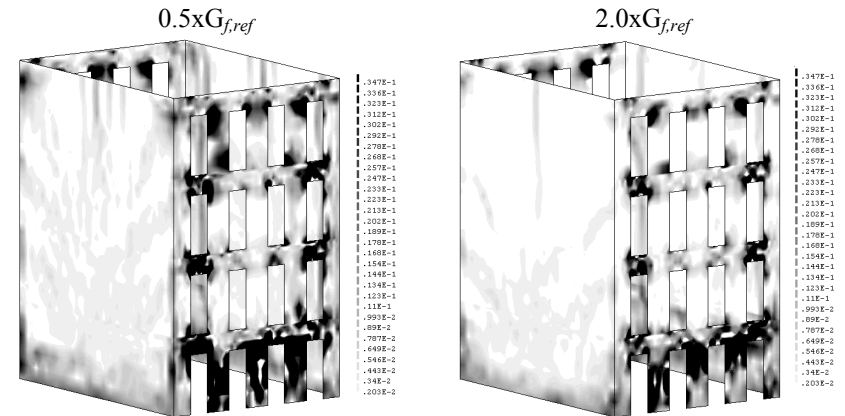
Maximum out-of-plane displacement at the middle of the wall:



Maximum in-plane drift of the wall:

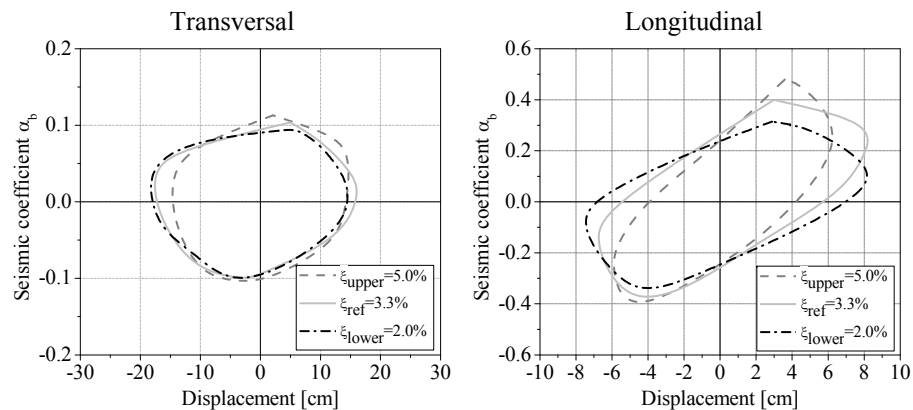


Maximum tensile principal strains at the external surface:

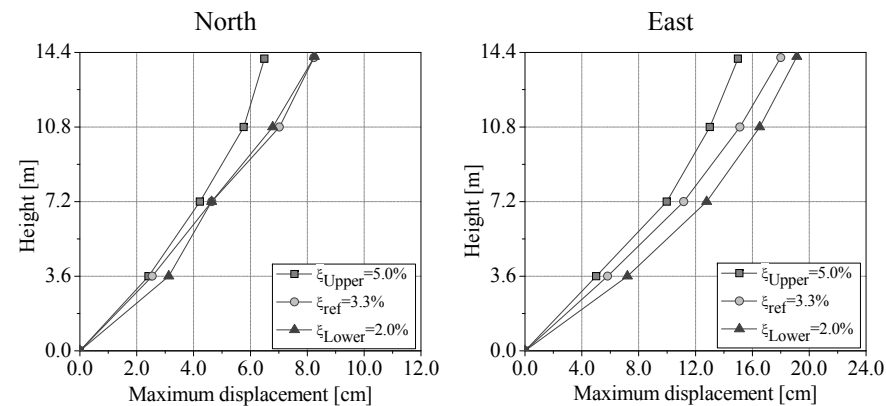


C.7 Damping ratio

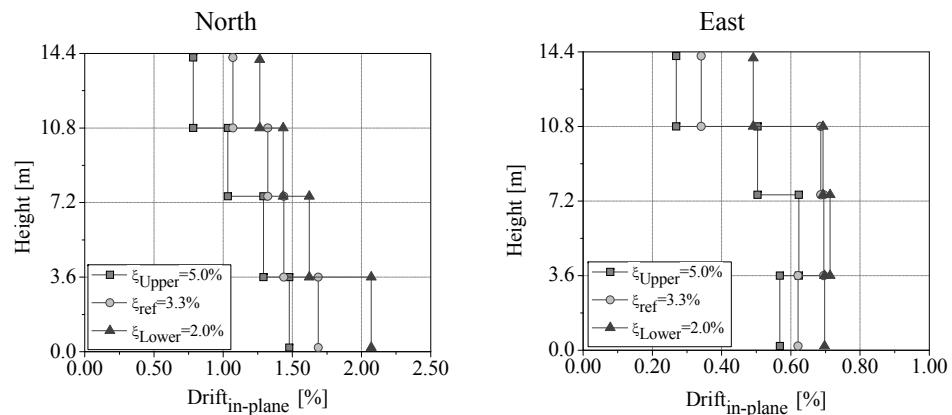
Envelope of the response in each direction:



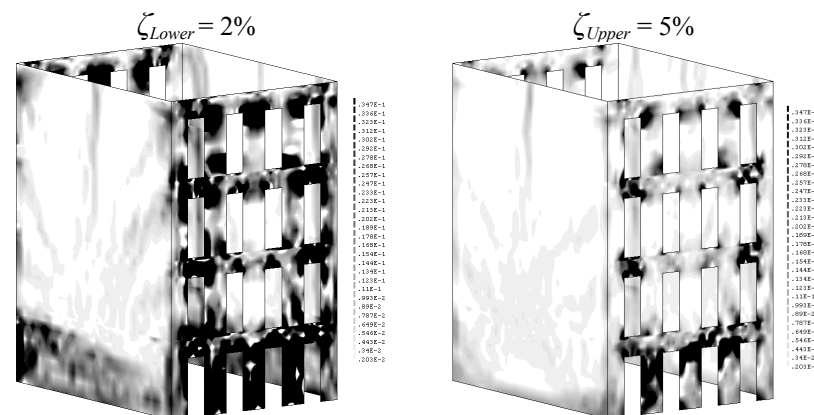
Maximum out-of-plane displacement at the middle of the wall:



Maximum in-plane drift of the wall:

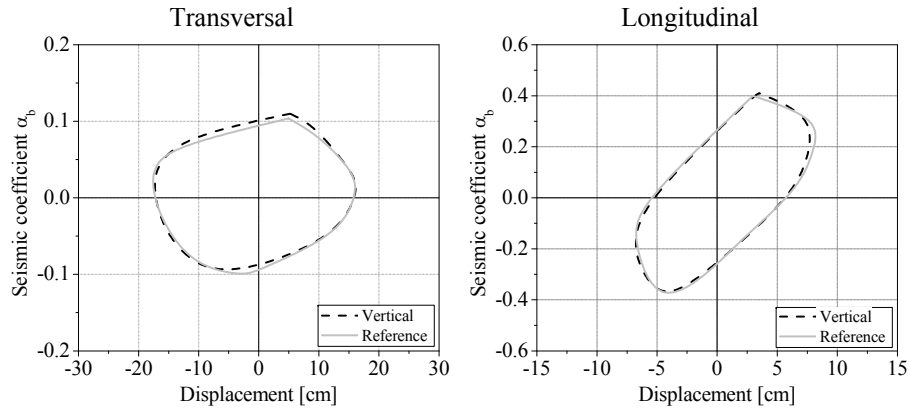


Maximum tensile principal strains at the external surface:

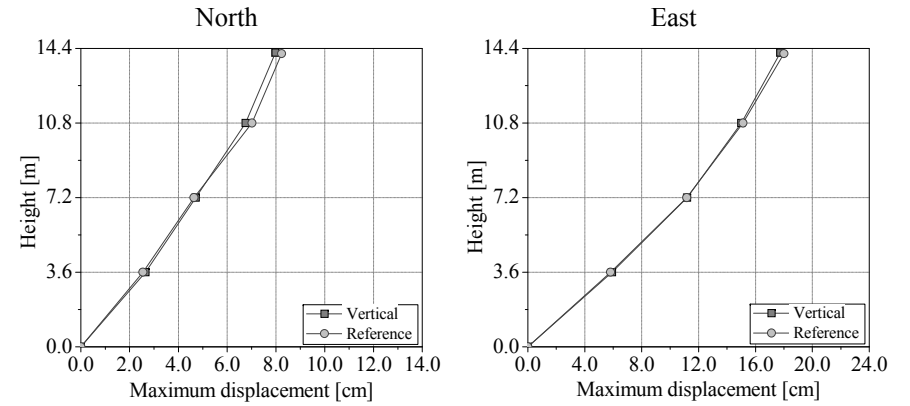


C.8 Vertical earthquake

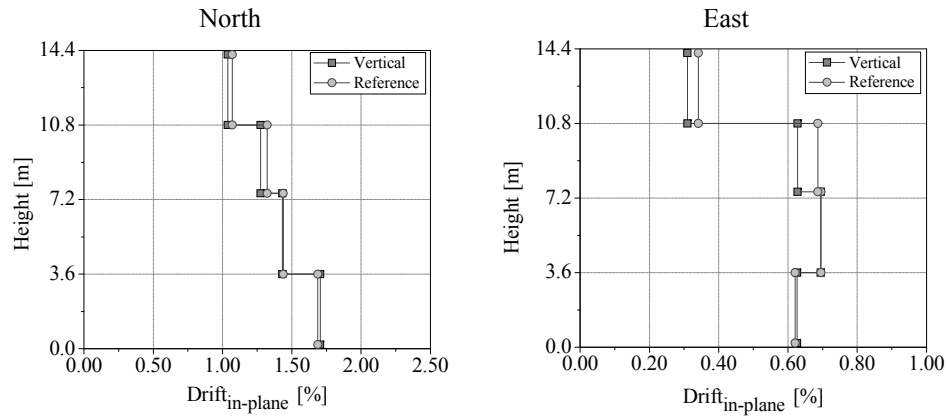
Envelope of the response in each direction:



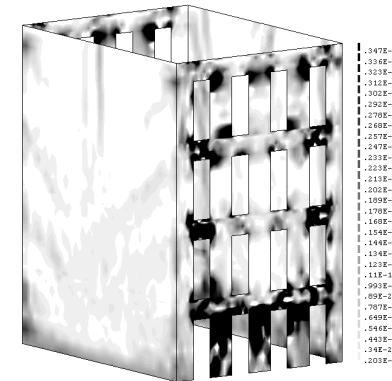
Maximum out-of-plane displacement at the middle of the wall:



Maximum in-plane drift of the wall:



Maximum tensile principal strains at the external surface:

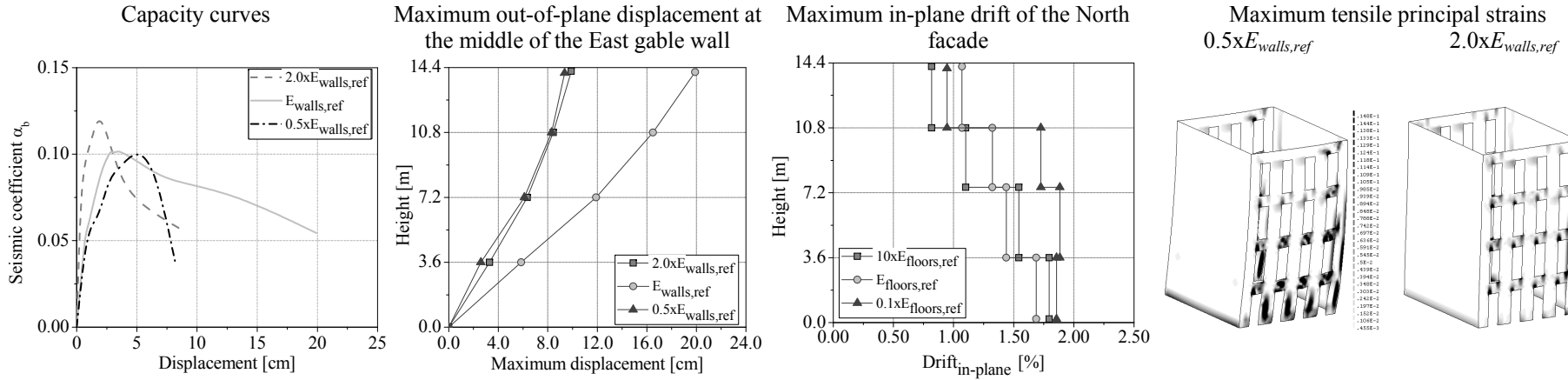


Annex D

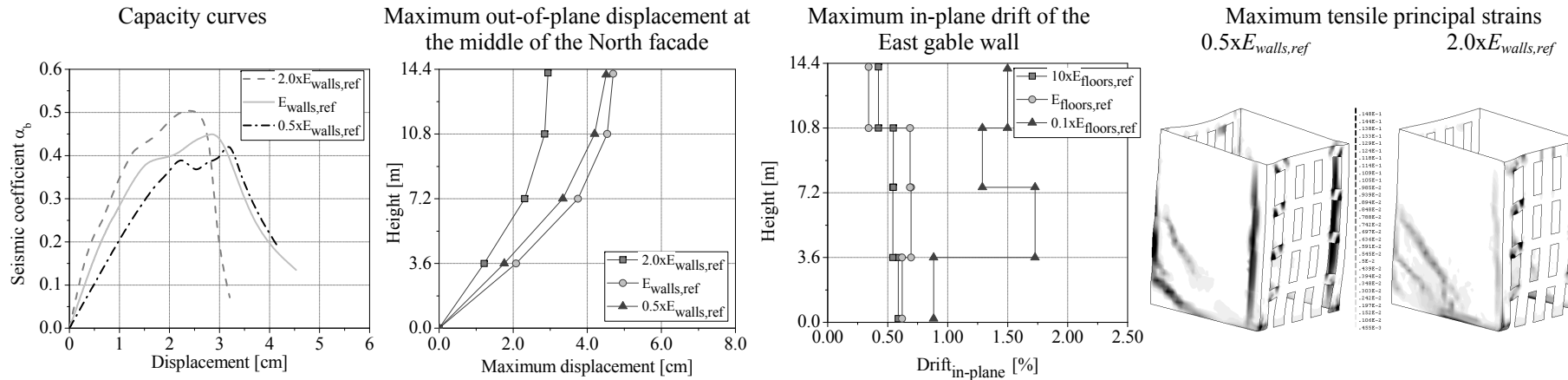
Pushover parametric analysis

D.1 Stiffness of the masonry walls

Pushover analyses in the transversal direction

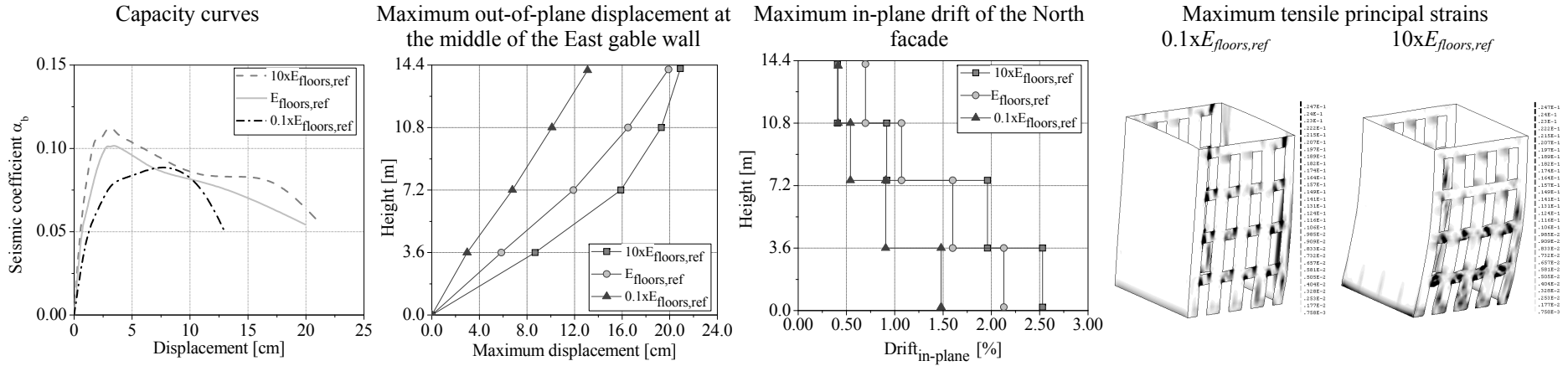


Pushover analyses in the longitudinal direction

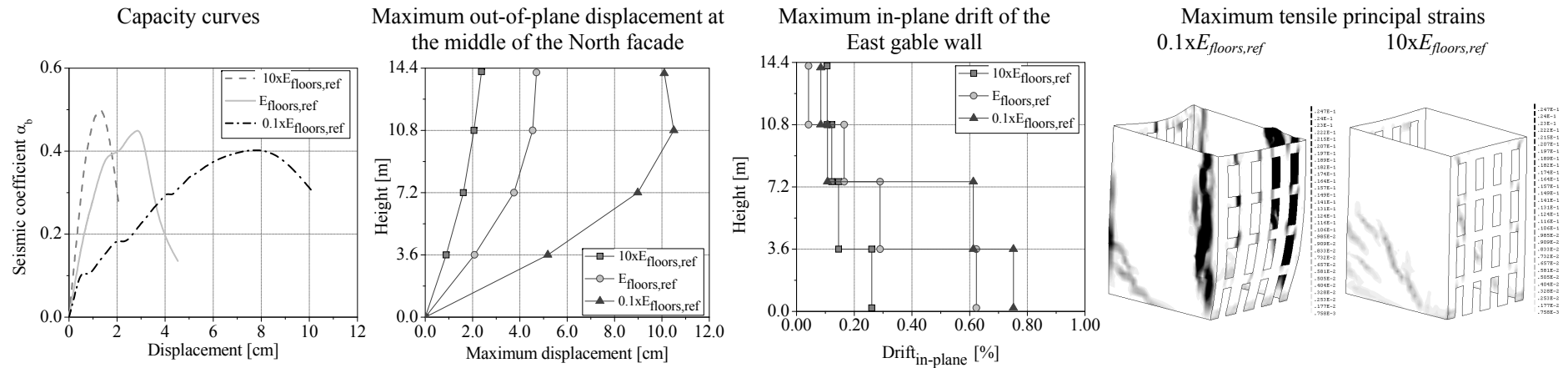


D.2 Stiffness of the timber floors

Pushover analyses in the transversal direction

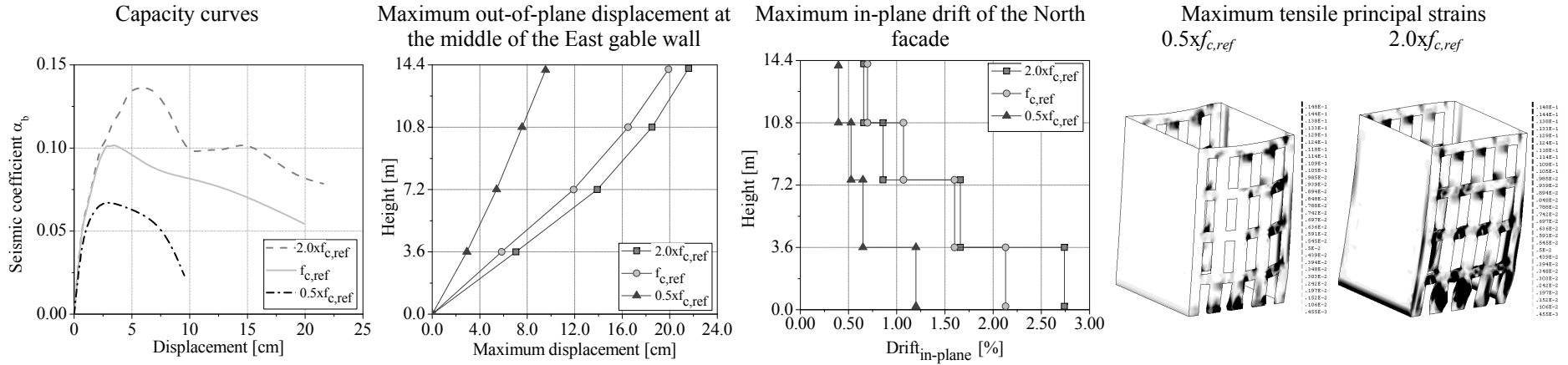


Pushover analyses in the longitudinal direction

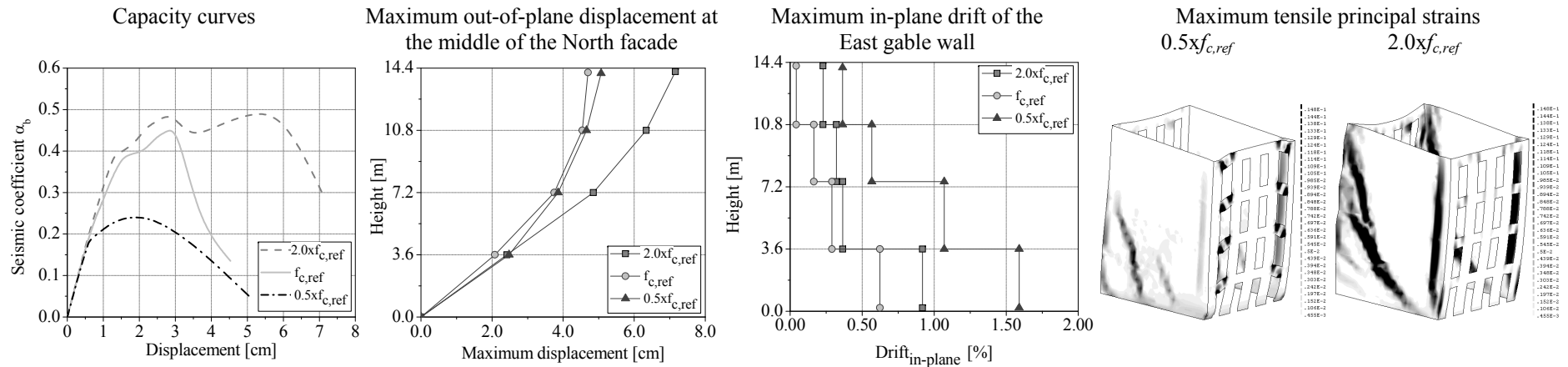


D.3 Compressive strength

Pushover analyses in the transversal direction

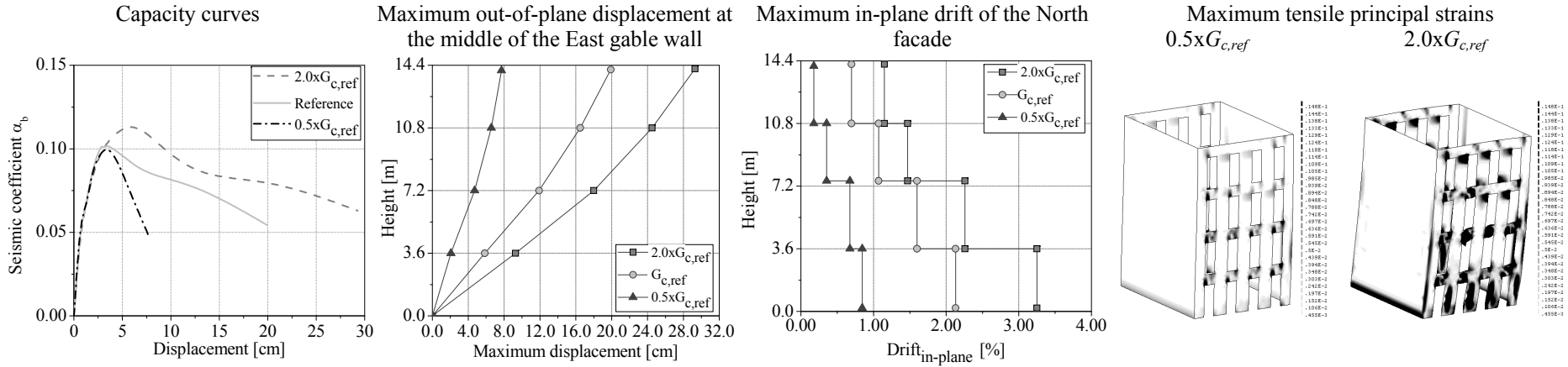


Pushover analyses in the longitudinal direction

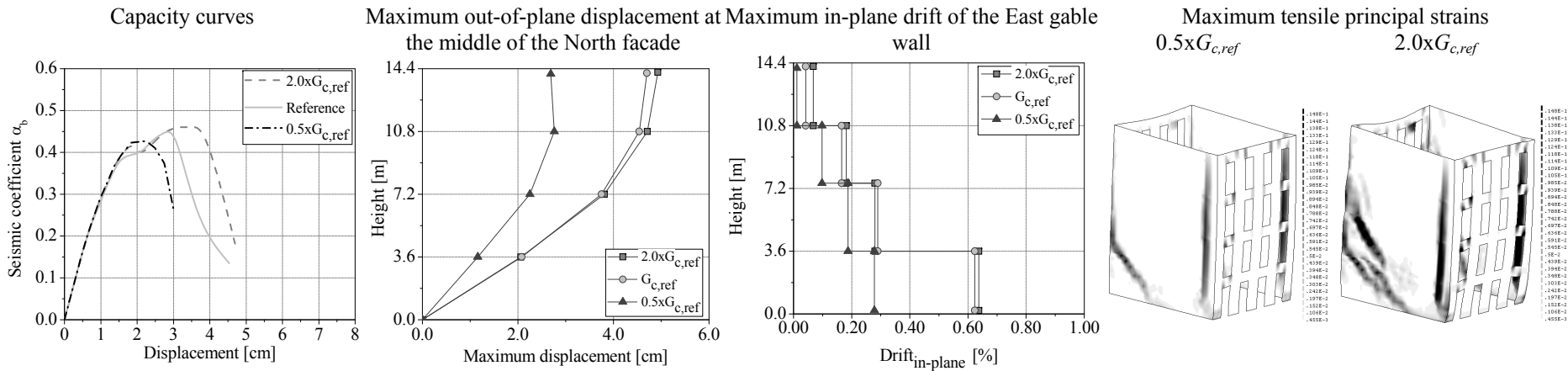


D.4 Compressive fracture energy

Pushover analyses in the transversal direction

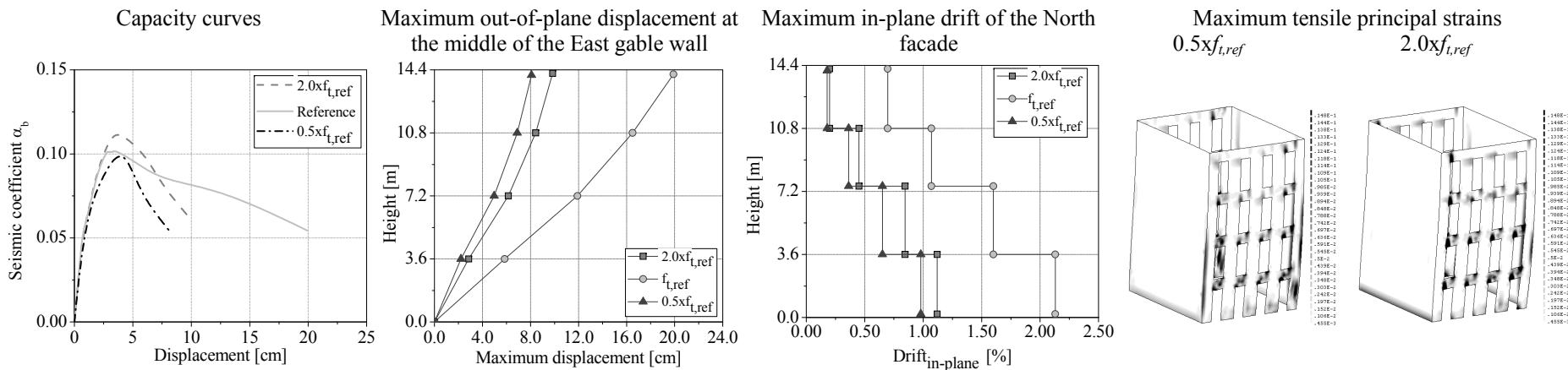


Pushover analyses in the longitudinal direction

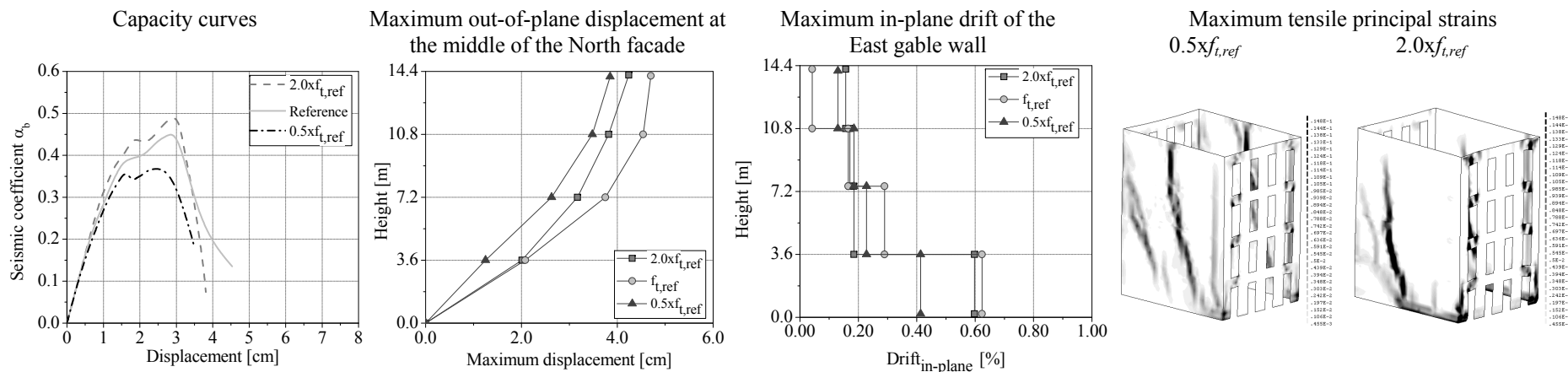


D.5 Tensile strength

Pushover analyses in the transversal direction

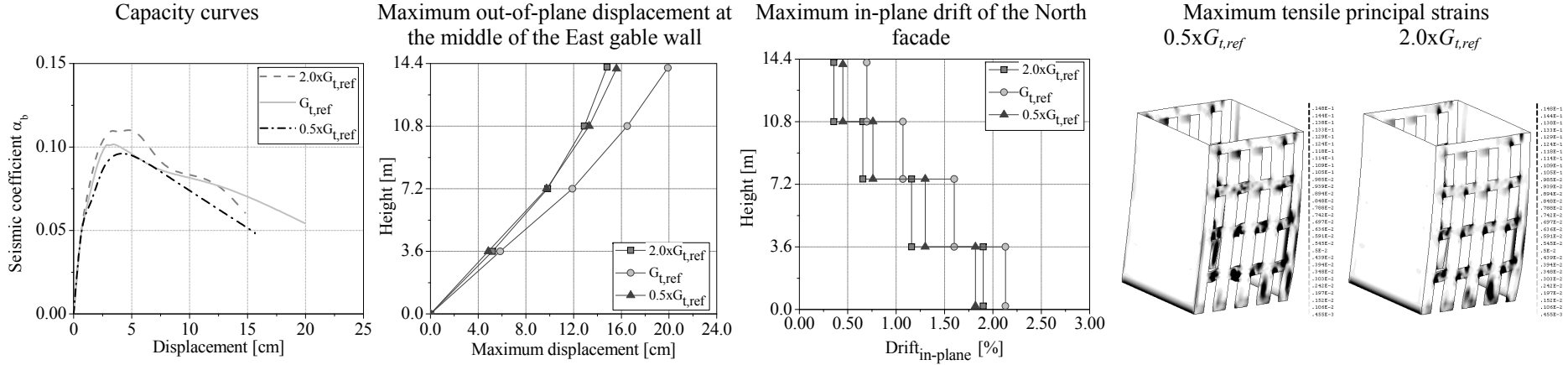


Pushover analyses in the longitudinal direction

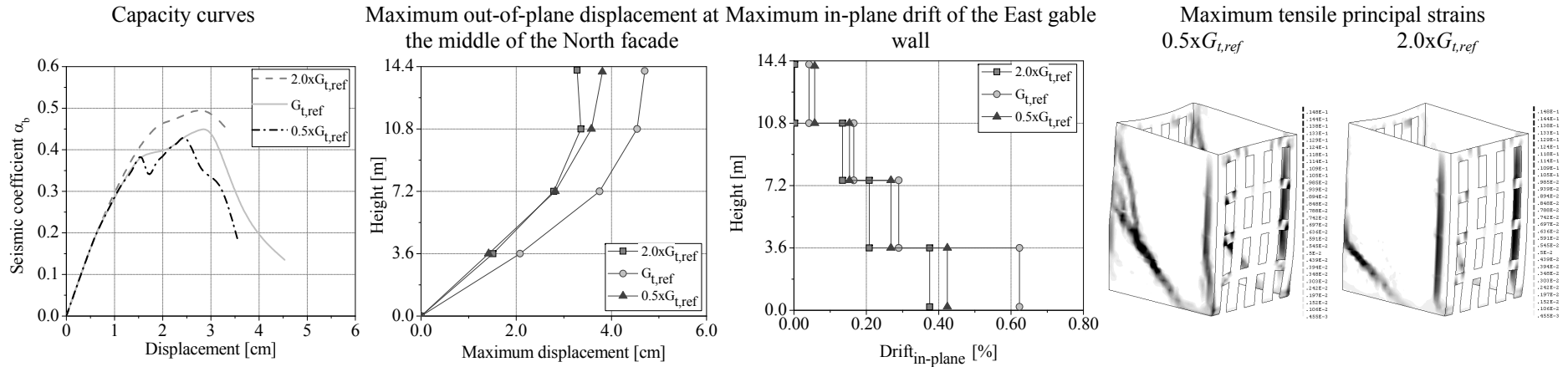


D.6 Tensile fracture energy

Pushover analyses in the transversal direction

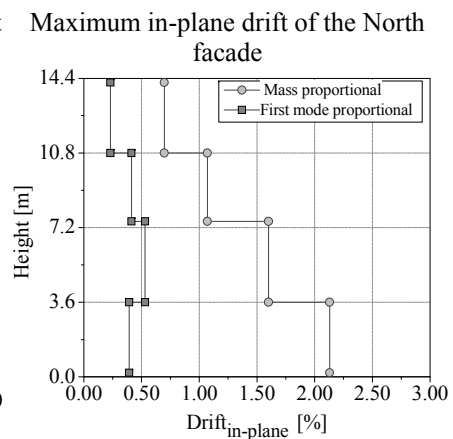
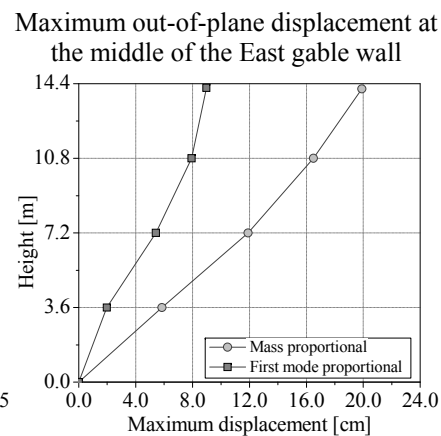
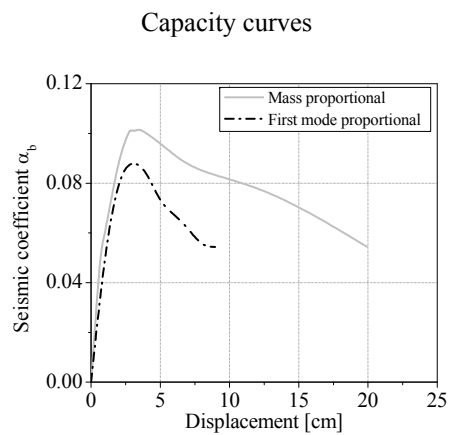


Pushover analyses in the longitudinal direction

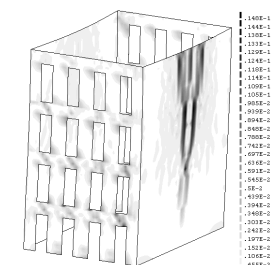


D.7 Pushover analysis proportional to the first mode

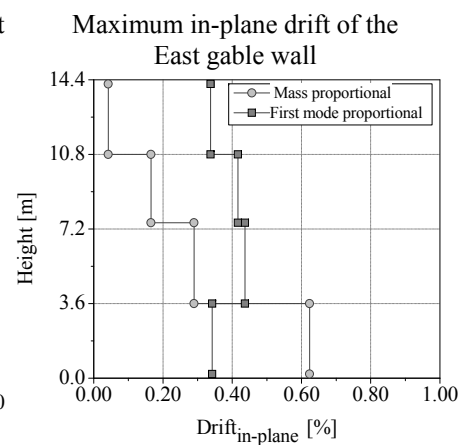
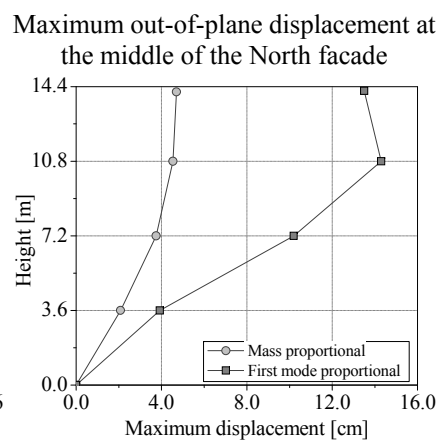
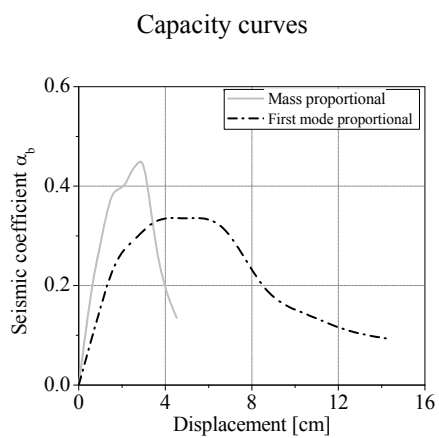
Pushover analyses in the transversal direction



Maximum tensile principal strains



Pushover analyses in the longitudinal direction



Maximum tensile principal strains

